

LIBRARY  
Michigan State  
University

This is to certify that the  
dissertation entitled

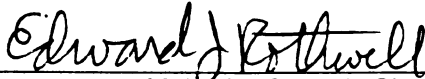
NATURAL RESONANCE REPRESENTATION OF THE  
TRANSIENT FIELD REFLECTED FROM A MULTILAYERED  
MATERIAL

presented by

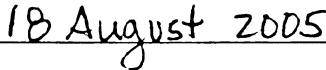
BRADLEY THOMAS PERRY

has been accepted towards fulfillment  
of the requirements for the

Ph.D. degree in Electrical and Computer  
Engineering



Major Professor's Signature



Date

**PLACE IN RETURN BOX** to remove this checkout from your record.  
**TO AVOID FINES** return on or before date due.  
**MAY BE RECALLED** with earlier due date if requested.

<b>DATE DUE</b>	<b>DATE DUE</b>	<b>DATE DUE</b>

**NATURAL RESONANCE REPRESENTATION OF THE  
TRANSIENT FIELD REFLECTED FROM A  
MULTILAYERED MATERIAL**

By

Bradley Thomas Perry

A DISSERTATION

Submitted to  
Michigan State University  
in partial fulfillment of the requirements  
for the degree of

DOCTOR OF PHILOSOPHY

Electrical and Computer Engineering

2005

## ABSTRACT

### NATURAL RESONANCE REPRESENTATION OF THE TRANSIENT FIELD REFLECTED FROM A MULTILAYERED MATERIAL

By

Bradley Thomas Perry

The transient reflection from a multilayered material structure is a deep and involved problem, even though closed form representations are available in the frequency domain. This thesis presents a novel approach for evaluating the transient field reflected from a layered material. Here a natural resonance representation is sought for the temporal response in both the late time of the layered structure, and the late time of individual substructures making up the layered material stack. In seeking this representation, a time domain reflection coefficient is defined, such that the convolution with a finite duration incident waveform yields the reflected field in the time domain. Through the definition of this time domain reflection coefficient, a methodology for obtaining the temporal response evolves. Questions on the source of the resonance response during various time periods are answered in this thesis, and the conditions for existence of the natural mode series are developed. It is found that for an  $n$ -layered material stack, a natural resonance representation can be found for the transient field if the backing material is either a perfect conductor, or a lossless medium. When the backing layer is lossy, a non-time limited branch cut contribution appears. It is also found that with the addition of a lossless layer, this branch cut contribution can be turned off. This is a valuable result with applications to non-destructive evaluation of materials.

Copyright by  
Bradley Thomas Perry  
2005

For Beckie and Alana

## ACKNOWLEDGMENTS

There are many people who deserve acknowledgement for both the work contained in this thesis, and the countless other things that I was able to be involved in during my time at Michigan State. First and foremost, a special thanks to Dr. Ed Rothwell for letting me walk my own paths. I have truly enjoyed my time as your student and feel fortunate to have been able to study under your guidance. To Dr. Leo Kempel, a special thanks for helping me decide to stay with this school thing after my undergraduate work. It is one of the best choices I have made, thank you for steering me in this direction. Also, thank you for the help in my job search, I know that you were, and always will be a valuable reference. Thanks to Dr. Shanker B. for teaching me some computational EM stuff that will help me for years to come. Also to Dr. Dennis Nyquist, for an invaluable experience of being in the last classes that you taught. A thank you is also in order for Dr. Guowei Wei, for agreeing to serve on my Ph.D. committee.

Thanks to Percy Pierre and Barbara O'Kelly for their support through the GAANN fellowship. A big thank you to Garrett Stenholm with AFRL, for supporting the experimental side of this research.

A special acknowledgement to my parents for their love and support always. Also to my in-laws who have loved and supported me like their own. Thank you for that. My deepest gratitude is reserved for my wife, Beckie, who has supported me throughout my studies and given me a beautiful daughter. Without your help, all this would not have been possible. I love you and Alana with all my heart and soul.



## TABLE OF CONTENTS

LIST OF TABLES . . . . .	ix
LIST OF FIGURES . . . . .	x
KEY TO SYMBOLS AND ABBREVIATIONS . . . . .	xiv
<b>CHAPTER 1</b>	
Introduction and Background . . . . .	1
1.1 Background and related work . . . . .	2
1.2 Overview of the research . . . . .	3
<b>CHAPTER 2</b>	
Frequency Domain and Time Domain Reflection Coefficients . . . . .	7
2.1 The plane wave field . . . . .	7
2.2 Interfacial reflection and transmission coefficients . . . . .	10
2.2.1 Parallel polarization . . . . .	11
2.2.2 Perpendicular polarization . . . . .	15
2.3 Wave matrix method . . . . .	18
2.3.1 Frequency domain reflection coefficient for two-layered geometries . . . . .	22
2.4 Time domain reflection coefficient . . . . .	24
2.4.1 Propagation through lossy media - wave velocity and transit time . . . . .	25
2.4.2 Simulation based comparison of NMS to IFFT . . . . .	28
<b>CHAPTER 3</b>	
Air-backed Lossy Layer in the Presence of a Conducting Screen . . . . .	43
3.1 Laplace domain representation . . . . .	45
3.2 The time domain reflection coefficient . . . . .	47
3.2.1 Singularities of the frequency domain reflection coefficient . . . . .	49
3.2.2 Evaluation of the time domain reflection coefficient . . . . .	49
3.2.2.1 Early time: $t < T_1$ . . . . .	50
3.2.2.2 Middle time: $T_1 < t < T_1 + T_2$ . . . . .	52
3.2.2.3 Late time: $t > T_1 + T_2$ . . . . .	54
<b>CHAPTER 4</b>	
Material-backed material layers . . . . .	78
4.1 Laplace domain representation . . . . .	80
4.2 The time domain reflection coefficient . . . . .	82
4.2.1 Singularities of the frequency domain reflection coefficient . . . . .	83
4.2.2 Evaluation of the time domain reflection coefficient . . . . .	84

4.2.2.1	Early time: $t < T_1$ . . . . .	84
4.2.2.2	Late time: $t > T_1$ . . . . .	85
<b>CHAPTER 5</b>		
Two Material Layers Backed by a Perfectly Conducting Screen . . . . .		112
5.1	Laplace domain representation . . . . .	114
5.2	The time domain reflection coefficient . . . . .	117
5.2.1	Singularities of the frequency domain reflection coefficient . . . . .	118
5.2.2	Evaluation of the time domain reflection coefficient . . . . .	119
5.2.2.1	Early time: $t < T_1$ . . . . .	119
5.2.2.2	Middle time: $T_1 < t < T_1 + T_2$ . . . . .	120
5.2.2.3	Late time: $t > T_1 + T_2$ . . . . .	123
<b>CHAPTER 6</b>		
N-Layered Material Problems . . . . .		148
6.1	Evaluation of the Laplace inversion integral . . . . .	149
6.1.1	Left half plane closure . . . . .	149
6.1.1.1	Contributions from the outer contour, $C$ . . . . .	150
6.1.1.2	Contributions from the inner contour, $C'$ . . . . .	152
6.1.2	Right half plane closure . . . . .	154
6.2	Form of the reduced reflection coefficient . . . . .	155
6.3	Decomposition of the temporal response using substructure responses . . . . .	171
6.4	Determination of the branch cut contribution . . . . .	177
6.4.1	Form of the denominator . . . . .	181
6.4.1.1	Equations for the $i$ -th layer . . . . .	182
6.4.1.2	N-Layer geometry . . . . .	185
6.4.2	Form of the numerator . . . . .	195
6.4.2.1	Equations for the $i$ -th layer . . . . .	195
6.4.2.2	N-Layer geometry . . . . .	199
6.4.3	Form of the reflection coefficient . . . . .	211
<b>CHAPTER 7</b>		
Time and Frequency Domain Measurements . . . . .		222
7.1	Measurement Systems . . . . .	222
7.1.1	Time Domain Measurement System . . . . .	223
7.1.1.1	Benefits of the time-domain system . . . . .	224
7.1.1.2	Drawbacks of the time-domain system . . . . .	225
7.1.2	Frequency Domain Measurement System . . . . .	226
7.1.2.1	Benefits of the frequency-domain system . . . . .	227
7.1.2.2	Drawbacks of the frequency-domain system . . . . .	228
7.1.3	Arch Range Calibration . . . . .	229
7.2	Experimental Procedures . . . . .	232

7.2.1	Determination of Experiment Parameters . . . . .	232
7.2.1.1	Time Domain Measurement System . . . . .	233
7.2.1.2	Frequency Domain Measurement System . . . . .	234
7.2.2	Calibration of the Time Domain System . . . . .	235
7.2.3	Calibration of the Frequency Domain System . . . . .	236
7.3	Measurement Results . . . . .	238
7.3.1	Time Domain System Measurements . . . . .	238
7.3.2	Frequency Domain System Measurements . . . . .	239
7.3.3	Comparison of Results from the Time-Domain and Frequency-Domain Systems . . . . .	240
CHAPTER 8		
	Conclusions . . . . .	291
8.1	Suggestions for Future Work . . . . .	293
	BIBLIOGRAPHY . . . . .	296

## LIST OF TABLES

Table 2.1	Natural mode frequencies and coupling coefficients for the problem of Figure 2.8 . . . . .	30
Table 2.2	Natural mode frequencies and coupling coefficients for the problem of Figure 2.10 . . . . .	31
Table 7.1	Percent difference between measurement with given number of averages, and measurement with 256 averages . . . . .	242
Table 7.2	Percent difference between measurement with given number of averages, and measurement with 512 averages . . . . .	243

## LIST OF FIGURES

Figure 2.1	A discontinuity interface between two material regions . . . . .	32
Figure 2.2	Fields at an interface between two materials for parallel polarization	33
Figure 2.3	Fields at an interface between two materials for perpendicular polarization . . . . .	34
Figure 2.4	Fields at a discontinuity for incidence from each direction . . . . .	35
Figure 2.5	An $n$ -material cascade of planar layers . . . . .	36
Figure 2.6	Geometry for a two layered material stack . . . . .	37
Figure 2.7	Timing diagram for determining transit time in a lossy material layer	38
Figure 2.8	A two-layered, air-backed geometry . . . . .	39
Figure 2.9	Time domain reflection coefficient for a two-layered, air-backed geometry . . . . .	40
Figure 2.10	A two-layered, PEC-backed geometry . . . . .	41
Figure 2.11	Time domain reflection coefficient for a two-layered, PEC-backed geometry . . . . .	42
Figure 3.1	Air Lossy Air PEC . . . . .	69
Figure 3.2	Single interface between free-space and a lossy dielectric . . . . .	70
Figure 3.3	Closure of the Bromwich contour in the right half plane. $ b  \rightarrow \infty, 0 < c < \infty$ . . . . .	71
Figure 3.4	Interfacial reflection coefficient for the first interface . . . . .	72
Figure 3.5	Air-backed lossy dielectric layer . . . . .	73
Figure 3.6	Temporal response from an air-backed lossy layer . . . . .	74
Figure 3.7	Closure of the Bromwich contour in the left half plane. $ a ,  b  \rightarrow \infty, 0 < c < \infty$ . . . . .	75
Figure 3.8	Inner contour integration paths for left half plane closure . . . . .	76
Figure 3.9	Temporal response of an air-backed lossy layer in the presence of a conducting screen . . . . .	77
Figure 4.1	Material-backed lossy dielectric layer . . . . .	107
Figure 4.2	Single interface between free-space and a lossy dielectric . . . . .	108
Figure 4.3	Closure of the Bromwich contour in the right half plane. $ b  \rightarrow \infty, 0 < c < \infty$ . . . . .	109
Figure 4.4	Closure of the Bromwich contour in the left half plane. $ a ,  b  \rightarrow \infty, 0 < c < \infty$ . . . . .	110
Figure 4.5	Inner contour integration paths for left half plane closure . . . . .	111

Figure 5.1	Air Lossy PEC . . . . .	142
Figure 5.2	Single interface between free-space and a lossy dielectric . . . . .	143
Figure 5.3	Closure of the Bromwich contour in the right half plane. $ b  \rightarrow \infty, 0 < c < \infty$ . . . . .	144
Figure 5.4	Material-backed lossy dielectric layer . . . . .	145
Figure 5.5	Closure of the Bromwich contour in the left half plane. $ a ,  b  \rightarrow \infty, 0 < c < \infty$ . . . . .	146
Figure 5.6	Inner contour integration paths for left half plane closure . . . . .	147
Figure 6.1	Singularities of the frequency domain reflection coefficient . . . . .	213
Figure 6.2	Left half plane closure of the integration path. $ a ,  b  \rightarrow \infty, 0 < c < \infty$ . . . . .	214
Figure 6.3	Right half plane closure of the integration path. $ b  \rightarrow \infty, 0 < c < \infty$ . . . . .	215
Figure 6.4	Single interface between two material half spaces . . . . .	216
Figure 6.5	Single layer geometry backed by a material half space . . . . .	217
Figure 6.6	Two layer geometry backed by a material half space . . . . .	218
Figure 6.7	Three layer geometry backed by a material half space . . . . .	219
Figure 6.8	N-layered structure backed by a material half space . . . . .	220
Figure 6.9	Inner contour integration paths for left half plane closure . . . . .	221
Figure 7.1	Arch range setup for the time-domain measurement system . . . . .	244
Figure 7.2	Step output from channel 3 of the HP54750A used as trigger for the PSPL 4015B step generator . . . . .	245
Figure 7.3	Transmitted pulse created by the PSPL 5208 pulse-generating network . . . . .	246
Figure 7.4	Spectrum of transmitted pulse created by the PSPL 5208 pulse-generating network . . . . .	247
Figure 7.5	Top view of arch range setup . . . . .	248
Figure 7.6	Arch range setup for the frequency-domain measurement system . . . . .	249
Figure 7.7	Block diagram of the measurement system . . . . .	250
Figure 7.8	Comparison of raw measured data for a conducting plate measured with a metallic pedestal and a styrofoam pedestal . . . . .	251
Figure 7.9	Comparison of raw measured data for a 14 inch sphere measured with a metallic pedestal and a styrofoam pedestal . . . . .	252
Figure 7.10	Raw measurement for a conductor-backed garolite sheet . . . . .	253

Figure 7.11	A typical background measurement for the time-domain measurement system (Note the change in scale) . . . . .	254
Figure 7.12	Raw conducting-plate calibration measurement . . . . .	255
Figure 7.13	Time-gated conducting-plate calibrator measurement . . . . .	256
Figure 7.14	System response for the time-domain measurement system . . . . .	257
Figure 7.15	Time-gated, Fourier transformed PEC-backed material measurement	258
Figure 7.16	Measured PEC-backed garolite data after division by system response	259
Figure 7.17	Spectrum of PEC-backed garolite sheet weighted by a cosine taper	260
Figure 7.18	Calibrated temporal response of PEC-backed garolite sheet measured with the time-domain system . . . . .	261
Figure 7.19	System response of the frequency-domain measurement system . . . . .	262
Figure 7.20	Comparison of the system responses for the time-domain and frequency-domain measurement systems . . . . .	263
Figure 7.21	Spectrum of a PEC-backed garolite sheet measured using the frequency-domain system . . . . .	264
Figure 7.22	Spectrum of a PEC-backed garolite sheet measured using the frequency-domain system and weighted with a cosine taper window . . . . .	265
Figure 7.23	Calibrated temporal response of PEC-backed garolite sheet measured with the frequency domain system . . . . .	266
Figure 7.24	PEC-backed acrylic - Measurement using time-domain system (a)temporal response and (b)spectral response . . . . .	267
Figure 7.25	Air-backed acrylic - Measurement using time-domain system (a)temporal response and (b)spectral response . . . . .	268
Figure 7.26	PEC-backed garolite - Measurement using time-domain system (a)temporal response and (b)spectral response . . . . .	269
Figure 7.27	Air-backed garolite - Measurement using time-domain system (a)temporal response and (b)spectral response . . . . .	270
Figure 7.28	PEC-backed PVC - Measurement using time-domain system (a)temporal response and (b)spectral response . . . . .	271
Figure 7.29	Air-backed PVC - Measurement using time-domain system (a)temporal response and (b)spectral response . . . . .	272
Figure 7.30	PEC-backed garolite-acrylic stack - Measurement using time-domain system (a)temporal response and (b)spectral response . . . . .	273
Figure 7.31	Air-backed garolite-acrylic stack - Measurement using time-domain system (a)temporal response and (b)spectral response . . . . .	274

Figure 7.32	Air-backed acrylic-garolite stack - Measurement using time-domain system (a)temporal response and (b)spectral response . . . . .	275
Figure 7.33	PEC-backed acrylic - Measurement using frequency-domain system (a)temporal response and (b)spectral response . . . . .	276
Figure 7.34	Air-backed acrylic - Measurement using frequency-domain system (a)temporal response and (b)spectral response . . . . .	277
Figure 7.35	PEC-backed garolite - Measurement using frequency-domain system (a)temporal response and (b)spectral response . . . . .	278
Figure 7.36	Air-backed garolite - Measurement using frequency-domain system (a)temporal response and (b)spectral response . . . . .	279
Figure 7.37	PEC-backed PVC - Measurement using frequency-domain system (a)temporal response and (b)spectral response . . . . .	280
Figure 7.38	Air-backed PVC - Measurement using frequency-domain system (a)temporal response and (b)spectral response . . . . .	281
Figure 7.39	PEC-backed garolite-acrylic stack - Measurement using frequency-domain system (a)temporal response and (b)spectral response . .	282
Figure 7.40	PEC-backed PVC-garolite stack - Measurement using frequency-domain system (a)temporal response and (b)spectral response . .	283
Figure 7.41	PEC-backed acrylic - Comparison of measurement systems (a)temporal response and (b)spectral response . . . . .	284
Figure 7.42	Air-backed acrylic - Comparison of measurement systems (a)temporal response and (b)spectral response . . . . .	285
Figure 7.43	PEC-backed garolite - Comparison of measurement systems (a)temporal response and (b)spectral response . . . . .	286
Figure 7.44	Air-backed garolite - Comparison of measurement systems (a)temporal response and (b)spectral response . . . . .	287
Figure 7.45	PEC-backed PVC - Comparison of measurement systems (a)temporal response and (b)spectral response . . . . .	288
Figure 7.46	Air-backed PVC - Comparison of measurement systems (a)temporal response and (b)spectral response . . . . .	289
Figure 7.47	PEC-backed garolite-acrylic stack - Comparison of measurement systems (a)temporal response and (b)spectral response . . . . .	290



## KEY TO SYMBOLS AND ABBREVIATIONS

**NMS:** Natural Mode Series

**IFFT:** Inverse fast-Fourier Transform

**SEM:** Singularity Expansion Method

**VNA:** Vector Network Analyzer

**DSO:** Digital Sampling Oscilloscope

**TDR:** Time Domain Reflectometry

**SNR:** Signal-to-Noise Ratio

## CHAPTER 1

### INTRODUCTION AND BACKGROUND

Time domain electromagnetics has been utilized for many applications, such as radar target discrimination [1]-[3] and materials characterization [4],[5], mainly due to its adaptability to broadband signals. The singularity expansion method (SEM) [6], which views the late time of a temporal response of a scatterer as a series of residues at the poles of the Green's function [7], has been used by many for radar target discrimination. This late time is defined as the time period after the entire scatterer has been illuminated by the incident wave and the scattered field has returned to the observer. Applications of SEM and its limitations are the subject of [8]-[10].

The extinction pulse (E-pulse) technique [1]-[3] is a target identification scheme which was born out of the singularity expansion method. This technique uses a natural mode series representation of the late time response to devise a waveform that will extinguish the modes present in a measured response through a convolution. The E-pulse consists of a series of pulses and is designed for a given radar target. For convolution of the E-pulse with the intended target, all modes in the band of the response are annihilated, giving zero energy from the convolution in the late time. In addition to radar target discrimination, the E-pulse technique has been applied in non-destructive evaluation of materials [4],[5]. Here, E-pulses are created from baseline measurements of known materials, and convolution with an identical material measurement will yield zero energy in the late time. Experimental results have shown that the E-pulse technique can work well for material testing. The validity of the E-pulse technique for non-destructive evaluation is the motivation of the study of the form of the transient field, which is done analytically in this thesis.

## 1.1 Background and related work

There is a lack of detailed analysis for the transient response of a layered medium in terms of a resonance series, except for work done by Tihuis and Block in 1984 [11],[12], and more recent work performed by Oh [13] and Suk [14].

In the work of Tihuis and Block, the transient scattering of a normally incident plane wave from a lossy dielectric slab is considered using the singularity expansion method. Their work, however, is semi-analytic and does not clearly show that the late-time response can be expressed as a pure natural resonance series, due to difficulty in evaluating the branch cut contributions and infinite contour contributions needed to evaluate the Laplace inversion integrals.

Oh also considers the reflection from single layers of materials backed by free space, or by a perfect conductor. This work is rigorous and shows that a natural resonance representation is valid for the reflection from an air-backed lossy material layer, as well as a conductor-backed one. Consideration is given to oblique incidence, and the behavior of the poles of the frequency domain reflection coefficient with changing incidence angle are analyzed heavily. Early time responses from these material slabs are found to be identical to the response from the single interfacial reflection, which is considered in detail by Suk.

Suk analyzes the transient response for plane-wave reflection from a single planar interface between two material half spaces. This is a rigorous development which shows that the interfacial reflection from a dissipative material is composed of both an impulsive component and an infinite tail, which has to do with conduction currents in the lossy medium.

The work presented in this thesis looks to expand on the work done by Oh and Suk by considering multilayered material problems. Since these problems involve various material regions, the interfacial reflection coefficients developed by Suk are valuable.

Also, the method employed for the factorization of the frequency domain reflection coefficient for a multilayered material problem is based on the approach used by Oh in his single material layer analysis.

## 1.2 Overview of the research

This thesis is presented as a series of postulates on the form of the late time temporal response for various geometries, along with verifications of these postulates, which lead to a general property describing the late time behavior of an  $n$ -layer structure. Chapters 3 through 5 consider simple problems, the solutions to which provide sufficient evidence to form a hypothesis about the behavior of an  $n$ -layer structure. This hypothesis is verified through the developments of Chapter 6.

Oh showed that the late time response of a single layer backed by either free space or a conductor is a natural mode series. This leads one to consider the question ‘can the late time response of a material stack with more than a single layer also be a natural mode series?’, and, if so, ‘under what conditions will this be true?’. To answer these questions, the reflection from an air backed single lossy layer terminated by a perfect electric conductor is first considered. Physical reasoning suggests that there should be a ‘middle time’ period during which the response of the structure is a natural mode series identical to that of the single air-backed layer, since the incident wave will not have reached the conductor backing and thus no information about the position of this backing can be available in the reflected response. After this middle time period there should be a late time during which the response differs from that of the air-backed layer. An important question is ‘will this late time response, which must include information about the entire structure, also be a natural mode series?’, and, if so, the additional question of ‘will the natural frequencies be the same as those of the middle time response, or will an entirely new natural mode series arise, either replacing or augmenting the middle time series?’ must be considered.

Examining the temporal response of the air backed lossy layer terminated by a conducting screen, the time domain response is found to have a natural mode series representation once the response from the reflection off of the second interface is observed at the observation plane; this provides a definitive turn on time for the natural mode series and marks the beginning of the middle time period that was speculated. Further, it is found that the natural resonance representation during the middle time period is given in terms of the poles of the frequency domain reflection coefficient for the air-backed lossy layer, as physical reasoning would suggest. The observation of the response from the reflection off of the conductor returning to the observation plane is the event that marks the end of the middle time period. After this event occurs, the time domain reflection coefficient is found to have an entirely new natural resonance representation related to the poles of the frequency domain reflection coefficient for the entire problem. Hence, the response of the air-backed lossy layer present during the middle time period is turned off, and replaced by a different natural mode response.

With this knowledge, the next question to consider is 'does the presence of a pure natural mode series in the late time have anything to do with the properties of the backing layer?'. To study this, a single lossy layer, backed by a material layer, either lossless or lossy, is considered.

In examining the response from a single lossy layer backed by a material half space, it is found that whether or not the late time response of this structure is a natural mode series is dependent only on the properties of the material backing. When a lossless half space is considered, the response is found to have a natural resonance representation in the late time. However, when a lossy half space is considered, it is found that a pure natural resonance representation is not possible, as there may be a branch cut contribution to the temporal response. This is found to be the case regardless of the properties of the first material layer.

Combining this with the results from Oh, a statement can now be made that a single lossy layer, backed by a perfect conductor, or a lossless half space, will have a late time response that is a pure natural mode series. However, when that same layer is backed by a lossy region, the late time natural mode response will be augmented by a branch cut contribution which is not time-limited. The portion of the response due to this branch cut contribution is an infinite tail which pollutes the natural mode response.

These results lead to one last question, that is, ‘is it the properties of the final backing layer in an  $n$ -layer material stack that determine the form of the response in the late time of the structure?’. To explore this, a stack consisting of two lossy layers backed by a perfect conductor is considered.

It is found in this exploration that the response of the two-layered material structure backed by a perfect conductor is a natural mode series during the late time. This implies that the branch cut contribution that is present in the middle time of the response is turned off when the reflection from the conductor backing reaches the observation plane; that is, at the start of the late time. Thus, the presence of the conductor terminates the infinite tail in the response of the single layer backed by a lossy layer, and initiates a pure natural mode series.

These results lead to the following hypothesis about the response of an  $n$ -layer system:

1. The late time reflected field response of an  $n$ -layer system is a pure natural mode series if the backing layer is lossless or a perfect electric conductor. If the backing layer is lossy, the late time reflected field response is a natural mode series augmented by a non-time limited branch cut contribution.
2. If an additional interface is added to produce a new  $n + 1$  layer structure, the early time response will be the same as the total response of the  $n$ -layer structure. This response will turn off completely at a time associated with the reflection from the new

interface with the backing material, and a late time response will turn on consisting of a natural mode series that is augmented by a branch cut contribution only if the new backing is lossy. If the  $n$ -layer structure had a non-time limited component in its late time, this component will turn off at the start of the late time of the  $n + 1$  layer structure. This hypothesis is verified in Chapter 6 by decomposing an  $n$ -layer structure into simpler substructures and continuing the decomposition until one of the simple problems of Chapters 3 through 5 is reached.

## CHAPTER 2

### FREQUENCY DOMAIN AND TIME DOMAIN REFLECTION COEFFICIENTS

In order to consider the transient field reflected from a multiply layered dielectric, begin by examining the frequency domain reflection coefficient. This reflection coefficient has a closed form representation for planarly layered materials, which can be found using various approaches, including the wave matrix method [16] and iterative approaches [17]. In both of these approaches, the frequency domain reflection coefficient for a layered material is written in terms of interfacial reflection and transmission coefficients, which are found for interfaces between two material regions of semi-infinite extent. The derivation of these reflection and transmission coefficients are outlined in Section 2.2. For this work, the wave matrix method is utilized and an explanation of this method is included in Section 2.3.

The time domain reflection coefficient is defined in Section 2.4, such that the reflected field in the time domain is given as the convolution of this time domain reflection coefficient with an incident field of finite duration.

#### 2.1 The plane wave field

For a source-free region of linear, isotropic, homogeneous material, Maxwell's equations in terms of the fields  $\vec{E}$  and  $\vec{H}$  are given in point form as

$$\nabla \times \vec{E} = -j\omega\mu\vec{H} \quad (2.1)$$

$$\nabla \times \vec{H} = j\omega\epsilon^c\vec{E} \quad (2.2)$$

$$\nabla \cdot \vec{E} = 0 \quad (2.3)$$

$$\nabla \cdot \vec{H} = 0 \quad (2.4)$$



where  $\epsilon^c(\omega)$  is the frequency dependent complex permittivity, which is defined by  $\epsilon^c(\omega) = \epsilon + \sigma/j\omega$ . Here, dielectric loss is included through the conductivity,  $\sigma$ . Taking the curl of Faraday's law, which is given in (2.1), gives

$$\begin{aligned}\nabla \times \nabla \times \vec{E} &= -j\omega\mu(\nabla \times \vec{H}) \\ &= \omega^2\mu\epsilon^c\vec{E}\end{aligned}\tag{2.5}$$

where Ampere's law, given by (2.2) has been utilized. Using  $\nabla \times \nabla \times \vec{E} = \nabla(\nabla \cdot \vec{E}) - \nabla^2\vec{E}$  and Gauss's law, given in (2.3), Equation (2.5) can be written as

$$\nabla^2\vec{E} + k^2\vec{E} = 0\tag{2.6}$$

where  $k = \omega\sqrt{\mu\epsilon^c}$  is the wave number of the medium. Similarly, taking the curl of Ampere's law, which is given in (2.2), gives

$$\begin{aligned}\nabla \times \nabla \times \vec{H} &= j\omega\epsilon^c(\nabla \times \vec{E}) \\ &= \omega^2\mu\epsilon^c\vec{H}\end{aligned}\tag{2.7}$$

where Faraday's law, given by (2.1) has been utilized. Using  $\nabla \times \nabla \times \vec{H} = \nabla(\nabla \cdot \vec{H}) - \nabla^2\vec{H}$  and Gauss's magnetic law, given in (2.4), Equation (2.7) can be written as

$$\nabla^2\vec{H} + k^2\vec{H} = 0\tag{2.8}$$

Equations (2.6) and (2.8) are the homogeneous vector Helmholtz equations. In rectangular coordinates, the vector Helmholtz equations reduce to three scalar Helmholtz equations of the form

$$\nabla^2\psi + k^2\psi = 0\tag{2.9}$$

where  $\psi$  is representative of the  $x$ ,  $y$ , and  $z$  components of the electric and magnetic fields. Equation (2.9) has a product solution in terms of a linear combinations of harmonic functions, which can be found through a separation of variables. Since exponentials describe propagating wave functions, the scalar term  $\psi$  is written as

$$\psi = A(\omega)e^{\pm jk_x(\omega)x}e^{\pm jk_y(\omega)y}e^{\pm jk_z(\omega)z} \quad (2.10)$$

where  $A(\omega)$  is the amplitude spectrum of the plane wave and  $k_x^2 + k_y^2 + k_z^2 = k^2$ . Using this solution for each component of the electric field, the solution to (2.6) is given by

$$\vec{E}(\vec{r}, \omega) = \vec{E}_0(\omega)e^{\pm jk_x(\omega)x}e^{\pm jk_y(\omega)y}e^{\pm jk_z(\omega)z} \quad (2.11)$$

where  $\vec{E}_0(\omega)$  is the vector amplitude spectrum of the electric field. Defining the wave vector as

$$\vec{k}(\omega) = \hat{x}k_x(\omega) + \hat{y}k_y(\omega) + \hat{z}k_z(\omega), \quad (2.12)$$

the electric field can be written as

$$\vec{E}(\vec{r}, \omega) = \vec{E}_0(\omega)e^{-j\vec{k}(\omega) \cdot \vec{r}}. \quad (2.13)$$

where  $\vec{r}$  is the position vector given by  $\vec{r} = \hat{x}x + \hat{y}y + \hat{z}z$ . Here, the negative sign has been taken in the exponential function, allowing the wave vector components to be either positive or negative, depending on the physics of a given problem. For a uniform plane wave, electric and magnetic fields are related by

$$\vec{H} = \frac{\vec{k} \times \vec{E}}{\omega\mu}. \quad (2.14)$$

The plane-wave field, which has  $\vec{E}$  and  $\vec{H}$  mutually orthogonal to one another, and to the wave vector, is said to be transverse electromagnetic, or TEM, to the direction

of propagation.

## 2.2 Interfacial reflection and transmission coefficients

Consider a uniform plane wave incident on a planar interface between two regions of space, as shown in Figure 2.1. The material in each region is assumed to be isotropic and homogeneous with material parameters  $(\mu_i, \epsilon_i^c)$ . Here,  $\mu_i$  is the frequency independent permeability of the  $i^{\text{th}}$  region, and  $\epsilon_i^c$  is the frequency dependent complex permittivity of that region, which is a complex number that includes dielectric loss. Since the incident field is uniform, the wave vector associated with this field may be written as

$$\vec{k}^i = \hat{k}^i k_1^i \quad (2.15)$$

where

$$k_1^i(\omega) = \omega \sqrt{\mu_1 \epsilon_1^c(\omega)} \quad (2.16)$$

Without loss of generality, it can be assumed that the unit vector  $\hat{k}^i$  lies in the  $xz$ -plane and makes an angle  $\theta_{in}$  with the interface normal, as shown in Figure 2.1. The angle  $\theta_{in}$  is the angle between the direction of propagation of the planar phase fronts of the incident field, and the normal to the interface. This angle is referred to as the incidence angle of the incident field. With this, the wave vector can be written as

$$\vec{k}^i = \hat{x} k_1 \sin \theta_{in} + \hat{z} k_1 \cos \theta_{in} = \hat{x} k_x^i + \hat{z} k_z^i \quad (2.17)$$

The fields in each region of space are solved for directly in the frequency domain. The incident electric and magnetic field are given by (2.13) and (2.14) as

$$\vec{E}^i(\vec{r}, \omega) = \vec{E}_0^i(\omega) e^{-j \vec{k}^i(\omega) \cdot \vec{r}} \quad (2.18a)$$

$$\vec{H}^i = \frac{\vec{k}^i \times \vec{E}^i}{\omega \mu_1}. \quad (2.18b)$$

To proceed, note that a uniform plane wave can be decomposed into two orthogonal components. The two components are distinguished from one another by the plane in which the electric field lies. The first of these is parallel polarization, in which the electric field lies in the plane containing the interface normal and the direction of propagation, as shown in Figure 2.2. The form of the interfacial reflection coefficient for this polarization is the subject of Section 2.2.1. The second case is when the electric field vector is perpendicular to this plane (perpendicular polarization), as shown in Figure 2.3. The derivation of the interfacial reflection coefficient for perpendicular polarization is the subject of Section 2.2.2. A solution for both of these polarizations is sufficient to characterize any arbitrary incident uniform plane wave. The total field in any region of space is given as a superposition of the fields found for each polarization.

### 2.2.1 Parallel polarization

For parallel polarization, where the electric field lies in the plane containing the interface normal and the direction of propagation, the incident field is given using (2.18) and examining Figure 2.2 as

$$\vec{E}_{\parallel}^i = E_0^i \left( \hat{x} \frac{k_z^i}{k_1} - \hat{z} \frac{k_x^i}{k_1} \right) e^{-j(k_x^i x + k_z^i z)} \quad (2.19)$$

$$\vec{H}_{\parallel}^i = \hat{y} \frac{E_0^i}{\eta_1} e^{-j(k_x^i x + k_z^i z)}. \quad (2.20)$$

Here  $\eta_1 = \sqrt{\mu_1/\epsilon_1^c}$  is the frequency dependent intrinsic impedance of region 1.

It is hypothesized that the total field in region 1 will be given by the incident field superposed with a reflected plane-wave field with wave vector,  $\vec{k}^r$ , while the field in region 2 is given by a single transmitted plane-wave field having wave vector,  $\vec{k}^t$ . Although the reflected and transmitted fields are not known explicitly at this point, their form is known. This is because the reflected and transmitted fields cannot

have vector components that are not present in the incident field, in order to satisfy boundary conditions at the interface. Letting  $E_0^r$  be the amplitude of the reflected field gives

$$\vec{E}_{\parallel}^r = E_0^r \left( \hat{x} \frac{k_z^r}{k_1} - \hat{z} \frac{k_x^r}{k_1} \right) e^{-j(k_x^r x + k_z^r z)} \quad (2.21)$$

$$\vec{H}_{\parallel}^r = \hat{y} \frac{E_0^r}{\eta_1} e^{-j(k_x^r x + k_z^r z)} \quad (2.22)$$

for parallel polarization. Similarly, letting  $E_0^t$  be the amplitude of the transmitted field gives

$$\vec{E}_{\parallel}^t = E_0^t \left( \hat{x} \frac{k_z^t}{k_2} - \hat{z} \frac{k_x^t}{k_2} \right) e^{-j(k_x^t x + k_z^t z)} \quad (2.23)$$

$$\vec{H}_{\parallel}^t = \hat{y} \frac{E_0^t}{\eta_2} e^{-j(k_x^t x + k_z^t z)}. \quad (2.24)$$

where  $\eta_2 = \sqrt{\mu_2/\epsilon_2^c}$  is the frequency dependent intrinsic impedance of region 2. In region 2,  $k_2^2 = (k_x^t)^2 + (k_z^t)^2$ , with the amplitude given by the wave number,  $k_2 = \omega \sqrt{\mu_2 \epsilon_2^c}$ .

In order to satisfy continuity of tangential electric and magnetic fields over the entire interface, the x-variation of all three partial fields, that is the incident, reflected, and transmitted fields, must be identical; i.e.,

$$k_x^i = k_x^r = k_x^t \quad (2.25)$$

These constraints on  $k_x^r$  and  $k_x^t$  also place constraints on  $k_z^r$  and  $k_z^t$ . Thus,  $(k_x^i)^2 + (k_z^i)^2 = (k_x^r)^2 + (k_z^r)^2 = k_1^2$ , which requires  $k_z^r = \pm k_z^i$ . Here  $k_z^r = -k_z^i$  is chosen to give propagation of the planar wave fronts away from the interface.

The boundary condition on continuity of tangential electric field requires

$$\hat{z} \times (\vec{E}_{\parallel}^i + \vec{E}_{\parallel}^r)|_{z=0} = \hat{z} \times \vec{E}_{\parallel}^t|_{z=0} \quad (2.26)$$

Using the constraint on the x-component of the various wave numbers and the boundary condition on the electric field leads to

$$\frac{k_z^i}{k_1} E_0^i + \frac{k_z^r}{k_1} E_0^r = \frac{k_z^t}{k_2} E_0^t. \quad (2.27)$$

Dividing (2.27) by the amplitude of the incident field,  $E_0^i$ , gives

$$1 + \frac{k_z^r}{k_z^i} \frac{E_0^r}{E_0^i} = \frac{k_z^t}{k_z^i} \frac{k_1}{k_2} \frac{E_0^t}{E_0^i}. \quad (2.28)$$

The boundary condition on the magnetic field at the  $z = 0$  interface also requires continuity. Thus, with the hypothesized form of the fields in each region, continuity of tangential magnetic field requires

$$\hat{z} \times (\vec{H}_{\parallel}^i + \vec{H}_{\parallel}^r)|_{z=0} = \hat{z} \times \vec{H}_{\parallel}^t|_{z=0} \quad (2.29)$$

Using the constraint on the x-component of the various wave numbers and the boundary condition on the magnetic field leads to

$$\frac{E_0^i}{\eta_1} + \frac{E_0^r}{\eta_1} = \frac{E_0^t}{\eta_2}. \quad (2.30)$$

Rearranging terms in this equation gives

$$1 + \frac{E_0^r}{E_0^i} = \frac{\eta_1}{\eta_2} \frac{E_0^t}{E_0^i}. \quad (2.31)$$

The addition of (2.28) and (2.31), along with  $k_z^r = -k_z^i$  gives

$$\begin{aligned}\frac{E_0^t}{E_0^i} &= \frac{2Z_2^{\parallel}}{Z_2^{\parallel} + Z_1^{\parallel}} \frac{k_z^i k_2}{k_1 k_z^t} \\ &= T^{\parallel} \frac{k_z^i k_2}{k_1 k_z^t}\end{aligned}\quad (2.32)$$

where, using (2.17) and (2.25),

$$Z_1^{\parallel} = \frac{k_z^i \eta_1}{k_1} = \eta_1 \cos \theta_{in} \quad (2.33a)$$

$$Z_2^{\parallel} = \frac{k_z^t \eta_2}{k_2} = \frac{\eta_2}{k_2} \left( k_2^2 - (k_x^t)^2 \right)^{1/2} = \frac{\eta_2}{k_2} \left( k_2^2 - k_1^2 \sin^2 \theta_{in} \right)^{1/2}. \quad (2.33b)$$

Here  $T^{\parallel}$  is a frequency-dependent transmission coefficient that relates the tangential components of the incident and transmitted fields for parallel polarization. This will be referred to throughout this thesis as the interfacial transmission coefficient. The relationship of this transmission coefficient to the total fields is given by

$$T^{\parallel} = \frac{2Z_2^{\parallel}}{Z_2^{\parallel} + Z_1^{\parallel}} = \frac{E_{\parallel,x}^t}{E_{\parallel,x}^i} = \frac{E_0^t (k_z^t / k_2)}{E_0^i (k_z^i / k_1)}. \quad (2.34)$$

Plugging the interfacial transmission coefficient back into (2.28) gives

$$T^{\parallel} = 1 + \frac{k_z^r}{k_z^i} \frac{E_0^r}{E_0^i} = 1 + R^{\parallel}. \quad (2.35)$$

Here  $R^{\parallel}$  is a frequency-dependent reflection coefficient that relates the tangential components of the incident and reflected fields for parallel polarization. This will be referred to throughout this thesis as the interfacial reflection coefficient. The

relationship of this reflection coefficient to the total fields is given by

$$R^{\parallel} = \frac{k_z^r E_0^r}{k_z^i E_0^i} = -\frac{E_0^r}{E_0^i} = \frac{E_{\parallel,x}^r}{E_{\parallel,x}^i} = \frac{Z_2^{\parallel} - Z_1^{\parallel}}{Z_2^{\parallel} + Z_1^{\parallel}} \quad (2.36)$$

with  $Z_1^{\parallel}$  and  $Z_2^{\parallel}$  given by (2.33).

### 2.2.2 Perpendicular polarization

For perpendicular polarization, where the electric field lies perpendicular to the plane containing the interface normal and the direction of propagation, the incident field is given using (2.18) and examining Figure 2.3 as

$$\vec{E}_{\perp}^i = \hat{y} E_0^i e^{-j(k_x^i x + k_z^i z)} \quad (2.37)$$

$$\vec{H}_{\perp}^i = \frac{E_0^i}{\eta_1} \left( -\hat{x} \frac{k_z^i}{k_1} + \hat{z} \frac{k_x^i}{k_1} \right) e^{-j(k_x^i x + k_z^i z)} \quad (2.38)$$

It is hypothesized that the total field in region 1 will be given by the incident field superposed with a reflected plane-wave field with wave vector,  $\vec{k}^r$ , while the field in region 2 is given by a single transmitted plane-wave field having wave vector,  $\vec{k}^t$ . Although the reflected and transmitted fields are not known explicitly at this point, their form is known. This is because the reflected and transmitted fields cannot have vector components that are not present in the incident field, in order to satisfy boundary conditions at the interface. Letting  $E_0^r$  be the amplitude of the reflected field gives

$$\vec{E}_{\perp}^r = \hat{y} E_0^r e^{-j(k_x^r x + k_z^r z)} \quad (2.39)$$

$$\vec{H}_{\perp}^r = \frac{E_0^r}{\eta_1} \left( -\hat{x} \frac{k_z^r}{k_1} + \hat{z} \frac{k_x^r}{k_1} \right) e^{-j(k_x^r x + k_z^r z)} \quad (2.40)$$



for perpendicular polarization. Similarly, letting  $E_0^t$  be the amplitude of the transmitted field gives

$$\vec{E}_\perp^t = \hat{y}E_0^t e^{-j(k_x^t x + k_z^t z)} \quad (2.41)$$

$$\vec{H}_\perp^t = \frac{E_0^t}{\eta_2} \left( -\hat{x} \frac{k_z^t}{k_2} + \hat{z} \frac{k_x^t}{k_2} \right) e^{-j(k_x^t x + k_z^t z)} \quad (2.42)$$

In order to satisfy continuity of tangential electric and magnetic fields over the entire interface, the x-variation of all three partial fields, that is the incident, reflected, and transmitted fields, must be identical; i.e.,

$$k_x^i = k_x^r = k_x^t \quad (2.43)$$

The constraints on  $k_x^r$  and  $k_x^t$  also place constraints on  $k_z^r$  and  $k_z^t$ . Thus,  $(k_x^i)^2 + (k_z^i)^2 = (k_x^r)^2 + (k_z^r)^2 = k_1^2$ , which requires  $k_z^r = \pm k_z^i$ . Here  $k_z^r = -k_z^i$  is chosen to give propagation of the planar wave fronts away from the interface.

The boundary condition on continuity of tangential electric field requires

$$\hat{z} \times (\vec{E}_\perp^i + \vec{E}_\perp^r) \Big|_{z=0} = \hat{z} \times \vec{E}_\perp^t \Big|_{z=0} \quad (2.44)$$

Using the constraint on the x-component of the various wave numbers and the boundary condition on the electric field leads to

$$E_0^i + E_0^r = E_0^t \quad (2.45)$$

Dividing (2.45) by the amplitude of the incident field,  $E_0^i$ , gives

$$1 + \frac{E_0^r}{E_0^i} = \frac{E_0^t}{E_0^i} \quad (2.46)$$

The boundary condition on the magnetic field at the  $z = 0$  interface also requires continuity. Thus, with the hypothesized form of the fields in each region, continuity of tangential magnetic field requires

$$\hat{z} \times (\vec{H}_{\perp}^i + \vec{H}_{\perp}^r) \Big|_{z=0} = \hat{z} \times \vec{H}_{\perp}^t \Big|_{z=0} \quad (2.47)$$

Using the constraint on the x-component of the various wave numbers and the boundary condition on the magnetic field leads to

$$\frac{k_z^i E_0^i}{k_1 \eta_1} + \frac{k_z^r E_0^r}{k_1 \eta_1} = \frac{k_z^t E_0^t}{k_2 \eta_2} \quad (2.48)$$

rearranging terms in this equation gives

$$1 + \frac{k_z^r E_0^r}{k_z^i E_0^i} = \frac{\eta_1 k_z^t k_1 E_0^t}{\eta_2 k_2 k_z^i E_0^i}. \quad (2.49)$$

The addition of (2.46) and (2.49), using  $k_z^r = -k_z^i$ , gives

$$\begin{aligned} \frac{E_0^t}{E_0^i} &= \frac{2Z_2^{\perp}}{Z_2^{\perp} + Z_1^{\perp}} \\ &= T^{\perp} \end{aligned} \quad (2.50)$$

where, using (2.17) and (2.43),

$$Z_1^{\perp} = \frac{k_1 \eta_1}{k_z^i} = \eta_1 / \cos \theta_{in} \quad (2.51a)$$

$$Z_2^{\perp} = \frac{k_2 \eta_2}{k_z^t} = k_2 \eta_2 \left( k_2^2 - k_1^2 \sin^2 \theta_{in} \right)^{-1/2}. \quad (2.51b)$$

Here  $T^{\perp}$  is a frequency-dependent transmission coefficient that relates the tangential components of the incident and transmitted fields for perpendicular polarization. This will be referred to throughout this thesis as the interfacial transmission coefficient.

Plugging the interfacial transmission coefficient back into (2.46) gives

$$T^\perp = 1 + \frac{E_0^r}{E_0^i} = 1 + R^\perp \quad (2.52)$$

or

$$R^\perp = \frac{E_0^r}{E_0^i} = \frac{Z_2^\perp - Z_1^\perp}{Z_2^\perp + Z_1^\perp}. \quad (2.53)$$

Here  $R^\perp$  is a frequency-dependent reflection coefficient that relates the tangential components of the incident and reflected fields for perpendicular polarization. This will be referred to throughout this thesis as the interfacial reflection coefficient.

### 2.3 Wave matrix method

The wave matrix method is used to obtain the frequency domain reflection coefficient of a multilayered medium in terms of the interfacial reflection and transmission coefficients derived in Section 2.2. Consider a plane wave with amplitude  $c_1$  incident from the left and another plane wave with amplitude  $b_2$  incident from the right on the planar interface shown in Figure 2.4. In region 1 there will be a wave which is partially made up of a reflected wave and partially made up of a wave transmitted past the discontinuity from the right, propagating in the negative  $z$  direction. In region 2 there will be a wave which is partially made up of a reflected wave and partially made up of a wave transmitted past the discontinuity from the left, propagating in the positive  $z$  direction. Letting the amplitude of the wave propagating in the negative  $z$  direction and the amplitude of the positive  $z$  propagating wave be given by  $b_1$  and  $c_2$ , respectively, these waves can be written as

$$\begin{aligned} b_1 &= R_1^+ c_1 + T_1^- b_2 \\ c_2 &= T_1^+ c_1 + R_1^- b_2 \end{aligned} \quad (2.54a)$$

or

$$\begin{aligned} b_1 &= \left( T_1^- - \frac{R_1^+ R_1^-}{T_1^+} \right) b_2 + \frac{R_1^+}{T_1^+} c_2 \\ c_1 &= \frac{1}{T_1^+} (c_2 - R_1^- b_2) \end{aligned} \quad (2.55a)$$

where  $R_1^+$  and  $R_1^-$  are the interfacial reflection coefficients for waves incident from the left and right, respectively. The terms  $T_1^+$  and  $T_1^-$  are interfacial transmission coefficients. Equations (2.55) can be written in matrix form as

$$\begin{bmatrix} c_1 \\ b_1 \end{bmatrix} = \frac{1}{T_1^+} \begin{bmatrix} 1 & R_1^+ \\ -R_1^- & T_1^+ T_1^- - R_1^+ R_1^- \end{bmatrix} \begin{bmatrix} c_2 \\ b_2 \end{bmatrix} = \begin{bmatrix} A_{11} & A_{21} \\ A_{12} & A_{22} \end{bmatrix} \begin{bmatrix} c_2 \\ b_2 \end{bmatrix} \quad (2.56)$$

The matrix  $[A]$  is termed the wave-transmission chain matrix because it relates the amplitudes of the waves on one side of a discontinuity interface to the amplitudes of the waves on the other side. For the case of planar discontinuities, the elements of the wave-transmission matrix are given as

$$\begin{aligned} A_{11} &= \frac{1}{T_1^+} \\ A_{21} &= \frac{R_1^+}{T_1^+} \\ A_{12} &= \frac{-R_1^-}{T_1^+} = \frac{R_1^+}{T_1^+} \\ A_{22} &= \frac{T_1^+ T_1^- - R_1^+ R_1^-}{T_1^+} = \frac{(1 - R_1^+)(1 + R_1^+) + (R_1^+)^2}{T_1^+} = \frac{1}{T_1^+} \end{aligned}$$

since  $R_1^+ = -R_1^-$  using (2.36) and (2.53) for parallel and perpendicular polarizations. Here  $T_1^+ = 1 + R_1^+$  and  $T_1^- = 1 + R_1^-$  are the interfacial transmission coefficients for transmission from the left and right, respectively, and are given by (2.34) and (2.50) for parallel and perpendicular polarizations. Since only the interfacial reflection and

transmission coefficients for incidence from the left onto the planar interface appear, the simpler notation of  $R_1 = R_1^+$  and  $T_1 = T_1^+$  will be utilized. Equation (2.56) can thus be written as

$$\begin{bmatrix} c_1 \\ b_1 \end{bmatrix} = \frac{1}{T_1} \begin{bmatrix} 1 & R_1 \\ R_1 & 1 \end{bmatrix} \begin{bmatrix} c_2 \\ b_2 \end{bmatrix} \quad (2.57)$$

Before considering a cascade connection of  $n$  layers, the wave-transmission matrix for a *length of unbounded space* needs consideration. Consider a wave  $c_1 e^{-jk_z z}$  which propagates in the positive  $z$  direction, and another wave  $b_1 e^{jk_z z}$  propagating in the negative  $z$  direction. At  $z = 0$ , the amplitudes of the waves are  $c_1$  and  $b_1$ , respectively. At another terminal plane,  $z = z_1$ , the complex wave amplitudes are given by  $c_2 = c_1 e^{-jk_z z_1}$  and  $b_2 = b_1 e^{jk_z z_1}$ . The wave amplitudes at  $z = 0$  can thus be related to those at  $z = z_1$  by

$$c_1 = c_2 e^{jk_z z_1} \quad (2.58)$$

$$b_1 = b_2 e^{-jk_z z_1} \quad (2.59)$$

These equations are written in matrix form as

$$\begin{bmatrix} c_1 \\ b_1 \end{bmatrix} = \begin{bmatrix} e^{jk_z z_1} & 0 \\ 0 & e^{-jk_z z_1} \end{bmatrix} \begin{bmatrix} c_2 \\ b_2 \end{bmatrix} \quad (2.60)$$

The diagonal matrix

$$\begin{bmatrix} e^{jk_z z_1} & 0 \\ 0 & e^{-jk_z z_1} \end{bmatrix} \quad (2.61)$$

relates the amplitudes of the waves propagating in the positive  $z$  and negative  $z$  directions at one plane to those of the same waves at another terminal plane an electrical distance  $k_z z_1$  away. With this, a cascade connection of  $n$  material regions can be examined.

Consider the  $n$ -material stack shown in Figure 2.5, where each material layer is of thickness  $\Delta_i$  and the  $i^{th}$  interface is located to the left of the  $i^{th}$  layer. Each material layer has parameters  $(\mu_i, \epsilon_i, \sigma_i)$  which may differ between individual layers, or remain the same, without invalidating the results contained here. Using the developments of (2.56) through (2.61), the complex wave amplitudes to the left of the  $i^{th}$  interface can be related to the amplitudes to the left of the  $(i + 1)^{th}$  interface, with propagation occurring in region  $i$ , as

$$\begin{bmatrix} c_i \\ b_i \end{bmatrix} = \frac{1}{T_i} \begin{bmatrix} 1 & R_i \\ R_i & 1 \end{bmatrix} \begin{bmatrix} e^{jk_{z,i}\Delta_i} & 0 \\ 0 & e^{-jk_{z,i}\Delta_i} \end{bmatrix} \begin{bmatrix} c_{i+1} \\ b_{i+1} \end{bmatrix}. \quad (2.62)$$

Using this, the complex wave amplitudes at the first interface to the  $n$  layered material structure can be written in terms of the amplitudes at the second interface as

$$\begin{bmatrix} c_1 \\ b_1 \end{bmatrix} = \frac{1}{T_1} \begin{bmatrix} e^{jk_{z,1}\Delta_1} & R_1 e^{-jk_{z,1}\Delta_1} \\ R_1 e^{jk_{z,1}\Delta_1} & e^{-jk_{z,1}\Delta_1} \end{bmatrix} \begin{bmatrix} c_2 \\ b_2 \end{bmatrix} \quad (2.63)$$

Thus, if  $c_2$  and  $b_2$  are now written in terms of  $c_3$  and  $b_3$  using (2.62), and  $c_3$  and  $b_3$  in terms of  $c_4$  and  $b_4$ , and so on, the amplitudes  $c_1$  and  $b_1$  can be found as a matrix product of  $n$  matrices which characterize propagation through each layer of material. The complex wave amplitudes at the input to the first layer are thus given in terms of the amplitudes at the output from region  $n$  as

$$\begin{bmatrix} c_1 \\ b_1 \end{bmatrix} = \prod_{i=1}^n \frac{1}{T_i} \begin{bmatrix} e^{jk_{z,i}\Delta_i} & R_i e^{-jk_{z,i}\Delta_i} \\ R_i e^{jk_{z,i}\Delta_i} & e^{-jk_{z,i}\Delta_i} \end{bmatrix} \begin{bmatrix} c_{n+1} \\ b_{n+1} \end{bmatrix} \quad (2.64)$$

The frequency domain reflection coefficient at the input to the layered material is found using (2.64) as  $\Gamma = b_1/c_1$ . The interfacial reflection coefficients, which are needed to compute  $\Gamma$ , are given for parallel and perpendicular polarization by (2.36)

and (2.53) as

$$R_i = \frac{Z_i - Z_{i-1}}{Z_i + Z_{i-1}} \quad (2.65)$$

and the interfacial transmission coefficients from (2.34) and (2.50) as

$$T_i = 1 + R_i. \quad (2.66)$$

Here, the wave impedances used to determine the interfacial reflection and transmission coefficients for each polarization are given for region 0 by

$$Z_0 = \begin{cases} \eta_0 \cos \theta_{in} & \text{parallel polarization} \\ \eta_0 (\cos \theta_{in})^{-1} & \text{perpendicular polarization} \end{cases} \quad (2.67)$$

and for the  $i^{th}$  region as

$$Z_i = \begin{cases} \frac{\eta_i}{k_i} (k_i^2 - k_0^2 \sin^2 \theta_{in})^{1/2} & \text{parallel polarization} \\ \eta_i k_i (k_i^2 - k_0^2 \sin^2 \theta_{in})^{-1/2} & \text{perpendicular polarization} \end{cases} \quad (2.68)$$

where  $\theta_{in}$  is the incidence angle for the wave impinging on the interface between region 0 and region 1.

### 2.3.1 Frequency domain reflection coefficient for two-layered geometries

The geometries which are rigorously considered in Chapters 3 and 5 are cases of two-layered geometries. For this reason, and to provide an example using the wave matrix method, the derivation of the frequency domain reflection coefficient for this specific geometry will be shown here.

Beginning with (2.64) and examining Figure 2.6, the forward and backward travelling waves at the  $z = 0$  interface can be found in terms of the fields at the output

from the second layer as

$$\begin{bmatrix} c_1 \\ b_1 \end{bmatrix} = \frac{1}{T_1 T_2} \begin{bmatrix} e^{jk_{z,1}\Delta_1} & R_1 e^{-jk_{z,1}\Delta_1} \\ R_1 e^{jk_{z,1}\Delta_1} & e^{-jk_{z,1}\Delta_1} \end{bmatrix} \begin{bmatrix} e^{jk_{z,2}\Delta_2} & R_2 e^{-jk_{z,2}\Delta_2} \\ R_2 e^{jk_{z,2}\Delta_2} & e^{-jk_{z,2}\Delta_2} \end{bmatrix} \begin{bmatrix} c_3 \\ b_3 \end{bmatrix} \quad (2.69)$$

where dependance on the angular frequency,  $\omega$ , is understood for the wave numbers,  $k_i$ , and the interfacial reflection coefficients,  $R_i$ . Defining the propagation factors  $P_1 = e^{-jk_{z,1}\Delta_1}$  and  $P_2 = e^{-jk_{z,2}\Delta_2}$  and carrying out the matrix multiplication gives

$$\begin{bmatrix} c_1 \\ b_1 \end{bmatrix} = \frac{1}{T_1 T_2 P_1 P_2} \begin{bmatrix} 1 + R_1 R_2 P_1^2 & R_2 P_2^2 + R_1 P_1^2 P_2^2 \\ R_1 + R_2 P_1^2 & R_1 R_2 P_2^2 + P_1^2 P_2^2 \end{bmatrix} \begin{bmatrix} c_3 \\ b_3 \end{bmatrix} \quad (2.70)$$

The frequency domain reflection coefficient can be found as the ratio of backward travelling to forward travelling waves at the  $z = 0$  interface, or

$$\Gamma(\omega) = \frac{b_1}{c_1} = \frac{(R_1(\omega) + R_2(\omega)P_1^2(\omega))c_3 + (R_1(\omega)R_2(\omega)P_2^2(\omega) + P_1^2(\omega)P_2^2(\omega))b_3}{(1 + R_1(\omega)R_2(\omega)P_1^2(\omega))c_3 + (R_2(\omega)P_2^2(\omega) + R_1(\omega)P_1^2(\omega)P_2^2(\omega))b_3} \quad (2.71)$$

dividing through by the complex amplitude of the forward travelling wave at the third interface and using  $R_3 = b_3/c_3$ , gives the frequency domain reflection coefficient from the two-layered geometry as

$$\Gamma(\omega) = \frac{b_1}{c_1} = \frac{R_1(\omega) + R_2(\omega)P_1^2(\omega) + (R_1(\omega)R_2(\omega)P_2^2(\omega) + P_1^2(\omega)P_2^2(\omega))R_3(\omega)}{1 + R_1(\omega)R_2(\omega)P_1^2(\omega) + (R_2(\omega)P_2^2(\omega) + R_1(\omega)P_1^2(\omega)P_2^2(\omega))R_3(\omega)} \quad (2.72)$$

For the special case of a conductor backed geometry, where the interfacial reflection coefficient  $R_3 = -1$ , the frequency domain reflection coefficient is given by

$$\Gamma(\omega) = \frac{R_1(\omega) + R_2(\omega)P_1^2(\omega) - P_1^2(\omega)P_2^2(\omega) - R_1(\omega)R_2(\omega)P_2^2(\omega)}{1 + R_1(\omega)R_2(\omega)P_1^2(\omega) - R_1(\omega)P_1^2(\omega)P_2^2(\omega) - R_2(\omega)P_2^2(\omega)}. \quad (2.73)$$

Since the frequency domain reflection coefficient,  $\Gamma(\omega)$  exists, a Laplace domain rep-



resentation also exists. This quantity is given by  $\Gamma(s) = \Gamma(\omega) \Big|_{\omega = \frac{s}{j}}$ .

## 2.4 Time domain reflection coefficient

To define the time domain reflection coefficient, begin by considering the response due to a finite duration input waveform. Letting the input waveform be given by  $g(t)$ , where  $G(s) = \mathcal{L}\{g(t)\}$ , the frequency domain response is given by

$$F(s) = G(s)\Gamma(s) \quad (2.74)$$

where  $\Gamma(s)$  is the frequency domain reflection coefficient found in Section 2.3. The time domain response of the system is thus given as

$$f(t) = \mathcal{L}^{-1}\{F(s)\} = \mathcal{L}^{-1}\{G(s)\Gamma(s)\}. \quad (2.75)$$

Although this is the temporal response of the system, the response cannot be written as  $g(t) * \mathcal{L}^{-1}\{\Gamma(s)\}$ , because the inverse Laplace transform of  $\Gamma(s)$  either may not exist, or may be difficult to compute. This is because the frequency domain reflection coefficient,  $\Gamma(s)$ , does not go to zero uniformly on all of the infinite contours used in evaluating the Laplace inversion integral. However, by neglecting the contributions from these infinite contours, since  $G(s)$  does go to zero on them, a new quantity,  $\tilde{\Gamma}(s)$  is defined. This quantity is identical to  $\Gamma(s)$ , except for its behavior as  $|s| \rightarrow \infty$ . The quantity  $\tilde{\Gamma}(s)$  will satisfy

$$\mathcal{L}^{-1}\{G(s)\tilde{\Gamma}(s)\} = \mathcal{L}^{-1}\{G(s)\Gamma(s)\} = f(t), \quad (2.76)$$

since  $G(s)$  goes to zero on the infinite contours. With the infinite contour contributions neglected, the inverse transform exists, and by the convolution theorem,

$$f(t) = g(t) * \Gamma(t) \quad (2.77)$$

where  $\Gamma(t) = \mathcal{L}^{-1}\{\tilde{\Gamma}(s)\}$  is defined as the time domain reflection coefficient. Note that this time domain reflection coefficient, when convolved with a finite duration incident waveform, gives the reflected field.

Exploration into the form of the time domain reflection coefficient is given for specific geometries in Chapters 3 through 5, and for the  $n$ -layer case in Chapter 6.

#### 2.4.1 Propagation through lossy media - wave velocity and transit time

To determine the start and end of the various time periods, a complex-analysis based approach is taken in Chapters 3 through 6. To relate the distinction of the various time periods to physical events, the propagation of a plane wave through a dispersive medium is considered. To do this, consider the solution for the total field of a plane wave propagating in a homogeneous region of permittivity,  $\epsilon$ , permeability,  $\mu$ , and conductivity,  $\sigma$ , reflected from a perfect conductor.

In a source free region, the electric and magnetic fields,  $\vec{E}$  and  $\vec{H}$ , satisfy identical wave equations given in the time domain by

$$\frac{\partial^2 E(z, t)}{\partial z^2} - \mu\sigma \frac{\partial E(z, t)}{\partial t} - \mu\epsilon \frac{\partial^2 E(z, t)}{\partial t^2} = 0 \quad (2.78)$$

and

$$\frac{\partial^2 H(z, t)}{\partial z^2} - \mu\sigma \frac{\partial H(z, t)}{\partial t} - \mu\epsilon \frac{\partial^2 H(z, t)}{\partial t^2} = 0 \quad (2.79)$$

Here it is assumed that the plane of field invariance is the  $xy$ -plane, with generalization to any planar surface obtained through a simple rotation of the coordinate axes. Thus, propagation of the plane-wave occurs in the  $\pm\hat{z}$ -direction.

Begin by considering the lossless ( $\sigma = 0$ ) case, assuming the region  $z < 0$  contains a perfect conductor. Boundary conditions at the conductor require the tangential component of the electric field to vanish. Since the electric field is orthogonal to  $\hat{z}$ , requiring

$$\left. \frac{\partial H(z, t)}{\partial z} \right|_{z=0} = 0$$

gives  $\vec{E}(0, t) = 0$  and thus satisfies boundary conditions. The solution to (2.79), subject to the above boundary condition, and assuming  $H(0, t) = H_0 f(t)$ , is given by

$$H(z, t) = \frac{H_0}{2} f\left(t - \frac{z}{v}\right) + \frac{H_0}{2} f\left(t + \frac{z}{v}\right), \quad (2.80)$$

where  $v = 1/(\mu\epsilon)^{1/2}$ . With the solution for the magnetic field,  $H$ , the electric field is obtained as

$$E(z, t) = \frac{v\mu H_0}{2} f\left(t - \frac{z}{v}\right) - \frac{v\mu H_0}{2} f\left(t + \frac{z}{v}\right), \quad (2.81)$$

Examining this solution for the electric and magnetic fields, the term  $f(t + z/v)$  can be interpreted as a wave field disturbance propagating in the  $-z$ -direction with a velocity  $v$ . Similarly, the term  $f(t - z/v)$  can be interpreted as a wave field disturbance propagating in the  $+z$ -direction with the same velocity  $v$ .

Now consider the case of propagation through a lossy medium, again assuming the region  $z < 0$  contains a perfect conductor. The solution to (2.79), with the boundary condition of vanishing tangential electric field at the conductor, assuming  $H(0, t) = H_0 f(t)$ , is given in [17] by

$$H(z, t) = \frac{H_0}{2} e^{-\frac{\sigma}{2\epsilon v} z} f\left(t - \frac{z}{v}\right) + \frac{H_0}{2} e^{\frac{\sigma}{2\epsilon v} z} f\left(t + \frac{z}{v}\right) - \frac{z\sigma^2 H_0}{8\epsilon v} e^{-\frac{\sigma}{2\epsilon} t} \int_{t-z/v}^{t+z/v} f(u) e^{\frac{\sigma}{2\epsilon} u} \frac{J_1\left(\frac{\sigma}{2\epsilon v} \sqrt{z^2 - (t-u)^2 v^2}\right)}{\frac{\sigma}{2\epsilon v} \sqrt{z^2 - (t-u)^2 v^2}} du, \quad (2.82)$$

where  $v = 1/(\mu\epsilon)^{1/2}$ , as in the lossless case. The first two terms of this solution

are similar to the terms in the lossless case, modified by an exponential damping factor. This term gives the necessary decay associated with propagation through a dissipative material. The interpretation of these two terms as propagating wave field disturbances remains valid, with propagation velocity,  $v$ . The remaining term, which only appears in the case of a lossy medium, results in an extension of the disturbance through the medium, due to currents induced by the passing wavefront. This response will be a remnant left behind as the wavefront passes.

The important result for defining the time periods of the transient response from a layered material is that the leading edge of the wavefront propagates with wave velocity  $v$ , which is again defined by

$$v = \frac{1}{\sqrt{\mu\epsilon}} \quad (2.83)$$

where  $\mu = \mu_r \mu_0$  and  $\epsilon = \epsilon_r \epsilon_0$  are the frequency independent permeability and permittivity of the material. Note that in free space, this wave velocity is given by the speed of light,  $c$ .

With the wave velocity of a plane wave propagating in a lossy medium known, the two-way transit time in a layer of material can now be considered. It is important to note that this transit time is not just the propagation time for the wave to travel through the slab. The timing between the initially-reflected wave, which sets the time-reference of the transient response, and the subsequent response due to various reflections inside the material layer can only be properly described by considering the field over an observation plane.[17] Consider the observation plane designated  $P$ - $P$  in Figure 2.7. This plane intersects the first interface at the first “exit point” of the wave that is initially transmitted into the layer. To arrive at this plane, the

initially-reflected wave takes the path  $B$ , arriving at the observation plane at a time

$$\frac{D \sin \theta_{in}}{v_0} \quad (2.84)$$

after the initial reflection. Here  $v_0$  is the wave velocity in region 0. To arrive at this same plane, the wave that penetrates the surface takes the path  $A$ , arriving back at the reference plane at a time

$$\frac{2\Delta_1}{v_1 \cos \theta_t}, \quad (2.85)$$

where  $\theta_t$  is the transmission angle into region 1, and  $v_1$  is the wave velocity in the medium. Noting that  $D = 2\Delta_1 \tan \theta_t$ , the time difference between these two waves arriving at the reference plane is given by

$$T_1 = \frac{2\Delta_1}{v_1 \cos \theta_t} \left[ 1 - \frac{\sin \theta_t \sin \theta_{in}}{v_0/v_1} \right]. \quad (2.86)$$

Utilizing Snell's law of refraction, which gives

$$\frac{v_0}{v_1} = \frac{\sin \theta_{in}}{\sin \theta_t} \quad (2.87)$$

the two-way transit time of the material layer is found to be

$$T_1 = 2 \frac{\Delta_1 \cos \theta_t}{v_1}. \quad (2.88)$$

This quantity appears in the complex-analysis based approach taken in Chapters 3 through 6, and is found to determine the start and end of the various time periods.

#### 2.4.2 Simulation based comparison of NMS to IFFT

For purposes of comparing the natural mode series (NMS) to the inverse fast-Fourier transform (IFFT), the reflection coefficients of several layered arrangements are com-

puted. Consider the two layer material stack shown in Figure 2.8, with layer thicknesses of 25 and 24 millimeters and material parameters of  $(\mu_0, 4.8\epsilon_0)$  and  $(\mu_0, 2.5\epsilon_0)$ . Using the wave matrix method detailed in Section 2.3, the reflection coefficient can be found and an inverse fast-Fourier transform can be performed. This procedure gives the time domain reflection coefficient, however it gives no physical insight into the source of the response. To gain this insight, a natural mode series representation is found using the poles of the frequency domain reflection coefficient. These poles are found using the secant method, with initial guesses generated using an E-pulse program on the time domain reflection coefficient found by an IFFT. Figure 2.9 is a comparison of the IFFT of the reflection coefficient with the resulting natural mode series representation for the air-backed case found using (3.16); here the first 7 modes are used to construct the natural mode series, as listed in Table 2.1. For the conductor-backed case shown in Figure 2.10, a comparison of the IFFT to the NMS for the conductor-backed case, using the 8 modes listed in Table 2.2 to construct the natural mode series is shown in Figure 2.11.

Note that, in each case, there is no difference between the IFFT and the NMS results after the reflection from the second interface has returned to the observation plane. This implies that the natural mode series is a valid representation of the temporal response for times after the reflection from the first material-material interface is seen at the observation plane. This is an interesting result, since the late time is generally taken as starting after the wave has completely penetrated the entire stack of materials and has been reflected from the last interface. A rigorous, complex-analysis-based approach is given in Chapter 6 to evaluate the contributions of branch cuts to the time domain reflection coefficient, and to accurately determine where the late-time period begins. In this chapter the reflection coefficient is decomposed into various components which are used to validate the natural mode series representation for both the  $n$ -layer material stack in the late time, and portions of the early time.

Mode	Pole Amplitude		Natural Mode Amplitude	
	Real Part	Imaginary Part	Real Part	Imaginary Part
6	$-0.41045 \times 10^{10}$	$0.90877 \times 10^{11}$	$0.35161 \times 10^{10}$	$-0.23713 \times 10^9$
5	$-0.40353 \times 10^{10}$	$0.81846 \times 10^{11}$	$0.36648 \times 10^{10}$	$0.24961 \times 10^9$
4	$-0.38304 \times 10^{10}$	$0.70678 \times 10^{11}$	$0.40979 \times 10^{10}$	$-0.16679 \times 10^9$
3	$-0.42604 \times 10^{10}$	$0.61114 \times 10^{11}$	$0.31807 \times 10^{10}$	$0.74073 \times 10^8$
2	$-0.41727 \times 10^{10}$	$0.40177 \times 10^{11}$	$0.33693 \times 10^{10}$	$-0.20099 \times 10^9$
1	$-0.39591 \times 10^{10}$	$0.31051 \times 10^{11}$	$0.38275 \times 10^{10}$	$0.24041 \times 10^9$
0	$-0.3889 \times 10^{10}$	$0.19793 \times 10^{11}$	$0.39755 \times 10^{10}$	$-0.21095 \times 10^9$

Table 2.1. Natural mode frequencies and coupling coefficients for the problem of Figure 2.8

Mode	Pole Amplitude		Natural Mode Amplitude	
	Real Part	Imaginary Part	Real Part	Imaginary Part
7	$-0.14262 \times 10^{10}$	$0.96877 \times 10^{11}$	$0.33152 \times 10^{10}$	$-0.14396 \times 10^9$
6	$-0.18016 \times 10^{10}$	$0.8627 \times 10^{11}$	$0.42388 \times 10^{10}$	$0.23251 \times 10^8$
5	$-0.17131 \times 10^{10}$	$0.66496 \times 10^{11}$	$0.4025 \times 10^{10}$	$-0.16103 \times 10^9$
4	$-0.16018 \times 10^{10}$	$0.553 \times 10^{11}$	$0.37517 \times 10^{10}$	$0.20664 \times 10^9$
3	$-0.14772 \times 10^{10}$	$0.46196 \times 10^{11}$	$0.34423 \times 10^{10}$	$-0.18384 \times 10^9$
2	$-0.17866 \times 10^{10}$	$0.35327 \times 10^{11}$	$0.4203 \times 10^{10}$	$0.73224 \times 10^8$
1	$-0.13724 \times 10^{10}$	$0.2531 \times 10^{11}$	$0.31817 \times 10^{10}$	$0.32635 \times 10^8$
0	$-0.17567 \times 10^{10}$	$0.15598 \times 10^{11}$	$0.41304 \times 10^{10}$	$-0.12013 \times 10^9$

Table 2.2. Natural mode frequencies and coupling coefficients for the problem of Figure 2.10



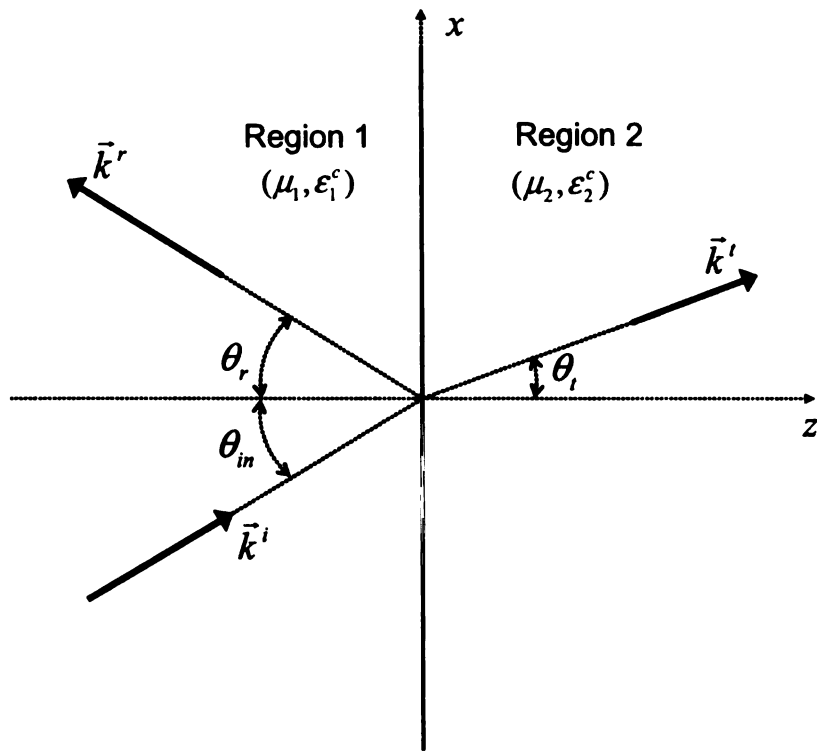


Figure 2.1. A discontinuity interface between two material regions

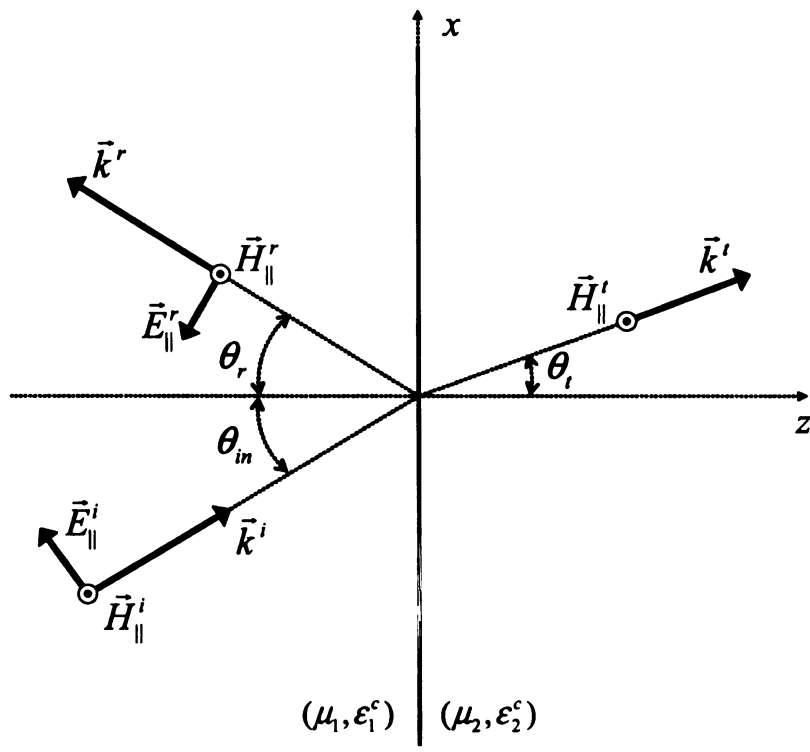


Figure 2.2. Fields at an interface between two materials for parallel polarization

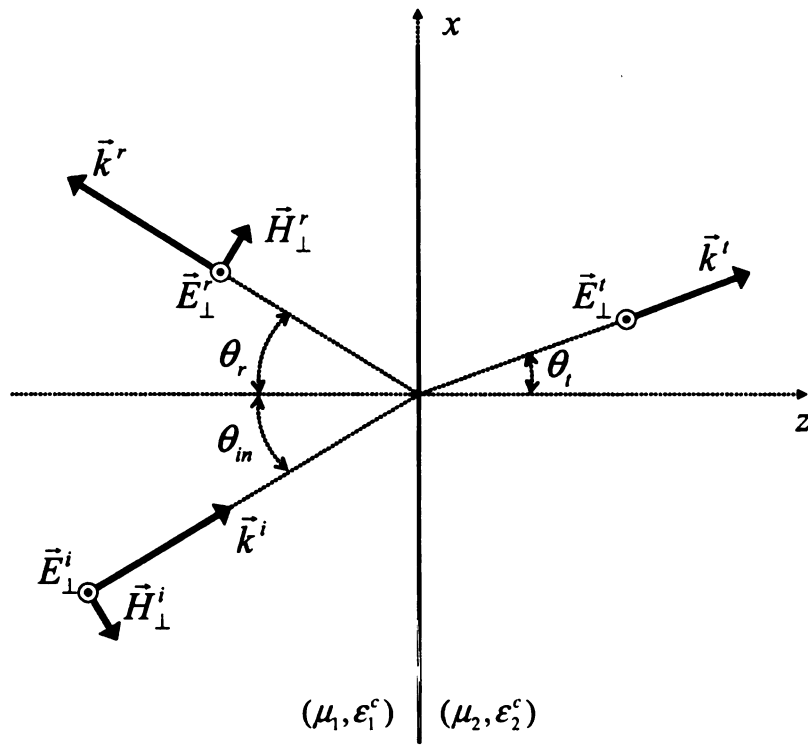


Figure 2.3. Fields at an interface between two materials for perpendicular polarization

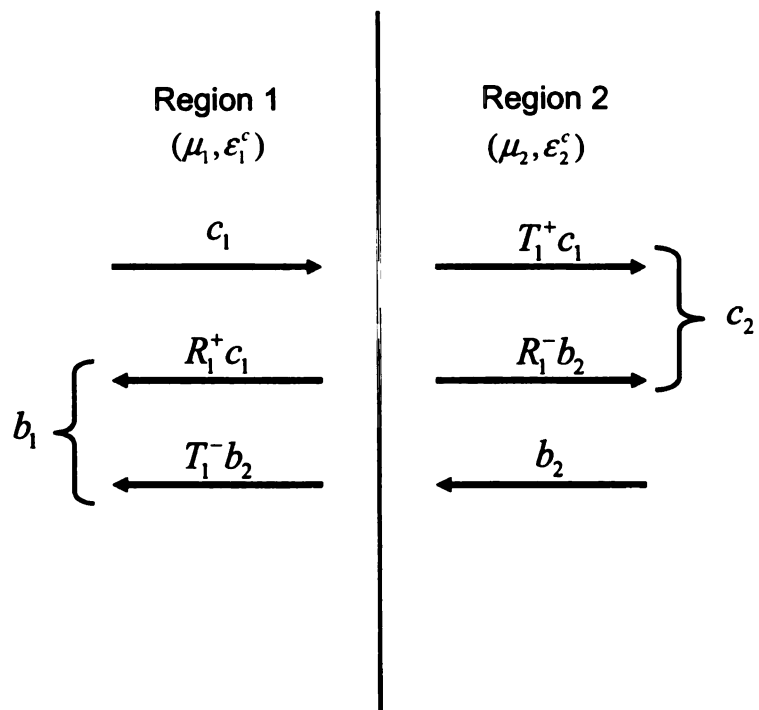


Figure 2.4. Fields at a discontinuity for incidence from each direction

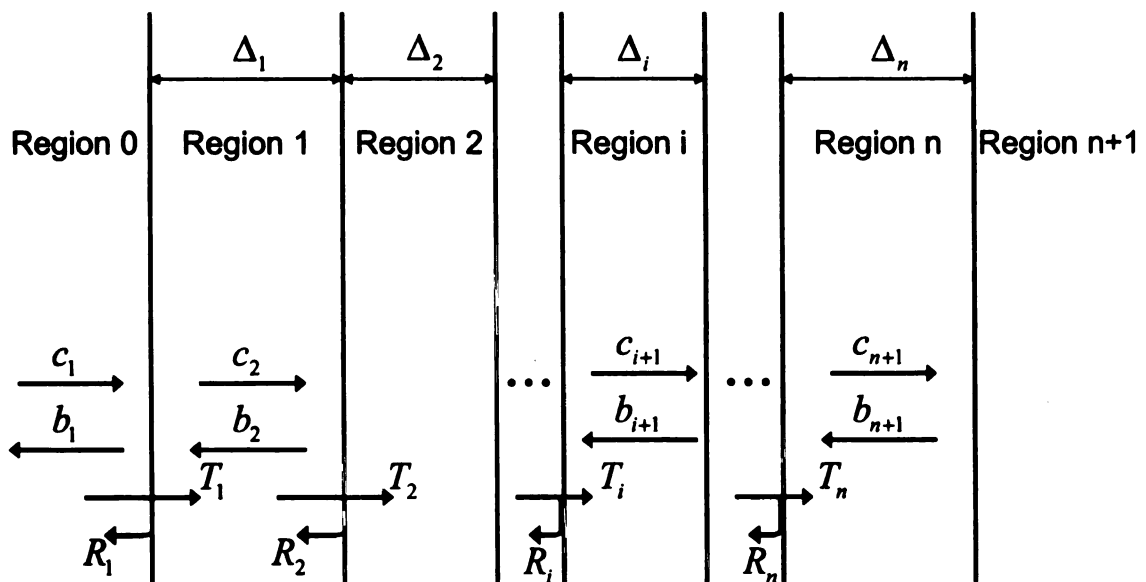


Figure 2.5. An n-material cascade of planar layers

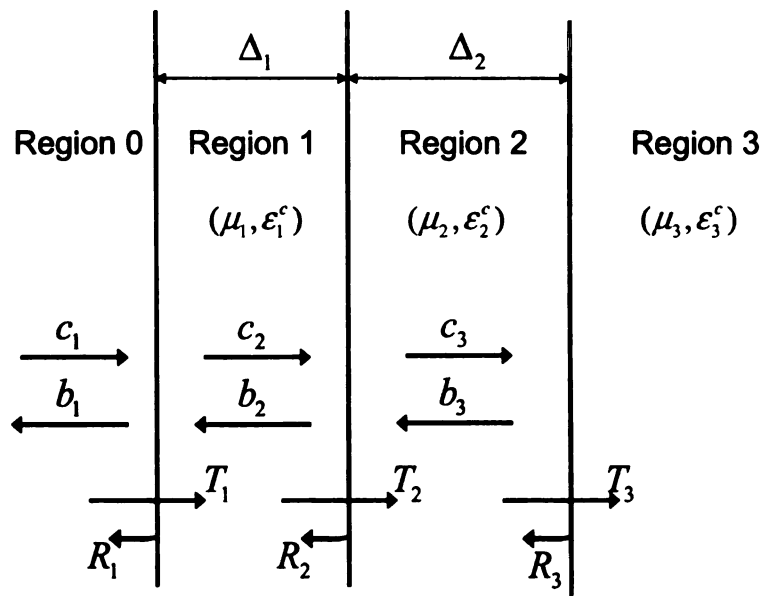


Figure 2.6. Geometry for a two layered material stack

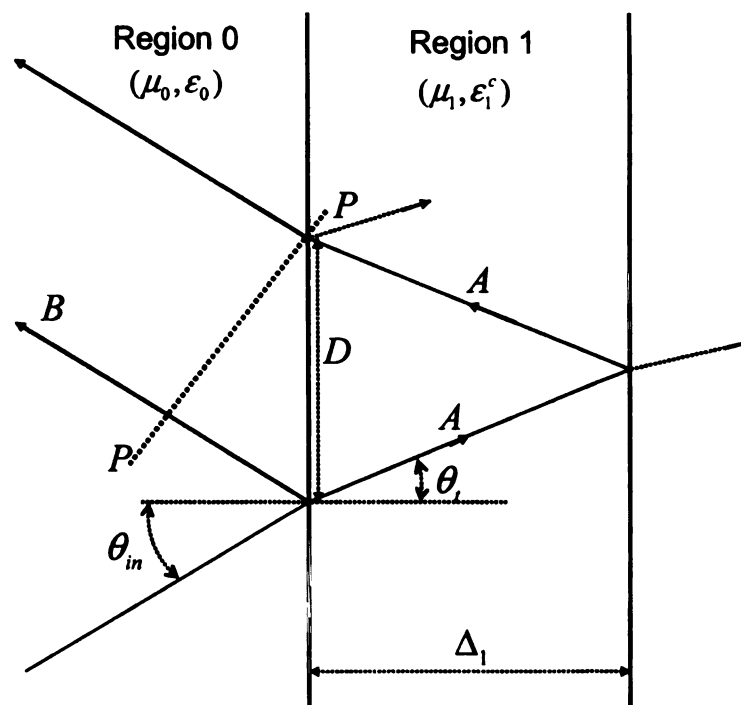


Figure 2.7. Timing diagram for determining transit time in a lossy material layer

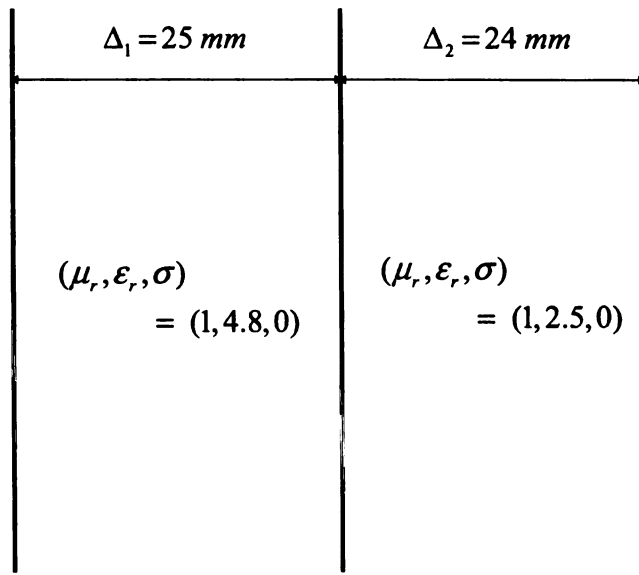


Figure 2.8. A two-layered, air-backed geometry



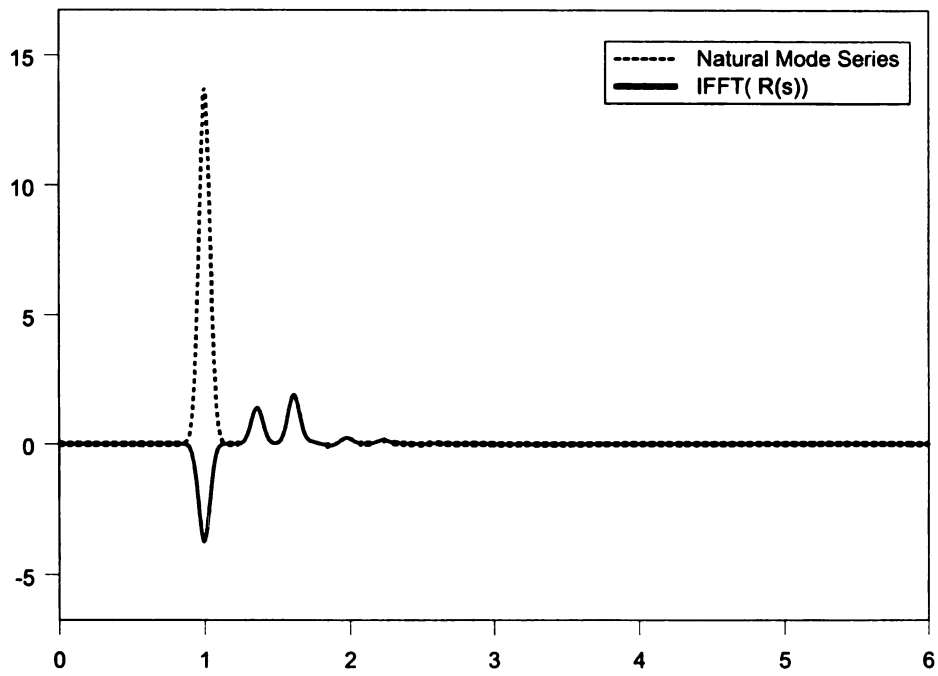


Figure 2.9. Time domain reflection coefficient for a two-layered, air-backed geometry

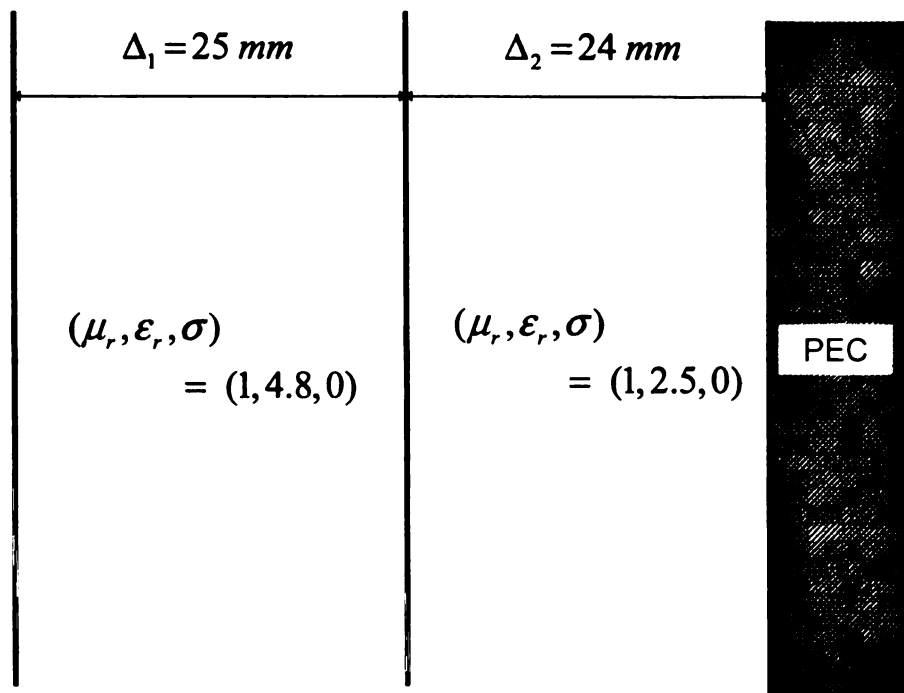


Figure 2.10. A two-layered, PEC-backed geometry

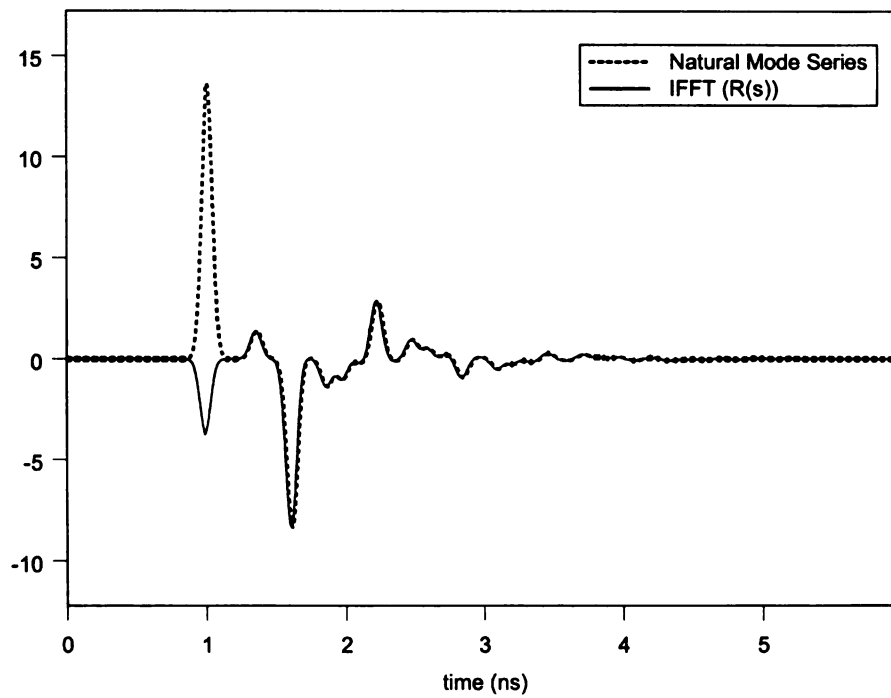


Figure 2.11. Time domain reflection coefficient for a two-layered, PEC-backed geometry

## CHAPTER 3

### AIR-BACKED LOSSY LAYER IN THE PRESENCE OF A CONDUCTING SCREEN

As a first step towards the development of a procedure for multiply layered materials, an air-backed lossy layer in the presence of a conducting screen is considered. The geometry is shown in Figure 3.1. This builds upon the work completed in [13], where the transient reflection from an air-backed lossy layer was rigorously developed. As shown in Chapter 2, the frequency domain reflection coefficient for a two-layered geometry backed by a perfect electric conductor is given using the wave matrix method as

$$\Gamma(\omega) = \frac{R_1(\omega) + R_2(\omega)P_1^2(\omega) - P_1^2(\omega)P_2^2(\omega) - R_1(\omega)R_2(\omega)P_2^2(\omega)}{1 + R_1(\omega)R_2(\omega)P_1^2(\omega) - R_1(\omega)P_1^2(\omega)P_2^2(\omega) - R_2(\omega)P_2^2(\omega)}, \quad (3.1)$$

with interfacial reflection coefficients

$$R_1(\omega) = \frac{Z_1(\omega) - Z_0}{Z_1(\omega) + Z_0}, \quad (3.2a)$$

$$R_2(\omega) = \frac{Z_2(\omega) - Z_1(\omega)}{Z_2(\omega) + Z_1(\omega)}, \quad (3.2b)$$

where  $Z_1(\omega)$  and  $Z_2(\omega)$  are the wave impedances in the material layers given for parallel (TM) and perpendicular (TE) polarizations, respectively, by

$$Z_i^{\parallel}(\omega) = \frac{k_{z,i}(\omega)\eta_i(\omega)}{k_i(\omega)} \quad (3.3a)$$

$$Z_i^{\perp}(\omega) = \frac{k_i(\omega)\eta_i(\omega)}{k_{z,i}(\omega)} \quad (3.3b)$$

where  $\eta_i(\omega) = \sqrt{\mu_i/\epsilon_i^c}$  is the frequency dependent intrinsic impedance in region  $i$ .  $Z_0$  is the wave impedance in free space, which takes on the same forms as (3.3), but with

frequency independent intrinsic impedance,  $\eta_0$ .  $P_1(\omega)$  and  $P_2(\omega)$  are propagation factors given by

$$P_1(\omega) = e^{-jk_{z,1}d} \quad (3.4a)$$

$$P_2(\omega) = e^{-jk_{z,2}h}. \quad (3.4b)$$

Examining the geometry of Figure 3.1, it can be seen that  $R_1(\omega) = -R_2(\omega)$ , so (3.1) can be rewritten in terms of just the first interfacial reflection coefficient,  $R_1(\omega)$ , and the propagation factors given in (3.4) as

$$\Gamma(\omega) = \frac{R_1(\omega) - R_1(\omega)P_1^2(\omega) - P_1^2(\omega)P_2^2(\omega) + R_1^2(\omega)P_2^2(\omega)}{1 - R_1^2(\omega)P_1^2(\omega) - R_1(\omega)P_1^2(\omega)P_2^2(\omega) + R_1(\omega)P_2^2(\omega)}. \quad (3.5)$$

Since  $k_i^2 = k_{x,i}^2 + k_{z,i}^2$  and  $k_{x,i} = k_{x,0} = k_0 \sin \theta_{in}$  to satisfy boundary conditions at all points on the planar surfaces, the wave impedances will take the forms

$$Z_i^{\parallel}(\omega) = \frac{\eta_i}{k_i} \sqrt{k_i^2 - k_0^2 \sin^2 \theta_{in}}, \quad Z_0^{\parallel} = \eta_0 \cos \theta_{in} \quad (3.6a)$$

$$Z_i^{\perp}(\omega) = \frac{k_i \eta_i}{\sqrt{k_i^2 - k_0^2 \sin^2 \theta_{in}}}, \quad Z_0^{\perp} = \frac{\eta_0}{\cos \theta_{in}} \quad (3.6b)$$

for parallel and perpendicular polarizations, respectively. For notational purposes, the propagation factors will be written in the form

$$P_i^2(\omega) = e^{-j\omega\tau_i(\omega)}, \quad (3.7)$$

where the expressions contained in the exponent are given by

$$\begin{aligned}
\omega\tau_1(\omega) &= 2k_{z,1}d \\
&= 2d\sqrt{k_1^2 - k_0^2 \sin^2 \theta_{in}} \\
&= \omega \frac{2d}{c} \sqrt{\frac{\epsilon_1^c}{\epsilon_0} - \sin^2 \theta_{in}}
\end{aligned} \tag{3.8}$$

$$\begin{aligned}
\omega\tau_2(\omega) &= 2k_{z,0}h \\
&= \omega \frac{2h}{c} \cos \theta_{in}.
\end{aligned} \tag{3.9}$$

Here, the complex permittivity is given by  $\epsilon_1^c(\omega) = \epsilon_{1r}\epsilon_0 + \sigma/j\omega$ , and a nonmagnetic material layer is assumed; i.e.,  $\mu_1 = \mu_0$ . To simplify notation, the quantity  $\bar{\epsilon}_1 = \epsilon_{1r} - \sin^2 \theta_{in}$  is defined, giving

$$\tau_1(\omega) = \frac{2d}{c} \sqrt{\bar{\epsilon}_1 + \frac{\sigma}{j\omega\epsilon_0}}. \tag{3.10}$$

### 3.1 Laplace domain representation

Since the frequency domain reflection coefficient,  $\Gamma(\omega)$ , exists, a Laplace domain representation also exists. This quantity is given by

$$\begin{aligned}
\Gamma(s) &= \Gamma(\omega) \Big|_{\omega=\frac{s}{j}} \\
&= \frac{R_1(s) - R_1(s)P_1^2(s) - P_1^2(s)P_2^2(s) + R_1^2(s)P_2^2(s)}{1 - R_1^2(s)P_1^2(s) - R_1(s)P_1^2(s)P_2^2(s) + R_1(s)P_2^2(s)} \\
&= \frac{R_1(s) - R_1(s)e^{-s\tau_1(s)} - e^{-s(\tau_1(s)+\tau_2(s))} + R_1^2(s)e^{-s\tau_2(s)}}{1 - R_1^2(s)e^{-s\tau_1(s)} - R_1(s)e^{-s(\tau_1(s)+\tau_2(s))} + R_1(s)e^{-s\tau_2(s)}}
\end{aligned} \tag{3.11}$$

with expressions appearing in the exponentials given by

$$\begin{aligned}
s\tau_1(s) &= j\omega\tau_1(\omega)\Big|_{\omega=\frac{s}{j}} \\
&= s\frac{2d}{c}\sqrt{\bar{\epsilon}_1 + \frac{\sigma}{s\epsilon_0}} \\
&= \frac{2d}{c}\sqrt{\bar{\epsilon}_1}\sqrt{s}\sqrt{s + \frac{\sigma}{\bar{\epsilon}_1\epsilon_0}} \\
&= \frac{2d}{c}\sqrt{\bar{\epsilon}_1}\sqrt{s}\sqrt{s - s_1}
\end{aligned} \tag{3.12}$$

$$\begin{aligned}
s\tau_2(s) &= j\omega\tau_2(\omega)\Big|_{\omega=\frac{s}{j}} \\
&= s\frac{2h}{c}\cos\theta_{in} = s\tau_2
\end{aligned} \tag{3.13}$$

where the quantity  $s_1 = -\sigma/\bar{\epsilon}_1\epsilon_0$  has been defined. The interfacial reflection coefficient for the first interface is given simply as  $R_1(s) = R_1(\omega)\Big|_{\omega=\frac{s}{j}}$ . The wave impedances, which are needed to compute the interfacial reflection coefficient by (3.2), are given for parallel polarization as

$$\begin{aligned}
Z_1^{\parallel}(s) &= Z_1^{\parallel}(\omega)\Big|_{\omega=\frac{s}{j}} \\
&= \frac{\eta_1}{k_1}\sqrt{k_1^2 - k_0^2\sin^2\theta_{in}} \\
&= \frac{k_0\eta_1}{k_1}\sqrt{\frac{\epsilon_1^c}{\epsilon_0} - \sin^2\theta_{in}} \\
&= \frac{\eta_0}{(\epsilon_1^c/\epsilon_0)}\sqrt{\bar{\epsilon}_1 + \frac{\sigma}{s\epsilon_0}} \\
&= \frac{\eta_0\sqrt{\bar{\epsilon}_1}\sqrt{s}\sqrt{s - s_1}}{s\epsilon_{1r} + \sigma/\epsilon_0}.
\end{aligned} \tag{3.14a}$$

and for perpendicular polarization by

$$\begin{aligned}
Z_1^\perp(s) &= Z_1^\perp(\omega) \Big|_{\omega=\frac{s}{j}} \\
&= \frac{k_1 \eta_1}{\sqrt{k_1^2 - k_0^2 \sin^2 \theta_{in}}} \\
&= \frac{k_1 \eta_1}{k_0 \sqrt{\frac{\epsilon_1^c}{\epsilon_0} - \sin^2 \theta_{in}}} \\
&= \frac{\eta_0}{\sqrt{\bar{\epsilon}_1 + \frac{\sigma}{s \epsilon_0}}} \\
&= \frac{\eta_0 s}{\sqrt{\bar{\epsilon}_1} \sqrt{s} \sqrt{s - s_1}}
\end{aligned} \tag{3.14b}$$

The interfacial reflection coefficient,  $R_1(s)$ , can thus be written for parallel and perpendicular polarizations using (3.2), as

$$R_1(s) = \begin{cases} \frac{\sqrt{\bar{\epsilon}_1} \sqrt{s} \sqrt{s - s_1} - (s \epsilon_{1r} + \frac{\sigma}{\epsilon_0}) \cos \theta_{in}}{\sqrt{\bar{\epsilon}_1} \sqrt{s} \sqrt{s - s_1} + (s \epsilon_{1r} + \frac{\sigma}{\epsilon_0}) \cos \theta_{in}} & \text{parallel polarization} \\ \frac{s \cos \theta_{in} - \sqrt{\bar{\epsilon}_1} \sqrt{s} \sqrt{s - s_1}}{s \cos \theta_{in} + \sqrt{\bar{\epsilon}_1} \sqrt{s} \sqrt{s - s_1}} & \text{perpendicular polarization} \end{cases} \tag{3.15}$$

### 3.2 The time domain reflection coefficient

Using the frequency domain reflection coefficient found in Section 3.1, the time domain reflection coefficient of the material stack,  $\Gamma(t)$ , which is defined through an inverse temporal transform, can be found. This time domain reflection coefficient, when convolved with a finite duration incident waveform, gives the reflected field in the time domain.

In order to use the extinction pulse technique, it must be shown that the time domain reflection coefficient can be represented in terms of a natural mode series, after a finite period called the early time. The time period during which the natural mode series is an accurate representation of the time domain reflection coefficient



is commonly referred to as the late time. Thus, in the late time, the time domain reflection coefficient should take the form:

$$\Gamma(t) = \sum_{n=1}^{\infty} A_n e^{s_n t} \quad (3.16)$$

where  $A_n$  is the amplitude coefficient associated with the  $n^{\text{th}}$  pole,  $s_n = \sigma_n + j\omega_n$ , of the frequency domain reflection coefficient. This representation of the temporal field is found by taking the inverse Laplace transform of (3.11), neglecting infinite contour contributions for which (3.11) does not approach zero uniformly. To perform this inverse transform, the singularities of the frequency domain reflection coefficient are explored, and the evaluation of the integral

$$\int_{Br} \Gamma(s) e^{st} ds \quad (3.17)$$

is carried out through complex plane integration for several ranges of time,  $t$ . Here, the integration is carried out along the contour  $Br$ , which is the Bromwich path. The Bromwich path, which defines the inverse Laplace transform, is a path in the complex  $s$ -plane which is taken parallel to the imaginary axis, to the right of all singular points. Evaluation of the integral in (3.17) gives the time domain reflection coefficient as

$$\Gamma(t) = \frac{1}{j2\pi} \int_{Br} \Gamma(s) e^{st} ds \quad (3.18)$$

when infinite contour contributions are neglected. In order to carry out the contour integration involved with the evaluation of this integral, singularities of the integrand need to be determined, and appropriate branches defined.

### 3.2.1 Singularities of the frequency domain reflection coefficient

Singularities of the frequency domain reflection coefficient take on various forms. First,  $s\tau_1(s)$  and  $Z_1(s)$ , given by equations (3.12) and (3.14), respectively, contain complex square roots which lead to branch points at  $s = 0$  and  $s = s_1$ . Correspondingly, branch cuts are taken along the negative real axis to define the principal branches of the square root functions. In addition, observing that the frequency domain reflection coefficient may be written as

$$\Gamma(s) = \frac{N(s)}{D(s)}, \quad (3.19)$$

there are poles associated with the zeros of the denominator,  $D(s)$ . These poles will appear in the left half of the complex  $s$ -plane, with some lying on the real axis, and the rest occurring in conjugate pairs.

### 3.2.2 Evaluation of the time domain reflection coefficient

Evaluation of the time domain reflection coefficient is carried out by factoring the frequency domain reflection coefficient such that the inverse Laplace transform of the individual components are physically meaningful during various time periods. The definition of these time periods, the factorization used in each time period, and the implications of these developments are the subjects of Sections 3.2.2.1 through 3.2.2.3.

In evaluating the Laplace inversion integral, *Jordan's Lemma* is used many times to evaluate the integral contributions from various contours. This lemma is given by [15] as

**Theorem 3.1** (*Jordan's Lemma*) *If  $H(z)$  is an analytic function having the property*

$$\lim_{R \rightarrow \infty} H(Re^{j\theta}) = 0, \quad -\frac{\pi}{2} \leq \theta \leq \frac{\pi}{2} \quad \text{or} \quad \frac{\pi}{2} \leq \theta \leq \frac{3\pi}{2}$$

uniformly with respect to  $\theta$ , then, if  $b$  is a nonzero real number,

$$\begin{aligned}\lim_{R \rightarrow \infty} \int_{C_1} H(z) e^{bz} dz &= 0, \quad \text{if } b < 0 \\ \lim_{R \rightarrow \infty} \int_{C_2} H(z) e^{bz} dz &= 0, \quad \text{if } b > 0\end{aligned}$$

where  $C_1$  and  $C_2$  are semicircles in the right and left half planes, respectively, centered at the origin and of radius  $R$ .

### 3.2.2.1 Early time: $t < T_1$

The early time is defined as the time period before a response is observed at the observation plane due to reflection from the second interface, as discussed in Section 2.4.1. This response should be identical to the interfacial reflection for two semi-infinite media during this time period. Because of this, the frequency domain reflection coefficient is factored into the sum of the interfacial reflection coefficient of the first interface,  $R_1(s)$ , and a reduced reflection coefficient defined by

$$\begin{aligned}\Gamma'(s) &= \Gamma(s) - R_1(s) \\ &= \frac{-(1 - R_1^2(s))(R_1(s)e^{-s\tau_1(s)} + e^{-s(\tau_1(s)+\tau_2(s))})}{1 - R_1^2(s)e^{-s\tau_1(s)} - R_1(s)e^{-s(\tau_1(s)+\tau_2)} + R_1(s)e^{-s\tau_2(s)}}.\end{aligned}\quad (3.20)$$

Since the inverse Laplace transform is a linear operation, the time domain reflection coefficient for the entire structure is given as a sum of the inverse Laplace transforms of the two components of the frequency domain reflection coefficient. The inverse Laplace transform of the interfacial reflection coefficient, given by  $R_1(t)$ , is rigorously developed in [14]. The evaluation of the inverse Laplace transform of the reduced reflection coefficient remains; this is given by  $\Gamma'(t) = \mathcal{L}^{-1}\{\tilde{\Gamma}'(s)\}$ , where  $\tilde{\Gamma}'(s)$  is identical to  $\Gamma'(s)$ , except for its behavior at infinity. This inverse transform is found

by evaluating

$$\frac{1}{j2\pi} \int_{Br} \Gamma'(s)e^{st} ds, \quad (3.21)$$

neglecting infinite contour contributions for which  $\Gamma'(s)$  does not go to zero uniformly.

On an infinite contour,  $C_\infty$ , exponential terms appearing in the numerator of the reduced reflection coefficient are given using (3.12) as,

$$\lim_{|s| \rightarrow \infty} \left\{ \frac{2d}{c} \sqrt{\bar{\epsilon}_1 + \frac{\sigma_1}{s\epsilon_0}} \right\} = \frac{2d}{c} \sqrt{\bar{\epsilon}_1} \triangleq T_1 \quad (3.22)$$

Letting  $t_1 = t - T_1$ , which is negative for  $t < T_1$ , evaluation of the integration along the Bromwich contour in (3.21) is obtained by closing the integration contour in the right half of the complex  $s$ -plane, as shown in Figure 3.3. Right half plane closure is justified here, since  $t_1$  is negative for the time period  $t < T_1$ . Note that  $T_1$  is the two-way transit time of the first material region, as discussed in 2.4.1. The early time is thus given by the time period  $t < T_1$ . The integration on the infinite contour  $C_\infty$  is given by

$$\int_{C_\infty} \Gamma'(s)e^{st} ds = \int_{C_\infty} \Gamma'(s)e^{sT_1} e^{st_1} ds \quad (3.23)$$

Here, *Jordan's Lemma* cannot be directly applied to evaluate the integral contribution over  $C_\infty$ , because the integrand does not go to zero as  $|s| \rightarrow \infty$  at all points on the contour. However, it is possible to apply *Jordan's Lemma*, when the following theorem from [15] is used:

**Theorem 3.2** *Let  $f(t)$  be a function which is APC (almost piecewise continuous) and which is identically zero for  $t$  greater than some number  $T$ . Then the Laplace transform of  $f(t)$  approaches zero uniformly as  $s$  becomes infinite in a right half plane,*

$$|\arg(s - c_0)| \leq \frac{\pi}{2},$$

where  $c_0 = \sigma_0 + j\omega_0$  is any complex constant in the  $s$  plane.

To use this theorem, recall that the time domain reflection coefficient is always convolved with a finite duration incident waveform. Letting this waveform be given by  $g(t)$  and noting that this waveform is APC, the spectral response of the system is  $G(s)\Gamma'(s)$ , where  $G(s) = \mathcal{L}\{g(t)\}$ . Using Theorem 3.2,  $G(s)$  will approach zero on the infinite contour,  $C_\infty$ . The response of the system thus approaches zero on the contour. Defining  $\tilde{\Gamma}'(s)$  as a function which approaches zero uniformly on the infinite contour, and which satisfies  $\mathcal{L}^{-1}\{G(s)\Gamma'(s)\} = \mathcal{L}^{-1}\{G(s)\tilde{\Gamma}'(s)\}$ , the infinite contour contribution is neglected to give the time domain reflection coefficient as  $\Gamma'(t) = \mathcal{L}^{-1}\{\tilde{\Gamma}'(s)\}$ . Thus, the time domain reflection coefficient in the early time is identical to the inverse Laplace transform of the interfacial reflection coefficient, as developed in [14].

### 3.2.2.2 Middle time: $T_1 < t < T_1 + T_2$

The middle time for this structure is defined as the time period between the observation of the reflection from the second interface at the observation plane, as discussed in Section 2.4.1, and the observation of the reflection from the conductor. During this time period, physical reasoning suggests that the temporal response should be identical to the reflection from the first layer of material backed by free space. Because of this, the frequency domain reflection coefficient is factored into the sum of the reflection coefficient for a single air-backed lossy layer, which is rigorously developed in [13], and a reduced reflection coefficient defined by the difference between the total reflection coefficient and the frequency domain reflection coefficient for the

single air-backed lossy layer. The reduced reflection coefficient is thus given by

$$\begin{aligned}
\Gamma'_{2lay}(s) &= \Gamma(s) - \Gamma_{1lay}(s) \\
&= \Gamma(s) - \frac{R_1(s)(1 - R_2(s)e^{-s\tau_1(s)})}{1 - R_1^2(s)e^{-s\tau_1(s)}} \\
&= \frac{-e^{-s(\tau_1(s)+\tau_2)}}{1 - R_1^2(s)e^{-s\tau_1(s)}} \times \\
&\quad \times \frac{(1 - R_1^2(s))^2}{1 - R_1^2(s)e^{-s\tau_1(s)} - R_1(s)e^{-s(\tau_1(s)+\tau_2)} + R_1(s)e^{-s\tau_2(s)}} \quad (3.24)
\end{aligned}$$

Since the inverse Laplace transform is a linear operation, the time domain reflection coefficient for the entire structure is given as a sum of the inverse Laplace transforms of the two components of the frequency domain reflection coefficient. The inverse Laplace transform of an air-backed lossy layer is rigorously developed in [13]. The evaluation of the inverse transform of the reduced reflection coefficient remains; this is given by  $\Gamma'_{2lay}(t) = \mathcal{L}^{-1}\{\tilde{\Gamma}'_{2lay}(s)\}$ , where  $\tilde{\Gamma}'_{2lay}(s)$  is identical to  $\Gamma'_{2lay}(s)$ , except for its behavior at infinity. This inverse transform is found by evaluating

$$\frac{1}{j2\pi} \int_{Br} \Gamma'_{2lay}(s)e^{st} ds, \quad (3.25)$$

neglecting infinite contour contributions. On an infinite contour,  $C_\infty$ , exponential terms appearing in the numerator of the reduced reflection coefficient are given using (3.12) and (3.13) as,

$$\lim_{|s| \rightarrow \infty} \left\{ \frac{2d}{c} \sqrt{\bar{\epsilon}_1 + \frac{\sigma}{s\epsilon_0}} + \frac{2h}{c} \cos \theta_{in} \right\} = \frac{2d}{c} \sqrt{\bar{\epsilon}_1} + \frac{2h}{c} \cos \theta_{in} \triangleq T_1 + T_2 \quad (3.26)$$

where  $T_1$  and  $T_2$  are the two-way transit times of the first and second layer, respectively, as discussed in 2.4.1. Letting  $t_2 = t - (T_1 + T_2)$ , which is negative for  $t < T_1 + T_2$ , evaluation along the Bromwich contour in (3.24) is obtained by closing

the integration contour in the right half plane of the complex  $s$ -plane, as shown in Figure 3.3. Right half plane closure is justified here, since  $t_2$  is negative during this time period. The end of the middle-time period is defined by (3.26). The integration on the infinite contour  $C_\infty$  is given by

$$\int_{C_\infty} \Gamma'(s)e^{st} ds = \int_{C_\infty} \Gamma'(s)e^{s(T_1+T_2)} e^{st_1} ds \quad (3.27)$$

It is not possible to apply *Jordan's Lemma* directly to this integral, since the integrand does not go to zero uniformly on the entire contour,  $C_\infty$ . However, by definition of the time domain reflection coefficient, the infinite contour contribution is to be neglected. Thus, during the middle-time period, the time domain reflection coefficient is identical to the time domain reflection coefficient for the air-backed lossy layer, which is rigorously developed in [13]. It is found in [13] that after the time  $T_1$ , the time domain reflection coefficient for the air-backed lossy layer is given by a natural mode series.

### 3.2.2.3 Late time: $t > T_1 + T_2$

The late time of the response for this geometry is defined as the portion of the transient response after a response from a reflection off of the conductor backing arrives at the observation plane, as discussed in Section 2.4.1. For this time period, the frequency domain reflection coefficient is factored into the sum of the reflection coefficient for a single air-backed lossy layer, which is rigorously developed in [13], and a reduced reflection coefficient defined by the difference between the total reflection coefficient and the frequency domain reflection coefficient for the single air-backed lossy layer, as is done for the middle time. The reason for this factorization is two-fold. First, the time domain reflection coefficient for the air-backed lossy layer is known to be a natural mode series after the time  $T_1$ , thus only the reduced reflection coefficient needs to be addressed. Second, by examining the properties of the individual components of the time domain reflection coefficient, some insight into the transient response can

be obtained. The reduced reflection coefficient is given by (3.24), and repeated here as

$$\begin{aligned}
 \Gamma'_{2lay}(s) &= \Gamma(s) - \Gamma_{1lay}(s) \\
 &= \Gamma(s) - \frac{R_1(s)(1 - R_2(s)e^{-s\tau_1(s)})}{1 - R_1^2(s)e^{-s\tau_1(s)}} \\
 &= \frac{-e^{-s(\tau_1(s)+\tau_2)}}{1 - R_1^2(s)e^{-s\tau_1(s)}} \times \\
 &\quad \times \frac{(1 - R_1^2(s))^2}{1 - R_1^2(s)e^{-s\tau_1(s)} - R_1(s)e^{-s(\tau_1(s)+\tau_2)} + R_1(s)e^{-s\tau_2}} \quad (3.28)
 \end{aligned}$$

Evaluation of the inverse transform of the reduced reflection coefficient is carried out through the integration along the Bromwich path, neglecting infinite contour contributions; this integration is given by

$$\frac{1}{j2\pi} \int_{Br} \Gamma'_{2lay}(s) e^{st} ds. \quad (3.29)$$

On an infinite contour,  $C_\infty$ , exponential terms appearing in the numerator of the reduced reflection coefficient include the two-way transit times of the two layers,  $T_1$  and  $T_2$  as in (3.26). Letting  $t_2 = t - (T_1 + T_2)$ , which is positive for  $t > T_1 + T_2$ , evaluation along the Bromwich contour in (3.28) is obtained by closing the integration contour in the left half of the complex  $s$ -plane, as shown in Figure 3.7. When closure is taken in the left half plane, many integration paths are involved. In this discussion, these integration paths will be referred to in two groups, the outer contour,  $C$ , which includes integration paths parameterized by quantities receding towards infinity, and the inner contour,  $C'$ , which includes integration paths taken along the branch cut.



These integration contours are given by

$$C = Br \cup L_1 \cup C_\infty^+ \cup C_\infty^- \cup L_2$$

$$C' = l_A \cup \gamma_1 \cup \gamma_2 \cup \dots \cup \gamma_7 \cup l_1 \cup l_2 \cup \dots \cup l_6 \cup l_B$$

Then, by Cauchy's residue theorem

$$\oint_{C \cup C'} \Gamma'_{2lay}(s) e^{st} ds = j2\pi \sum Res[\Gamma'_{2lay}(s) e^{st}, \text{complex poles}]. \quad (3.30)$$

Thus, determination of the time domain reflection coefficient is possible provided the integral contribution from each path is known.

### 3.2.2.3.1 Contributions from the outer contour, C .

The Laplace inversion integral is found by computing (3.30) for the Bromwich path contribution in terms of the contributions from all other integration paths and computation of the residues from the enclosed simple poles. The outer contour, C, consists of various integration paths that are parameterized by quantities that recede towards infinity, including the Bromwich path which defines the inverse Laplace transform.

#### Contributions from $C_\infty^+$ and $C_\infty^-$

Integral contributions from  $C_\infty^+$  and  $C_\infty^-$  are given directly by *Jordan's lemma*, as stated in Theorem 3.1, since  $\Gamma'_{2lay}(s) \rightarrow 0$  on the infinite contours. Thus, direct application of *Jordan's lemma* gives

$$\int_{C_\infty^+} \Gamma'_{2lay}(s) e^{st} ds = 0 \quad (3.31)$$

$$\int_{C_\infty^-} \Gamma'_{2lay}(s) e^{st} ds = 0. \quad (3.32)$$

#### Contributions from $L_1$ and $L_2$

On  $L_1$  and  $L_2$ , *Jordan's Lemma* cannot be directly applied to evaluate the integral

contributions, because the integrand does not go to zero as  $|s| \rightarrow \infty$  at all points on the contours. However, by definition of the time domain reflection coefficient, contributions from  $L_1$  and  $L_2$  are to be neglected, as discussed in Section 2.4.

### 3.2.2.3.2 Contributions from the inner contour, $C'$

The segments of the inner contour  $C'$ , which enclose the branch cut, can be broken into three groups. The first group consists of the contours  $\gamma_2$ ,  $\gamma_3$ ,  $\gamma_5$ , and  $\gamma_6$ , etc, which enclose the real poles on the branch cut. Note that two poles are shown on the real axis here, but more may appear depending on the properties of the material layers, and the incidence angle. The second group is made up of contours  $\gamma_1$ ,  $\gamma_4$ , and  $\gamma_7$  that enclose the branch points. The straight line segments immediately above and below the branch cut make up the final group. Within this group, the segments  $l_A$  and  $l_B$ , which lie to the left of all of the branch points will be handled separately from the segments  $l_1$  through  $l_6$ .

#### Contributions from $\gamma_2$ , $\gamma_3$ , $\gamma_5$ , and $\gamma_6$

The integral contributions from the first group of contours, which enclose the poles on the negative real axis, can be found by calculating the residues of  $\Gamma'_{2lay}(s)e^{st}$  at the poles. It is found that all of the poles of  $\Gamma'_{2lay}(s)$  are of first order and thus the residues may be found from

$$Res[\Gamma'_{2lay}(s)e^{st}, poles] \Big|_{s=s_k} = \lim_{s \rightarrow s_k} (s - s_k) [\Gamma'_{2lay}(s)e^{st}] = A_k e^{s_k t} \quad (3.33)$$

where

$$A_k = \frac{e^{-s_k(\tau_1(s_k) + \tau_2)} (1 - R_1^2(s_k))^2}{\frac{d}{ds} [M(s)] \Big|_{s=s_k}} \quad (3.34)$$

is the complex mode amplitude, and the denominator of the reduced reflection coefficient has been written as  $1 - M(s)$ . Note that l'Hôpital's rule has been used to obtain the form of the complex mode amplitude shown here. Carrying out the details

of the differentiation gives

$$\begin{aligned}
\frac{d}{ds} [M(s)] &= \frac{d}{ds} \left[ R_1^2(s) e^{-s\tau_1(s)} + (1 - R_1^2(s) e^{-s\tau_1(s)}) \times \right. \\
&\quad \left. \times (R_1^2(s) e^{-s\tau_1(s)} + R_1(s) e^{-s(\tau_1(s)+\tau_2)} - R_1(s) e^{-s\tau_2(s)}) \right] \\
&= [2(1 - R_1^2(s) e^{-s\tau_1(s)}) - R_1(s)(e^{-s(\tau_1(s)+\tau_2)} - e^{-s\tau_2})] \frac{d}{ds} [R_1^2(s) e^{-s\tau_1(s)}] \\
&\quad + (1 - R_1^2(s) e^{-s\tau_1(s)}) \frac{d}{ds} [R_1(s)(e^{-s(\tau_1(s)+\tau_2)} - e^{-s\tau_2})] \\
&= [2R_1(s) e^{-s\tau_1(s)} (2(1 - R_1^2(s) e^{-s\tau_1(s)}) - R_1(s)(e^{-s(\tau_1(s)+\tau_2)} - e^{-s\tau_2})) \\
&\quad + (1 - R_1^2(s) e^{-s\tau_1(s)})(e^{-s(\tau_1(s)+\tau_2)} - e^{-s\tau_2})] \frac{d}{ds} [R_1(s)] \\
&\quad + R_1^2(s) (2(1 - R_1^2(s) e^{-s\tau_1(s)}) - R_1(s)(e^{-s(\tau_1(s)+\tau_2)} - e^{-s\tau_2})) \frac{d}{ds} [e^{-s\tau_1(s)}] \\
&\quad + R_1(s) (1 - R_1^2(s) e^{-s\tau_1(s)}) \frac{d}{ds} [e^{-s(\tau_1(s)+\tau_2)} - e^{-s\tau_2}] \tag{3.35}
\end{aligned}$$

with the derivatives of the exponential terms given by

$$\frac{d}{ds} [e^{-s(\tau_1(s)+\tau_2)} - e^{-s\tau_2}] = - \left[ \left( \frac{d}{c} \sqrt{\bar{\epsilon}_1} \frac{2s - s_1}{\sqrt{s}\sqrt{s - s_1}} + \frac{2h}{c} \right) e^{-s(\tau_1(s)+\tau_2)} - \left( \frac{2h}{c} \right) e^{-s\tau_2} \right]$$

and

$$\frac{d}{ds} [e^{-s\tau_1(s)}] = - \left[ \frac{d}{c} \sqrt{\bar{\epsilon}_1} \frac{2s - s_1}{\sqrt{s}\sqrt{s - s_1}} e^{-s\tau_1(s)} \right]$$

The derivative of the first interfacial reflection coefficient is found using (3.15) as

$$\frac{d}{ds} [R_1(s)] = \frac{\Upsilon(s)}{\Omega(s)} \tag{3.36}$$

where, for parallel polarization,

$$\begin{aligned}
\Upsilon(s) &= \sqrt{\bar{\epsilon}_1} \frac{2s^2 - ss_1}{\sqrt{s}\sqrt{s - s_1}} \left( s\epsilon_{1r} + \frac{\sigma}{\epsilon_0} \right) \cos \theta_{in} - 2\epsilon_{1r} \sqrt{\bar{\epsilon}_1} \sqrt{s}\sqrt{s - s_1} \cos \theta_{in} \\
\Omega(s) &= \left( s\epsilon_{1r} + \frac{\sigma}{\epsilon_0} \right)^2 \cos^2 \theta_{in} + 2 \left( s\epsilon_{1r} + \frac{\sigma}{\epsilon_0} \right) \sqrt{\bar{\epsilon}_1} \sqrt{s}\sqrt{s - s_1} \cos \theta_{in} + \bar{\epsilon}_1 s(s - s_1)
\end{aligned}$$

and for perpendicular polarization,

$$\begin{aligned}\Upsilon(s) &= 2\sqrt{\bar{\epsilon}_1}\sqrt{s}\sqrt{s-s_1}\cos\theta_{in} - \cos\theta_{in}\sqrt{\bar{\epsilon}_1}\frac{2s^2-ss_1}{\sqrt{s}\sqrt{s-s_1}} \\ \Omega(s) &= s^2\cos^2\theta_{in} + 2\cos\theta_{in}s\sqrt{\bar{\epsilon}_1}\sqrt{s}\sqrt{s-s_1} + \bar{\epsilon}_1s(s-s_1)\end{aligned}$$

Here it is noted that the residues of the poles located on the branch cut must be evaluated carefully, taking into account the value of functions on each side of the branch cut. For this particular problem, the reduced reflection coefficient is even about the branch cut, as discussed on pages 62 through 67, so the values on each side of the branch cut are the same. This allows the evaluation of the residues from each side to be combined into one evaluation, where all of the residues are evaluated using (3.33).

#### Contributions from $\gamma_1$ , $\gamma_4$ , and $\gamma_7$

The integral contribution from the contour surrounding the branch point at  $s = 0$  can be computed by denoting the radius of  $\gamma_4$  as  $r_0$  and letting  $\phi_0$  be an angle measured counterclockwise from the real axis to the point on  $\gamma_4$ . This allows any point on the contour to be located as  $s = r_0e^{j\phi_0}$ . The reflection coefficient on the  $\gamma_4$  contour is given in the limit of  $r_0 \rightarrow 0$ , i.e.,  $s \rightarrow 0$ , as

$$R_1(s) = \begin{cases} \frac{\sqrt{\bar{\epsilon}_1}\sqrt{s}\sqrt{s-s_1} - (s\epsilon_{1r} + \frac{\sigma}{\epsilon_0})\cos\theta_{in}}{\sqrt{\bar{\epsilon}_1}\sqrt{s}\sqrt{s-s_1} + (s\epsilon_{1r} + \frac{\sigma}{\epsilon_0})\cos\theta_{in}} \rightarrow -1 & \text{parallel polarization} \\ \frac{\sqrt{s}\cos\theta_{in} - \sqrt{\bar{\epsilon}_1}\sqrt{s-s_1}}{\sqrt{s}\cos\theta_{in} + \sqrt{\bar{\epsilon}_1}\sqrt{s-s_1}} \rightarrow -1 & \text{perpendicular polarization} \end{cases} \quad (3.37)$$

For parallel polarization, as  $s \rightarrow 0$  terms in the numerator of the reduced reflection

coefficient are given by

$$\begin{aligned}
1 - R_1^2(s) &= 1 - \frac{(\sqrt{\epsilon_1} \sqrt{s} \sqrt{s - s_1} - (s\epsilon_{1r} + \frac{\sigma}{\epsilon_0}) \cos \theta_{in})^2}{(\sqrt{\epsilon_1} \sqrt{s} \sqrt{s - s_1} + (s\epsilon_{1r} + \frac{\sigma}{\epsilon_0}) \cos \theta_{in})^2} \\
&= \frac{4\sqrt{\epsilon_1} \sqrt{s} \sqrt{s - s_1} ((s\epsilon_{1r} + \frac{\sigma}{\epsilon_0}) \cos \theta_{in})}{(\sqrt{\epsilon_1} \sqrt{s} \sqrt{s - s_1} + (s\epsilon_{1r} + \frac{\sigma}{\epsilon_0}) \cos \theta_{in})^2} \\
&= \frac{4\sqrt{\epsilon_1} \sqrt{s} \sqrt{s - s_1} ((s\epsilon_{1r} + \frac{\sigma}{\epsilon_0}) \cos \theta_{in})}{(\frac{\sigma}{\epsilon_0} \cos \theta_{in})^2} \left( 1 + \frac{\sqrt{\epsilon_1} \sqrt{s} \sqrt{s - s_1} + s\epsilon_{1r} \cos \theta_{in}}{\frac{\sigma}{\epsilon_0} \cos \theta_{in}} \right)^{-2}
\end{aligned}$$

Using the first two terms of the binomial expansion, this can be written as

$$\begin{aligned}
1 - R_1^2(s) &= \frac{4\sqrt{\epsilon_1} \sqrt{s} \sqrt{s - s_1} ((s\epsilon_{1r} + \frac{\sigma}{\epsilon_0}) \cos \theta_{in})}{(\frac{\sigma}{\epsilon_0} \cos \theta_{in})^2} \left[ 1 - 2 \frac{\sqrt{\epsilon_1} \sqrt{s} \sqrt{s - s_1} + s\epsilon_{1r} \cos \theta_{in}}{\frac{\sigma}{\epsilon_0} \cos \theta_{in}} \right] \\
&= 4 \frac{\sqrt{\epsilon_1} \sqrt{s} \sqrt{s - s_1}}{(\sigma/\epsilon_0) \cos \theta_{in}} \left( \frac{s\epsilon_{1r}}{(\sigma/\epsilon_0)} + 1 \right) \left[ 1 - 2 \frac{\sqrt{\epsilon_1} \sqrt{s} \sqrt{s - s_1}}{(\sigma/\epsilon_0) \cos \theta_{in}} - 2 \frac{s\epsilon_{1r}}{(\sigma/\epsilon_0)} \right] \sim \sqrt{s}
\end{aligned} \tag{3.38}$$

Thus, the numerator of the reduced reflection coefficient is proportional to  $s$  as  $s \rightarrow 0$  for parallel polarization, using (3.28). Similarly, for perpendicular polarization, as  $s \rightarrow 0$  terms in the numerator of the reduced reflection coefficient are given by

$$\begin{aligned}
1 - R_1^2(s) &= 1 - \frac{(\sqrt{s} \cos \theta_{in} - \sqrt{\epsilon_1} \sqrt{s - s_1})^2}{(\sqrt{s} \cos \theta_{in} + \sqrt{\epsilon_1} \sqrt{s - s_1})^2} \\
&= \frac{4\sqrt{\epsilon_1} \sqrt{s} \sqrt{s - s_1} \cos \theta_{in}}{(\sqrt{s} \cos \theta_{in} + \sqrt{\epsilon_1} \sqrt{s - s_1})^2} \\
&= 4 \frac{\sqrt{s} \cos \theta_{in}}{\sqrt{\epsilon_1} \sqrt{s - s_1}} \left( 1 + \frac{\sqrt{s} \cos \theta_{in}}{\sqrt{\epsilon_1} \sqrt{s - s_1}} \right)^{-2}
\end{aligned}$$

Using the first two terms of the binomial expansion, this can be written as

$$1 - R_1^2(s) = 4 \frac{\sqrt{s} \cos \theta_{in}}{\sqrt{\epsilon_1} \sqrt{s - s_1}} \left( 1 - 2 \frac{\sqrt{s} \cos \theta_{in}}{\sqrt{\epsilon_1} \sqrt{s - s_1}} \right) \sim \sqrt{s} \tag{3.39}$$

Thus, the numerator of the reduced reflection coefficient is proportional to  $s$  as  $s \rightarrow 0$

for perpendicular polarization, using (3.28).

For both polarizations, terms in the denominator are given, as  $s \rightarrow 0$ , by

$$\begin{aligned}
1 - R_1^2(s)e^{-s\tau_1(s)} &= 1 - R_1^2(s) + R_1^2(s) - R_1^2(s)e^{-s\tau_1(s)} \\
&= 1 - R_1^2(s) + R_1^2(s)(1 - e^{-s\tau_1(s)}) \\
&\sim \sqrt{s} + s\tau_1(s) \sim \sqrt{s}(1 + s) \sim \sqrt{s} \quad (3.40)
\end{aligned}$$

and

$$R_1(s)e^{s\tau_2}(1 - e^{-s\tau_1(s)}) \sim (s\tau_1(s)) \sim s\sqrt{s} \quad (3.41)$$

where (3.38) and (3.39) are utilized. Thus, the denominator of the reflection coefficient is also proportional to  $s$ , as  $s \rightarrow 0$  for each polarization. The reduced reflection coefficient, for both parallel and perpendicular polarization, is then given using (3.28), (3.38), and (3.39) as  $s \rightarrow 0$  by

$$\begin{aligned}
\Gamma'_{2lay}(s) &= \frac{-(1 - R_1^2(s))^2 e^{-s(\tau_1(s) + \tau_2)}}{(1 - R_1^2(s)e^{-s\tau_1(s)})(1 - R_1^2(s)e^{-s\tau_1(s)} - R_1(s)(e^{-s(\tau_1(s) + \tau_2)} - e^{-s\tau_2}))} \\
&\rightarrow D^{\parallel, \perp} \quad (3.42)
\end{aligned}$$

Since the numerator and denominator of the reduced reflection coefficient are both proportional to  $s$  for each polarization, as  $r_0 \rightarrow 0$ , the reduced reflection coefficient goes to a constant,  $D^{\parallel, \perp}$ . Thus,

$$\Gamma(s)e^{st} = D^{\parallel, \perp} e^{st}$$

and

$$|\Gamma(s)e^{st}| \leq |D^{\parallel, \perp}| e^{r_0 t}.$$

Therefore

$$\left| \int_{\gamma_4} \Gamma(s) e^{st} ds \right| \leq 2\pi r_0 |D^{\parallel, \perp}| e^{r_0 t} \rightarrow 0, \quad (r_0 \rightarrow 0).$$

As a result, the integral contribution from the contour around the branch point at  $s = 0$  is given by

$$\int_{\gamma_4} \Gamma'_{2lay}(s) e^{st} ds = 0 \quad (3.43)$$

The integral contributions from the contours surrounding the branch point at  $s = s_1$  can be computed by denoting the radius of both  $\gamma_1$  and  $\gamma_7$  as  $r_1$  and letting  $\phi_1$  be an angle measured counterclockwise from the real axis to a point on either  $\gamma_1$  or  $\gamma_7$ . This allows any point on the contours to be located as  $s = s_1 + r_1 e^{j\phi_1}$ . The reflection coefficient on the contours are given in the limit of  $r_1 \rightarrow 0$ , i.e.,  $s \rightarrow s_1$ , as

$$R_1(s) = \begin{cases} \frac{\sqrt{\epsilon_1} \sqrt{s} \sqrt{s - s_1} - (s\epsilon_{1r} + \frac{\sigma}{\epsilon_0}) \cos \theta_{in}}{\sqrt{\epsilon_1} \sqrt{s} \sqrt{s - s_1} + (s\epsilon_{1r} + \frac{\sigma}{\epsilon_0}) \cos \theta_{in}} \rightarrow -1 & \text{parallel polarization} \\ \frac{s \cos \theta_{in} - \sqrt{\epsilon_1} \sqrt{s} \sqrt{s - s_1}}{s \cos \theta_{in} + \sqrt{\epsilon_1} \sqrt{s} \sqrt{s - s_1}} \rightarrow 1 & \text{perpendicular polarization} \end{cases} \quad (3.44)$$

In an analogous development to the one for the branch point at  $s = 0$ , it can again be shown the both the numerator and denominator of (3.28) are proportional to  $s$ , and thus  $\Gamma'_{2lay}(s)$  becomes constant on the contour. This leads to

$$\int_{\gamma_1} \Gamma'_{2lay} e^{st} ds = \int_{\gamma_7} \Gamma'_{2lay}(s) e^{st} ds = 0. \quad (3.45)$$

### Contributions from segments above and below the branch cuts

The contributions from the straight line segments of the inner contour immediately above and below the branch cuts are separated into two groups. The first group is given by  $l_A$  and  $l_B$ , which lie to the left of the branch points. The rest of the contours,  $l_1$  through  $l_6$ , lie to the right of the leftmost branch point. Note that if more than two poles lie on the real axis, more contours would be included in at least one of

these groups. The developments here will remain valid for any number of integration contours along the branch cut.

Branch cuts which define the principal branches of the complex square root functions of the wave impedances and propagation factors are taken along the negative real axis. These branches are defined by  $-\pi < \phi_0 \leq \pi$ , and  $-\pi < \phi_1 \leq \pi$ . Looking at Figure 3.8, begin by examining the integration paths designated as  $A_+$  and  $A_-$ . For the contour  $A_+$ ,  $\phi_0 = \phi_1 = \pi$ . Letting  $s = -x$ , where  $x$  is a nonnegative real number, denote a point on the negative real axis, the product of the square root functions found in the wave impedances and propagation terms take the form

$$\sqrt{s}\sqrt{s-s_1} = \sqrt{r_0}\sqrt{r_1}e^{j(\phi_0+\phi_1)/2} = \sqrt{x}\sqrt{x+s_1}e^{j\pi} = -\sqrt{x}\sqrt{x+s_1}. \quad (3.46)$$

On  $A_-$ ,  $\phi_0 = \phi_1 = -\pi$ , and the product of square roots is given by

$$\sqrt{s}\sqrt{s-s_1} = \sqrt{x}\sqrt{x+s_1}e^{-j\pi} = -\sqrt{x}\sqrt{x+s_1}. \quad (3.47)$$

Thus, the products of the square roots are analytic on the  $A$  contours, and

$$\Gamma'_{2lay}(s)\Big|_{A_+} = \Gamma'_{2lay}(s)\Big|_{A_-}. \quad (3.48)$$

Since the integrations above and below the branch cut are taken in opposite directions,

$$\int_{l_A} \Gamma'_{2lay}(s)e^{st}ds + \int_{l_B} \Gamma'_{2lay}(s)e^{st}ds = 0 \quad (3.49)$$

On  $B_+$ ,  $\phi_0 = \pi$ ,  $\phi_1 = 0$ , and the product of square root functions found in the wave impedances and propagation terms is given by

$$\sqrt{s}\sqrt{s-s_1} = \sqrt{x}\sqrt{-x-s_1}e^{j\pi/2} = j\sqrt{x}\sqrt{-x-s_1}. \quad (3.50)$$



Similarly, on  $B_-$ ,  $\phi_0 = -\pi$ ,  $\phi_1 = 0$ , and

$$\sqrt{s}\sqrt{s-s_1} = \sqrt{x}\sqrt{-x-s_1}e^{-j\pi/2} = -j\sqrt{x}\sqrt{-x-s_1}. \quad (3.51)$$

The product of square roots on the  $B$  contours is not found to be analytic, so further investigation into the form of the reduced reflection coefficient is needed. Plugging (3.50) into (3.12) gives the term  $s\tau_1(s)$  on a contour directly above the branch cut as

$$s\tau_1(s)\Big|_{B_+} = j\frac{2d}{c}\sqrt{\epsilon_1}\sqrt{x}\sqrt{-x-s_1} = j2\Phi_1\Big|_{B_+} \quad (3.52)$$

where  $\Phi_1|_{B_+} = \frac{d}{c}\sqrt{\epsilon_1}\sqrt{x}\sqrt{-x-s_1}$  has been defined. The wave impedances, which are needed to compute the interfacial reflection coefficient by (3.2), are given by (3.14) on the contour  $B_+$  as

$$Z_1^{\parallel}(s)\Big|_{B_+} = j\frac{\eta_0\sqrt{\epsilon_1}\sqrt{x}\sqrt{-x-s_1}}{-x\epsilon_{1r} + \sigma/\epsilon_0} \quad (3.53a)$$

for parallel polarization, and as

$$Z_1^{\perp}(s)\Big|_{B_+} = j\frac{\eta_0 x}{\sqrt{\epsilon_1}\sqrt{x}\sqrt{-x-s_1}} \quad (3.53b)$$

for perpendicular polarization. Plugging (3.51) into (3.12) gives the term  $s\tau_1(s)$  on a contour directly below the branch cut as

$$s\tau_1(s)\Big|_{B_-} = -j\frac{2d}{c}\sqrt{\epsilon_1}\sqrt{x}\sqrt{-x-s_1} = j2\Phi_1\Big|_{B_-} \quad (3.54)$$

where  $\Phi_1|_{B_-} = -\frac{d}{c}\sqrt{\epsilon_1}\sqrt{x}\sqrt{-x-s_1}$  has been defined. The wave impedances are

given for parallel and perpendicular polarizations, respectively, by (3.14) as

$$Z_1^{\parallel}(s)\Big|_{B-} = -j \frac{\eta_0 \sqrt{\epsilon_1} \sqrt{x} \sqrt{-x - s_1}}{-x \epsilon_{1r} + \sigma / \epsilon_0} \quad (3.55a)$$

$$Z_1^{\perp}(s)\Big|_{B-} = -j \frac{\eta_0 x}{\sqrt{\epsilon_1} \sqrt{x} \sqrt{-x - s_1}} \quad (3.55b)$$

on the contour  $B_-$ . Thus, odd symmetry is seen about the branch cut along the  $B$  contours for both the propagation terms and the wave impedances; i.e.,

$$Z_1\Big|_{B+} = -Z_1\Big|_{B-} \quad (3.56)$$

$$\Phi_1\Big|_{B+} = -\Phi_1\Big|_{B-} \quad (3.57)$$

Plugging  $R_1(s)$  into (3.28) and multiplying top and bottom through by  $(Z_1 + Z_0)^4$ , the reduced reflection coefficient takes on the form

$$\begin{aligned} \Gamma'_{2lay}(s) &= \frac{-e^{s(\tau_1(s)+\tau_2)}}{(Z_1 + Z_0)^2 - (Z_1 - Z_0)^2 e^{-s\tau_1(s)}} \times \\ &\times \frac{((Z_1 - Z_0)^2 - (Z_1 + Z_0)^2)^2}{(Z_1 + Z_0)^2 - (Z_1 - Z_0)^2 e^{-s\tau_1(s)} - (Z_1 - Z_0)(Z_1 - Z_0)(e^{s(\tau_1(s)+\tau_2)} - e^{s\tau_2})} \\ &= -16Z_1^2 Z_0^2 / \tilde{D}(s) \end{aligned} \quad (3.58)$$

where the products in the numerator have been carried out and  $e^{-s(\tau_1(s)+\tau_2)}$  has

been moved into the denominator term,  $\tilde{D}(s)$ . This term is given by

$$\begin{aligned}
\tilde{D}(s) &= e^{s(\tau_1(s)+\tau_2)} \left[ (Z_1 + Z_0)^4 - 2(Z_1 + Z_0)^2(Z_1 - Z_0)^2 e^{-s\tau_1(s)} \right. \\
&\quad \left. + (Z_1 - Z_0)^4 e^{-2s\tau_1(s)} - (Z_1^2 - Z_0^2) [(Z_1 + Z_0)^2 - (Z_1 - Z_0)^2 e^{-s\tau_1(s)}] \times \right. \\
&\quad \left. \times (e^{-s(\tau_1(s)+\tau_2)} - e^{-s\tau_2}) \right] \\
&= e^{s(\tau_1(s)+\tau_2)} \left[ (Z_1 + Z_0)^4 - 2(Z_1 + Z_0)^2(Z_1 - Z_0)^2 e^{-s\tau_1(s)} \right. \\
&\quad \left. + (Z_1 - Z_0)^4 e^{-2s\tau_1(s)} - [(Z_1^4 + 2Z_1(Z_1^2 Z_0 - Z_0^3) + Z_0^4) \right. \\
&\quad \left. - (Z_1^4 - 2Z_1(Z_1^2 Z_0 - Z_0^3) + Z_0^4) e^{-s\tau_1(s)}] (e^{-s(\tau_1(s)+\tau_2)} - e^{-s\tau_2}) \right] \quad (3.59)
\end{aligned}$$

Multiplying the exponential term  $e^{s(\tau_1(s)+\tau_2)}$  into the square brackets and expanding some of the bracketed wave impedance terms gives

$$\begin{aligned}
\tilde{D}(s) &= (Z_1^2 + 2Z_1 Z_0 + Z_0^2)^2 e^{s(\tau_1(s)+\tau_2)} - 2(Z_1 + Z_0)^2 (Z_1 - Z_0)^2 e^{s\tau_2} \\
&\quad + (Z_1^2 - 2Z_1 Z_0 + Z_0^2)^2 e^{-s(\tau_1(s)-\tau_2)} - (Z_1^4 + 2Z_1(Z_1^2 Z_0 - Z_0^3) + Z_0^4) \times \\
&\quad \times (1 - e^{s\tau_1(s)}) + (Z_1^4 - 2Z_1(Z_1^2 Z_0 - Z_0^3) + Z_0^4) (e^{-s\tau_1(s)} - 1) \quad (3.60)
\end{aligned}$$

Continuing to multiply out the bracketed wave impedance terms and regrouping gives

$$\begin{aligned}
\tilde{D}(s) &= \left[ Z_1^4 (e^{s\tau_2} + 1) + Z_0^4 (e^{s\tau_2} - 1) + 6Z_1^2 Z_0^2 e^{s\tau_2} \right] (e^{s\tau_1(s)} + e^{-s\tau_1(s)}) \\
&\quad - 2 \left[ Z_1^4 (e^{s\tau_2} + 1) + Z_0^4 (e^{s\tau_2} - 1) - 2Z_1^2 Z_0^2 e^{s\tau_2} \right] \\
&\quad + 2 \left[ Z_1^2 Z_0 (2e^{s\tau_2} + 1) + Z_0^3 (2e^{s\tau_2} - 1) \right] Z_1 (e^{s\tau_1(s)} - e^{-s\tau_1(s)}) \quad (3.61)
\end{aligned}$$

Using  $\Phi_1 = (s\tau_1(s)/2j)$  from Equations (3.52) and (3.54), the denominator of the

reduced reflection coefficient becomes

$$\begin{aligned}
\tilde{D}(s) &= \left[ Z_1^4(e^{s\tau_2} + 1) + Z_0^4(e^{s\tau_2} - 1) + 6Z_1^2 Z_0^2 e^{s\tau_2} \right] (e^{j2\Phi_1} + e^{-j2\Phi_1}) \\
&\quad - 2 \left[ Z_1^4(e^{s\tau_2} + 1) + Z_0^4(e^{s\tau_2} - 1) - 2Z_1^2 Z_0^2 e^{s\tau_2} \right] \\
&\quad + 2 \left[ Z_1^2 Z_0 (2e^{s\tau_2} + 1) + Z_0^3 (2e^{s\tau_2} - 1) \right] Z_1 (e^{j2\Phi_1} - e^{-j2\Phi_1}) \\
&= 2 \left[ Z_1^4(e^{s\tau_2} + 1) + Z_0^4(e^{s\tau_2} - 1) + 6Z_1^2 Z_0^2 e^{s\tau_2} \right] \cos 2\Phi_1 \\
&\quad - 2 \left[ Z_1^4(e^{s\tau_2} + 1) + Z_0^4(e^{s\tau_2} - 1) - 2Z_1^2 Z_0^2 e^{s\tau_2} \right] \\
&\quad + 4j \left[ Z_1^2 Z_0 (2e^{s\tau_2} + 1) + Z_0^3 (2e^{s\tau_2} - 1) \right] (Z_1 \sin 2\Phi_1) \tag{3.62}
\end{aligned}$$

Note that the wave impedance,  $Z_1$ , appears in  $\tilde{D}(s)$  either raised to an even power, or multiplied by  $(\sin 2\Phi_1)$ . Since regions 0 and 2 are free space, using (3.56) through (3.62) gives

$$\Gamma'_{2lay}(s) \Big|_{B+} = \Gamma'_{2lay}(s) \Big|_{B-}. \tag{3.63}$$

Since the integrations above and below the branch cut are taken in opposite directions, the evenness about the branch cut of the reduced reflection coefficient gives

$$\int_{l_1 \cup l_2 \cup l_3} \Gamma'_{2lay}(s) e^{st} ds + \int_{l_4 \cup l_5 \cup l_6} \Gamma'_{2lay}(s) e^{st} ds = 0 \tag{3.64}$$

The time domain reduced reflection coefficient is thus given in the late time by (3.30) as

$$\begin{aligned}
\Gamma'_{2lay} &= \sum Res[\Gamma'_{2lay}(s) e^{st}, \text{complex poles}] + \sum Res[\Gamma'_{2lay}(s) e^{st}, \text{real poles}] \\
&= \sum Res[\Gamma'_{2lay}(s) e^{st}, \text{poles}] = \sum_k A_k e^{s_k t} \tag{3.65}
\end{aligned}$$

which is a pure natural mode series with amplitude coefficients given by (3.34). Note that the complete pole series gives this response, with residue contributions due to

both the complex poles and the poles on the branch cut.

Since the two components of the time domain reflection coefficient are each given by a natural mode series by [13] and (3.65), the time domain reflection coefficient is also a natural mode series during this time period. It is important to note that the poles of the total reflection coefficient do not include the poles of the reflection coefficient for the air-backed slab. The poles of the air-backed slab reflection coefficient are in fact cancelled by poles of the reduced reflection coefficient, once this response turns on at the start of the late time. This cancellation gives a response that is a natural mode series based just on the poles of the total reflection coefficient, rather than some superset of the poles of the substructure reflection coefficients.

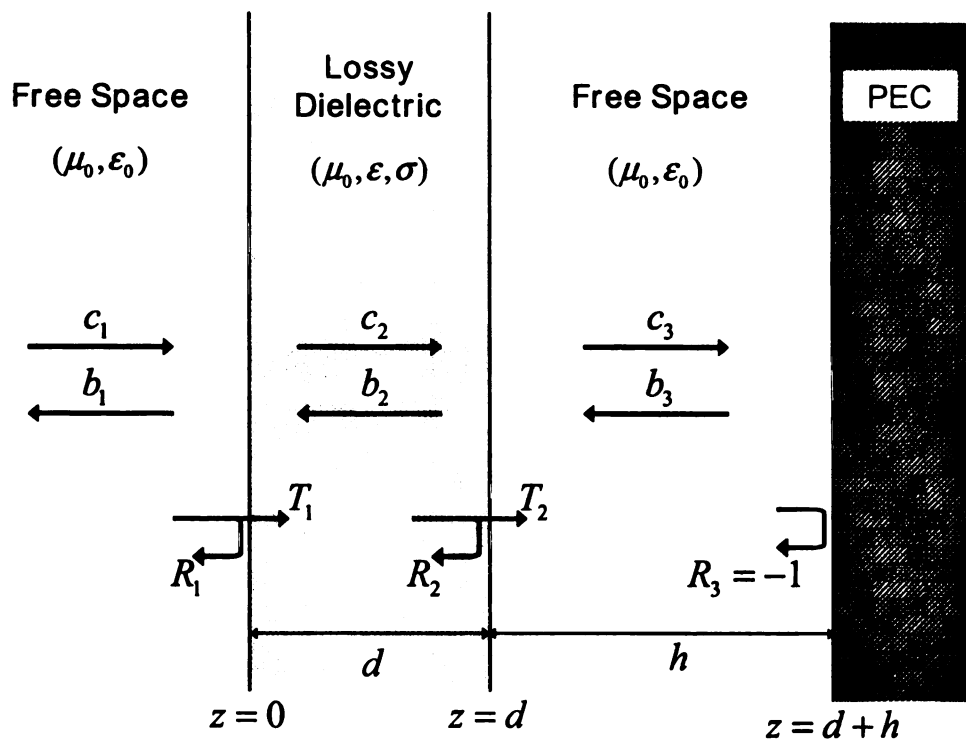


Figure 3.1. Air Lossy Air PEC

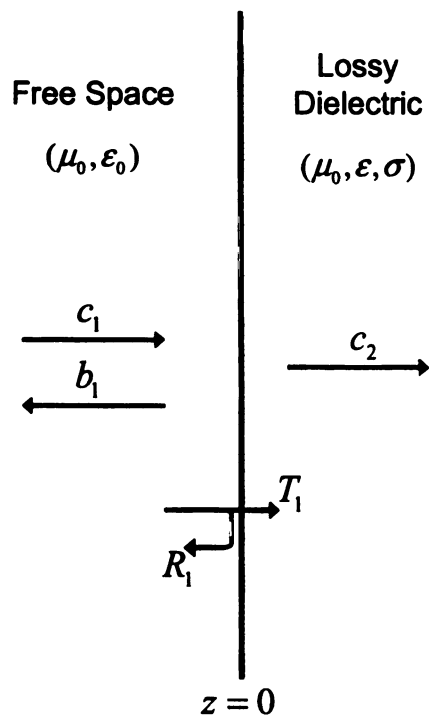


Figure 3.2. Single interface between free-space and a lossy dielectric

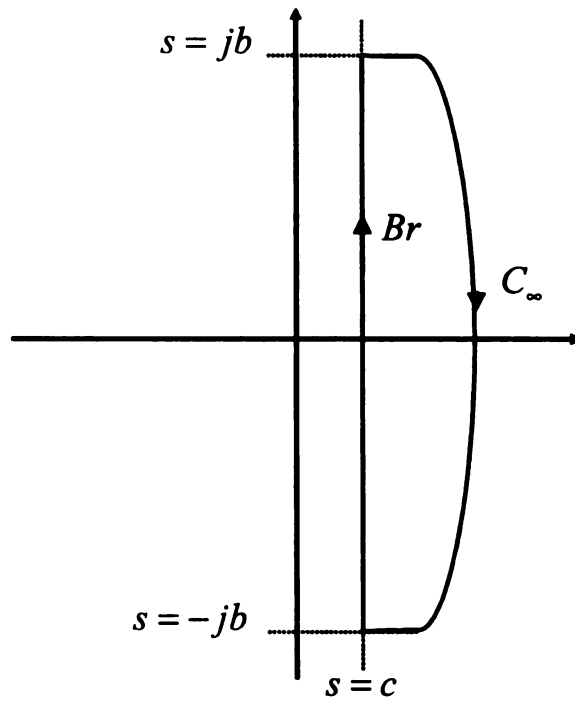


Figure 3.3. Closure of the Bromwich contour in the right half plane.  
 $|b| \rightarrow \infty, 0 < c < \infty$



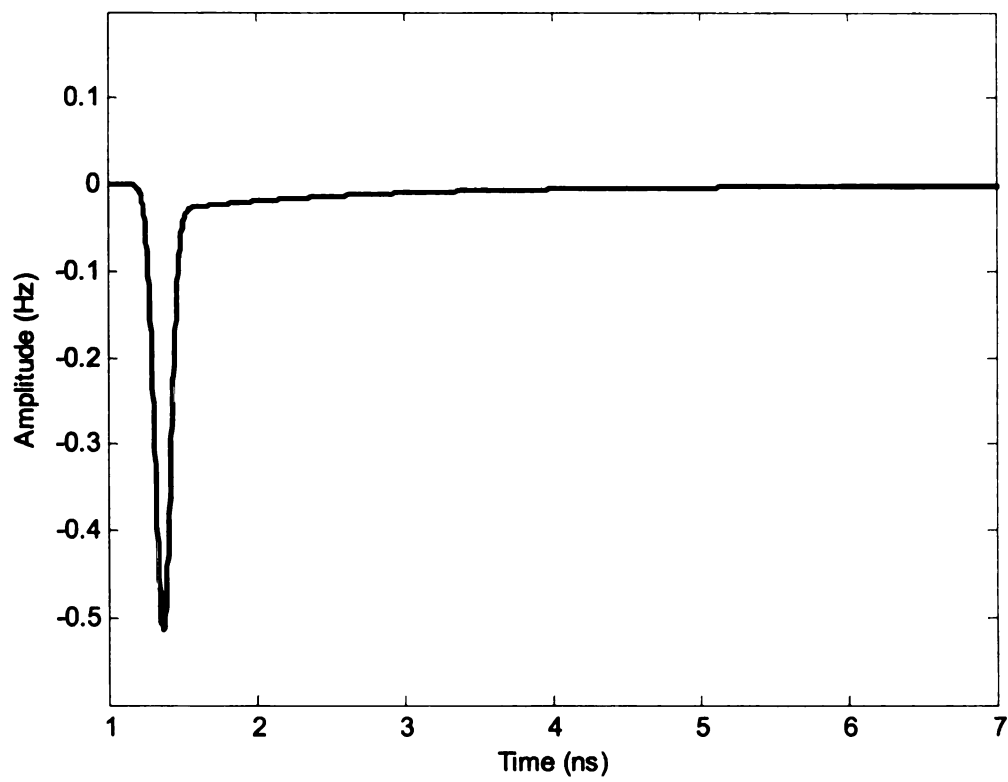


Figure 3.4. Interfacial reflection coefficient for the first interface

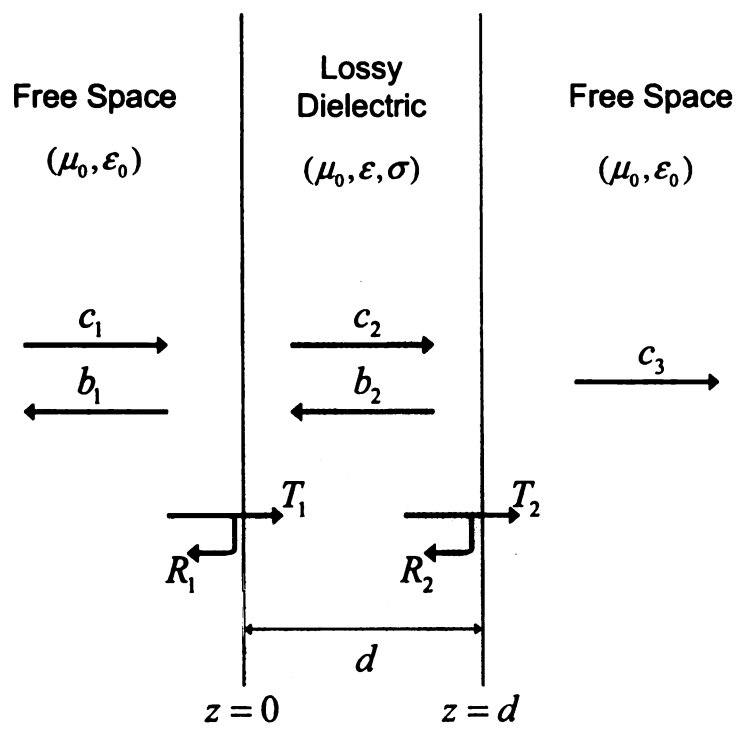


Figure 3.5. Air-backed lossy dielectric layer

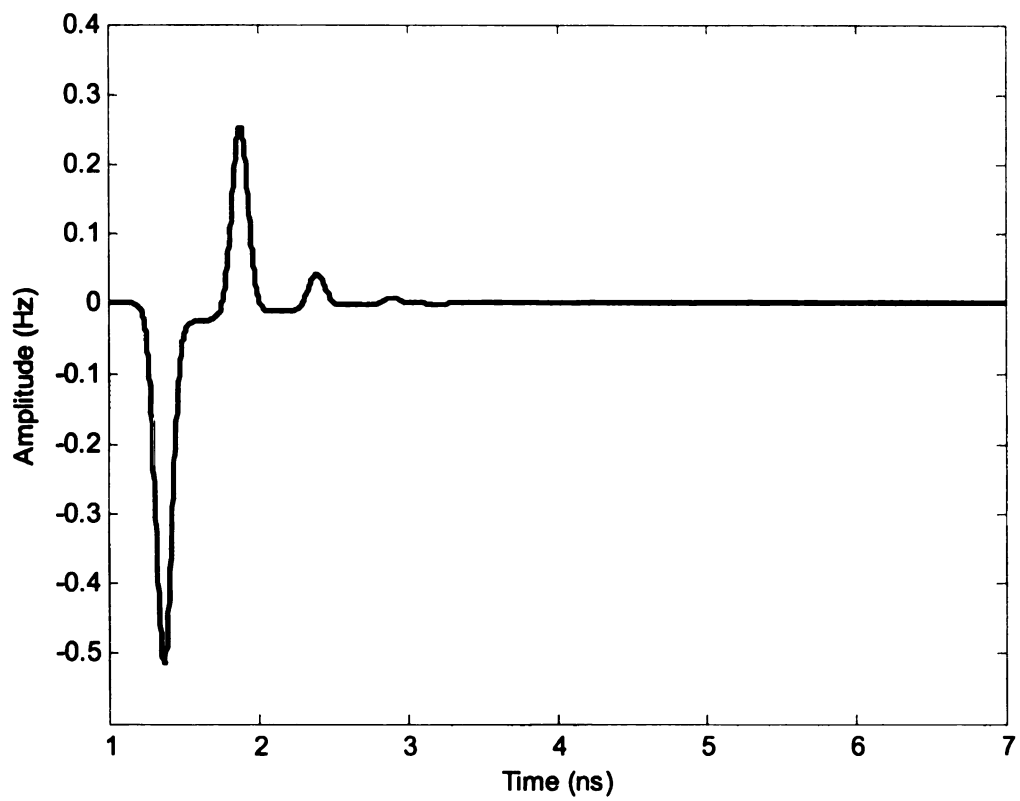


Figure 3.6. Temporal response from an air-backed lossy layer

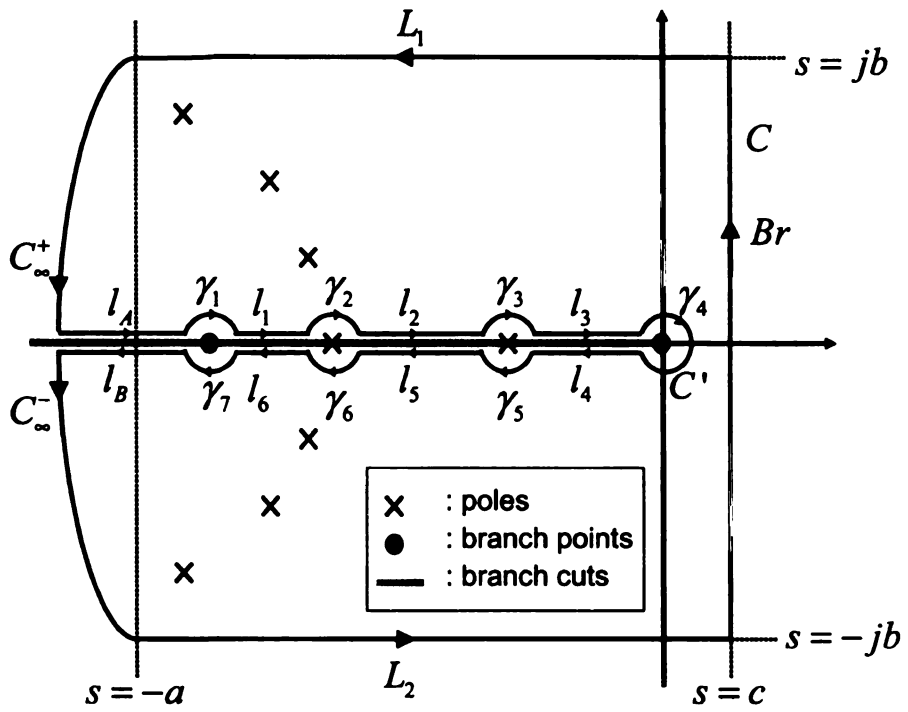


Figure 3.7. Closure of the Bromwich contour in the left half plane.  
 $|a|, |b| \rightarrow \infty, 0 < c < \infty$

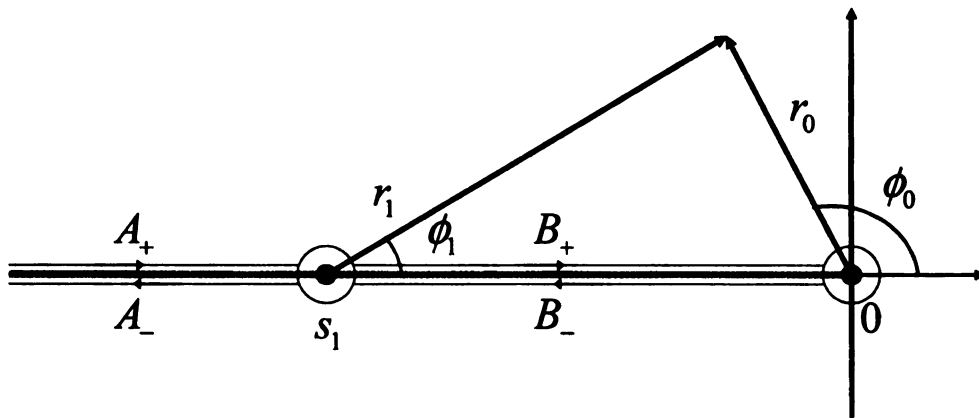


Figure 3.8. Inner contour integration paths for left half plane closure

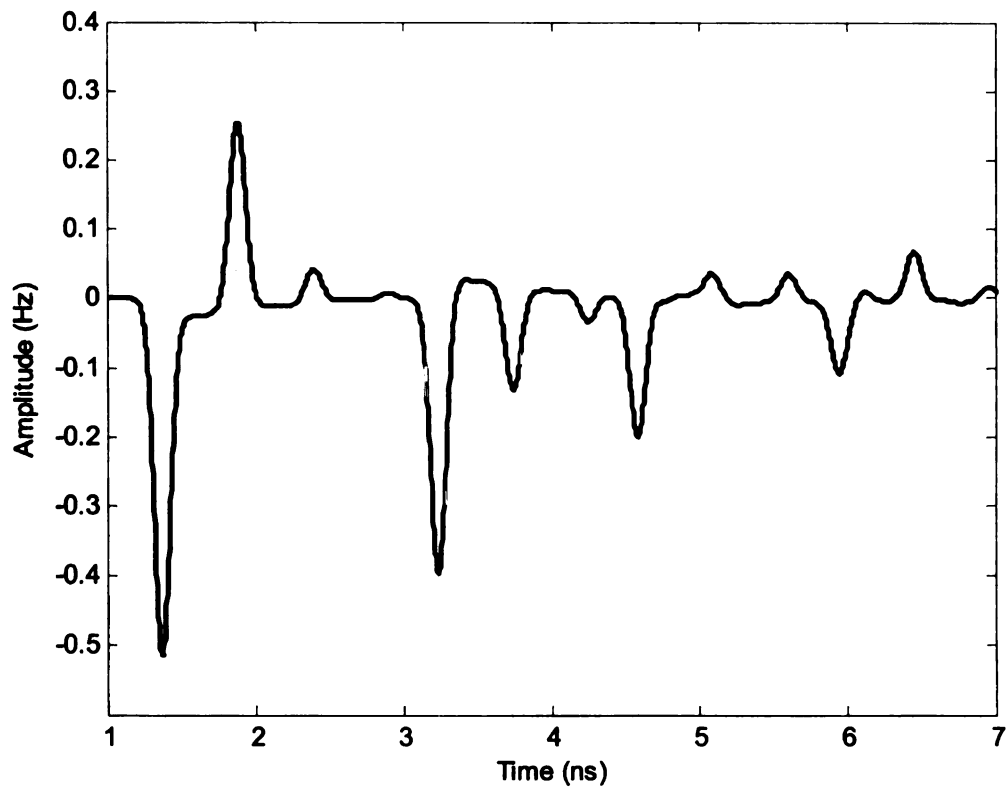


Figure 3.9. Temporal response of an air-backed lossy layer in the presence of a conducting screen

## CHAPTER 4

### MATERIAL-BACKED MATERIAL LAYERS

Having considered the addition of an interface to a geometry which was known to have a natural mode series representation after a finite time period in Chapter 3, the next step is to consider a single material layer backed by some material. Doing this, with the consideration that either the material layer, the backing layer, or both, are lossy, allows the examination of the effect of loss in one or both of the materials on the response of the system. This is also the first consideration of a backing layer other than free space or a perfect conductor.

As shown in Chapter 2, the frequency domain reflection coefficient can be obtained using the wave matrix method. For the single layer with a material backing, this reflection coefficient is given as

$$\Gamma(\omega) = \frac{R_1(\omega) + R_2(\omega)P_1^2(\omega)}{1 + R_1(\omega)R_2(\omega)P_1^2(\omega)}, \quad (4.1)$$

with interfacial reflection coefficients

$$R_1(\omega) = \frac{Z_1(\omega) - Z_0}{Z_1(\omega) + Z_0}, \quad (4.2a)$$

$$R_2(\omega) = \frac{Z_2(\omega) - Z_1(\omega)}{Z_2(\omega) + Z_1(\omega)}. \quad (4.2b)$$

Here  $Z_1(\omega)$  and  $Z_2(\omega)$  are the wave impedances in the material layers given for parallel (TM) and perpendicular (TE) polarizations, respectively, by

$$Z_i^{\parallel}(\omega) = \frac{k_{z,i}(\omega)\eta_i(\omega)}{k_i(\omega)} \quad (4.3a)$$

$$Z_i^{\perp}(\omega) = \frac{k_i(\omega)\eta_i(\omega)}{k_{z,i}(\omega)} \quad (4.3b)$$

where  $\eta_1(\omega)$  and  $\eta_2(\omega)$  are the frequency dependent intrinsic impedances of the material layers, given in terms of the complex permittivities,  $\epsilon_1^c(\omega)$  and  $\epsilon_2^c(\omega)$ , and permeabilities,  $\mu_1$  and  $\mu_2$ , as

$$\eta_1(\omega) = \sqrt{\frac{\mu_1}{\epsilon_1^c(\omega)}}, \quad \epsilon_1^c(\omega) = \epsilon_{1r}\epsilon_0 + \frac{\sigma_1}{j\omega}, \quad (4.4)$$

$$\eta_2(\omega) = \sqrt{\frac{\mu_2}{\epsilon_2^c(\omega)}}, \quad \epsilon_2^c(\omega) = \epsilon_{2r}\epsilon_0 + \frac{\sigma_2}{j\omega}, \quad (4.5)$$

Here,  $\epsilon_{1r}$  and  $\epsilon_{2r}$  are frequency independent relative permittivities, and  $\sigma_1$  and  $\sigma_2$  are the frequency independent conductivities of the first and second material, respectively. In this development, only nonmagnetic materials will be considered, thus  $\mu_1 = \mu_2 = \mu_0$ . The wave impedance in free space,  $Z_0$ , takes on the same forms as (4.3), but with frequency independent intrinsic impedance,  $\eta_0$ . Since  $k_i^2 = k_{x,i}^2 + k_{z,i}^2$  and  $k_{x,i} = k_{x,0} = k_0 \sin \theta_{in}$  to satisfy boundary conditions at all points on the planar surfaces, the wave impedances take the forms

$$Z_i^{\parallel}(\omega) = \frac{\eta_i}{k_i} \sqrt{k_i^2 - k_0^2 \sin^2 \theta_{in}}, \quad Z_0^{\parallel} = \eta_0 \cos \theta_{in} \quad (4.6a)$$

$$Z_i^{\perp}(\omega) = \frac{k_i \eta_i}{\sqrt{k_i^2 - k_0^2 \sin^2 \theta_{in}}}, \quad Z_0^{\perp} = \frac{\eta_0}{\cos \theta_{in}} \quad (4.6b)$$

for parallel and perpendicular polarizations, respectively.  $P_1(\omega)$  is a propagation factor given by

$$P_1(\omega) = e^{-jk_{z,1}d} \quad (4.7)$$

where  $d$  is the physical thickness of the material layer, and  $k_{z,1}$  is the z-directed wave number in region 1. For notational purposes, the propagation factor is written in the form

$$P_1^2(\omega) = e^{-j\omega\tau_1(\omega)}, \quad (4.8)$$



where the expression contained in the exponent is given by

$$\begin{aligned}
\omega\tau_1(\omega) &= 2k_{z,1}d \\
&= 2d\sqrt{k_1^2 - k_0^2 \sin^2 \theta_{in}} \\
&= \omega \frac{2d}{c} \sqrt{\frac{\epsilon_1^c}{\epsilon_0} - \sin^2 \theta_{in}}
\end{aligned} \tag{4.9}$$

To simplify notation, the quantity  $\bar{\epsilon}_1 = \epsilon_{1r} - \sin^2 \theta_{in}$  is defined, giving

$$\tau_1(\omega) = \frac{2d}{c} \sqrt{\bar{\epsilon}_1 + \frac{\sigma_1}{j\omega\epsilon_0}} \tag{4.10}$$

#### 4.1 Laplace domain representation

Since the frequency domain reflection coefficient,  $\Gamma(\omega)$ , exists, a Laplace domain representation also exists. This quantity is given, inserting the propagation factor,  $P_1(\omega)$ , from (4.8), as

$$\Gamma(s) = \Gamma(\omega) \Big|_{\omega=\frac{s}{j}} = \frac{R_1(s) + R_2(s)e^{-s\tau_1(s)}}{1 + R_1(s)R_2(s)e^{-s\tau_1(s)}} \tag{4.11}$$

with the expression appearing in the exponential term given by

$$\begin{aligned}
s\tau_1(s) &= j\omega\tau_1(\omega) \Big|_{\omega=\frac{s}{j}} \\
&= s \frac{2d}{c} \sqrt{\bar{\epsilon}_1 + \frac{\sigma_1}{s\epsilon_0}} \\
&= \frac{2d}{c} \sqrt{\bar{\epsilon}_1} \sqrt{s} \sqrt{s + \frac{\sigma_1}{\bar{\epsilon}_1\epsilon_0}} \\
&= \frac{2d}{c} \sqrt{\bar{\epsilon}_1} \sqrt{s} \sqrt{s - s_1}
\end{aligned} \tag{4.12}$$

where the quantity  $s_1 = -\sigma_1/\bar{\epsilon}_1\epsilon_0$  is defined. The interfacial reflection coefficients are given using (4.2) as  $R_1(s) = R_1(\omega) \Big|_{\omega=\frac{s}{j}}$  and  $R_2(s) = R_2(\omega) \Big|_{\omega=\frac{s}{j}}$ . The wave

impedances, which are needed to compute the interfacial reflection coefficients, are given for parallel polarization as

$$\begin{aligned}
Z_i^{\parallel}(s) &= Z_i^{\parallel}(\omega) \Big|_{\omega=\frac{s}{j}} \\
&= \frac{\eta_i}{k_i} \sqrt{k_i^2 - k_0^2 \sin^2 \theta_{in}} \\
&= \frac{k_0 \eta_i}{k_i} \sqrt{\frac{\epsilon_i^c}{\epsilon_0} - \sin^2 \theta_{in}} \\
&= \frac{\eta_0}{(\epsilon_i^c/\epsilon_0)} \sqrt{\bar{\epsilon}_i + \frac{\sigma_i}{s\epsilon_0}} \\
&= \frac{\eta_0 \sqrt{\bar{\epsilon}_i} \sqrt{s} \sqrt{s - s_i}}{s\epsilon_{ir} + \sigma_i/\epsilon_0},
\end{aligned} \tag{4.13a}$$

and for perpendicular polarization by

$$\begin{aligned}
Z_i^{\perp}(s) &= Z_i^{\perp}(\omega) \Big|_{\omega=\frac{s}{j}} \\
&= \frac{k_i \eta_i}{\sqrt{k_i^2 - k_0^2 \sin^2 \theta_{in}}} \\
&= \frac{k_i \eta_i}{k_0 \sqrt{(\epsilon_i^c/\epsilon_0) - \sin^2 \theta_{in}}} \\
&= \frac{\eta_0}{\sqrt{\bar{\epsilon}_i + (\sigma_i/s\epsilon_0)}} \\
&= \frac{\eta_0 s}{\sqrt{\bar{\epsilon}_i} \sqrt{s} \sqrt{s - s_i}}.
\end{aligned} \tag{4.13b}$$

with  $s_i = -\sigma_i/\bar{\epsilon}_i\epsilon_0$ . The interfacial reflection coefficients can thus be written for parallel and perpendicular polarizations using (4.2) and (4.13), as

$$R_1(s) = \begin{cases} \frac{\sqrt{\bar{\epsilon}_1} \sqrt{s} \sqrt{s - s_1} - (s\epsilon_{1r} + (\sigma_1/\epsilon_0)) \cos \theta_{in}}{\sqrt{\bar{\epsilon}_1} \sqrt{s} \sqrt{s - s_1} + (s\epsilon_{1r} + (\sigma_1/\epsilon_0)) \cos \theta_{in}} & \text{parallel polarization} \\ \frac{s \cos \theta_{in} - \sqrt{\bar{\epsilon}_1} \sqrt{s} \sqrt{s - s_1}}{s \cos \theta_{in} + \sqrt{\bar{\epsilon}_1} \sqrt{s} \sqrt{s - s_1}} & \text{perpendicular polarization} \end{cases} \tag{4.14}$$

and

$$R_2(s) = \begin{cases} \frac{(s\epsilon_{1r} + \frac{\sigma_1}{\epsilon_0})\sqrt{\epsilon_2}\sqrt{s}\sqrt{s-s_2} - (s\epsilon_{2r} + \frac{\sigma_2}{\epsilon_0})\sqrt{\epsilon_1}\sqrt{s}\sqrt{s-s_1}}{(s\epsilon_{1r} + \frac{\sigma_1}{\epsilon_0})\sqrt{\epsilon_2}\sqrt{s}\sqrt{s-s_2} + (s\epsilon_{2r} + \frac{\sigma_2}{\epsilon_0})\sqrt{\epsilon_1}\sqrt{s}\sqrt{s-s_1}} & \parallel \text{-pol} \\ \frac{\sqrt{\epsilon_1}\sqrt{s}\sqrt{s-s_1} - \sqrt{\epsilon_2}\sqrt{s}\sqrt{s-s_2}}{\sqrt{\epsilon_1}\sqrt{s}\sqrt{s-s_1} + \sqrt{\epsilon_2}\sqrt{s}\sqrt{s-s_2}} & \perp \text{-pol} \end{cases} \quad (4.15)$$

## 4.2 The time domain reflection coefficient

Using the frequency domain reflection coefficient found in Section 4.1, the time domain reflection coefficient of the material stack,  $\Gamma(t)$ , which is defined through an inverse temporal transform, can be found. This time domain reflection coefficient, when convolved with a finite duration incident waveform, gives the reflected field in the time domain.

In order to use the extinction pulse technique, it must be shown that the time domain reflection coefficient can be represented in terms of a natural mode series, after a finite period called the early time. The time period during which the natural mode series is an accurate representation of the time domain reflection coefficient is commonly referred to as the late time. Thus, in the late time, the time domain reflection coefficient should take the form:

$$\Gamma(t) = \sum_{n=1}^{\infty} A_n e^{s_n t} \quad (4.16)$$

where  $A_n$  is the amplitude coefficient associated with the  $n^{th}$  pole,  $s_n = \sigma_n + j\omega_n$ , of the frequency domain reflection coefficient. This representation of the temporal field is found by taking the inverse Laplace transform of (4.11), neglecting infinite contour contributions for which (4.11) does not approach zero uniformly. To perform this inverse transform, the singularities of the frequency domain reflection coefficient

are explored, and the evaluation of the integral

$$\int_{Br} \Gamma(s)e^{st} ds \quad (4.17)$$

is carried out through complex plane integration. This is done in several steps, corresponding to several ranges of time,  $t$ . Here, the integration is carried out along the contour  $Br$ , which is the Bromwich path. The Bromwich path, which defines the inverse Laplace transform, is a path in the complex  $s$ -plane which is taken parallel to the imaginary axis, to the right of all singular points. Evaluation of the integral in (4.17) gives the time domain reflection coefficient as

$$\Gamma(t) = \frac{1}{j2\pi} \int_{Br} \Gamma(s)e^{st} ds \quad (4.18)$$

when infinite contour contributions are neglected. In order to carry out the contour integration involved with the evaluation of this integral, singularities of the integrand need to be determined, and appropriate branches defined. These are explored in Section 4.2.1.

#### 4.2.1 Singularities of the frequency domain reflection coefficient

Singularities of the frequency domain reflection coefficient take on various forms. First,  $s\tau_1(s)$  and  $Z_i(s)$ , given by equations (4.12) and (4.13), respectively, contain complex square roots which lead to branch points at  $s = 0$ ,  $s = s_1$ , and  $s = s_2$ . Correspondingly, branch cuts are taken along the negative real axis to define the principal branches of the square root functions. In addition, observing that the frequency domain reflection coefficient may be written as

$$\Gamma(s) = \frac{N(s)}{D(s)}, \quad (4.19)$$

there are poles associated with the zeros of the denominator,  $D(s)$ . These poles will appear in the left half of the complex  $s$ -plane, with some lying on the real axis, and the rest occurring in conjugate pairs.

#### 4.2.2 Evaluation of the time domain reflection coefficient

Evaluation of the time domain reflection coefficient is carried out by factoring the frequency domain reflection coefficient such that the inverse Laplace transform of the individual components are physically meaningful during various time periods. The definition of these time periods, the factorization used in each time period, and the implications of these developments are the subjects of Sections 4.2.2.1 and 4.2.2.2.

##### 4.2.2.1 Early time: $t < T_1$

The early time is defined as the time period before a response is observed at the observation plane due to reflection from the second interface, as discussed in Section 2.4.1. The temporal response should be identical to the interfacial reflection between two semi-infinite media during this time period. Because of this, the frequency domain reflection coefficient is factored into the sum of the interfacial reflection coefficient of the first interface,  $R_1(s)$ , and a reduced reflection coefficient defined by

$$\begin{aligned}\Gamma'(s) &= \Gamma(s) - R_1(s) \\ &= \frac{(1 - R_1^2(s))R_2(s)e^{-s\tau_1(s)}}{1 + R_1(s)R_2(s)e^{-s\tau_1(s)}}.\end{aligned}\tag{4.20}$$

Since the inverse Laplace transform is a linear operation, the time domain reflection coefficient for the entire structure is given as a sum of the inverse Laplace transforms of the two components of the frequency domain reflection coefficient. The inverse Laplace transform of the interfacial reflection coefficient, given by  $R_1(t)$ , is rigorously developed in [14]. The evaluation of the inverse Laplace transform of the reduced reflection coefficient remains; this is given by  $\Gamma'(t) = \mathcal{L}^{-1}\{\tilde{\Gamma}'(s)\}$ , where  $\tilde{\Gamma}'(s)$  is identical to  $\Gamma'(s)$ , except for its behavior at infinity. This inverse transform is found

by evaluating

$$\frac{1}{j2\pi} \int_{Br} \Gamma'(s) e^{st} ds, \quad (4.21)$$

neglecting infinite contour contributions for which  $\Gamma'(s)$  does not go to zero uniformly.

On an infinite contour,  $C_\infty$ , exponential terms appearing in the numerator of the reduced reflection coefficient are given using (4.12) as,

$$\lim_{|s| \rightarrow \infty} \left\{ \frac{2d}{c} \sqrt{\bar{\epsilon}_1 + \frac{\sigma_1}{s\epsilon_0}} \right\} = \frac{2d}{c} \sqrt{\bar{\epsilon}_1} \triangleq T_1 \quad (4.22)$$

Letting  $t_1 = t - T_1$ , which is negative for  $t < T_1$ , evaluation of the integration along the Bromwich contour in (4.21) is obtained by closing the integration contour in the right half of the complex  $s$ -plane, as shown in Figure 4.3. Right half plane closure is justified here, since  $t_1$  is negative for the time period  $t < T_1$ . Note that  $T_1$  is the two-way transit time of the first material region, as discussed in Section 2.4.1. The early time is thus given by the time period  $t < T_1$ . The integration on the infinite contour  $C_\infty$  is given by

$$\int_{C_\infty} \Gamma'(s) e^{st} ds = \int_{C_\infty} \Gamma'(s) e^{sT_1} e^{st_1} ds \quad (4.23)$$

Here, *Jordan's Lemma* cannot be directly applied to evaluate the integral contributions over  $C_\infty$ , because the integrand does not go to zero as  $|s| \rightarrow \infty$  at all points on the contour. However, by definition of the time domain reflection coefficient, the infinite contour contribution is to be neglected, as discussed in Section 2.4. Thus, the time domain reflection coefficient in the early time is identical to the inverse Laplace transform of the interfacial reflection coefficient, as developed in [14].

#### 4.2.2.2 Late time: $t > T_1$

The late time of the response for this geometry is defined as the portion of the transient response after a response from a reflection off of the second interface arrives at the

observation plane, as discussed in Section 2.4.1. For this time period, the frequency domain reflection coefficient for the entire geometry, given by (4.11), is considered. Evaluation of the inverse transform of the reflection coefficient is carried out through the integration along the Bromwich path, neglecting infinite contour contributions; this integration is given by

$$\frac{1}{j2\pi} \int_{Br} \Gamma(s)e^{st} ds. \quad (4.24)$$

On an infinite contour,  $C_\infty$ , the exponential term appearing in the numerator of the reflection coefficient is given using the two-way transit time of the material layer,  $T_1$ , as in (4.22). Letting  $t_1 = t - T_1$ , which is positive for  $t > T_1$ , evaluation along the Bromwich contour in (4.24) is obtained by closing the integration contour in the left half of the complex  $s$ -plane, as shown in Figure 4.4. For closure of the integration contour in the left half plane many integration paths are involved. In this discussion, these integration paths will be referred to in two groups, the outer contour,  $C$ , which includes integration paths parameterized by quantities receding towards infinity, and the inner contour,  $C'$ , which includes integration paths taken along the branch cut. These integration contours are given by

$$C = Br \cup L_1 \cup C_\infty^+ \cup C_\infty^- \cup L_2$$

$$C' = l_A \cup \gamma_1 \cup \gamma_2 \cup \dots \cup \gamma_9 \cup l_1 \cup l_2 \cup \dots \cup l_8 \cup l_B$$

Using Cauchy's residue theorem, evaluation of the closed contour integration is given by

$$\oint_{C \cup C'} \Gamma(s)e^{st} ds = j2\pi \sum Res[\Gamma(s)e^{st}, \text{complex poles}]. \quad (4.25)$$

Thus, determination of the time domain reflection coefficient is possible provided the integral contribution from each path is known.

**Contributions from the outer contour,  $C$ .**

The Laplace inversion integral is found by computing (4.25) for the Bromwich path contribution in terms of the contributions from all other integration paths and computation of the residues from the enclosed simple poles. The outer contour,  $C$ , consists of various integration paths that are parameterized by quantities that recede towards infinity, including the Bromwich path which defines the inverse Laplace transform.

### Contributions from $C_{\infty}^+$ and $C_{\infty}^-$

Integral contributions from  $C_{\infty}^+$  and  $C_{\infty}^-$  are given directly by *Jordan's lemma*, as stated in Theorem 3.1. Since  $\Gamma(s) \rightarrow 0$  on the infinite contours,  $C_{\infty}^+$  and  $C_{\infty}^-$ , direct application of *Jordan's lemma* gives

$$\int_{C_{\infty}^+} \Gamma(s)e^{st} ds = 0 \quad (4.26)$$

$$\int_{C_{\infty}^-} \Gamma(s)e^{st} ds = 0. \quad (4.27)$$

### Contributions from $L_1$ and $L_2$

On  $L_1$  and  $L_2$ , *Jordan's Lemma* cannot be directly applied to evaluate the integral contributions because the integrand does not go to zero as  $|s| \rightarrow \infty$  at all points on the contours. However, by definition of the time domain reflection coefficient, the infinite contour contribution is to be neglected, as discussed in Section 2.4.

### Contributions from the inner contour, $C'$ .

The segments of the inner contour  $C'$ , which enclose the branch cut, can be broken into three groups. The first group consists of the contours  $\gamma_2$ ,  $\gamma_4$ ,  $\gamma_6$ , and  $\gamma_8$ , etc, which enclose the real poles on the branch cut. Note that two poles are shown on the real axis here, but more may appear depending on the properties of the material layers and the incidence angle. The second group is made up of contours  $\gamma_1$ ,  $\gamma_3$ ,  $\gamma_5$ ,  $\gamma_7$ , and  $\gamma_9$  that enclose the branch points. The straight line segments immediately above and below the branch cut make up the final group. Within this group, the segments  $l_A$  and  $l_B$ , which lie to the left of all of the branch points will be handled



separately from the segments  $l_1$  through  $l_8$ .

### Contributions from $\gamma_2$ , $\gamma_4$ , $\gamma_6$ , and $\gamma_8$

The integral contributions from the first group of contours, which enclose poles located on the branch cut, can be found by calculating the residues of  $\Gamma(s)e^{st}$  at the poles. It is found that all of the poles of  $\Gamma(s)$  are of first order and thus the residues may be found from

$$\text{Res}[\Gamma(s)e^{st}, \text{poles}] \Big|_{s=s_k} = \lim_{s \rightarrow s_k} (s - s_k) [\Gamma(s)e^{st}] = A_k e^{s_k t} \quad (4.28)$$

where

$$A_k = \frac{R_1(s_k) + R_2(s_k)e^{-s_k \tau_1(s_k)}}{\frac{d}{ds} [R_1(s)R_2(s)e^{-s\tau_1(s)}] \Big|_{s=s_k}} \quad (4.29)$$

is the complex mode amplitude, using l'Hôpital's rule to obtain the form shown here.

Carrying out the details of the differentiation gives

$$\begin{aligned} \frac{d}{ds} [R_1(s)R_2(s)e^{-s\tau_1(s)}] &= [R_2(s)e^{-s\tau_1(s)}] \frac{d}{ds} [R_1(s)] + [R_1(s)e^{-s\tau_1(s)}] \frac{d}{ds} [R_2(s)] \\ &\quad + [R_1(s)R_2(s)] \frac{d}{ds} [e^{-s\tau_1(s)}] \end{aligned}$$

with the derivative of the exponential term given by

$$\frac{d}{ds} [e^{-s\tau_1(s)}] = - \left[ \frac{d}{c} \sqrt{\bar{\epsilon}_1} \frac{2s - s_1}{\sqrt{s}\sqrt{s - s_1}} e^{-s\tau_1(s)} \right].$$

The derivative of the first interfacial reflection coefficient is found using (4.14) as

$$\frac{d}{ds} [R_1(s)] = \frac{\Upsilon_1(s)}{\Omega_1(s)}$$

where, for parallel polarization

$$\Upsilon_1(s) = \sqrt{\bar{\epsilon}_1} \frac{2s^2 - ss_1}{\sqrt{s}\sqrt{s-s_1}} \left( s\epsilon_{1r} + \frac{\sigma_1}{\epsilon_0} \right) \cos \theta_{in} - 2\epsilon_{1r} \sqrt{\bar{\epsilon}_1} \sqrt{s}\sqrt{s-s_1} \cos \theta_{in}$$

$$\Omega_1(s) = \left( s\epsilon_{1r} + \frac{\sigma_1}{\epsilon_0} \right)^2 \cos^2 \theta_{in} + 2 \left( s\epsilon_{1r} + \frac{\sigma_1}{\epsilon_0} \right) \sqrt{\bar{\epsilon}_1} \sqrt{s}\sqrt{s-s_1} \cos \theta_{in} + \bar{\epsilon}_1 s(s-s_1)$$

and for perpendicular polarization

$$\Upsilon_1(s) = 2\sqrt{\bar{\epsilon}_1} \sqrt{s}\sqrt{s-s_1} \cos \theta_{in} - \cos \theta_{in} \sqrt{\bar{\epsilon}_1} \frac{2s^2 - ss_1}{\sqrt{s}\sqrt{s-s_1}}$$

$$\Omega_1(s) = s^2 \cos^2 \theta_{in} + 2 \cos \theta_{in} s \sqrt{\bar{\epsilon}_1} \sqrt{s}\sqrt{s-s_1} + \bar{\epsilon}_1 s(s-s_1)$$

The derivative of the second interfacial reflection coefficient is found using (4.15) as

$$\frac{d}{ds} [R_2(s)] = \frac{\Upsilon_2(s)}{\Omega_2(s)}$$

where, for parallel polarization

$$\begin{aligned} \Upsilon_2(s) = \sqrt{\bar{\epsilon}_1} \sqrt{\bar{\epsilon}_2} \left[ \left( \epsilon_{1r} \frac{\sigma_2}{\epsilon_0} - \epsilon_{2r} \frac{\sigma_1}{\epsilon_0} \right) s \sqrt{s-s_1} \sqrt{s-s_2} \right. \\ \left. + \frac{1}{2} \frac{s(s_1-s_2)}{\sqrt{s-s_1} \sqrt{s-s_2}} \left( s\epsilon_{1r} + \frac{\sigma_1}{\epsilon_0} \right) \left( s\epsilon_{2r} + \frac{\sigma_2}{\epsilon_0} \right) \right] \end{aligned}$$

$$\begin{aligned} \Omega_2(s) = \left( s\epsilon_{1r} + \frac{\sigma_1}{\epsilon_0} \right)^2 \bar{\epsilon}_2 s(s-s_2) + \left( s\epsilon_{2r} + \frac{\sigma_2}{\epsilon_0} \right)^2 \bar{\epsilon}_1 s(s-s_1) \\ + 2 \left( s\epsilon_{1r} + \frac{\sigma_1}{\epsilon_0} \right) \left( s\epsilon_{2r} + \frac{\sigma_2}{\epsilon_0} \right) \sqrt{\bar{\epsilon}_1} \sqrt{\bar{\epsilon}_2} s \sqrt{s-s_1} \sqrt{s-s_2} \end{aligned}$$

and for perpendicular polarization as

$$\Upsilon_2(s) = \sqrt{\bar{\epsilon}_1} \sqrt{\bar{\epsilon}_2} \frac{s(s_1 - s_2)}{\sqrt{s - s_1} \sqrt{s - s_2}}$$

$$\Omega_2(s) = \bar{\epsilon}_2 s(s - s_2) + \bar{\epsilon}_1 s(s - s_1) + 2\sqrt{\bar{\epsilon}_1} \sqrt{\bar{\epsilon}_2} s \sqrt{s - s_1} \sqrt{s - s_2}$$

Here it is noted that the residues of the poles located on the branch cut must be evaluated carefully, taking into account the value of functions on each side of the branch cut. The evaluation of the integral contributions from each of the contours which combine to enclose the poles on the real axis are thus given as

$$\begin{aligned} \int_{\gamma_{2,74}} \Gamma(s) e^{st} ds &= -j\pi \sum \text{Res}[\Gamma(s)]_{(+)} e^{st}, \text{ real poles}, \\ \int_{\gamma_{6,78}} \Gamma(s) e^{st} ds &= -j\pi \sum \text{Res}[\Gamma(s)]_{(-)} e^{st}, \text{ real poles}, \end{aligned} \quad (4.30)$$

where the designators (+) and (-) correspond to the values of the frequency domain reflection coefficient above and below the branch cut, respectively.

#### Contributions from $\gamma_1$ , $\gamma_3$ , $\gamma_5$ , $\gamma_7$ , and $\gamma_9$

The integral contribution from the contour surrounding the branch point at  $s = 0$  can be computed by denoting the radius of  $\gamma_5$  as  $r_0$  and letting  $\phi_0$  be an angle measured counterclockwise from the real axis to the point on  $\gamma_5$ . This allows any point on the contour to be located as  $s = r_0 e^{j\phi_0}$ . The reflection coefficients on the  $\gamma_5$  contour are given in the limit of  $r_0 \rightarrow 0$ , i.e.,  $s \rightarrow 0$ , as

$$R_1(s) = \begin{cases} \frac{\sqrt{\bar{\epsilon}_1} \sqrt{s} \sqrt{s - s_1} - (s\epsilon_{1r} + \frac{\sigma_1}{\epsilon_0}) \cos \theta_{in}}{\sqrt{\bar{\epsilon}_1} \sqrt{s} \sqrt{s - s_1} + (s\epsilon_{1r} + \frac{\sigma_1}{\epsilon_0}) \cos \theta_{in}} \rightarrow -1 & \text{parallel polarization} \\ \frac{\sqrt{s} \cos \theta_{in} - \sqrt{\bar{\epsilon}_1} \sqrt{s - s_1}}{\sqrt{s} \cos \theta_{in} + \sqrt{\bar{\epsilon}_1} \sqrt{s - s_1}} \rightarrow -1 & \text{perpendicular polarization} \end{cases}$$

$$R_2(s) \rightarrow \begin{cases} \frac{(\frac{\sigma_1}{\epsilon_0})\sqrt{\epsilon_2}\sqrt{-s_2} - (\frac{\sigma_2}{\epsilon_0})\sqrt{\epsilon_1}\sqrt{-s_1}}{(\frac{\sigma_1}{\epsilon_0})\sqrt{\epsilon_2}\sqrt{-s_2} + (\frac{\sigma_2}{\epsilon_0})\sqrt{\epsilon_1}\sqrt{-s_1}} \triangleq C_1^{\parallel} & \text{parallel polarization} \\ \frac{\sqrt{\epsilon_1}\sqrt{-s_1} - \sqrt{\epsilon_2}\sqrt{-s_2}}{\sqrt{\epsilon_1}\sqrt{-s_1} + \sqrt{\epsilon_2}\sqrt{-s_2}} \triangleq C_1^{\perp} & \text{perpendicular polarization} \end{cases}$$

This gives the reflection coefficient from (4.11) as

$$\Gamma(s) = \frac{-1 + C_1^{\parallel, \perp}}{1 - C_1^{\parallel, \perp}} = -1$$

Thus,

$$\Gamma(s)e^{st} = -e^{st}$$

and

$$|\Gamma(s)e^{st}| \leq e^{r_0 t}.$$

Therefore

$$\left| \int_{\gamma_5} \Gamma(s)e^{st} ds \right| \leq 2\pi r_0 e^{r_0 t} \rightarrow 0, \quad (r_0 \rightarrow 0).$$

As a result, the integral contribution from the contour around the branch point at  $s = 0$  is given by

$$\int_{\gamma_5} \Gamma(s)e^{st} ds = 0. \quad (4.31)$$

The integral contributions from the contours surrounding the branch point at  $s = s_1$  can be computed by denoting the radius of both  $\gamma_3$  and  $\gamma_7$  as  $r_1$  and letting  $\phi_1$  be an angle measured counterclockwise from the real axis to a point on either  $\gamma_3$  or  $\gamma_7$ . This allows any point on the contours to be located as  $s = s_1 + r_1 e^{j\phi_1}$ . The reflection coefficients on the contours are given in the limit of  $r_1 \rightarrow 0$ , i.e.,  $s \rightarrow s_1$ , as

$$R_1(s) = \begin{cases} \frac{\sqrt{\epsilon_1}\sqrt{s}\sqrt{s-s_1} - (s\epsilon_{1r} + \frac{\sigma_1}{\epsilon_0})\cos\theta_{in}}{\sqrt{\epsilon_1}\sqrt{s}\sqrt{s-s_1} + (s\epsilon_{1r} + \frac{\sigma_1}{\epsilon_0})\cos\theta_{in}} \rightarrow -1 & \text{parallel polarization} \\ \frac{s\cos\theta_{in} - \sqrt{\epsilon_1}\sqrt{s}\sqrt{s-s_1}}{s\cos\theta_{in} + \sqrt{\epsilon_1}\sqrt{s}\sqrt{s-s_1}} \rightarrow 1 & \text{perpendicular polarization} \end{cases}$$

$$R_2(s) = \begin{cases} \frac{(s\epsilon_{1r} + \frac{\sigma_1}{\epsilon_0})\sqrt{\epsilon_2}\sqrt{s}\sqrt{s-s_2} - (s\epsilon_{2r} + \frac{\sigma_2}{\epsilon_0})\sqrt{\epsilon_1}\sqrt{s}\sqrt{s-s_1}}{(s\epsilon_{1r} + \frac{\sigma_1}{\epsilon_0})\sqrt{\epsilon_2}\sqrt{s}\sqrt{s-s_2} + (s\epsilon_{2r} + \frac{\sigma_2}{\epsilon_0})\sqrt{\epsilon_1}\sqrt{s}\sqrt{s-s_1}} \rightarrow 1 & \parallel \text{-pol} \\ \frac{\sqrt{\epsilon_1}\sqrt{s}\sqrt{s-s_1} - \sqrt{\epsilon_2}\sqrt{s}\sqrt{s-s_2}}{\sqrt{\epsilon_1}\sqrt{s}\sqrt{s-s_1} + \sqrt{\epsilon_2}\sqrt{s}\sqrt{s-s_2}} \rightarrow -1 & \perp \text{-pol} \end{cases}$$

This gives the reflection coefficient from (4.11) as

$$\Gamma(s) = \frac{\mp 1 \pm e^{-s\tau_1(s)}}{1 - e^{-s\tau_1(s)}} = \mp 1$$

Thus,

$$\Gamma(s)e^{st} = \mp e^{st}$$

and

$$|\Gamma(s)e^{st}| \leq e^{(s_1+r_1)t}.$$

Therefore

$$\left| \int_{\gamma_3, \gamma_7} \Gamma(s)e^{st} ds \right| \leq \pi r_1 e^{(s_1+r_1)t} \rightarrow 0, \quad (r_1 \rightarrow 0).$$

As a result, the integral contribution from the contour around the branch point at  $s = s_1$  is given by

$$\int_{\gamma_3, \gamma_7} \Gamma(s)e^{st} ds = 0. \quad (4.32)$$

The integral contributions from the contours surrounding the branch point at  $s = s_2$  can be computed by denoting the radius of both  $\gamma_1$  and  $\gamma_9$  as  $r_2$  and letting  $\phi_2$  be an angle measured counterclockwise from the real axis to a point on either  $\gamma_1$  or  $\gamma_9$ . This allows any point on the contours to be located as  $s = s_2 + r_2 e^{j\phi_2}$ . The reflection coefficients on the contours are given in the limit of  $r_2 \rightarrow 0$ , i.e.,  $s \rightarrow s_2$ , as

$$R_1(s) \rightarrow \begin{cases} \frac{\sqrt{\epsilon_1}\sqrt{s_2}\sqrt{s_2-s_1} - (s_2\epsilon_{1r} + \frac{\sigma_1}{\epsilon_0})\cos\theta_{in}}{\sqrt{\epsilon_1}\sqrt{s_2}\sqrt{s_2-s_1} + (s_2\epsilon_{1r} + \frac{\sigma_1}{\epsilon_0})\cos\theta_{in}} \triangleq C_2^{\parallel} & \parallel \text{-polarization} \\ \frac{s_2\cos\theta_{in} - \sqrt{\epsilon_1}\sqrt{s_2}\sqrt{s_2-s_1}}{s_2\cos\theta_{in} + \sqrt{\epsilon_1}\sqrt{s_2}\sqrt{s_2-s_1}} \triangleq C_2^{\perp} & \perp \text{-polarization} \end{cases}$$

$$R_2(s) = \begin{cases} \frac{(s\epsilon_{1r} + \frac{\sigma_1}{\epsilon_0})\sqrt{\epsilon_2}\sqrt{s}\sqrt{s-s_2} - (s\epsilon_{2r} + \frac{\sigma_2}{\epsilon_0})\sqrt{\epsilon_1}\sqrt{s}\sqrt{s-s_1}}{(s\epsilon_{1r} + \frac{\sigma_1}{\epsilon_0})\sqrt{\epsilon_2}\sqrt{s}\sqrt{s-s_2} + (s\epsilon_{2r} + \frac{\sigma_2}{\epsilon_0})\sqrt{\epsilon_1}\sqrt{s}\sqrt{s-s_1}} \rightarrow -1 & \parallel \text{-pol} \\ \frac{\sqrt{\epsilon_1}\sqrt{s}\sqrt{s-s_1} - \sqrt{\epsilon_2}\sqrt{s}\sqrt{s-s_2}}{\sqrt{\epsilon_1}\sqrt{s}\sqrt{s-s_1} + \sqrt{\epsilon_2}\sqrt{s}\sqrt{s-s_2}} \rightarrow 1 & \perp \text{-pol} \end{cases}$$

This gives the reflection coefficient from (4.11) as

$$\Gamma(s) = \frac{C_2^{\parallel, \perp} \mp e^{-s\tau_1(s)}}{1 \mp C_2^{\parallel, \perp} e^{-s\tau_1(s)}} \triangleq D^{\parallel, \perp}$$

Thus,

$$\Gamma(s)e^{st} = D^{\parallel, \perp} e^{st}$$

and

$$|\Gamma(s)e^{st}| \leq |D^{\parallel, \perp}| e^{(s_2+r_2)t}.$$

Therefore

$$\left| \int_{\gamma_1, \gamma_9} \Gamma(s)e^{st} ds \right| \leq \pi r_2 |D^{\parallel, \perp}| e^{(s_2+r_2)t} \rightarrow 0, \quad (r_2 \rightarrow 0).$$

As a result, the integral contribution from the contour around the branch point at  $s = s_2$  is given by

$$\int_{\gamma_1, \gamma_9} \Gamma(s)e^{st} ds = 0. \quad (4.33)$$

### Contributions from segments above and below the branch cuts

The contributions from the straight line segments of the inner contour immediately above and below the branch cuts are separated into two groups. The first group is given by  $l_A$  and  $l_B$ , which lie to the left of all the branch points. The rest of the contours,  $l_1$  through  $l_8$ , lie to the right of the leftmost branch point. Note that if more than two poles lie on the real axis, more contours would be included in at least one of these groups. The developments here will remain valid for any number of integration contours along the branch cut.

Using (4.11), and noting that this equation can be written simply as  $\Gamma(s) = N(s)/D(s)$ , the numerator and denominator of the frequency domain reflection coefficient can be put into the forms

$$\begin{aligned}
N(s) &= (Z_1 - Z_0)(Z_2 + Z_1) + (Z_2 - Z_1)(Z_1 + Z_0)e^{-s\tau_1(s)} \\
&= (Z_1Z_2 - Z_0Z_1)(1 + e^{-s\tau_1(s)}) + (Z_1^2 - Z_0Z_2)(1 - e^{-s\tau_1(s)}) \\
&= (Z_1Z_2 - Z_0Z_1) \cos\left(\frac{s\tau_1(s)}{2j}\right) + j(Z_1^2 - Z_0Z_2) \sin\left(\frac{s\tau_1(s)}{2j}\right) \\
&= \mathcal{X} - \mathcal{Y},
\end{aligned} \tag{4.34}$$

and

$$\begin{aligned}
D(s) &= (Z_1 + Z_0)(Z_2 + Z_1) + (Z_1 - Z_0)(Z_2 - Z_1)e^{-s\tau_1(s)} \\
&= (Z_1Z_2 + Z_0Z_1)(1 + e^{-s\tau_1(s)}) + (Z_1^2 + Z_0Z_2)(1 - e^{-s\tau_1(s)}) \\
&= (Z_1Z_2 + Z_0Z_1) \cos\left(\frac{s\tau_1(s)}{2j}\right) + j(Z_1^2 + Z_0Z_2) \sin\left(\frac{s\tau_1(s)}{2j}\right) \\
&= \mathcal{X} + \mathcal{Y},
\end{aligned} \tag{4.35}$$

where a multiplication and division by  $2e^{s\tau_1/2}$  has been used, and the quantities  $\mathcal{X}$  and  $\mathcal{Y}$  have been defined as

$$\mathcal{X} = Z_1Z_2 \cos\left(\frac{s\tau_1(s)}{2j}\right) + jZ_1^2 \sin\left(\frac{s\tau_1(s)}{2j}\right) \tag{4.36}$$

$$\mathcal{Y} = Z_0Z_1 \cos\left(\frac{s\tau_1(s)}{2j}\right) + jZ_0Z_2 \sin\left(\frac{s\tau_1(s)}{2j}\right) \tag{4.37}$$

This allows the frequency domain reflection coefficient to be written as

$$\begin{aligned}
\Gamma(s) &= \frac{\mathcal{X} - \mathcal{Y}}{\mathcal{X} + \mathcal{Y}} \\
&= \frac{\mathcal{X}^2 - 2\mathcal{X}\mathcal{Y} + \mathcal{Y}^2}{\mathcal{X}^2 + \mathcal{Y}^2}.
\end{aligned} \tag{4.38}$$

Using this expression, the behavior of the reflection coefficient about the branch cut can be examined by evaluating the quantities  $\mathcal{X}^2$ ,  $\mathcal{Y}^2$ , and  $\mathcal{X}\mathcal{Y}$  about the branch cut.

Defining the quantity  $\Phi_1 = \frac{s\tau_1(s)}{2j}$  and writing these expressions out gives

$$\mathcal{X}^2 = Z_1^2 Z_2^2 \cos^2 \Phi_1 + j2Z_1^2 Z_2 (Z_1 \sin \Phi_1) \cos \Phi_1 - Z_1^4 \sin^2 \Phi_1 \quad (4.39)$$

$$\mathcal{Y}^2 = Z_0^2 Z_1^2 \cos^2 \Phi_1 + j2Z_0^2 Z_2 (Z_1 \sin \Phi_1) \cos \Phi_1 - Z_0^2 Z_2^2 \sin^2 \Phi_1 \quad (4.40)$$

$$\mathcal{X}\mathcal{Y} = Z_0 Z_1^2 Z_2 [\cos^2 \Phi_1 - \sin^2 \Phi_1] + j[Z_2^2 + Z_1^2] Z_0 (Z_1 \sin \Phi_1) \cos \Phi_1 \quad (4.41)$$

Branch cuts which define the principal branches of the complex square root functions of the wave impedances and propagation factors are taken along the negative real axis. These branches are defined by  $-\pi < \phi_0 \leq \pi$ , and  $-\pi < \phi_i \leq \pi$ . Looking at Figure 4.5, begin by examining the integration paths designated as  $A_+$  and  $A_-$ . For the contour  $A_+$ ,  $\phi_1 = \phi_\alpha = \phi_\beta = \pi$ . Letting  $s = -x$ , where  $x$  is a nonnegative real number, denote a point on the negative real axis, the product of the square root functions found in the wave impedances and exponential terms take the form

$$\sqrt{s}\sqrt{s-s_\alpha} = \sqrt{\tau_1}\sqrt{\tau_\alpha}e^{j(\phi_1+\phi_\alpha)/2} = \sqrt{x}\sqrt{x+s_\alpha}e^{j\pi} = -\sqrt{x}\sqrt{x+s_\alpha} \quad (4.42)$$

$$\sqrt{s}\sqrt{s-s_\beta} = \sqrt{\tau_1}\sqrt{\tau_\beta}e^{j(\phi_1+\phi_\beta)/2} = \sqrt{x}\sqrt{x+s_\beta}e^{j\pi} = -\sqrt{x}\sqrt{x+s_\beta} \quad (4.43)$$

where  $s_\alpha$  and  $s_\beta$  represent the two branch points  $s_1$  and  $s_2$ , such that  $|s_\alpha| \leq |s_\beta|$ . Which of the branch points  $s_1$  and  $s_2$  correspond to  $s_\alpha$ , and which to  $s_\beta$ , depends on material properties in each region, and incidence angle. Every case will be examined in this section.

On  $A_-$ ,  $\phi_1 = \phi_\alpha = \phi_\beta = -\pi$ , and the products of square roots found in the wave



impedances and exponential terms are given by

$$\sqrt{s}\sqrt{s-s_\alpha} = \sqrt{x}\sqrt{x+s_\alpha}e^{-j\pi} = -\sqrt{x}\sqrt{x+s_\alpha} \quad (4.44)$$

$$\sqrt{s}\sqrt{s-s_\beta} = \sqrt{x}\sqrt{x+s_\beta}e^{-j\pi} = -\sqrt{x}\sqrt{x+s_\beta} \quad (4.45)$$

Thus, the products of these square roots are analytic on the  $A$  contours, and

$$\Gamma(s)\Big|_{A+} = \Gamma(s)\Big|_{A-}. \quad (4.46)$$

Since the integrations above and below the branch cut are taken in opposite directions,

$$\int_{l_A} \Gamma(s)e^{st}ds + \int_{l_B} \Gamma(s)e^{st}ds = 0 \quad (4.47)$$

On  $B_+$ ,  $\phi_1 = \phi_\alpha = \pi$ ,  $\phi_\beta = 0$ , and the products of square root functions found in the wave impedances and exponential terms are given by

$$\sqrt{s}\sqrt{s-s_\alpha} = \sqrt{x}\sqrt{x+s_\alpha}e^{j\pi} = -\sqrt{x}\sqrt{x+s_\alpha} \quad (4.48)$$

$$\sqrt{s}\sqrt{s-s_\beta} = \sqrt{x}\sqrt{-x-s_\beta}e^{j\pi/2} = j\sqrt{x}\sqrt{-x-s_\beta} \quad (4.49)$$

Similarly, on  $B_-$ ,  $\phi_1 = \phi_\alpha = -\pi$ ,  $\phi_\beta = 0$

$$\sqrt{s}\sqrt{s-s_\alpha} = \sqrt{x}\sqrt{x+s_\alpha}e^{-j\pi} = -\sqrt{x}\sqrt{x+s_\alpha} \quad (4.50)$$

$$\sqrt{s}\sqrt{s-s_\beta} = \sqrt{x}\sqrt{-x-s_\beta}e^{-j\pi/2} = -j\sqrt{x}\sqrt{-x-s_\beta} \quad (4.51)$$

On  $C_+$ ,  $\phi_1 = \pi$ ,  $\phi_\alpha = \phi_\beta = 0$ , and the products of square root functions found in

the wave impedances and exponential terms are given by

$$\sqrt{s}\sqrt{s-s_\alpha} = \sqrt{x}\sqrt{-x-s_\alpha}e^{j\pi/2} = j\sqrt{x}\sqrt{-x-s_\alpha} \quad (4.52)$$

$$\sqrt{s}\sqrt{s-s_\beta} = \sqrt{x}\sqrt{-x-s_\beta}e^{j\pi/2} = j\sqrt{x}\sqrt{-x-s_\beta} \quad (4.53)$$

Similarly, on  $C_-$ ,  $\phi_1 = -\pi$ ,  $\phi_\alpha = \phi_\beta = 0$

$$\sqrt{s}\sqrt{s-s_\alpha} = \sqrt{x}\sqrt{-x-s_\alpha}e^{-j\pi/2} = -j\sqrt{x}\sqrt{-x-s_\alpha} \quad (4.54)$$

$$\sqrt{s}\sqrt{s-s_\beta} = \sqrt{x}\sqrt{-x-s_\beta}e^{-j\pi/2} = -j\sqrt{x}\sqrt{-x-s_\beta} \quad (4.55)$$

The products of square roots along the  $B$  and  $C$  contours are not found to be analytic when moving from a point on one side of the branch cut to a point on the other side, so further investigation into the form of the reflection coefficient is needed. To do this, individual consideration is given to various combinations of lossy and lossless materials.

#### 4.2.2.2.1 Lossy layer backed by a lossless half space .

For a lossy layer backed by a lossless half space, the branch point at  $s = s_2$ , where  $s_2 = -\sigma_2/\bar{\epsilon}_2\epsilon_0$ , disappears, and only the paths  $C_+$  and  $C_-$  need to be considered, since  $s_\alpha = s_2 = 0$ . Note that the wave impedance in region 2 becomes  $Z_2 = \eta_0\sqrt{\bar{\epsilon}_2}/\epsilon_{2r}$ , which is not a function of  $s$ . Taking  $s_\beta = s_1$ , the wave impedance of region 1 is given using (4.53) and (4.55) by

$$Z_1|_{C_+} = \frac{-\eta_0 x}{j\sqrt{\bar{\epsilon}_1}\sqrt{x}\sqrt{-x-s_1}} = Z_{1+} \quad (4.56)$$

$$Z_1|_{C_-} = \frac{-\eta_0 x}{-j\sqrt{\bar{\epsilon}_1}\sqrt{x}\sqrt{-x-s_1}} = Z_{1-} \quad (4.57)$$

Similarly, the term  $\Phi_1 = s\tau_1(s)/2j$  is given by

$$\Phi_1 \Big|_{C_+} = \frac{d}{c} \sqrt{\epsilon_1} \sqrt{x} \sqrt{-x - s_1} = \Phi_{1+} \quad (4.58)$$

$$\Phi_1 \Big|_{C_-} = -\frac{d}{c} \sqrt{\epsilon_1} \sqrt{x} \sqrt{-x - s_1} = \Phi_{1-} \quad (4.59)$$

Thus, on the contour  $C_+$ , the terms which determine the behavior of the reflection coefficient are given by

$$\mathcal{X}^2 = Z_{1+}^2 Z_2^2 \cos^2 \Phi_{1+} + j2Z_{1+}^2 Z_2 (Z_{1+} \sin \Phi_{1+}) \cos \Phi_{1+} - Z_{1+}^4 \sin^2 \Phi_{1+}$$

$$\mathcal{Y}^2 = Z_0^2 Z_{1+}^2 \cos^2 \Phi_{1+} + j2Z_0^2 Z_2 (Z_{1+} \sin \Phi_{1+}) \cos \Phi_{1+} - Z_0^2 Z_2^2 \sin^2 \Phi_{1+}$$

$$\mathcal{X}\mathcal{Y} = Z_0 Z_{1+}^2 Z_2 [\cos^2 \Phi_{1+} - \sin^2 \Phi_{1+}] + j[Z_2^2 + Z_{1+}^2] Z_0 (Z_{1+} \sin \Phi_{1+}) \cos \Phi_{1+}$$

Similarly, on the contour,  $C_-$ ,

$$\mathcal{X}^2 = Z_{1-}^2 Z_2^2 \cos^2 \Phi_{1-} + j2Z_{1-}^2 Z_2 (Z_{1-} \sin \Phi_{1-}) \cos \Phi_{1-} - Z_{1-}^4 \sin^2 \Phi_{1-}$$

$$\mathcal{Y}^2 = Z_0^2 Z_{1-}^2 \cos^2 \Phi_{1-} + j2Z_0^2 Z_2 (Z_{1-} \sin \Phi_{1-}) \cos \Phi_{1-} - Z_0^2 Z_2^2 \sin^2 \Phi_{1-}$$

$$\mathcal{X}\mathcal{Y} = Z_0 Z_{1-}^2 Z_2 [\cos^2 \Phi_{1-} - \sin^2 \Phi_{1-}] + j[Z_2^2 + Z_{1-}^2] Z_0 (Z_{1-} \sin \Phi_{1-}) \cos \Phi_{1-}$$

Note that wave impedances that change sign as a point moves from  $C_+$  to  $C_-$  across the branch cut appear raised to even powers, or grouped with a sine function that also changes sign upon crossing the branch cut. Thus, the quantities  $\mathcal{X}^2$ ,  $\mathcal{Y}^2$ , and  $\mathcal{X}\mathcal{Y}$  are even about the branch cut, and by (4.38),

$$\Gamma(s) \Big|_{C_+} = \Gamma(s) \Big|_{C_-} \quad (4.60)$$

So, for the lossy layer backed by a lossless half space, the integral contributions from

contours above and below the branch cut are given by

$$\int_{l_1 \cup l_2 \cup l_3 \cup l_4} \Gamma(s) e^{st} ds + \int_{l_5 \cup l_6 \cup l_7 \cup l_8} \Gamma(s) e^{st} ds = 0 \quad (4.61)$$

since integrations are taken in opposite directions.

#### 4.2.2.2.2 Lossless layer backed by a lossy half space .

For a lossless layer backed by a lossy half space, the branch point at  $s = s_1$ , where  $s_1 = -\sigma_1/\bar{\epsilon}_1\epsilon_0$ , disappears, and only the paths  $C_+$  and  $C_-$  need to be considered, since  $s_\alpha = s_1 = 0$ . Note that the wave impedance in region 1 becomes  $Z_1 = \eta_0\sqrt{\bar{\epsilon}_1}/\epsilon_{1r}$ , which is not a function of  $s$ . Also, the term  $\tau_1(s)$  becomes a constant; this gives  $\Phi_1$  proportional to  $s$ , which is analytic across the branch cut. Thus, taking  $s_\beta = s_2$ , the wave impedance of region 2 is given using (4.53) and (4.55) by

$$Z_2 \Big|_{C_+} = \frac{-\eta_0 x}{j\sqrt{\bar{\epsilon}_2}\sqrt{x}\sqrt{-x-s_2}} = Z_{2+} \quad (4.62)$$

$$Z_2 \Big|_{C_-} = \frac{\eta_0 x}{j\sqrt{\bar{\epsilon}_2}\sqrt{x}\sqrt{-x-s_2}} = Z_{2-} \quad (4.63)$$

Thus, on the contour  $C_+$ , the terms which determine the behavior of the reflection coefficient are given by

$$\mathcal{X}^2 = Z_1^2 Z_{2+}^2 \cos^2 \Phi_1 + j2Z_1^2 Z_{2+} (Z_1 \sin \Phi_1) \cos \Phi_1 - Z_1^4 \sin^2 \Phi_1$$

$$\mathcal{Y}^2 = Z_0^2 Z_1^2 \cos^2 \Phi_1 + j2Z_0^2 Z_{2+} (Z_1 \sin \Phi_1) \cos \Phi_1 - Z_0^2 Z_{2+}^2 \sin^2 \Phi_1$$

$$\mathcal{X}\mathcal{Y} = Z_0 Z_1^2 Z_{2+} [\cos^2 \Phi_1 - \sin^2 \Phi_1] + j[Z_{2+}^2 + Z_1^2] Z_0 (Z_1 \sin \Phi_1) \cos \Phi_1$$

Similarly, on the contour,  $C_-$ ,

$$\begin{aligned}\mathcal{X}^2 &= Z_1^2 Z_{2-}^2 \cos^2 \Phi_1 + j2Z_1^2 Z_{2-} (Z_1 \sin \Phi_1) \cos \Phi_1 - Z_1^4 \sin^2 \Phi_1 \\ \mathcal{Y}^2 &= Z_0^2 Z_1^2 \cos^2 \Phi_1 + j2Z_0^2 Z_{2-} (Z_1 \sin \Phi_1) \cos \Phi_1 - Z_0^2 Z_{2-}^2 \sin^2 \Phi_1 \\ \mathcal{X}\mathcal{Y} &= Z_0 Z_1^2 Z_{2-} [\cos^2 \Phi_1 - \sin^2 \Phi_1] + j[Z_{2-}^2 + Z_1^2] Z_0 (Z_1 \sin \Phi_1) \cos \Phi_1\end{aligned}$$

Note that wave impedances that change sign as a point moves from  $C_+$  to  $C_-$  across the branch cut are not grouped with a sine function that changes sign between the contours. Thus, the quantities  $\mathcal{X}^2$ ,  $\mathcal{Y}^2$ , and  $\mathcal{X}\mathcal{Y}$  are not even about the branch cut for the lossless layer backed by a lossy half space. Thus, using (4.38),

$$\Gamma(s)\Big|_{C_+} \neq \Gamma(s)\Big|_{C_-} \quad (4.64)$$

This is an important result, because the time domain reflection coefficient will not be given by a pure natural mode series in the late time since the integral contributions from contours above and below the branch cut do not cancel; i.e.

$$\int_{l_1 \cup l_2 \cup l_3 \cup l_4} \Gamma(s) e^{st} ds + \int_{l_5 \cup l_6 \cup l_7 \cup l_8} \Gamma(s) e^{st} ds \neq 0. \quad (4.65)$$

#### 4.2.2.2.3 Lossy layer backed by a lossy half space .

For the case of the lossy layer backed by a lossy half space, evaluation of the contours above and below the branch cut are examined in three cases. These cases represent combinations of material parameters for which  $|s_1| < |s_2|$ ,  $|s_1| > |s_2|$ , and  $|s_1| = |s_2|$ .

**Case 1:**  $(\sigma_1/\bar{\epsilon}_1) < (\sigma_2/\bar{\epsilon}_2)$

Examining each combination of material parameters for the two material regions, beginning with the case of  $(\sigma_1/\bar{\epsilon}_1) < (\sigma_2/\bar{\epsilon}_2)$ , the behavior of the frequency domain

reflection coefficient on each side of the branch cut is determined. For this first case,  $s_\alpha = s_1$  and  $s_\beta = s_2$ . Using (4.48)-(4.55), wave impedances on each integration path take on the form

$$Z_1 \Big|_{B_+} = Z_1 \Big|_{B_-} = \frac{\eta_0 x}{\sqrt{\epsilon_1} \sqrt{x} \sqrt{x + s_1}} = Z_1 \quad (4.66)$$

$$Z_1 \Big|_{C_+} = \frac{-\eta_0 x}{j \sqrt{\epsilon_1} \sqrt{x} \sqrt{-x - s_1}} = Z_{1+} \quad (4.67)$$

$$Z_1 \Big|_{C_-} = \frac{\eta_0 x}{j \sqrt{\epsilon_1} \sqrt{x} \sqrt{-x - s_1}} = Z_{1-} \quad (4.68)$$

$$Z_2 \Big|_{B_+, C_+} = \frac{-\eta_0 x}{j \sqrt{\epsilon_2} \sqrt{x} \sqrt{-x - s_2}} = Z_{2+} \quad (4.69)$$

$$Z_2 \Big|_{B_-, C_-} = \frac{\eta_0 x}{j \sqrt{\epsilon_2} \sqrt{x} \sqrt{-x - s_2}} = Z_{2-} \quad (4.70)$$

thus,  $Z_{1+} = -Z_{1-}$ ,  $Z_{2+} = -Z_{2-}$ . The exponential terms appearing in the frequency domain reflection coefficient are given using

$$s\tau_1 \Big|_{B_+} = s\tau_1 \Big|_{B_-} = -\frac{2d}{c} \sqrt{\epsilon_1} \sqrt{x} \sqrt{x + s_1} = -2\Phi_1 \quad (4.71)$$

$$s\tau_1 \Big|_{C_+} = j \frac{2d}{c} \sqrt{\epsilon_1} \sqrt{x} \sqrt{-x - s_1} = j2\Phi_{1+} \quad (4.72)$$

$$s\tau_1 \Big|_{C_-} = -j \frac{2d}{c} \sqrt{\epsilon_1} \sqrt{x} \sqrt{-x - s_1} = j2\Phi_{1-} \quad (4.73)$$

where the quantity  $\Phi_1 = (s\tau_1(s)/2j)$  is defined. It is important to note that  $\Phi_{1+} = -\Phi_{1-}$ .

On  $B_+$ , plugging (4.66) through (4.73) into (4.36) and (4.37) gives

$$\mathcal{X}^2 = Z_1^2 Z_{2+}^2 \cos^2 \Phi_1 + j2Z_1^2 Z_{2+} (Z_1 \sin \Phi_1) \cos \Phi_1 - Z_1^4 \sin^2 \Phi_1$$

$$\mathcal{Y}^2 = Z_0^2 Z_1^2 \cos^2 \Phi_1 + j2Z_0^2 Z_{2+} (Z_1 \sin \Phi_1) \cos \Phi_1 - Z_0^2 Z_{2+}^2 \sin^2 \Phi_1$$

$$\mathcal{X}\mathcal{Y} = Z_0 Z_1^2 Z_{2+} [\cos^2 \Phi_1 - \sin^2 \Phi_1] + j[Z_{2+}^2 + Z_1^2] Z_0 (Z_1 \sin \Phi_1) \cos \Phi_1$$

Similarly, on the contour,  $B_-$ ,

$$\begin{aligned}\mathcal{X}^2 &= Z_1^2 Z_{2-}^2 \cos^2 \Phi_1 + j2Z_1^2 Z_{2-} (Z_1 \sin \Phi_1) \cos \Phi_1 - Z_1^4 \sin^2 \Phi_1 \\ \mathcal{Y}^2 &= Z_0^2 Z_1^2 \cos^2 \Phi_1 + j2Z_0^2 Z_{2-} (Z_1 \sin \Phi_1) \cos \Phi_1 - Z_0^2 Z_{2-}^2 \sin^2 \Phi_1 \\ \mathcal{X}\mathcal{Y} &= Z_0 Z_1^2 Z_{2-} [\cos^2 \Phi_1 - \sin^2 \Phi_1] + j[Z_{2-}^2 + Z_1^2] Z_0 (Z_1 \sin \Phi_1) \cos \Phi_1\end{aligned}$$

Note that wave impedances that change sign as a point moves from  $B_+$  to  $B_-$  across the branch cuts are not grouped with a sine function that changes sign crossing the branch cut. Thus, the quantities  $\mathcal{X}^2$ ,  $\mathcal{Y}^2$ , and  $\mathcal{X}\mathcal{Y}$  are not even about the portion of the branch cut for which the  $B$  contours run. Thus, by (4.38),

$$\Gamma(s)\Big|_{B_+} \neq \Gamma(s)\Big|_{B_-}. \quad (4.74)$$

For the contour  $C_+$ ,

$$\begin{aligned}\mathcal{X}^2 &= Z_{1+}^2 Z_{2+}^2 \cos^2 \Phi_{1+} + j2Z_{1+}^2 Z_{2+} (Z_{1+} \sin \Phi_{1+}) \cos \Phi_{1+} - Z_{1+}^4 \sin^2 \Phi_{1+} \\ \mathcal{Y}^2 &= Z_0^2 Z_{1+}^2 \cos^2 \Phi_{1+} + j2Z_0^2 Z_{2+} (Z_{1+} \sin \Phi_{1+}) \cos \Phi_{1+} - Z_0^2 Z_{2+}^2 \sin^2 \Phi_{1+} \\ \mathcal{X}\mathcal{Y} &= Z_0 Z_{1+}^2 Z_{2+} [\cos^2 \Phi_{1+} - \sin^2 \Phi_{1+}] + j[Z_{2+}^2 + Z_{1+}^2] Z_0 (Z_{1+} \sin \Phi_{1+}) \cos \Phi_{1+}\end{aligned}$$

Similarly, on the contour,  $C_-$ ,

$$\begin{aligned}\mathcal{X}^2 &= Z_{1-}^2 Z_{2-}^2 \cos^2 \Phi_{1-} + j2Z_{1-}^2 Z_{2-} (Z_{1-} \sin \Phi_{1-}) \cos \Phi_{1-} - Z_{1-}^4 \sin^2 \Phi_{1-} \\ \mathcal{Y}^2 &= Z_0^2 Z_{1-}^2 \cos^2 \Phi_{1-} + j2Z_0^2 Z_{2-} (Z_{1-} \sin \Phi_{1-}) \cos \Phi_{1-} - Z_0^2 Z_{2-}^2 \sin^2 \Phi_{1-} \\ \mathcal{X}\mathcal{Y} &= Z_0 Z_{1-}^2 Z_{2-} [\cos^2 \Phi_{1-} - \sin^2 \Phi_{1-}] + j[Z_{2-}^2 + Z_{1-}^2] Z_0 (Z_{1-} \sin \Phi_{1-}) \cos \Phi_{1-}\end{aligned}$$

Note that wave impedance,  $Z_1$ , which corresponds to the lossy material in region 1, only appears raised to even powers, or grouped with a sine function that changes sign

upon moving from the  $C_+$  to the  $C_-$  contour, as the wave impedance does. However, for  $Z_2$ , which is the wave impedance in the backing material of region 2, sign changes occur which change the values of the quantities  $\mathcal{X}^2$ ,  $\mathcal{Y}^2$ , and  $\mathcal{X}\mathcal{Y}$  on opposite sides of the branch cut. Thus, since  $\mathcal{X}^2$ ,  $\mathcal{Y}^2$ , and  $\mathcal{X}\mathcal{Y}$  are not even about the branch cut, thus

$$\Gamma(s)\Big|_{C_+} \neq \Gamma(s)\Big|_{C_-}. \quad (4.75)$$

**Case 2:**  $(\sigma_1/\bar{\epsilon}_1) > (\sigma_2/\bar{\epsilon}_2)$

For this case,  $s_\alpha = s_2$  and  $s_\beta = s_1$ . Using (4.48) through (4.55), wave impedances on each integration path take on the form

$$Z_1\Big|_{B_+,C_+} = \frac{-\eta_0 x}{j\sqrt{\bar{\epsilon}_1}\sqrt{x}\sqrt{-x-s_1}} = Z_{1+} \quad (4.76)$$

$$Z_1\Big|_{B_-,C_-} = \frac{\eta_0 x}{j\sqrt{\bar{\epsilon}_1}\sqrt{x}\sqrt{-x-s_1}} = Z_{1-} \quad (4.77)$$

$$Z_2\Big|_{B_+} = Z_2\Big|_{B_-} = \frac{\eta_0 x}{\sqrt{\bar{\epsilon}_2}\sqrt{x}\sqrt{x+s_2}} = Z_2 \quad (4.78)$$

$$Z_2\Big|_{C_+} = \frac{-\eta_0 x}{j\sqrt{\bar{\epsilon}_2}\sqrt{x}\sqrt{-x-s_2}} = Z_{2+} \quad (4.79)$$

$$Z_2\Big|_{C_-} = \frac{\eta_0 x}{j\sqrt{\bar{\epsilon}_2}\sqrt{x}\sqrt{-x-s_2}} = Z_{2-} \quad (4.80)$$

Thus,  $Z_{1+} = -Z_{1-}$ ,  $Z_{2+} = -Z_{2-}$ . The exponential terms appearing in the frequency domain reflection coefficient are given using

$$s\tau_1\Big|_{B_+,C_+} = j\frac{2d}{c}\sqrt{\bar{\epsilon}_1}\sqrt{x}\sqrt{-x-s_1} = j2\Phi_{1+} \quad (4.81)$$

$$s\tau_1\Big|_{B_-,C_-} = -j\frac{2d}{c}\sqrt{\bar{\epsilon}_1}\sqrt{x}\sqrt{-x-s_1} = j2\Phi_{1-} \quad (4.82)$$



On  $B_+$ , plugging (4.76) through (4.82) into (4.36) and (4.37) gives

$$\begin{aligned}\mathcal{X}^2 &= Z_{1+}^2 Z_2^2 \cos^2 \Phi_{1+} + j2Z_{1+}^2 Z_2 (Z_{1+} \sin \Phi_{1+}) \cos \Phi_{1+} - Z_{1+}^4 \sin^2 \Phi_{1+} \\ \mathcal{Y}^2 &= Z_0^2 Z_{1+}^2 \cos^2 \Phi_{1+} + j2Z_0^2 Z_2 (Z_{1+} \sin \Phi_{1+}) \cos \Phi_{1+} - Z_0^2 Z_2^2 \sin^2 \Phi_{1+} \\ \mathcal{X}\mathcal{Y} &= Z_0 Z_{1+}^2 Z_2 [\cos^2 \Phi_{1+} - \sin^2 \Phi_{1+}] + j[Z_2^2 + Z_{1+}^2] Z_0 (Z_{1+} \sin \Phi_{1+}) \cos \Phi_{1+}\end{aligned}$$

Similarly, on the contour,  $B_-$ ,

$$\begin{aligned}\mathcal{X}^2 &= Z_{1-}^2 Z_2^2 \cos^2 \Phi_{1-} + j2Z_{1-}^2 Z_2 (Z_{1-} \sin \Phi_{1-}) \cos \Phi_{1-} - Z_{1-}^4 \sin^2 \Phi_{1-} \\ \mathcal{Y}^2 &= Z_0^2 Z_{1-}^2 \cos^2 \Phi_{1-} + j2Z_0^2 Z_2 (Z_{1-} \sin \Phi_{1-}) \cos \Phi_{1-} - Z_0^2 Z_2^2 \sin^2 \Phi_{1-} \\ \mathcal{X}\mathcal{Y} &= Z_0 Z_{1-}^2 Z_2 [\cos^2 \Phi_{1-} - \sin^2 \Phi_{1-}] + j[Z_2^2 + Z_{1-}^2] Z_0 (Z_{1-} \sin \Phi_{1-}) \cos \Phi_{1-}\end{aligned}$$

Note that wave impedances that change sign when moving from a point on the  $B_+$  contour to a point on the  $B_-$  contour across the branch cut appear raised to even powers, or grouped with a sine function that also changes sign crossing the branch cut. Thus, the quantities  $\mathcal{X}^2$ ,  $\mathcal{Y}^2$ , and  $\mathcal{X}\mathcal{Y}$  are even about the branch cut, and by (4.38),

$$\Gamma(s) \Big|_{B_+} = \Gamma(s) \Big|_{B_-}. \quad (4.83)$$

The expressions for  $\mathcal{X}^2$ ,  $\mathcal{Y}^2$ , and  $\mathcal{X}\mathcal{Y}$  on the integration paths  $C_+$  and  $C_-$  are given by the same equations as in case 1, since the wave impedances and propagation factors are identical for these paths for all combinations of  $(\sigma_1/\bar{\epsilon}_1)$  and  $(\sigma_2/\bar{\epsilon}_2)$ . Therefore, as in case 1,

$$\Gamma(s) \Big|_{C_+} \neq \Gamma(s) \Big|_{C_-}. \quad (4.84)$$

**Case 3:**  $(\sigma_1/\bar{\epsilon}_1) = (\sigma_2/\bar{\epsilon}_2)$

For this case, the integration paths  $B_+$  and  $B_-$  disappear, leaving just the integration paths along  $C_+$  and  $C_-$ . These expressions are the same as in the first two

cases, thus

$$\Gamma(s)\Big|_{C_+} \neq \Gamma(s)\Big|_{C_-}. \quad (4.85)$$

This is an important result, because the response will not be given by a pure natural mode series in the late time, since the integral contributions from contours above and below the branch cut do not cancel; i.e.

$$\int_{l_1 \cup l_2 \cup l_3 \cup l_4} \Gamma(s)e^{st} ds + \int_{l_5 \cup l_6 \cup l_7 \cup l_8} \Gamma(s)e^{st} ds \neq 0 \quad (4.86)$$

#### 4.2.2.2.4 Conclusions for the late time period for material-backed material layers .

In the late time, the time domain reflection coefficient may or may not be a pure natural mode series, since a branch cut contribution can exist. The time domain reflection coefficient is given by (4.25) as

$$\begin{aligned} \Gamma(t) = & \sum Res[\Gamma(s)e^{st}, \text{complex poles}] + \frac{1}{2} \sum Res[\Gamma(s)\Big|_+ e^{st}, \text{real poles}] \\ & + \frac{1}{2} \sum Res[\Gamma(s)\Big|_- e^{st}, \text{real poles}] - \frac{1}{j2\pi} \sum_i \int_{l_i} \Gamma(s)e^{st} ds \end{aligned} \quad (4.87)$$

Here, the pole contributions from the complex poles included inside the closed contour, and the contributions from the poles on the real axis combine to give the complete pole series, where all of the residues are evaluated using (4.28). It should be emphasized here that caution needs to be exercised in evaluating these residues, as the correct value for the frequency domain reflection coefficient on each side of the branch cut needs to be used in order to obtain the correct solution.

Note that this response, unlike the air-backed and conductor-backed cases considered in [13], may include a branch cut contribution in the late time of the system. This is the case when the backing material is lossy. It is assumed that this response will be a non-time limited response, as it is for the reflection for a single interface

involving lossy material. Note also that the first material layer can be either lossy or lossless, yielding a branch cut contribution in either case.

Another important result to note here that the integral contributions from the contours along the branch cut disappear when the backing material of region 2 is lossless. This is important because it shows that cancellation of a branch cut contribution from the interfacial reflection occurs upon the return of the reflection from the second interface to the observation plane. This has implications in a multilayered problem, where some of the layers may be lossless, yielding a pure natural mode series representation during portions of the early time of the system. This is explored in detail in Chapter 6.

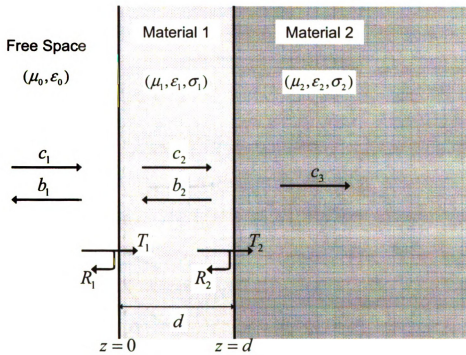


Figure 4.1. Material-backed lossy dielectric layer

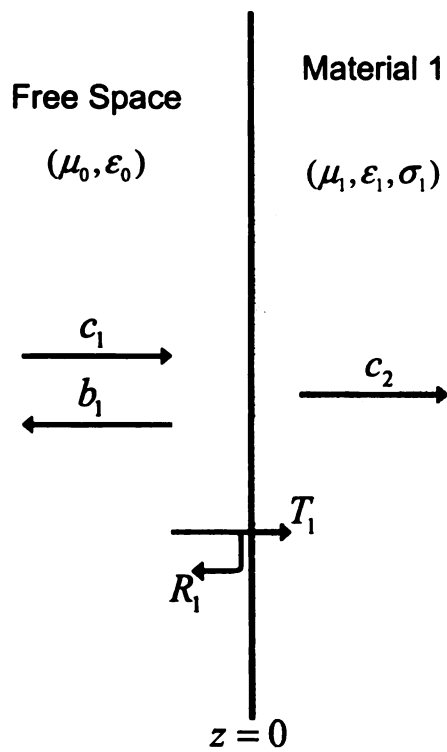


Figure 4.2. Single interface between free-space and a lossy dielectric

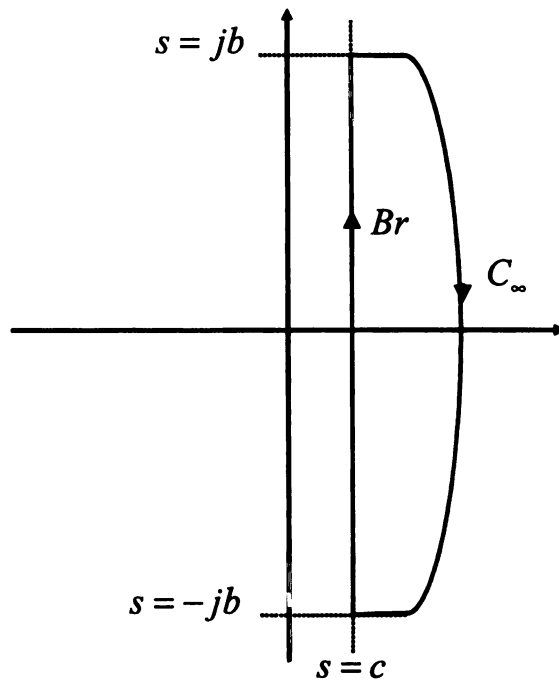


Figure 4.3. Closure of the Bromwich contour in the right half plane.  
 $|b| \rightarrow \infty, 0 < c < \infty$

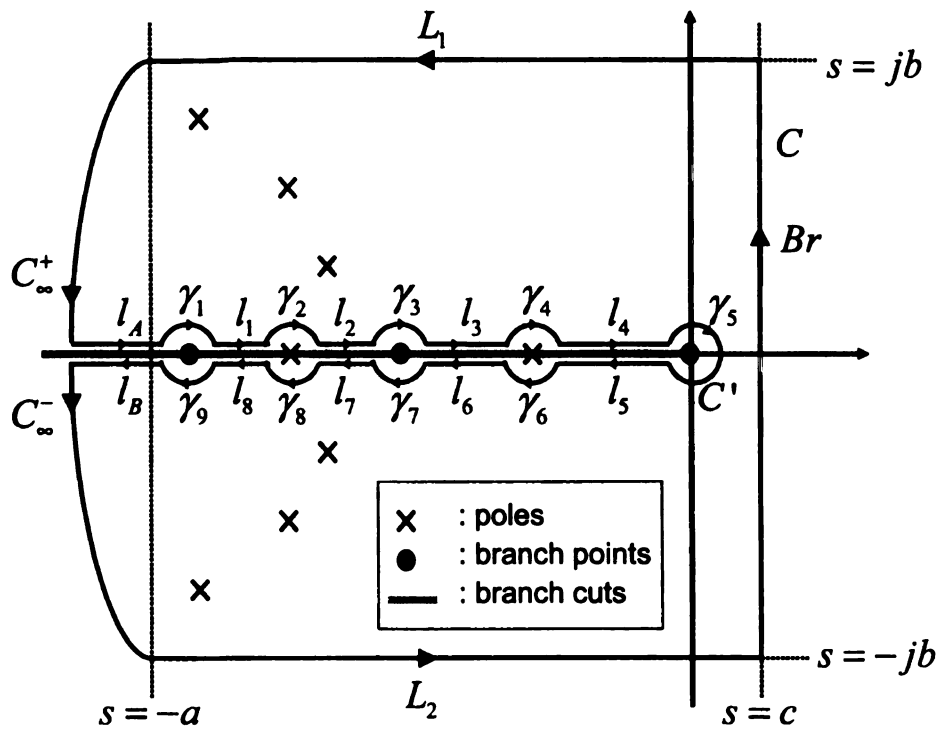


Figure 4.4. Closure of the Bromwich contour in the left half plane.  
 $|a|, |b| \rightarrow \infty, 0 < c < \infty$

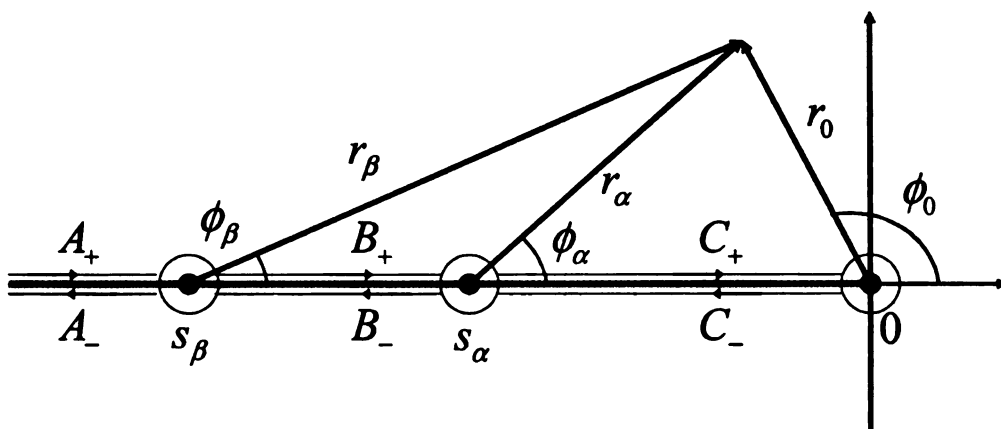


Figure 4.5. Inner contour integration paths for left half plane closure



## CHAPTER 5

### TWO MATERIAL LAYERS BACKED BY A PERFECTLY CONDUCTING SCREEN

Having examined the various subproblems associated with the geometry of Figure 5.1, the temporal response for two planar material layers backed by a perfect electric conductor is considered. This geometry is interesting because, unlike the structure considered in Chapter 3, the middle time response of this structure does not necessarily have a pure natural mode series representation. Evaluation of this geometry thus gives insight into the behavior of the response in regard to a turn on and turn off behavior of various components.

As shown in Chapter 2, the frequency domain reflection coefficient for a two-layered geometry backed by a perfect electric conductor is given using the wave matrix method as

$$\Gamma(\omega) = \frac{R_1(\omega) + R_2(\omega)P_1^2(\omega) - P_1^2(\omega)P_2^2(\omega) - R_1(\omega)R_2(\omega)P_2^2(\omega)}{1 + R_1(\omega)R_2(\omega)P_1^2(\omega) - R_1(\omega)P_1^2(\omega)P_2^2(\omega) - R_2(\omega)P_2^2(\omega)}, \quad (5.1)$$

with interfacial reflection coefficients

$$R_1(\omega) = \frac{Z_1(\omega) - Z_0}{Z_1(\omega) + Z_0}, \quad (5.2a)$$

$$R_2(\omega) = \frac{Z_2(\omega) - Z_1(\omega)}{Z_2(\omega) + Z_1(\omega)}. \quad (5.2b)$$

Here  $Z_1(\omega)$  and  $Z_2(\omega)$  are the wave impedances in the material layers given for parallel

(TM) and perpendicular (TE) polarizations, respectively, by

$$Z_i^{\parallel}(\omega) = \frac{k_{z,i}(\omega)\eta_i(\omega)}{k_i(\omega)} \quad (5.3a)$$

$$Z_i^{\perp}(\omega) = \frac{k_i(\omega)\eta_i(\omega)}{k_{z,i}(\omega)} \quad (5.3b)$$

where  $\eta_1(\omega)$  and  $\eta_2(\omega)$  are the frequency dependent intrinsic impedances of the material layers, given in terms of the complex permittivities,  $\epsilon_1^c(\omega)$  and  $\epsilon_2^c(\omega)$ , and permeabilities  $\mu_1$  and  $\mu_2$ , as

$$\eta_1(\omega) = \sqrt{\frac{\mu_1}{\epsilon_1^c(\omega)}}, \quad \epsilon_1^c(\omega) = \epsilon_{1r}\epsilon_0 + \frac{\sigma_1}{j\omega}, \quad (5.4)$$

$$\eta_2(\omega) = \sqrt{\frac{\mu_2}{\epsilon_2^c(\omega)}}, \quad \epsilon_2^c(\omega) = \epsilon_{2r}\epsilon_0 + \frac{\sigma_2}{j\omega}, \quad (5.5)$$

In this development, only nonmagnetic materials will be considered, thus  $\mu_1 = \mu_2 = \mu_0$ . The wave impedance in free space,  $Z_0$ , takes on the same forms as (5.3), but with frequency independent intrinsic impedance,  $\eta_0$ . Since  $k_i^2 = k_{x,i}^2 + k_{z,i}^2$  and  $k_{x,i} = k_{x,0} = k_0 \sin \theta_{in}$  to satisfy boundary conditions at all points on the planar surfaces, the wave impedances take the forms

$$Z_i^{\parallel}(\omega) = \frac{\eta_i}{k_i} \sqrt{k_i^2 - k_0^2 \sin^2 \theta_{in}}, \quad Z_0^{\parallel} = \eta_0 \cos \theta_{in} \quad (5.6a)$$

$$Z_i^{\perp}(\omega) = \frac{k_i \eta_i}{\sqrt{k_i^2 - k_0^2 \sin^2 \theta_{in}}}, \quad Z_0^{\perp} = \frac{\eta_0}{\cos \theta_{in}} \quad (5.6b)$$

for parallel and perpendicular polarizations, respectively.  $P_1(\omega)$  and  $P_2(\omega)$  are propagation factors given by

$$P_1(\omega) = e^{-jk_{z,1}d} \quad (5.7a)$$

$$P_2(\omega) = e^{-jk_{z,2}h}. \quad (5.7b)$$

For notational purposes, the propagation factors will be written in the form

$$P_i^2(\omega) = e^{-j\omega\tau_i(\omega)}, \quad (5.8)$$

where the expressions contained in the exponent are given by

$$\begin{aligned} \omega\tau_1(\omega) &= 2k_{z,1}d \\ &= 2d\sqrt{k_1^2 - k_0^2 \sin^2 \theta_{in}} \\ &= \omega \frac{2d}{c} \sqrt{\frac{\epsilon_1^c}{\epsilon_0} - \sin^2 \theta_{in}} \end{aligned} \quad (5.9)$$

and

$$\begin{aligned} \omega\tau_2(\omega) &= 2k_{z,2}h \\ &= 2h\sqrt{k_2^2 - k_0^2 \sin^2 \theta_{in}} \\ &= \omega \frac{2h}{c} \sqrt{\frac{\epsilon_2^c}{\epsilon_0} - \sin^2 \theta_{in}}. \end{aligned} \quad (5.10)$$

To simplify notation, the quantities  $\bar{\epsilon}_1 = \epsilon_{1r} - \sin^2 \theta_{in}$  and  $\bar{\epsilon}_2 = \epsilon_{2r} - \sin^2 \theta_{in}$  are defined, giving

$$\tau_1(\omega) = \frac{2d}{c} \sqrt{\bar{\epsilon}_1 + \frac{\sigma_1}{j\omega\epsilon_0}} \quad (5.11a)$$

$$\tau_2(\omega) = \frac{2h}{c} \sqrt{\bar{\epsilon}_2 + \frac{\sigma_2}{j\omega\epsilon_0}} \quad (5.11b)$$

## 5.1 Laplace domain representation

Since the frequency domain reflection coefficient,  $\Gamma(\omega)$ , exists, a Laplace domain representation also exists. This quantity is given, inserting the propagation factors,

$P_1(\omega)$  and  $P_2(\omega)$ , as

$$\begin{aligned}\Gamma(s) &= \Gamma(\omega) \Big|_{\omega=\frac{s}{j}} \\ &= \frac{R_1(s) + R_2(s)e^{-s\tau_1(s)} - e^{-s(\tau_1(s)+\tau_2(s))} - R_1(s)R_2(s)e^{-s\tau_2(s)}}{1 + R_1(s)R_2(s)e^{-s\tau_1(s)} - R_1(s)e^{-s(\tau_1(s)+\tau_2(s))} - R_2(s)e^{-s\tau_2(s)}}\end{aligned}\quad (5.12)$$

with expressions appearing in the exponential terms given by

$$\begin{aligned}s\tau_1(s) &= j\omega\tau_1(\omega) \Big|_{\omega=\frac{s}{j}} \\ &= s\frac{2d}{c}\sqrt{\bar{\epsilon}_1 + \frac{\sigma_1}{s\epsilon_0}} \\ &= \frac{2d}{c}\sqrt{\bar{\epsilon}_1}\sqrt{s}\sqrt{s + \frac{\sigma_1}{\bar{\epsilon}_1\epsilon_0}} \\ &= \frac{2d}{c}\sqrt{\bar{\epsilon}_1}\sqrt{s}\sqrt{s - s_1}\end{aligned}\quad (5.13)$$

and

$$\begin{aligned}s\tau_2(s) &= j\omega\tau_2(\omega) \Big|_{\omega=\frac{s}{j}} \\ &= s\frac{2h}{c}\sqrt{\bar{\epsilon}_2 + \frac{\sigma_2}{s\epsilon_0}} \\ &= \frac{2h}{c}\sqrt{\bar{\epsilon}_2}\sqrt{s}\sqrt{s + \frac{\sigma_2}{\bar{\epsilon}_2\epsilon_0}} \\ &= \frac{2h}{c}\sqrt{\bar{\epsilon}_2}\sqrt{s}\sqrt{s - s_2}\end{aligned}\quad (5.14)$$

where the quantities  $s_1 = -\sigma_1/\bar{\epsilon}_1\epsilon_0$  and  $s_2 = -\sigma_2/\bar{\epsilon}_2\epsilon_0$  have been defined. The interfacial reflection coefficients are given using (5.2) as  $R_1(s) = R_1(\omega) \Big|_{\omega=\frac{s}{j}}$  and  $R_2(s) = R_2(\omega) \Big|_{\omega=\frac{s}{j}}$ . The wave impedances, which are needed to compute the inter-

facial reflection coefficients, are given for parallel polarization as

$$\begin{aligned}
Z_i^{\parallel}(s) &= Z_i^{\parallel}(\omega) \Big|_{\omega=\frac{s}{j}} \\
&= \frac{\eta_i}{k_i} \sqrt{k_i^2 - k_0^2 \sin^2 \theta_{in}} \\
&= \frac{k_0 \eta_i}{k_i} \sqrt{\frac{\epsilon_i^c}{\epsilon_0} - \sin^2 \theta_{in}} \\
&= \frac{\eta_0}{(\epsilon_i^c/\epsilon_0)} \sqrt{\bar{\epsilon}_i + \frac{\sigma_i}{s\epsilon_0}} \\
&= \frac{\eta_0 \sqrt{\bar{\epsilon}_i} \sqrt{s} \sqrt{s - s_i}}{s\epsilon_{ir} + \sigma_i/\epsilon_0}, \tag{5.15a}
\end{aligned}$$

and for perpendicular polarization by

$$\begin{aligned}
Z_i^{\perp}(s) &= Z_i^{\perp}(\omega) \Big|_{\omega=\frac{s}{j}} \\
&= \frac{k_i \eta_i}{\sqrt{k_i^2 - k_0^2 \sin^2 \theta_{in}}} \\
&= \frac{k_i \eta_i}{k_0 \sqrt{(\epsilon_i^c/\epsilon_0) - \sin^2 \theta_{in}}} \\
&= \frac{\eta_0}{\sqrt{\bar{\epsilon}_i + (\sigma_i/s\epsilon_0)}} \\
&= \frac{\eta_0 s}{\sqrt{\bar{\epsilon}_i} \sqrt{s} \sqrt{s - s_i}}. \tag{5.15b}
\end{aligned}$$

The interfacial reflection coefficients can thus be written for parallel and perpendicular polarizations using (5.2), as

$$R_1(s) = \begin{cases} \frac{\sqrt{\bar{\epsilon}_1} \sqrt{s} \sqrt{s - s_1} - (s\epsilon_{1r} + (\sigma_1/\epsilon_0)) \cos \theta_{in}}{\sqrt{\bar{\epsilon}_1} \sqrt{s} \sqrt{s - s_1} + (s\epsilon_{1r} + (\sigma_1/\epsilon_0)) \cos \theta_{in}} & \text{parallel polarization} \\ \frac{s \cos \theta_{in} - \sqrt{\bar{\epsilon}_1} \sqrt{s} \sqrt{s - s_1}}{s \cos \theta_{in} + \sqrt{\bar{\epsilon}_1} \sqrt{s} \sqrt{s - s_1}} & \text{perpendicular polarization} \end{cases} \tag{5.16}$$

and

$$R_2(s) = \begin{cases} \frac{(s\epsilon_{1r} + \frac{\sigma_1}{\epsilon_0})\sqrt{\epsilon_2}\sqrt{s}\sqrt{s-s_2} - (s\epsilon_{2r} + \frac{\sigma_2}{\epsilon_0})\sqrt{\epsilon_1}\sqrt{s}\sqrt{s-s_1}}{(s\epsilon_{1r} + \frac{\sigma_1}{\epsilon_0})\sqrt{\epsilon_2}\sqrt{s}\sqrt{s-s_2} + (s\epsilon_{2r} + \frac{\sigma_2}{\epsilon_0})\sqrt{\epsilon_1}\sqrt{s}\sqrt{s-s_1}} & \parallel \text{-pol} \\ \frac{\sqrt{\epsilon_1}\sqrt{s}\sqrt{s-s_1} - \sqrt{\epsilon_2}\sqrt{s}\sqrt{s-s_2}}{\sqrt{\epsilon_1}\sqrt{s}\sqrt{s-s_1} + \sqrt{\epsilon_2}\sqrt{s}\sqrt{s-s_2}} & \perp \text{-pol} \end{cases} \quad (5.17)$$

## 5.2 The time domain reflection coefficient

Using the frequency domain reflection coefficient found in Section 5.1, the time domain reflection coefficient of the material stack,  $\Gamma(t)$ , which is defined through an inverse temporal transform, can be found. This time domain reflection coefficient, when convolved with a finite duration incident waveform, gives the reflected field in the time domain.

In order to use the extinction pulse technique, it must be shown that the time domain reflection coefficient can be represented in terms of a natural mode series, after a finite period called the early time. The time period during which the natural mode series is an accurate representation of the time domain reflection coefficient is commonly referred to as the late time. Thus, in the late time, the time domain reflection coefficient should take the form:

$$\Gamma(t) = \sum_{n=1}^{\infty} A_n e^{s_n t} \quad (5.18)$$

where  $A_n$  is the amplitude coefficient associated with the  $n^{\text{th}}$  pole,  $s_n = \sigma_n + j\omega_n$ , of the frequency domain reflection coefficient. This representation of the temporal field is found by taking the inverse Laplace transform of (5.12), neglecting infinite contour contributions for which (5.12) does not approach zero uniformly. To perform this inverse transform, the singularities of the frequency domain reflection coefficient

are explored, and the evaluation of the integral

$$\int_{Br} \Gamma(s)e^{st} ds \quad (5.19)$$

is carried out through complex plane integration. This is done in several steps, corresponding to several ranges of time,  $t$ . Here, the integration is carried out along the contour  $Br$ , which is the Bromwich path. The Bromwich path, which defines the inverse Laplace transform, is a path in the complex  $s$ -plane which is taken parallel to the imaginary axis, to the right of all singular points. Evaluation of the integral in (5.19) gives the time domain reflection coefficient as

$$\Gamma(t) = \frac{1}{j2\pi} \int_{Br} \Gamma(s)e^{st} ds \quad (5.20)$$

when infinite contour contributions are neglected. In order to carry out the contour integration involved with the evaluation of this integral, singularities of the integrand need to be determined, and appropriate branches defined.

### 5.2.1 Singularities of the frequency domain reflection coefficient

Singularities of the frequency domain reflection coefficient take on various forms. First,  $s\tau_1(s)$ ,  $s\tau_2(s)$  and  $Z_i(s)$ , given by equations (5.13) through (5.15), contain complex square roots which lead to branch points at  $s = 0$ ,  $s = s_1$ , and  $s = s_2$ . Correspondingly, branch cuts are taken along the negative real axis to define the principal branches of the square root functions. In addition, observing that the frequency domain reflection coefficient may be written as

$$\Gamma(s) = \frac{N(s)}{D(s)}, \quad (5.21)$$

there are poles associated with the zeros of the denominator,  $D(s)$ . These poles will appear in the left half of the complex  $s$ -plane, with some lying on the real axis, and

the rest occurring in conjugate pairs.

## 5.2.2 Evaluation of the time domain reflection coefficient

Evaluation of the time domain reflection coefficient is carried out by factoring the frequency domain reflection coefficient such that the inverse Laplace transform of the individual components are physically meaningful during various time periods. The definition of these time periods, the factorization used in each time period, and the implications of these developments are the subjects of Sections 5.2.2.1 through 5.2.2.3.

### 5.2.2.1 Early time: $t < T_1$

The early time is defined as the time period before a response is observed at the observation plane due to reflection from the second interface, as discussed in Section 2.4.1. This response should be identical to the interfacial reflection between two semi-infinite media during this time period. Because of this, the frequency domain reflection coefficient is factored into the sum of the interfacial reflection coefficient of the first interface,  $R_1(s)$ , and a reduced reflection coefficient defined by

$$\begin{aligned}\Gamma'(s) &= \Gamma(s) - R_1(s) \\ &= \frac{(1 - R_1^2(s))(R_2(s) - e^{-s\tau_2(s)})e^{-s\tau_1(s)}}{1 + R_1(s)R_2(s)e^{-s\tau_1(s)} - R_1(s)e^{-s(\tau_1(s)+\tau_2(s))} - R_2(s)e^{-s\tau_2(s)}}.\end{aligned}\quad (5.22)$$

Since the inverse Laplace transform is a linear operation, the time domain reflection coefficient for the entire structure is given as a sum of the inverse Laplace transforms of the two components of the frequency domain reflection coefficient. The inverse Laplace transform of the interfacial reflection coefficient, given by  $R_1(t)$ , is rigorously developed in [14]. The evaluation of the inverse Laplace transform of the reduced reflection coefficient remains; this is given by  $\Gamma'(t) = \mathcal{L}^{-1}\{\tilde{\Gamma}'(s)\}$ , where  $\tilde{\Gamma}'(s)$  is identical to  $\Gamma'(s)$ , except for its behavior at infinity. This inverse transform is found



by evaluating

$$\frac{1}{j2\pi} \int_{Br} \Gamma'(s) e^{st} ds, \quad (5.23)$$

neglecting infinite contour contributions for which  $\Gamma'(s)$  does not go to zero uniformly.

On an infinite contour,  $C_\infty$ , exponential terms appearing in the numerator of the reduced reflection coefficient are given using (5.13) as,

$$\lim_{|s| \rightarrow \infty} \left\{ \frac{2d}{c} \sqrt{\bar{\epsilon}_1 + \frac{\sigma_1}{s\epsilon_0}} \right\} = \frac{2d}{c} \sqrt{\bar{\epsilon}_1} \triangleq T_1 \quad (5.24)$$

Letting  $t_1 = t - T_1$ , which is negative for  $t < T_1$ , evaluation of the integration along the Bromwich contour in (5.23) is obtained by closing the integration contour in the right half of the complex  $s$ -plane, as shown in Figure 5.3. Right half plane closure is justified here, since  $t_1$  is negative for the time period  $t < T_1$ . Note that  $T_1$  is the two-way transit time of the first material region, as discussed in Section 2.4.1. The early time is thus given by the time period  $t < T_1$ . The integration on the infinite contour  $C_\infty$  is given by

$$\int_{C_\infty} \Gamma'(s) e^{st} ds = \int_{C_\infty} \Gamma'(s) e^{sT_1} e^{st_1} ds \quad (5.25)$$

Here, *Jordan's Lemma* cannot be directly applied to evaluate the integral contribution over  $C_\infty$ , because the integrand does not go to zero as  $|s| \rightarrow \infty$  at all points on the contour. However, by definition of the time domain reflection coefficient, the infinite contour contribution is to be neglected, as discussed in Section 2.4. Thus, the time domain reflection coefficient in the early time is identical to the inverse Laplace transform of the interfacial reflection coefficient, as developed in [14].

### 5.2.2.2 Middle time: $T_1 < t < T_1 + T_2$

The middle time for this structure is defined as the time period between the observation of the reflection from the second interface at the observation plane, as discussed

in Section 2.4.1, and the observation of the reflection from the conductor. During this time period, physical reasoning suggests that the temporal response should be identical to the reflection from the first layer of material backed by a half space of the second material. Because of this, the frequency domain reflection coefficient is factored into the sum of the reflection coefficient for a single material-backed lossy layer, which is developed in Chapter 4, and a reduced reflection coefficient defined by the difference between the total reflection coefficient and the frequency domain reflection coefficient for the single material-backed lossy layer. The reduced reflection coefficient is thus given by

$$\begin{aligned}
\Gamma'_{2lay}(s) &= \Gamma(s) - \Gamma_{1lay}(s) \\
&= \Gamma(s) - \frac{R_1(s) + R_2(s)e^{-s\tau_1(s)}}{1 + R_1(s)R_2(s)e^{-s\tau_1(s)}} \\
&= \frac{-e^{-s(\tau_1(s)+\tau_2(s))}}{1 + R_1(s)R_2(s)e^{-s\tau_1(s)}} \times \\
&\quad \times \frac{(1 - R_1^2(s))(1 - R_2^2(s))}{1 + R_1(s)R_2(s)e^{-s\tau_1(s)} - R_1(s)e^{-s(\tau_1(s)+\tau_2(s))} - R_2(s)e^{-s\tau_2(s)}}
\end{aligned} \tag{5.26}$$

Since the inverse Laplace transform is a linear operation, the time domain reflection coefficient for the entire structure is given as a sum of the inverse Laplace transforms of the two components of the frequency domain reflection coefficient. The inverse Laplace transform of a material-backed lossy layer is developed in Chapter 4. The evaluation of the inverse transform of the reduced reflection coefficient remains; this is given by  $\Gamma'_{2lay}(t) = \mathcal{L}^{-1}\{\tilde{\Gamma}'_{2lay}(s)\}$ , where  $\tilde{\Gamma}'_{2lay}(s)$  is identical to  $\Gamma'_{2lay}(s)$ , except for its behavior at infinity. This inverse transform is found by evaluating

$$\frac{1}{j2\pi} \int_{Br} \Gamma'_{2lay}(s)e^{st} ds, \tag{5.27}$$

neglecting infinite contour contributions. On an infinite contour,  $C_\infty$ , exponential terms appearing in the numerator of the reduced reflection coefficient are given using (5.13) and (5.14) as,

$$\lim_{|s| \rightarrow \infty} \left\{ \frac{2d}{c} \sqrt{\bar{\epsilon}_1 + \frac{\sigma_1}{s\epsilon_0}} + \frac{2h}{c} \sqrt{\bar{\epsilon}_2 + \frac{\sigma_2}{s\epsilon_0}} \right\} = \frac{2d}{c} \sqrt{\bar{\epsilon}_1} + \frac{2h}{c} \sqrt{\bar{\epsilon}_2} \triangleq T_1 + T_2 \quad (5.28)$$

where  $T_1$  and  $T_2$  are the two-way transit times of the first and second material layer, respectively, as discussed in Section 2.4.1. Letting  $t_2 = t - (T_1 + T_2)$ , which is negative for  $t < T_1 + T_2$ , evaluation along the Bromwich contour in (5.26) is obtained by closing the integration contour in the right half of the complex  $s$ -plane, as shown in Figure 5.3. Right half plane closure is justified here, since  $t_2$  is negative during this time period. The end of the middle-time period is defined by (5.28). The integration on the infinite contour  $C_\infty$  is given by

$$\int_{C_\infty} \Gamma'(s) e^{st} ds = \int_{C_\infty} \Gamma'(s) e^{s(T_1+T_2)} e^{st_1} ds \quad (5.29)$$

It is not possible to apply *Jordan's Lemma* directly to this integral, since the integrand does not go to zero uniformly on the entire contour,  $C_\infty$ . However, by definition of the time domain reflection coefficient, the infinite contour contribution is to be neglected. Thus, during the middle-time period, the time domain reflection coefficient is identical to the the time domain reflection coefficient for the material-backed lossy layer, which is rigorously developed in Chapter 4. It is found in Chapter 4 that after the time  $T_1$ , the time domain reflection coefficient for the material-backed lossy layer will be given by a natural mode series if the material backing is lossless, otherwise a branch cut contribution may be present. This holds here as well, since the response is identical to that of the material-backed layer during the middle time period.

### 5.2.2.3 Late time: $t > T_1 + T_2$

The late time of the temporal response for this geometry is defined as the portion of the transient response after a response from a reflection from the conductor backing arrives at the observation plane, as discussed in Section 2.4.1. For this time period, the frequency domain reflection coefficient for the entire geometry, given by (5.1), is considered. Here the entire geometry is used because the middle time response is not necessarily a natural mode series. By examining the properties of the reflection coefficient for the entire structure, insight can be gained into the possible existence of a branch cut contribution in the late time. Also, insight can be obtained as to what happens to the the branch cut contribution that may be present in the response during the middle time, once the late time begins.

Evaluation of the inverse transform of the reflection coefficient is carried out through the integration along the Bromwich path, neglecting infinite contour contributions; this integration is given by

$$\frac{1}{j2\pi} \int_{Br} \Gamma(s) e^{st} ds. \quad (5.30)$$

On an infinite contour,  $C_\infty$ , exponential terms appearing in the numerator of the reflection coefficient include the two-way transit times of the two layers,  $T_1$  and  $T_2$  as in (5.28). Letting  $t_2 = t - (T_1 + T_2)$ , which is positive for  $t > T_1 + T_2$ , evaluation along the Bromwich contour in (5.30) is obtained by closing the integration contour in the left half of the complex  $s$ -plane, as shown in Figure 5.5. For closure of the integration contour in the left half plane many integration paths are involved. In this discussion, these integration paths will be referred to in two groups, the outer contour,  $C$ , which includes integration paths parameterized by quantities receding towards infinity, and the inner contour,  $C'$ , which includes integration paths taken along the branch cut.

These integration contours are given by

$$C = Br \cup L_1 \cup C_\infty^+ \cup C_\infty^- \cup L_2$$

$$C' = l_A \cup \gamma_1 \cup \gamma_2 \cup \dots \cup \gamma_9 \cup l_1 \cup l_2 \cup \dots \cup l_8 \cup l_B$$

Using Cauchy's residue theorem, evaluation of the closed contour integration is given by

$$\oint_{C \cup C'} \Gamma(s)e^{st} ds = j2\pi \sum \text{Res}[\Gamma(s)e^{st}, \text{complex poles}]. \quad (5.31)$$

Thus, determination of the time domain reflection coefficient is possible provided the integral contribution from each path is known.

### 5.2.2.3.1 Contributions from the outer contour, C .

The Laplace inversion integral is found by computing (5.31) for the Bromwich path contribution in terms of the contributions from all other integration paths and computation of the residues from the enclosed simple poles. The outer contour, C, consists of various integration paths that are parameterized by quantities that recede towards infinity, including the Bromwich path which defines the inverse Laplace transform.

#### Contributions from $C_\infty^+$ and $C_\infty^-$

Integral contributions from  $C_\infty^+$  and  $C_\infty^-$  are given directly by *Jordan's lemma*, as stated in Theorem 3.1, since  $\Gamma(s) \rightarrow 0$  on the contours. Thus, direct application of *Jordan's lemma* gives

$$\int_{C_\infty^+} \Gamma(s)e^{st} ds = 0 \quad (5.32)$$

$$\int_{C_\infty^-} \Gamma(s)e^{st} ds = 0. \quad (5.33)$$

#### Contributions from $L_1$ and $L_2$

On  $L_1$  and  $L_2$ , *Jordan's Lemma* cannot be directly applied to evaluate the integral

contributions, because the integrand does not go to zero as  $|s| \rightarrow \infty$  at all points on the contours. However, by definition of the time domain reflection coefficient, the infinite contour contribution is to be neglected, as discussed in Section 2.4.

### Contributions from the inner contour, $C'$

The segments of the inner contour  $C'$ , which enclose the branch cut, can be broken into three groups. The first group consists of the contours  $\gamma_2, \gamma_4, \gamma_6,$  and  $\gamma_8,$  etc, which enclose the real poles on the branch cut. Note that two poles are shown on the real axis here, but more may appear depending on the properties of each material layer, and the incidence angle. The second group is made up of contours  $\gamma_1, \gamma_3, \gamma_5, \gamma_7,$  and  $\gamma_9$  that enclose the branch points. The straight line segments immediately above and below the branch cut make up the final group. Within this group, the segments  $l_A$  and  $l_B$ , which lie to the left of all of the branch points are handled separately from the segments  $l_1$  through  $l_8$ .

### Contributions from $\gamma_2, \gamma_4, \gamma_6,$ and $\gamma_8$

The integral contributions from the first group of contours, which enclose poles on the branch cut, can be found by calculating the residues of  $\Gamma(s)e^{st}$  at the poles. It is found that all of the poles of  $\Gamma(s)$  are of first order and thus the residues may be found from

$$\text{Res}[\Gamma(s)e^{st}, \text{poles}] \Big|_{s=s_k} = \lim_{s \rightarrow s_k} (s - s_k) [\Gamma(s)e^{st}] = A_k e^{s_k t} \quad (5.34)$$

where

$$A_k = \frac{R_1(s_k) + R_2(s_k)e^{-s_k \tau_1(s_k)} - e^{-s_k(\tau_1(s_k) + \tau_2(s_k))} - R_1(s_k)R_2(s_k)e^{-s_k \tau_2(s_k)}}{-\frac{d}{ds}[M(s)] \Big|_{s=s_k}} \quad (5.35)$$

is the complex mode amplitude, with the denominator of the reflection coefficient written as  $1 - M(s)$ . Note that l'Hôpital's rule has been used to obtain the form of the

complex mode amplitude shown here. Carrying out the details of the differentiation gives

$$\begin{aligned}
\frac{d}{ds}[M(s)] &= \frac{d}{ds} \left[ R_2(s)e^{-s\tau_2(s)} + R_1(s)e^{-s(\tau_1(s)+\tau_2(s))} - R_1(s)R_2(s)e^{-s\tau_1(s)} \right] \\
&= \left[ e^{-s(\tau_1(s)+\tau_2(s))} - R_2(s)e^{-s\tau_1(s)} \right] \frac{d}{ds} [R_1(s)] \\
&\quad + \left[ e^{-s\tau_2(s)} - R_1(s)e^{-s\tau_1(s)} \right] \frac{d}{ds} [R_2(s)] \\
&\quad + \left[ R_1(s)e^{-s\tau_2(s)} - R_1(s)R_2(s) \right] \frac{d}{ds} [e^{-s\tau_1(s)}] \\
&\quad + \left[ R_2(s) + R_1(s)e^{-s\tau_1(s)} \right] \frac{d}{ds} [e^{-s\tau_2(s)}]
\end{aligned}$$

with the derivatives of the exponential terms given by

$$\frac{d}{ds} [e^{-s\tau_1(s)}] = - \left[ \frac{d}{c} \sqrt{\bar{\epsilon}_1} \frac{2s - s_1}{\sqrt{s}\sqrt{s - s_1}} e^{-s\tau_1(s)} \right]$$

and

$$\frac{d}{ds} [e^{-s\tau_2(s)}] = - \left[ \frac{h}{c} \sqrt{\bar{\epsilon}_2} \frac{2s - s_2}{\sqrt{s}\sqrt{s - s_2}} e^{-s\tau_2(s)} \right]$$

The derivative of the first interfacial reflection coefficient is found using (5.16) as

$$\frac{d}{ds} [R_1(s)] = \frac{\Upsilon_1(s)}{\Omega_1(s)}$$

where, for parallel polarization,

$$\Upsilon_1(s) = \sqrt{\bar{\epsilon}_1} \frac{2s^2 - ss_1}{\sqrt{s}\sqrt{s - s_1}} \left( s\epsilon_{1r} + \frac{\sigma_1}{\epsilon_0} \right) \cos \theta_{in} - 2\epsilon_{1r} \sqrt{\bar{\epsilon}_1} \sqrt{s}\sqrt{s - s_1} \cos \theta_{in}$$

$$\Omega_1(s) = \left( s\epsilon_{1r} + \frac{\sigma_1}{\epsilon_0} \right)^2 \cos^2 \theta_{in} + 2 \left( s\epsilon_{1r} + \frac{\sigma_1}{\epsilon_0} \right) \sqrt{\bar{\epsilon}_1} \sqrt{s}\sqrt{s - s_1} \cos \theta_{in} + \bar{\epsilon}_1 s(s - s_1)$$

and for perpendicular polarization

$$\Upsilon_1(s) = 2\sqrt{\bar{\epsilon}_1}\sqrt{s}\sqrt{s-s_1} \cos \theta_{in} - \cos \theta_{in} \sqrt{\bar{\epsilon}_1} \frac{2s^2 - ss_1}{\sqrt{s}\sqrt{s-s_1}}$$

$$\Omega_1(s) = s^2 \cos^2 \theta_{in} + 2 \cos \theta_{in} s \sqrt{\bar{\epsilon}_1}\sqrt{s}\sqrt{s-s_1} + \bar{\epsilon}_1 s(s-s_1)$$

The derivative of the second interfacial reflection coefficient is found using (5.17) as

$$\frac{d}{ds} [R_2(s)] = \frac{\Upsilon_2(s)}{\Omega_2(s)}$$

where, for parallel polarization

$$\begin{aligned} \Upsilon_2(s) = & \sqrt{\bar{\epsilon}_1}\sqrt{\bar{\epsilon}_2} \left[ \left( \epsilon_{1r} \frac{\sigma_2}{\epsilon_0} - \epsilon_{2r} \frac{\sigma_1}{\epsilon_0} \right) s \sqrt{s-s_1}\sqrt{s-s_2} \right. \\ & \left. + \frac{1}{2} \frac{s(s_2-s_1)}{\sqrt{s-s_1}\sqrt{s-s_2}} \left( s\epsilon_{1r} + \frac{\sigma_1}{\epsilon_0} \right) \left( s\epsilon_{2r} + \frac{\sigma_2}{\epsilon_0} \right) \right] \end{aligned}$$

$$\begin{aligned} \Omega_2(s) = & \left( s\epsilon_{1r} + \frac{\sigma_1}{\epsilon_0} \right)^2 \bar{\epsilon}_2 s(s-s_2) + \left( s\epsilon_{2r} + \frac{\sigma_2}{\epsilon_0} \right)^2 \bar{\epsilon}_1 s(s-s_1) \\ & + 2 \left( s\epsilon_{1r} + \frac{\sigma_1}{\epsilon_0} \right) \left( s\epsilon_{2r} + \frac{\sigma_2}{\epsilon_0} \right) \sqrt{\bar{\epsilon}_1}\sqrt{\bar{\epsilon}_2} s \sqrt{s-s_1}\sqrt{s-s_2} \end{aligned}$$

and for perpendicular polarization as

$$\Upsilon_2(s) = \sqrt{\bar{\epsilon}_1}\sqrt{\bar{\epsilon}_2} \frac{s(s_1-s_2)}{\sqrt{s-s_1}\sqrt{s-s_2}}$$

$$\Omega_2(s) = \bar{\epsilon}_2 s(s-s_2) + \bar{\epsilon}_1 s(s-s_1) + 2\sqrt{\bar{\epsilon}_1}\sqrt{\bar{\epsilon}_2} s \sqrt{s-s_1}\sqrt{s-s_2}$$

Here it is noted that the residues of the poles located on the branch cut must be



evaluated carefully, taking into account the value of functions on each side of the branch cut. For this particular problem, the reflection coefficient is even about the branch cut, as discussed on pages 131 through 140, so the values on each side of the branch cut are the same. This allows the evaluation of the residues from each side to be combined into one evaluation giving

$$\int_{\gamma_2 \cup \gamma_4 \cup \gamma_6 \cup \gamma_8} \Gamma(s)e^{st} ds = -j2\pi \sum \text{Res}[\Gamma(s)e^{st}, \text{real poles}]. \quad (5.36)$$

### Contributions from $\gamma_1$ , $\gamma_3$ , $\gamma_5$ , $\gamma_7$ , and $\gamma_9$

The integral contribution from the contour surrounding the branch point at  $s = 0$  can be computed by denoting the radius of  $\gamma_5$  as  $r_0$  and letting  $\phi_0$  be an angle measured counterclockwise from the real axis to the point on  $\gamma_5$ . This allows any point on the contour to be located as  $s = r_0 e^{j\phi_0}$ . The reflection coefficients on the  $\gamma_5$  contour are given in the limit of  $r_0 \rightarrow 0$ , i.e.,  $s \rightarrow 0$ , as

$$R_1(s) = \begin{cases} \frac{\sqrt{\epsilon_1} \sqrt{s} \sqrt{s-s_1} - (s\epsilon_{1r} + \frac{\sigma_1}{\epsilon_0}) \cos \theta_{in}}{\sqrt{\epsilon_1} \sqrt{s} \sqrt{s-s_1} + (s\epsilon_{1r} + \frac{\sigma_1}{\epsilon_0}) \cos \theta_{in}} \rightarrow -1 & \text{parallel polarization} \\ \frac{\sqrt{s} \cos \theta_{in} - \sqrt{\epsilon_1} \sqrt{s-s_1}}{\sqrt{s} \cos \theta_{in} + \sqrt{\epsilon_1} \sqrt{s-s_1}} \rightarrow -1 & \text{perpendicular polarization} \end{cases}$$

$$R_2(s) \rightarrow \begin{cases} \frac{(\frac{\sigma_1}{\epsilon_0}) \sqrt{\epsilon_2} \sqrt{-s_2} - (\frac{\sigma_2}{\epsilon_0}) \sqrt{\epsilon_1} \sqrt{-s_1}}{(\frac{\sigma_1}{\epsilon_0}) \sqrt{\epsilon_2} \sqrt{-s_2} + (\frac{\sigma_2}{\epsilon_0}) \sqrt{\epsilon_1} \sqrt{-s_1}} \triangleq C_1^{\parallel} & \text{parallel polarization} \\ \frac{\sqrt{\epsilon_1} \sqrt{-s_1} - \sqrt{\epsilon_2} \sqrt{-s_2}}{\sqrt{\epsilon_1} \sqrt{-s_1} + \sqrt{\epsilon_2} \sqrt{-s_2}} \triangleq C_1^{\perp} & \text{perpendicular polarization} \end{cases}$$

This gives the reflection coefficient from (5.12) as

$$\Gamma(s) = \frac{-1 + C_1^{\parallel, \perp} - 1 + C_1^{\parallel, \perp}}{1 - C_1^{\parallel, \perp} + 1 - C_1^{\parallel, \perp}} = -1$$

Thus,

$$\Gamma(s)e^{st} = -e^{st}$$

and

$$\left| \Gamma(s)e^{st} \right| \leq e^{r_0 t}.$$

Therefore

$$\left| \int_{\gamma_5} \Gamma(s)e^{st} ds \right| \leq 2\pi r_0 e^{r_0 t} \rightarrow 0, \quad (r_0 \rightarrow 0).$$

As a result, the integral contribution from the contour around the branch point at  $s = 0$  is given by

$$\int_{\gamma_5} \Gamma(s)e^{st} ds = 0. \quad (5.37)$$

The integral contributions from the contours surrounding the branch point at  $s = s_1$  can be computed by denoting the radius of both  $\gamma_3$  and  $\gamma_7$  as  $r_1$  and letting  $\phi_1$  be an angle measured counterclockwise from the real axis to a point on either  $\gamma_3$  or  $\gamma_7$ . This allows any point on the contours to be located as  $s = s_1 + r_1 e^{j\phi_1}$ . The reflection coefficients on the contours are given in the limit of  $r_1 \rightarrow 0$ , i.e.,  $s \rightarrow s_1$ , as

$$R_1(s) = \begin{cases} \frac{\sqrt{\epsilon_1} \sqrt{s} \sqrt{s-s_1} - (s\epsilon_{1r} + \frac{\sigma_1}{\epsilon_0}) \cos \theta_{in}}{\sqrt{\epsilon_1} \sqrt{s} \sqrt{s-s_1} + (s\epsilon_{1r} + \frac{\sigma_1}{\epsilon_0}) \cos \theta_{in}} \rightarrow -1 & \parallel \text{-pol} \\ \frac{s \cos \theta_{in} - \sqrt{\epsilon_1} \sqrt{s} \sqrt{s-s_1}}{s \cos \theta_{in} + \sqrt{\epsilon_1} \sqrt{s} \sqrt{s-s_1}} \rightarrow 1 & \perp \text{-pol} \end{cases}$$

$$R_2(s) = \begin{cases} \frac{(s\epsilon_{1r} + \frac{\sigma_1}{\epsilon_0}) \sqrt{\epsilon_2} \sqrt{s} \sqrt{s-s_2} - (s\epsilon_{2r} + \frac{\sigma_2}{\epsilon_0}) \sqrt{\epsilon_1} \sqrt{s} \sqrt{s-s_1}}{(s\epsilon_{1r} + \frac{\sigma_1}{\epsilon_0}) \sqrt{\epsilon_2} \sqrt{s} \sqrt{s-s_2} + (s\epsilon_{2r} + \frac{\sigma_2}{\epsilon_0}) \sqrt{\epsilon_1} \sqrt{s} \sqrt{s-s_1}} \rightarrow 1 & \parallel \text{-pol} \\ \frac{\sqrt{\epsilon_1} \sqrt{s} \sqrt{s-s_1} - \sqrt{\epsilon_2} \sqrt{s} \sqrt{s-s_2}}{\sqrt{\epsilon_1} \sqrt{s} \sqrt{s-s_1} + \sqrt{\epsilon_2} \sqrt{s} \sqrt{s-s_2}} \rightarrow -1 & \perp \text{-pol} \end{cases}$$

This gives the reflection coefficient from (5.12) as

$$\Gamma(s) = \frac{\mp 1 \pm e^{-s\tau_1(s)} - e^{-s(\tau_1(s)+\tau_2(s))} + e^{-s\tau_2(s)}}{1 - e^{-s\tau_1(s)} \pm e^{-s(\tau_1(s)+\tau_2(s))} \mp e^{-s\tau_2(s)}} = \mp 1$$

where the top sign is taken for parallel polarization, and the bottom sign for perpen-

dicular polarization. Thus,

$$\Gamma(s)e^{st} = \mp e^{st}$$

and

$$\left| \Gamma(s)e^{st} \right| \leq e^{(s_1+r_1)t}.$$

Therefore

$$\left| \int_{\gamma_3 \cup \gamma_7} \Gamma(s)e^{st} ds \right| \leq 2\pi r_1 e^{(s_1+r_1)t} \rightarrow 0, \quad (r_1 \rightarrow 0).$$

As a result, the integral contribution from the contour around the branch point at  $s = s_1$  is given by

$$\int_{\gamma_3 \cup \gamma_7} \Gamma(s)e^{st} ds = 0. \quad (5.38)$$

The integral contributions from the contours surrounding the branch point at  $s = s_2$  can be computed by denoting the radius of both  $\gamma_1$  and  $\gamma_9$  as  $r_2$  and letting  $\phi_2$  be an angle measured counterclockwise from the real axis to a point on either  $\gamma_1$  or  $\gamma_9$ . This allows any point on the contours to be located as  $s = s_2 + r_2 e^{j\phi_2}$ . The reflection coefficients on the contours are given in the limit of  $r_2 \rightarrow 0$ , i.e.,  $s \rightarrow s_2$ , as

$$R_1(s) \rightarrow \begin{cases} \frac{\sqrt{\epsilon_1} \sqrt{s_2} \sqrt{s_2 - s_1} - (s_2 \epsilon_{1r} + \frac{\sigma_1}{\epsilon_0}) \cos \theta_{in}}{\sqrt{\epsilon_1} \sqrt{s_2} \sqrt{s_2 - s_1} + (s_2 \epsilon_{1r} + \frac{\sigma_1}{\epsilon_0}) \cos \theta_{in}} \triangleq C_2^{\parallel} & \parallel \text{-pol} \\ \frac{s_2 \cos \theta_{in} - \sqrt{\epsilon_1} \sqrt{s_2} \sqrt{s_2 - s_1}}{s_2 \cos \theta_{in} + \sqrt{\epsilon_1} \sqrt{s_2} \sqrt{s_2 - s_1}} \triangleq C_2^{\perp} & \perp \text{-pol} \end{cases}$$

$$R_2(s) = \begin{cases} \frac{(s \epsilon_{1r} + \frac{\sigma_1}{\epsilon_0}) \sqrt{\epsilon_2} \sqrt{s} \sqrt{s - s_2} - (s \epsilon_{2r} + \frac{\sigma_2}{\epsilon_0}) \sqrt{\epsilon_1} \sqrt{s} \sqrt{s - s_1}}{(s \epsilon_{1r} + \frac{\sigma_1}{\epsilon_0}) \sqrt{\epsilon_2} \sqrt{s} \sqrt{s - s_2} + (s \epsilon_{2r} + \frac{\sigma_2}{\epsilon_0}) \sqrt{\epsilon_1} \sqrt{s} \sqrt{s - s_1}} \rightarrow -1 & \parallel \text{-pol} \\ \frac{\sqrt{\epsilon_1} \sqrt{s} \sqrt{s - s_1} - \sqrt{\epsilon_2} \sqrt{s} \sqrt{s - s_2}}{\sqrt{\epsilon_1} \sqrt{s} \sqrt{s - s_1} + \sqrt{\epsilon_2} \sqrt{s} \sqrt{s - s_2}} \rightarrow -1 & \perp \text{-pol} \end{cases}$$

This gives the reflection coefficient from (5.12) as

$$\Gamma(s) = \frac{C_2^{\parallel, \perp} \mp e^{-s\tau_1(s)} - e^{-s(\tau_1(s)+\tau_2(s))} \pm C_2^{\parallel, \perp} e^{-s\tau_2(s)}}{1 \mp C_2^{\parallel, \perp} e^{-s\tau_1(s)} - C_2^{\parallel, \perp} e^{-s(\tau_1(s)+\tau_2(s))} \pm e^{-s\tau_2(s)}} \triangleq D^{\parallel, \perp}$$

where the top sign is taken for parallel polarization, and the bottom sign for perpendicular polarization. Thus,

$$\Gamma(s)e^{st} = D^{\parallel,\perp}e^{st}$$

and

$$\left| \Gamma(s)e^{st} \right| \leq |D^{\parallel,\perp}|e^{(s_2+r_2)t}.$$

Therefore

$$\left| \int_{\gamma_1 \cup \gamma_9} \Gamma(s)e^{st} ds \right| \leq 2\pi r_2 |D^{\parallel,\perp}| e^{(s_2+r_2)t} \rightarrow 0, \quad (r_2 \rightarrow 0).$$

As a result, the integral contribution from the contour around the branch point at  $s = s_2$  is given by

$$\int_{\gamma_1 \cup \gamma_9} \Gamma(s)e^{st} ds = 0. \quad (5.39)$$

### Contributions from segments above and below the branch cuts

The contributions from the straight line segments of the inner contour immediately above and below the branch cuts are separated into two groups. The first group is given by  $l_A$  and  $l_B$ , which lie to the left of the branch points. The rest of the contours,  $l_1$  through  $l_6$ , lie to the right of the leftmost branch point. Note that if more than two poles lie on the real axis, more contours would be included in at least one of these groups. The developments here will remain valid for any number of integration contours along the branch cut.

Using (5.1), and noting that this equation can be written simply as  $\Gamma(s) = N(s)/D(s)$ , the numerator and denominator of the frequency domain reflection coef-

ficient can be put into the forms

$$\begin{aligned}
N(s) &= (Z_1 - Z_0)(Z_2 + Z_1) + (Z_2 - Z_1)(Z_1 + Z_0)e^{-s\tau_1(s)} \\
&\quad - (Z_1 + Z_0)(Z_2 + Z_1)e^{-s(\tau_1(s)+\tau_2(s))} - (Z_1 - Z_0)(Z_2 - Z_1)e^{-s\tau_2(s)} \\
&= Z_1Z_2(1 + e^{-s\tau_1(s)})(1 - e^{-s\tau_2(s)}) - Z_0Z_2(1 - e^{-s\tau_1(s)})(1 - e^{-s\tau_2(s)}) \\
&\quad - Z_0Z_1(1 + e^{-s\tau_1(s)})(1 + e^{-s\tau_2(s)}) + Z_1^2(1 - e^{-s\tau_1(s)})(1 + e^{-s\tau_2(s)}) \\
&= jZ_1Z_2 \cos\left(\frac{s\tau_1(s)}{2j}\right) \sin\left(\frac{s\tau_2(s)}{2j}\right) + Z_0Z_2 \sin\left(\frac{s\tau_1(s)}{2j}\right) \sin\left(\frac{s\tau_2(s)}{2j}\right) \\
&\quad - Z_0Z_1 \cos\left(\frac{s\tau_1(s)}{2j}\right) \cos\left(\frac{s\tau_2(s)}{2j}\right) + jZ_1^2 \sin\left(\frac{s\tau_1(s)}{2j}\right) \cos\left(\frac{s\tau_2(s)}{2j}\right) \\
&= \mathcal{X} + j\mathcal{Y}, \tag{5.40}
\end{aligned}$$

and

$$\begin{aligned}
D(s) &= (Z_1 + Z_0)(Z_2 + Z_1) + (Z_1 - Z_0)(Z_2 - Z_1)e^{-s\tau_1(s)} \\
&\quad - (Z_1 - Z_0)(Z_2 + Z_1)e^{-s(\tau_1(s)+\tau_2(s))} - (Z_2 - Z_1)(Z_1 + Z_0)e^{-s\tau_2(s)} \\
&= Z_1Z_2(1 + e^{-s\tau_1(s)})(1 - e^{-s\tau_2(s)}) + Z_0Z_2(1 - e^{-s\tau_1(s)})(1 - e^{-s\tau_2(s)}) \\
&\quad + Z_0Z_1(1 + e^{-s\tau_1(s)})(1 + e^{-s\tau_2(s)}) + Z_1^2(1 - e^{-s\tau_1(s)})(1 + e^{-s\tau_2(s)}) \\
&= jZ_1Z_2 \cos\left(\frac{s\tau_1(s)}{2j}\right) \sin\left(\frac{s\tau_2(s)}{2j}\right) - Z_0Z_2 \sin\left(\frac{s\tau_1(s)}{2j}\right) \sin\left(\frac{s\tau_2(s)}{2j}\right) \\
&\quad + Z_0Z_1 \cos\left(\frac{s\tau_1(s)}{2j}\right) \cos\left(\frac{s\tau_2(s)}{2j}\right) + jZ_1^2 \sin\left(\frac{s\tau_1(s)}{2j}\right) \cos\left(\frac{s\tau_2(s)}{2j}\right) \\
&= -\mathcal{X} + j\mathcal{Y}, \tag{5.41}
\end{aligned}$$

where a multiplication and division by  $e^{s(\tau_1/2+\tau_2/2)}$  has been used, and the quantities

$\mathcal{X}$  and  $\mathcal{Y}$  have been defined as

$$\mathcal{X} = Z_0Z_2 \sin\left(\frac{s\tau_1(s)}{2j}\right) \sin\left(\frac{s\tau_2(s)}{2j}\right) - Z_0Z_1 \cos\left(\frac{s\tau_1(s)}{2j}\right) \cos\left(\frac{s\tau_2(s)}{2j}\right) \tag{5.42}$$

$$\mathcal{Y} = Z_1Z_2 \cos\left(\frac{s\tau_1(s)}{2j}\right) \sin\left(\frac{s\tau_2(s)}{2j}\right) + Z_1^2 \sin\left(\frac{s\tau_1(s)}{2j}\right) \cos\left(\frac{s\tau_2(s)}{2j}\right) \tag{5.43}$$

This allows the frequency domain reflection coefficient to be written as

$$\begin{aligned}\Gamma(s) &= \frac{\mathcal{X} + j\mathcal{Y}}{-\mathcal{X} + j\mathcal{Y}} \\ &= \frac{-\mathcal{X}^2 - j2\mathcal{X}\mathcal{Y} + \mathcal{Y}^2}{\mathcal{X}^2 + \mathcal{Y}^2}.\end{aligned}\quad (5.44)$$

Using this expression for the reflection coefficient, even symmetry about the branch cut can be shown if the quantities  $\mathcal{X}^2$ ,  $\mathcal{Y}^2$ , and  $\mathcal{X}\mathcal{Y}$  are shown to have even symmetry about the branch cut. To show this, the behavior of each of these quantities on either side of the branch cut needs to be evaluated.

Branch cuts which define the principal branches of the complex square root functions of the wave impedances and propagation factors are taken along the negative real axis. These branches are defined by  $-\pi < \phi_0 \leq \pi$ , and  $-\pi < \phi_i \leq \pi$ . Looking at Figure 5.6, begin by examining the integration paths designated as  $A_+$  and  $A_-$ . For the contour  $A_+$ ,  $\phi_1 = \phi_\alpha = \phi_\beta = \pi$ . Letting  $s = -x$ , where  $x$  is a nonnegative real number, denote a point on the negative real axis, the products of the square root functions found in the wave impedances and exponential terms take the form

$$\sqrt{s}\sqrt{s - s_\alpha} = \sqrt{r_1}\sqrt{r_\alpha}e^{j(\phi_1 + \phi_\alpha)/2} = \sqrt{x}\sqrt{x + s_\alpha}e^{j\pi} = -\sqrt{x}\sqrt{x + s_\alpha} \quad (5.45)$$

$$\sqrt{s}\sqrt{s - s_\beta} = \sqrt{r_1}\sqrt{r_\beta}e^{j(\phi_1 + \phi_\beta)/2} = \sqrt{x}\sqrt{x + s_\beta}e^{j\pi} = -\sqrt{x}\sqrt{x + s_\beta} \quad (5.46)$$

where  $s_\alpha$  and  $s_\beta$  represent the two branch points  $s_1$  and  $s_2$ , such that  $|s_\alpha| \leq |s_\beta|$ . Which of the branch points  $s_1$  and  $s_2$  correspond to  $s_\alpha$ , and which to  $s_\beta$ , depends on the material properties of each region, and the incidence angle. Every case will be examined in this section.

On the contour  $A_-$ ,  $\phi_1 = \phi_\alpha = \phi_\beta = -\pi$ , and the products of square roots found

in the wave impedances and exponential terms are given by

$$\sqrt{s}\sqrt{s-s_\alpha} = \sqrt{x}\sqrt{x+s_\alpha}e^{-j\pi} = -\sqrt{x}\sqrt{x+s_\alpha} \quad (5.47)$$

$$\sqrt{s}\sqrt{s-s_\beta} = \sqrt{x}\sqrt{x+s_\beta}e^{-j\pi} = -\sqrt{x}\sqrt{x+s_\beta} \quad (5.48)$$

Thus, the products of these square roots are analytic for the portion of the branch cut which the  $A$  contours run, and

$$\Gamma(s)\Big|_{A+} = \Gamma(s)\Big|_{A-}. \quad (5.49)$$

Since the integrations above and below the branch cut are taken in opposite directions,

$$\int_{l_A} \Gamma(s)e^{st}ds + \int_{l_B} \Gamma(s)e^{st}ds = 0 \quad (5.50)$$

On the contour  $B_+$ ,  $\phi_1 = \phi_\alpha = \pi$ ,  $\phi_\beta = 0$ , and the products of square root functions found in the wave impedances and exponential terms are given by

$$\sqrt{s}\sqrt{s-s_\alpha} = \sqrt{x}\sqrt{x+s_\alpha}e^{j\pi} = -\sqrt{x}\sqrt{x+s_\alpha} \quad (5.51)$$

$$\sqrt{s}\sqrt{s-s_\beta} = \sqrt{x}\sqrt{-x-s_\beta}e^{j\pi/2} = j\sqrt{x}\sqrt{-x-s_\beta} \quad (5.52)$$

Similarly, on the contour  $B_-$ ,  $\phi_1 = \phi_\alpha = -\pi$ ,  $\phi_\beta = 0$

$$\sqrt{s}\sqrt{s-s_\alpha} = \sqrt{x}\sqrt{x+s_\alpha}e^{-j\pi} = -\sqrt{x}\sqrt{x+s_\alpha} \quad (5.53)$$

$$\sqrt{s}\sqrt{s-s_\beta} = \sqrt{x}\sqrt{-x-s_\beta}e^{-j\pi/2} = -j\sqrt{x}\sqrt{-x-s_\beta} \quad (5.54)$$

On  $C_+$ ,  $\phi_1 = \pi$ ,  $\phi_\alpha = \phi_\beta = 0$ , and the products of square root functions found in

the wave impedances and exponential terms are given by

$$\sqrt{s}\sqrt{s-s_\alpha} = \sqrt{x}\sqrt{-x-s_\alpha}e^{j\pi/2} = j\sqrt{x}\sqrt{-x-s_\alpha} \quad (5.55)$$

$$\sqrt{s}\sqrt{s-s_\beta} = \sqrt{x}\sqrt{-x-s_\beta}e^{j\pi/2} = j\sqrt{x}\sqrt{-x-s_\beta} \quad (5.56)$$

Similarly, on  $C_-$ ,  $\phi_1 = -\pi$ ,  $\phi_\alpha = \phi_\beta = 0$

$$\sqrt{s}\sqrt{s-s_\alpha} = \sqrt{x}\sqrt{-x-s_\alpha}e^{-j\pi/2} = -j\sqrt{x}\sqrt{-x-s_\alpha} \quad (5.57)$$

$$\sqrt{s}\sqrt{s-s_\beta} = \sqrt{x}\sqrt{-x-s_\beta}e^{-j\pi/2} = -j\sqrt{x}\sqrt{-x-s_\beta} \quad (5.58)$$

The products of square roots for the portion of the branch cuts which the  $B$  and  $C$  contours run are not found to be analytic, so further investigation into the form of the reflection coefficient is needed.

**Case 1:**  $(\sigma_1/\bar{\epsilon}_1) < (\sigma_2/\bar{\epsilon}_2)$

Examining each combination of material parameters for the first and second layer, beginning with the case of  $(\sigma_1/\bar{\epsilon}_1) < (\sigma_2/\bar{\epsilon}_2)$ , the behavior of the frequency domain reflection coefficient on each side of the branch cut is determined. For this first case,  $s_\alpha = s_1$  and  $s_\beta = s_2$ . Using (5.51) through (5.58), wave impedances on each integration path take on the form

$$Z_1|_{B_+} = Z_1|_{B_-} = \frac{\eta_0 x}{\sqrt{\bar{\epsilon}_1}\sqrt{x}\sqrt{x+s_1}} = Z_1 \quad (5.59)$$

$$Z_1|_{C_+} = \frac{-\eta_0 x}{j\sqrt{\bar{\epsilon}_1}\sqrt{x}\sqrt{-x-s_1}} = Z_{1+} \quad (5.60)$$

$$Z_1|_{C_-} = \frac{\eta_0 x}{j\sqrt{\bar{\epsilon}_1}\sqrt{x}\sqrt{-x-s_1}} = Z_{1-} \quad (5.61)$$

$$Z_2|_{B_+,C_+} = \frac{-\eta_0 x}{j\sqrt{\bar{\epsilon}_2}\sqrt{x}\sqrt{-x-s_2}} = Z_{2+} \quad (5.62)$$

$$Z_2|_{B_-,C_-} = \frac{\eta_0 x}{j\sqrt{\bar{\epsilon}_2}\sqrt{x}\sqrt{-x-s_2}} = Z_{2-} \quad (5.63)$$



so,  $Z_{1+} = -Z_{1-}$ ,  $Z_{2+} = -Z_{2-}$ . The exponential terms are given using

$$s\tau_1|_{B_+} = s\tau_1|_{B_-} = -\frac{2d}{c}\sqrt{\bar{\epsilon}_1}\sqrt{x}\sqrt{x+s_1} = -2\Phi_1 \quad (5.64)$$

$$s\tau_1|_{C_+} = j\frac{2d}{c}\sqrt{\bar{\epsilon}_1}\sqrt{x}\sqrt{-x-s_1} = j2\Phi_{1+} \quad (5.65)$$

$$s\tau_1|_{C_-} = -j\frac{2d}{c}\sqrt{\bar{\epsilon}_1}\sqrt{x}\sqrt{-x-s_1} = j2\Phi_{1-} \quad (5.66)$$

$$s\tau_2|_{B_+,C_+} = j\frac{2h}{c}\sqrt{\bar{\epsilon}_2}\sqrt{x}\sqrt{-x-s_2} = j2\Phi_{2+} \quad (5.67)$$

$$s\tau_2|_{B_-,C_-} = -j\frac{2h}{c}\sqrt{\bar{\epsilon}_2}\sqrt{x}\sqrt{-x-s_2} = j2\Phi_{2-} \quad (5.68)$$

where the quantity  $\Phi_i = (s\tau_i(s)/2j)$  has been defined. Note that  $\Phi_{i+} = -\Phi_{i-}$  in all cases.

On the contour  $B_+$ , plugging (5.59) through (5.68) into (5.42) and (5.43) gives

$$\begin{aligned} \mathcal{X}^2|_{B_+} &= Z_0^2 Z_{2+}^2 \sin^2(j\Phi_1) \sin^2 \Phi_{2+} - Z_0^2 Z_1^2 \cos^2(j\Phi_1) \cos^2 \Phi_{2+} \\ &\quad - 2Z_0^2 Z_1 Z_{2+} \sin(j\Phi_1) \cos(j\Phi_1) \sin \Phi_{2+} \cos \Phi_{2+} \end{aligned} \quad (5.69)$$

$$\begin{aligned} \mathcal{Y}^2|_{B_+} &= Z_1^2 Z_{2+}^2 \cos^2(j\Phi_1) \sin^2 \Phi_{2+} + Z_1^4 \sin^2(j\Phi_1) \cos^2 \Phi_{2+} \\ &\quad + 2Z_1^3 Z_{2+} \sin(j\Phi_1) \cos(j\Phi_1) \sin \Phi_{2+} \cos \Phi_{2+} \end{aligned} \quad (5.70)$$

$$\begin{aligned} \mathcal{X}\mathcal{Y}|_{B_+} &= \sin(j\Phi_1) \cos(j\Phi_1) (Z_0 Z_1 Z_{2+}^2 \sin^2 \Phi_{2+} - Z_0 Z_1^3 \cos^2 \Phi_{2+}) \\ &\quad + Z_0 Z_1^2 Z_{2+} \sin \Phi_{2+} \cos \Phi_{2+} (\sin^2(j\Phi_1) - \cos^2(j\Phi_1)) \end{aligned} \quad (5.71)$$

Similarly, on the contour  $B_-$ ,

$$\begin{aligned}\mathcal{X}^2\Big|_{B_-} &= Z_0^2 Z_{2-}^2 \sin^2(j\Phi_1) \sin^2 \Phi_{2-} - Z_0^2 Z_1^2 \cos^2(j\Phi_1) \cos^2 \Phi_{2-} \\ &\quad - 2Z_0^2 Z_1 Z_{2-} \sin(j\Phi_1) \cos(j\Phi_1) \sin \Phi_{2-} \cos \Phi_{2-}\end{aligned}\quad (5.72)$$

$$\begin{aligned}\mathcal{Y}^2\Big|_{B_-} &= Z_1^2 Z_{2-}^2 \cos^2(j\Phi_1) \sin^2 \Phi_{2-} + Z_1^4 \sin^2(j\Phi_1) \cos^2 \Phi_{2-} \\ &\quad + 2Z_1^3 Z_{2-} \sin(j\Phi_1) \cos(j\Phi_1) \sin \Phi_{2-} \cos \Phi_{2-}\end{aligned}\quad (5.73)$$

$$\begin{aligned}\mathcal{X}\mathcal{Y}\Big|_{B_-} &= \sin(j\Phi_1) \cos(j\Phi_1) (Z_0 Z_1 Z_{2-}^2 \sin^2 \Phi_{2-} - Z_0 Z_1^3 \cos^2 \Phi_{2-}) \\ &\quad + Z_0 Z_1^2 Z_{2-} \sin \Phi_{2-} \cos \Phi_{2-} (\sin^2(j\Phi_1) - \cos^2(j\Phi_1))\end{aligned}\quad (5.74)$$

Note that wave impedances that change sign as a point moves from  $B_+$  to  $B_-$  across the branch cut appear raised to even powers, or grouped with a sine function that also changes sign upon crossing the branch cut. Thus, the quantities  $\mathcal{X}^2$ ,  $\mathcal{Y}^2$ , and  $\mathcal{X}\mathcal{Y}$  are even about the branch cut, and by (5.44),

$$\Gamma(s)\Big|_{B_+} = \Gamma(s)\Big|_{B_-}.\quad (5.75)$$

For the contour  $C_+$ ,

$$\begin{aligned}\mathcal{X}^2\Big|_{C_+} &= Z_0^2 Z_{2+}^2 \sin^2 \Phi_{1+} \sin^2 \Phi_{2+} - Z_0^2 Z_1^2 \cos^2 \Phi_{1+} \cos^2 \Phi_{2+} \\ &\quad - 2Z_0^2 Z_1 Z_{2+} \sin \Phi_{1+} \cos \Phi_{1+} \sin \Phi_{2+} \cos \Phi_{2+}\end{aligned}\quad (5.76)$$

$$\begin{aligned}\mathcal{Y}^2\Big|_{C_+} &= Z_1^2 Z_{2+}^2 \cos^2 \Phi_{1+} \sin^2 \Phi_{2+} + Z_1^4 \sin^2 \Phi_{1+} \cos^2 \Phi_{2+} \\ &\quad + 2Z_1^3 Z_{2+} \sin \Phi_{1+} \cos \Phi_{1+} \sin \Phi_{2+} \cos \Phi_{2+}\end{aligned}\quad (5.77)$$

$$\begin{aligned}\mathcal{X}\mathcal{Y}\Big|_{C_+} &= \sin \Phi_{1+} \cos \Phi_{1+} (Z_0 Z_1 Z_{2+}^2 \sin^2 \Phi_{2+} - Z_0 Z_1^3 \cos^2 \Phi_{2+}) \\ &\quad + Z_0 Z_1^2 Z_{2+} \sin \Phi_{2+} \cos \Phi_{2+} (\sin^2 \Phi_{1+} - \cos^2 \Phi_{1+})\end{aligned}\quad (5.78)$$

Similarly, on  $C_-$ ,

$$\begin{aligned} \mathcal{X}^2 \Big|_{C_-} &= Z_0^2 Z_{2-}^2 \sin^2 \Phi_{1-} \sin^2 \Phi_{2-} - Z_0^2 Z_{1-}^2 \cos^2 \Phi_{1-} \cos^2 \Phi_{2-} \\ &\quad - 2Z_0^2 Z_{1-} Z_{2-} \sin \Phi_{1-} \cos \Phi_{1-} \sin \Phi_{2-} \cos \Phi_{2-} \end{aligned} \quad (5.79)$$

$$\begin{aligned} \mathcal{Y}^2 \Big|_{C_-} &= Z_{1-}^2 Z_{2-}^2 \cos^2 \Phi_{1-} \sin^2 \Phi_{2-} + Z_{1-}^4 \sin^2 \Phi_{1-} \cos^2 \Phi_{2-} \\ &\quad + 2Z_{1-}^3 Z_{2-} \sin \Phi_{1-} \cos \Phi_{1-} \sin \Phi_{2-} \cos \Phi_{2-} \end{aligned} \quad (5.80)$$

$$\begin{aligned} \mathcal{X}\mathcal{Y} \Big|_{C_-} &= \sin \Phi_{1-} \cos \Phi_{1-} (Z_0 Z_{1-} Z_{2-}^2 \sin^2 \Phi_{2-} - Z_0 Z_{1-}^3 \cos^2 \Phi_{2-}) \\ &\quad + Z_0 Z_{1-}^2 Z_{2-} \sin \Phi_{2-} \cos \Phi_{2-} (\sin^2 \Phi_{1-} - \cos^2 \Phi_{1-}) \end{aligned} \quad (5.81)$$

Note that wave impedances that change sign as a point moves from the  $C_+$  contour to the  $C_-$  contour across the branch cuts appear raised to even powers, or grouped with a sine function that also changes sign in crossing the branch cuts. Thus, the quantities  $\mathcal{X}^2$ ,  $\mathcal{Y}^2$ , and  $\mathcal{X}\mathcal{Y}$  are even about the branch cut, and by (5.44),

$$\Gamma(s) \Big|_{C_+} = \Gamma(s) \Big|_{C_-}. \quad (5.82)$$

**Case 2:**  $(\sigma_1/\bar{\epsilon}_1) > (\sigma_2/\bar{\epsilon}_2)$

For this case,  $s_\alpha = s_2$  and  $s_\beta = s_1$ . Using (5.51) through (5.58), wave impedances on each integration path take on the form

$$Z_1 \Big|_{B_+, C_+} = \frac{-\eta_0 x}{j\sqrt{\bar{\epsilon}_1} \sqrt{x} \sqrt{-x - s_1}} = Z_{1+} \quad (5.83)$$

$$Z_1 \Big|_{B_-, C_-} = \frac{-\eta_0 x}{-j\sqrt{\bar{\epsilon}_1} \sqrt{x} \sqrt{-x - s_1}} = Z_{1-} \quad (5.84)$$

$$Z_2 \Big|_{B_+} = Z_2 \Big|_{B_-} = \frac{-\eta_0 x}{-\sqrt{\bar{\epsilon}_2} \sqrt{x} \sqrt{x + s_2}} = Z_2 \quad (5.85)$$

$$Z_2 \Big|_{C_+} = \frac{-\eta_0 x}{j\sqrt{\bar{\epsilon}_2} \sqrt{x} \sqrt{-x - s_2}} = Z_{2+} \quad (5.86)$$

$$Z_2 \Big|_{C_-} = \frac{-\eta_0 x}{-j\sqrt{\bar{\epsilon}_2} \sqrt{x} \sqrt{-x - s_2}} = Z_{2-} \quad (5.87)$$

Thus,  $Z_{1+} = -Z_{1-}$ ,  $Z_{2+} = -Z_{2-}$ . The exponential terms are given using

$$s\tau_1 \Big|_{B_+, C_+} = j \frac{2d}{c} \sqrt{\epsilon_1} \sqrt{x} \sqrt{-x - s_1} = j2\Phi_{1+} \quad (5.88)$$

$$s\tau_1 \Big|_{B_-, C_-} = -j \frac{2d}{c} \sqrt{\epsilon_1} \sqrt{x} \sqrt{-x - s_1} = j2\Phi_{1-} \quad (5.89)$$

$$s\tau_2 \Big|_{B_+} = s\tau_2 \Big|_{B_-} = -\frac{2h}{c} \sqrt{\epsilon_2} \sqrt{x} \sqrt{x + s_2} = -2\Phi_2 \quad (5.90)$$

$$s\tau_2 \Big|_{C_+} = j \frac{2h}{c} \sqrt{\epsilon_2} \sqrt{x} \sqrt{-x - s_2} = j2\Phi_{2+} \quad (5.91)$$

$$s\tau_2 \Big|_{C_-} = -j \frac{2h}{c} \sqrt{\epsilon_2} \sqrt{x} \sqrt{-x - s_2} = j2\Phi_{2-} \quad (5.92)$$

On  $B_+$ , plugging (5.83) through (5.92) into (5.42) and (5.43) gives

$$\begin{aligned} \mathcal{X}^2 \Big|_{B_+} &= Z_0^2 Z_2^2 \sin^2 \Phi_{1+} \sin^2(j\Phi_2) - Z_0^2 Z_{1+}^2 \cos^2 \Phi_{1+} \cos^2(j\Phi_2) \\ &\quad - 2Z_0^2 Z_{1+} Z_2 \sin \Phi_{1+} \cos \Phi_{1+} \sin(j\Phi_2) \cos(j\Phi_2) \end{aligned} \quad (5.93)$$

$$\begin{aligned} \mathcal{Y}^2 \Big|_{B_+} &= Z_{1+}^2 Z_2^2 \cos^2 \Phi_{1+} \sin^2(j\Phi_2) + Z_{1+}^4 \sin^2 \Phi_{1+} \cos^2(j\Phi_2) \\ &\quad + 2Z_{1+}^3 Z_2 \sin \Phi_{1+} \cos \Phi_{1+} \sin(j\Phi_2) \cos(j\Phi_2) \end{aligned} \quad (5.94)$$

$$\begin{aligned} \mathcal{X}\mathcal{Y} \Big|_{B_+} &= \sin \Phi_{1+} \cos \Phi_{1+} (Z_0 Z_{1+} Z_2^2 \sin^2(j\Phi_2) - Z_0 Z_{1+}^3 \cos^2(j\Phi_2)) \\ &\quad + Z_0 Z_{1+}^2 Z_2 \sin(j\Phi_2) \cos \Phi_{2+} (\sin^2 \Phi_{1+} - \cos^2 \Phi_{1+}) \end{aligned} \quad (5.95)$$

Similarly, on  $B_-$ ,

$$\begin{aligned} \mathcal{X}^2 \Big|_{B_-} &= Z_0^2 Z_2^2 \sin^2 \Phi_{1-} \sin^2(j\Phi_2) - Z_0^2 Z_{1-}^2 \cos^2 \Phi_{1-} \cos^2(j\Phi_2) \\ &\quad - 2Z_0^2 Z_{1-} Z_2 \sin \Phi_{1-} \cos \Phi_{1-} \sin(j\Phi_2) \cos(j\Phi_2) \end{aligned} \quad (5.96)$$

$$\begin{aligned} \mathcal{Y}^2 \Big|_{B_-} &= Z_{1-}^2 Z_2^2 \cos^2 \Phi_{1-} \sin^2(j\Phi_2) + Z_{1-}^4 \sin^2 \Phi_{1-} \cos^2(j\Phi_2) \\ &\quad + 2Z_{1-}^3 Z_2 \sin \Phi_{1-} \cos \Phi_{1-} \sin(j\Phi_2) \cos(j\Phi_2) \end{aligned} \quad (5.97)$$

$$\begin{aligned} \mathcal{X}\mathcal{Y} \Big|_{B_-} &= \sin \Phi_{1-} \cos \Phi_{1-} (Z_0 Z_{1-} Z_2^2 \sin^2(j\Phi_2) - Z_0 Z_{1-}^3 \cos^2(j\Phi_2)) \\ &\quad + Z_0 Z_{1-}^2 Z_2 \sin(j\Phi_2) \cos(j\Phi_2) (\sin^2 \Phi_{1-} - \cos^2 \Phi_{1-}) \end{aligned} \quad (5.98)$$

Note that wave impedances that change sign as a point moves from  $B_+$  to  $B_-$  across the branch cuts appear raised to even powers, or grouped with a sine function that also changes sign upon crossing the branch cuts. Thus, the quantities  $\mathcal{X}^2$ ,  $\mathcal{Y}^2$ , and  $\mathcal{X}\mathcal{Y}$  are even about the branch cut, and by (5.44),

$$\Gamma(s)\Big|_{B_+} = \Gamma(s)\Big|_{B_-}. \quad (5.99)$$

The expressions for  $\mathcal{X}^2$ ,  $\mathcal{Y}^2$ , and  $\mathcal{X}\mathcal{Y}$  on the integration paths  $C_+$  and  $C_-$  are given by equations (5.76) through (5.81), since the wave impedances and phase factors are identical for these paths for all combinations of  $\left(\frac{\sigma_1}{\bar{\epsilon}_1}\right)$  and  $\left(\frac{\sigma_2}{\bar{\epsilon}_2}\right)$ . Therefore, as in case 1,

$$\Gamma(s)\Big|_{C_+} = \Gamma(s)\Big|_{C_-}. \quad (5.100)$$

**Case 3:**  $(\sigma_1/\bar{\epsilon}_1) = (\sigma_2/\bar{\epsilon}_2)$

For this case, the integration paths  $B_+$  and  $B_-$  disappear, leaving just the integration paths along  $C_+$  and  $C_-$ . These expressions are given by equations (5.76) through (5.81), as in the first two cases.

Thus, for all combinations of  $(\sigma_1/\bar{\epsilon}_1)$  and  $(\sigma_2/\bar{\epsilon}_2)$ , the frequency domain reflection coefficient displays an even symmetry about the branch cut along the entire negative real axis. Since integrations along the branch cut are taken in opposing directions, there will be no contributions from integrating along these paths; i.e.,

$$\begin{aligned} & \int_{l_1, l_2} \Gamma(s)\Big|_{B_+} e^{st} ds + \int_{l_3, l_4} \Gamma(s)\Big|_{C_+} e^{st} ds \\ & + \int_{l_5, l_6} \Gamma(s)\Big|_{B_-} e^{st} ds + \int_{l_7, l_8} \Gamma(s)\Big|_{C_-} e^{st} ds = 0. \end{aligned} \quad (5.101)$$

Thus, in the late time, the time domain reflection coefficient is given from (5.31)

as

$$\begin{aligned}
\Gamma(t) &= \frac{1}{j2\pi} \int_{Br} \Gamma(s)e^{st} ds \\
&= \sum Res[\Gamma(s)e^{st}, \text{complex poles}] + \sum Res[\Gamma(s)e^{st}, \text{real poles}] \\
&= \sum Res[\Gamma(s)e^{st}, \text{poles}] = \sum_k A_k e^{s_k t} \tag{5.102}
\end{aligned}$$

which is a pure natural mode series, with amplitude coefficients given by (5.35). Here, the pole contributions from the complex poles included inside the closed contour, and the contributions from the poles on the real axis are combined to give the complete pole series for this geometry, where all of the residues are evaluated using (5.34).

It is important to note that the response of the two-layered material structure backed by a perfect conductor is a natural mode series during the late time. This implies that the branch cut contribution that is present in the middle time of the response is turned off when the reflection from the conductor backing reaches the observation plane; that is, at the start of the late time. This has important implications in the form of the temporal response in that a turn on and turn off behavior can be identified. This behavior provides motivation for investigation into this occurrence for the  $n$ -layered case in Chapter 6.

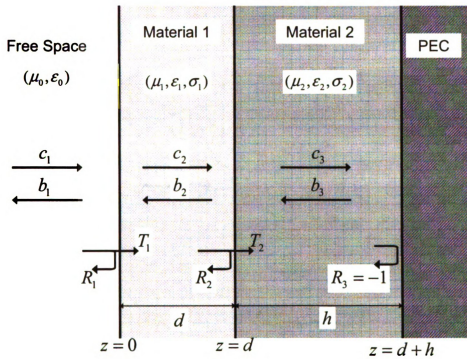


Figure 5.1. Air Lossy Lossy PEC

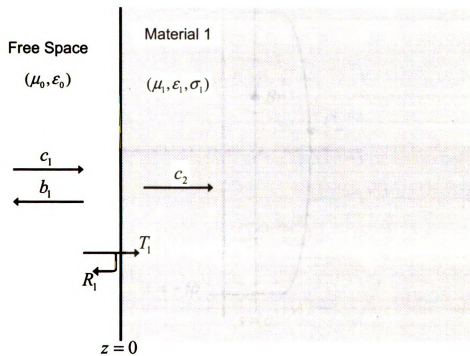


Figure 5.2. Single interface between free-space and a lossy dielectric



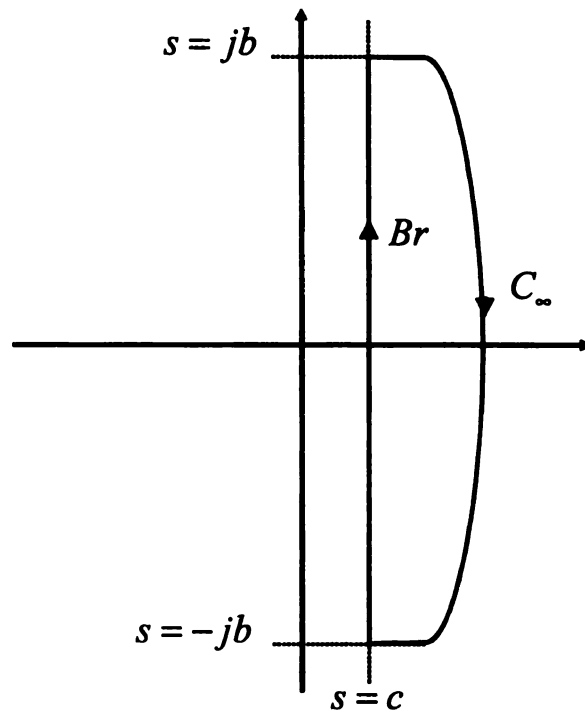


Figure 5.3. Closure of the Bromwich contour in the right half plane.  
 $|b| \rightarrow \infty, 0 < c < \infty$

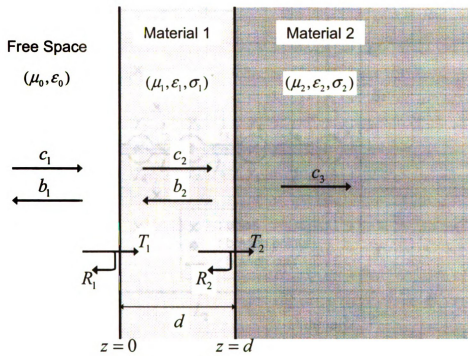


Figure 5.4. Material-backed lossy dielectric layer

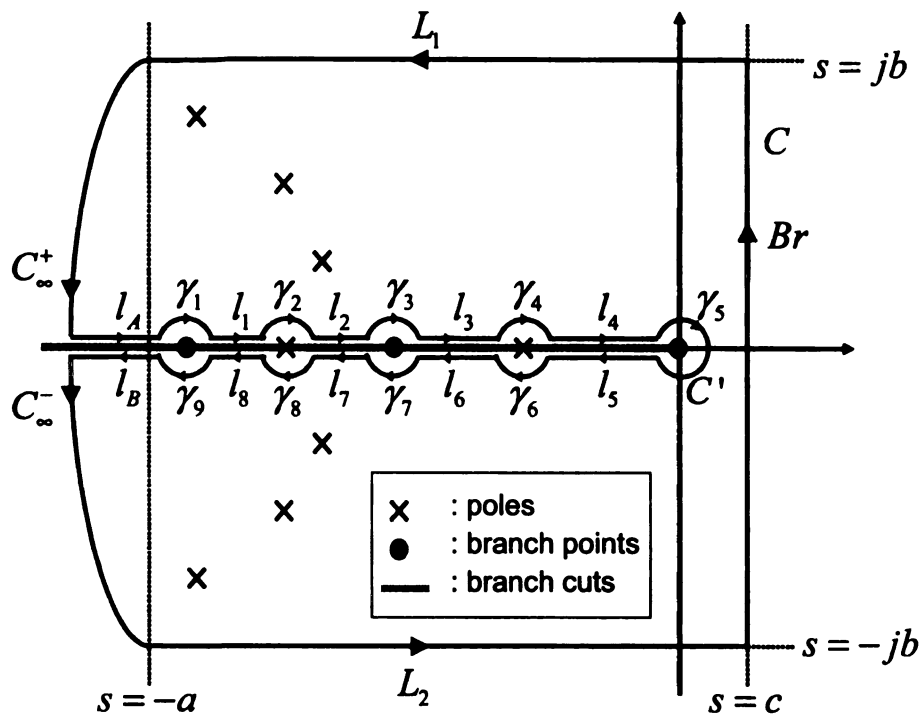


Figure 5.5. Closure of the Bromwich contour in the left half plane.  
 $|a|, |b| \rightarrow \infty, 0 < c < \infty$

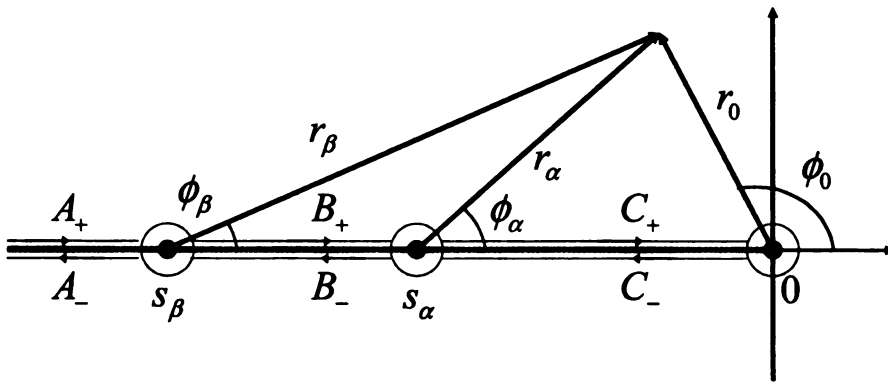


Figure 5.6. Inner contour integration paths for left half plane closure

## CHAPTER 6

### N-LAYERED MATERIAL PROBLEMS

The temporal response from a multilayered material backed by a material half space is obtained through the inverse Laplace transform of the frequency domain reflection coefficient. For a planar layered structure, this reflection coefficient is easily obtained in closed form using the wave matrix method. A methodology for performing the inverse Laplace transform on a general, multilayered material is developed here.

Calculation of the inverse Laplace transform for an N-layered material structure is broken up into various steps, corresponding to various time periods of the temporal response. Physically, these steps have to do with the time that it takes for an incident electromagnetic field to penetrate the multilayered structure. These time periods are determined by the thickness of each material layer, along with the speed of light in that layer. Further discussion on the definition of these time periods is given in Sections 6.2 and 6.3.

The inverse Laplace transform is defined by an integration in the complex  $s$ -plane along the Bromwich path. This is a path which is taken parallel to the imaginary axis, to the right of all singular points. Singularities in the frequency domain reflection coefficients occur in various forms. An example of the types and locations of these singularities is given in Figure 6.1. Examining the figure, one type of singularity present is simple poles, which will appear both on the real axis, and as complex conjugate pairs. Either type of pole will appear in the left half of the complex  $s$ -plane for this passive system. In addition to simple poles, the frequency domain reflection coefficient contains complex square roots due to the terms  $s\tau_i(s)$  and  $Z_i(s)$ . The

quantity  $s\tau_i(s)$  is given in Chapters 3 through 5 as

$$\begin{aligned} s\tau_i(s) &= \frac{2\Delta_i}{c} \sqrt{\bar{\epsilon}_i} \sqrt{s} \sqrt{s + \frac{\sigma_i}{\bar{\epsilon}_i \epsilon_0}} \\ &= \frac{2\Delta_i}{c} \sqrt{\bar{\epsilon}_i} \sqrt{s} \sqrt{s - s_i}. \end{aligned} \quad (6.1)$$

where  $\Delta_i$  is the physical thickness of the material layer,  $c$  is the speed of light in free space, and  $\bar{\epsilon}_i = \epsilon_{ir} - \sin^2 \theta_{in}$ . Here  $\epsilon_{ir}$  is the relative permittivity of region  $i$ , and  $\theta_{in}$  is the incidence angle of a wave in region 0 impinging on the first interface to the layered material. The wave impedance of region  $i$  is given by

$$Z_i(s) = \begin{cases} \frac{\eta_0 s}{\sqrt{\bar{\epsilon}_i} \sqrt{s} \sqrt{s - s_i}} & \text{perpendicular polarization} \\ \frac{\eta_0 \sqrt{\bar{\epsilon}_i} \sqrt{s} \sqrt{s - s_i}}{s\epsilon_{ir} + \sigma_i/\epsilon_0} & \text{parallel polarization} \end{cases} \quad (6.2)$$

In both the wave impedance and propagation terms, the product of complex square roots  $\sqrt{s} \sqrt{s - s_i}$  appears. These square roots will lead to branch points and corresponding branch cuts in the complex  $s$ -plane. The branch points are given by  $s = 0$  and  $s = s_i$ . The quantity  $s_i = -\sigma_i/\bar{\epsilon}_i \epsilon_0$  is a nonpositive real number, so the branch points are located on the real axis.

## 6.1 Evaluation of the Laplace inversion integral

In taking the inverse Laplace transform, closure of the integration path in the complex plane will take place in either the left or right half plane, depending on the behavior of the integrand on an infinite contour. The implications of closure in each half plane are discussed here.

### 6.1.1 Left half plane closure

When closure is taken in the left half of the complex  $s$ -plane, as shown in Figure 6.2, many integration paths are involved. In this discussion, these integration paths will

be referred to in two groups, the outer contour,  $C$ , which includes integration paths parameterized by quantities which recede towards infinity, and the inner contour,  $C'$ , which includes integration paths taken along the branch cut. These integration contours are given for the example of Figure 6.2 as

$$C = Br \cup L_1 \cup C_\infty^+ \cup C_\infty^- \cup L_2$$

$$C' = l_A \cup \gamma_1 \cup \gamma_2 \cup \dots \cup \gamma_7 \cup l_1 \cup l_2 \cup \dots \cup l_6 \cup l_B$$

Using Cauchy's residue theorem, evaluation of the closed contour integration is given by

$$\oint_{C \cup C'} f(s)e^{st} ds = j2\pi \sum \text{Res}[f(s)e^{st}, \text{poles}] \quad (6.3)$$

where  $f(s)$  represents the frequency domain reflection coefficient for which the inverse Laplace transform is sought. Thus, determination of the time domain reflection coefficient is possible provided the integral contribution from each path is known. Note that the singularities shown in the  $s$ -plane in Figure 6.2 are for illustration purposes, and the actual singularities associated with a given frequency domain reflection coefficient will vary. Thus, more poles, branch points, and branch cuts will occur in some cases, and additional segments will be added to the inner contour. The formulations included here are valid for any number of these contours.

#### 6.1.1.1 Contributions from the outer contour, $C$

The Laplace inversion integral is found by computing (6.3) for the Bromwich path contribution in terms of the contributions from all other integration paths and computation of the residues from the enclosed simple poles. The outer contour,  $C$ , consists of various integration paths that are parameterized by quantities that recede towards infinity, including the Bromwich path which defines the inverse Laplace transform.

#### Contributions from $C_\infty^+$ and $C_\infty^-$

When closure in the left half plane is warranted, that is for  $t > 0$ , integral contributions from  $C_\infty^+$  and  $C_\infty^-$  are given directly by *Jordan's lemma*. This is given in [15] as

**Theorem 6.1** (*Jordan's Lemma*) *If  $H(z)$  is an analytic function having the property*

$$\lim_{R \rightarrow \infty} H(Re^{j\theta}) = 0, \quad -\frac{\pi}{2} \leq \theta \leq \frac{\pi}{2} \quad \text{or} \quad \frac{\pi}{2} \leq \theta \leq \frac{3\pi}{2}$$

*uniformly with respect to  $\theta$ , then, if  $b$  is a nonzero real number,*

$$\lim_{R \rightarrow \infty} \int_{C_1} H(z)e^{bz} dz = 0, \quad \text{if } b < 0$$

$$\lim_{R \rightarrow \infty} \int_{C_2} H(z)e^{bz} dz = 0, \quad \text{if } b > 0$$

where  $C_1$  and  $C_2$  are semicircles in the right and left half planes, respectively, centered at the origin and of radius  $R$ .

Since  $f(s) \rightarrow 0$  on the infinite contours,  $C_\infty^+$  and  $C_\infty^-$ , for the reflection coefficients of interest here, application of *Jordan's lemma* gives

$$\int_{C_\infty^+} f(s)e^{st} ds = 0 \tag{6.4}$$

$$\int_{C_\infty^-} f(s)e^{st} ds = 0, \tag{6.5}$$

where  $t > 0$ .

### Contributions from $L_1$ and $L_2$

On  $L_1$  and  $L_2$ , *Jordan's Lemma* cannot be directly applied to evaluate the integral contributions, because the integrand does not go to zero as  $|s| \rightarrow \infty$  at all points on the contours. However, by definition of the time domain reflection coefficient, the infinite contour contributions are to be neglected, as discussed in Section 2.4.



### 6.1.1.2 Contributions from the inner contour, $C'$

The segments of the inner contour  $C'$ , which enclose the branch cut can be broken into three groups. The first group consists of the contours  $\gamma_2$ ,  $\gamma_3$ ,  $\gamma_5$ , and  $\gamma_6$ , etc., which enclose the real poles on the branch cut. Note that two poles are shown on the real axis here, but more may appear depending on both the properties of the material layers, and the incidence angle. The second group is made up of contours  $\gamma_1$ ,  $\gamma_4$ , and  $\gamma_7$  that enclose the branch points. The straight line segments immediately above and below the branch cut make up the final group. Within this group, the segments  $l_A$  and  $l_B$ , which lie to the left of all of the branch points will be handled separately from the segments  $l_1$  through  $l_6$ .

#### Contributions from $\gamma_2$ , $\gamma_3$ , $\gamma_5$ , and $\gamma_6$

The integral contributions from the first group of contours can be found by calculating the residues of  $f(s)e^{st}$  at the poles. For the reflection coefficients considered here, it is found that all poles of  $f(s)$  are first order and thus the residues may be found from

$$\text{Res}[f(s)e^{st}, \text{poles}] \Big|_{s=s_k} = \lim_{s \rightarrow s_k} (s - s_k)[f(s)e^{st}] \quad (6.6)$$

It is important that care be taken in evaluating the residues from poles residing on the branch cut. The formula for computing the residues given here is valid for poles on the branch cut, since there exists a neighborhood around the pole where the function  $f(s)$  is single valued, even though the neighborhood is in more than one Riemann sheet.[15] Since this is true, a semicircular integration path around the pole will yield  $j\pi$  times the residue, when the proper value of  $f(s)$  is taken. If  $f(s)$  is even about the branch cut, then the value on both sides is the same, and the distinction between the two sides need not be made. Explicit expressions for the residues can be found by evaluating (6.6), but they depend on the form of the reflection coefficient, and thus are not included in this general formulation.

### Contributions from $\gamma_1$ , $\gamma_4$ , and $\gamma_7$

The integral contribution from the contour surrounding the branch point at  $s = 0$  can be computed by denoting the radius of  $\gamma_4$  as  $r_0$  and letting  $\phi_0$  be an angle measured counterclockwise from the real axis to the point on  $\gamma_4$ . This allows any point on the contour to be located as  $s = r_0 e^{j\phi_0}$ . Computing the reflection coefficient on  $\gamma_4$  in the limit of  $r_0 \rightarrow 0$  it is anticipated that this will lead to the reflection coefficient approaching a constant on the contour, as has been the case in every geometry considered. If this constant is given by  $D$ , then

$$\Gamma(s)e^{st} = De^{st}$$

and

$$|\Gamma(s)e^{st}| \leq De^{r_0 t}.$$

Therefore

$$\left| \int_{\gamma_4} \Gamma(s)e^{st} ds \right| \leq 2\pi r_0 De^{r_0 t} \rightarrow 0, \quad (r_0 \rightarrow 0).$$

With this, the integral contribution from  $\gamma_4$  is given as

$$\int_{\gamma_4} f(s)e^{st} ds = 0 \tag{6.7}$$

Analogously, the integral contribution from the contours surrounding the branch point at  $s = s_1$  can be computed by denoting the radius of  $\gamma_1$  and  $\gamma_7$  as  $r_1$  and letting  $\phi_1$  be an angle measured counterclockwise from the real axis to a point on either  $\gamma_1$  or  $\gamma_7$ . This allows any point on the contours to be located as  $s = s_1 + r_1 e^{j\phi_1}$ . Computing the reflection coefficient on the contours as  $r_1 \rightarrow 0$ , it is anticipated that this will lead to

$$\int_{\gamma_1 \cup \gamma_7} f(s)e^{st} ds = 0. \tag{6.8}$$

## Contributions from segments above and below the branch cuts

The contributions from the straight line segments of the inner contour immediately above and below the branch cuts require further knowledge of the form of the frequency domain reflection coefficient. This is the focus of Section 6.4, which explores the conditions for the existence of a branch cut contribution. Discussion of the contributions due to the branch cuts will be deferred to that section, noting only that a branch cut contribution is possible, and the integral along the Bromwich path is thus given using (6.3) through (6.8) by

$$\begin{aligned}
 \int_{Br} f(s)e^{st} ds &= j2\pi \sum \text{Res}[f(s)e^{st}, \text{complex poles}] \\
 &\quad + j\pi \sum \text{Res}[f(s)|_+ e^{st}, \text{real poles}] \\
 &\quad + j\pi \sum \text{Res}[f(s)|_- e^{st}, \text{real poles}] \\
 &\quad - \sum_i \int_{l_i} f(s)e^{st} ds
 \end{aligned} \tag{6.9}$$

for closure in the left half plane.

### 6.1.2 Right half plane closure

When closure is taken in the right half of the complex s-plane, as shown in Figure 6.3, only two integration paths are involved, and no singularities of the reflection coefficient are contained within the closed contour. One of these paths is the Bromwich path, labelled  $Br$ , which defines the inverse Laplace transform, and the other is an infinite contour, marked  $C_\infty$ . Thus, by Cauchy's Integral theorem,

$$\oint_C f(s)e^{st} ds = \int_{Br} f(s)e^{st} ds + \int_{C_\infty} f(s)e^{st} ds = 0 \tag{6.10}$$

where  $f(s)$  is the frequency domain reflection coefficient for which the temporal response is desired. Using (6.10), the infinite contour contribution is all that is needed

to determine the inverse transform. For the reflection coefficients discussed here, direct application of *Jordan's Lemma* will not be possible in evaluating the contribution of the integral over  $C_\infty$ , since  $f(s)$  will not approach zero over the entire contour. However, by definition of the time domain reflection coefficient, the infinite contour contribution is to be neglected. Thus, when the closure of the Laplace inversion integral can be taken in the right half plane, which can be done if  $t < 0$ , the inverse Laplace transform of the reflection coefficient is equal to zero. This is used in Section 6.3 to establish a factorization of the frequency domain reflection coefficient into substructure responses which occur during certain time periods associated with the transit times of the material regions.

## 6.2 Form of the reduced reflection coefficient

To examine the transient reflected field from a layered material in terms of the layers which make up the structure, several substructures and the decomposition of their reflection coefficients will first be considered. These substructures are layered geometries which can be identified as components of the multilayered structure of interest. The choice of which substructure to use for the decomposition of the frequency domain reflection coefficient is based on the response seen at an observation plane during a given period of time. For example, if the time period of the response is between the two-way transit times of first two layers, then the substructure response used in the decomposition of the reflection coefficient is that of the first layer backed by a half space of the second material. This is used in decomposing the reflection coefficient into a reflection coefficient describing the response of the substructure, and a reduced reflection coefficient.

The earliest portion of the temporal response corresponds to a time period in which only a reflection from the first interface is seen at the observation plane. The

response for a single interface between two regions of space is given as

$$\Gamma(s) = R_1(s), \quad (6.11)$$

where  $R_1(s)$  is the interfacial reflection coefficient for the interface between region 0 and region 1. The interfacial reflection coefficient is computed for the interface between any two material regions as

$$R_i(s) = \frac{Z_i - Z_{i-1}}{Z_i + Z_{i-1}} \quad (6.12)$$

where  $Z_i$  is the wave impedance for the  $i^{\text{th}}$  region of space as given in (6.2).

Now consider the reflection from a single layer, backed by a material half space as shown in Figure 6.5. This is the geometry whose temporal response will appear after the two way transit time of the first layer. The frequency domain reflection coefficient for the single layer is found, using the wave matrix method discussed in Section 2.3, as

$$\begin{aligned} \Gamma_{1lay}(s) &= N_1(s)/D_1(s) \\ N_1(s) &= R_1(s) + R_2(s)P_1^2(s) \\ &= N_0 + R_2(s) \left[ P_1^2(s) \right] \end{aligned} \quad (6.13a)$$

$$\begin{aligned} D_1(s) &= 1 + R_1(s)R_2(s)P_1^2(s) \\ &= D_0 + R_2(s) \left[ R_1(s)P_1^2(s) \right] \end{aligned} \quad (6.13b)$$

where  $N_0 = R_1(s)$  and  $D_0 = 1$  are the numerator and denominator of the frequency domain reflection coefficient for a single interface, as given by (6.11). The interfacial reflection coefficients for the first and second interface are given by  $R_1(s)$  and  $R_2(s)$ , respectively, and  $P_1^2(s) = e^{-s\tau_1}$  is related to the propagation of a wave through

the material layer, with  $s\tau_1(s)$  given by (6.1).

To examine the response from this structure, the assumption is made that the early time response, which occurs prior to the two way transit time of the material layer, will be identical to the reflection from a single interface. Because of this, the frequency domain reflection coefficient is decomposed into two components. The first of these is the reflection coefficient for the single interface between two material half spaces, given by the interfacial reflection coefficient of the first interface, and the second is the reduced reflection coefficient. The reduced reflection coefficient for the single layer geometry is defined as the difference between the reflection coefficient for the two interface structure, and the one for the single interface. The reduced reflection coefficient is thus given by

$$\begin{aligned}
\Gamma'_{1lay}(s) &= \Gamma_{1lay}(s) - R_1(s) \\
&= (1 - R_1^2(s)) \frac{R_2(s)P_1^2(s)}{D_1(s)} \\
&= T_1^+(s)T_1^-(s) \frac{R_2(s)P_1^2(s)}{D_1(s)} \\
&= [T_1^+(s)P_1(s)] \left[ \frac{R_2(s)}{D_1(s)} \right] [T_1^-(s)P_1(s)], \tag{6.14}
\end{aligned}$$

where  $\Gamma_{1lay}(s)$  is the frequency domain reflection coefficient for the single layer geometry. Here  $T_1^+(s)$  and  $T_1^-(s)$  are the interfacial transmission coefficients for forward and backward transmission though the first interface,  $T_1^+(s) = 1 + R_1(s)$  and  $T_1^-(s) = 1 - R_1(s)$ , respectively. The reduced reflection coefficient is thus composed of the transfer functions for the direct path to and from the second interface, divided by the denominator of the reflection coefficient for the single layer structure.

Now consider adding a third interface to the layered structure, as shown in Figure 6.6. The frequency domain reflection coefficient is given using the wave matrix method

as

$$\Gamma_{2lay}(s) = N_2(s)/D_2(s)$$

$$\begin{aligned} N_2(s) &= R_1(s) + R_2(s)P_1^2(s) + R_3(s)P_1^2(s)P_2^2(s) + R_1(s)R_2(s)R_3(s)P_2^2(s) \\ &= N_1(s) + R_3(s) \left[ N_0(s)R_2(s)P_2^2(s) + P_1^2(s)P_2^2(s) \right] \end{aligned} \quad (6.15a)$$

$$\begin{aligned} D_2(s) &= 1 + R_1(s)R_2(s)P_1^2(s) + R_1(s)R_3(s)P_1^2(s)P_2^2(s) + R_2(s)R_3(s)P_2^2(s) \\ &= D_1(s) + R_3(s) \left[ D_0(s)R_2(s)P_2^2(s) + R_1(s)P_1^2(s)P_2^2(s) \right] \end{aligned} \quad (6.15b)$$

where  $N_1(s)$  and  $D_1(s)$  are the numerator and denominator for the single layer structure, as given by (6.13). Also,  $N_0(s)$  and  $D_0(s)$  are the numerator and denominator of the single interface structure, whose response is given by (6.11). The various exponential terms,  $P_1^2(s)$  and  $P_2^2(s)$ , describe the propagation through the first and second material layers, respectively.

To examine the response from the two layer structure, the assumption is made that the early time response, which occurs prior to the two way transit time of the two material layers, will be identical to the reflection from a single layered structure, backed by a material half space. Because of this, the frequency domain reflection coefficient is factored into two components. The first of these is the reflection coefficient for the single layered structure, given by (6.13), and the second is the reduced reflection coefficient. The reduced reflection coefficient is defined for the two layer structure as the difference between the reflection coefficient for the three interface structure, and the one for the two interface geometry. The reduced reflection coefficient is thus given by

$$\begin{aligned} \Gamma'_{2lay}(s) &= \Gamma_{2lay}(s) - \Gamma_{1lay}(s) \\ &= \frac{N_2(s)D_1(s) - N_1(s)D_2(s)}{D_2(s)D_1(s)} \end{aligned} \quad (6.16)$$

where the various terms in the numerator of the reduced reflection coefficient are given by

$$N_2(s)D_1(s) = (R_1 + R_2P_1^2 + R_3P_1^2P_2^2 + R_1R_2R_3P_2^2)(1 + R_1R_2P_1^2) \quad (6.17)$$

and

$$N_1(s)D_2(s) = (R_1 + R_2P_1^2)(1 + R_1R_2P_1^2 + R_1R_3P_1^2P_2^2 + R_2R_3P_2^2) \quad (6.18)$$

where dependence on the complex variable,  $s$ , is suppressed for brevity. The difference between the terms in (6.17) and (6.18) can be simplified to give

$$\begin{aligned} N_2(s)D_1(s) - N_1(s)D_2(s) &= R_3P_1^2P_2^2 + R_1^2R_2R_3P_1^2P_2^2 - R_1^2R_3P_1^2P_2^2 - R_2^2R_3P_1^2P_2^2 \\ &= R_3P_1^2P_2^2(1 + R_1^2R_2^2 - R_1^2 - R_2^2) \\ &= R_3P_1^2P_2^2(1 - R_1^2)(1 - R_2^2). \end{aligned} \quad (6.19)$$

The reduced reflection coefficient for the two layer case is thus given by

$$\begin{aligned} \Gamma'_{2lay}(s) &= (1 - R_1^2(s))(1 - R_2^2(s)) \frac{R_3(s)P_1^2(s)P_2^2(s)}{D_2(s)D_1(s)} \\ &= T_1^+(s)T_1^-(s)T_2^+(s)T_2^-(s) \frac{R_3(s)P_1^2(s)P_2^2(s)}{D_2(s)D_1(s)} \\ &= [T_1^+(s)P_1(s)T_2^+(s)P_2(s)] \left[ \frac{R_3(s)}{D_2(s)D_1(s)} \right] [T_1^-(s)P_1(s)T_2^-(s)P_2(s)], \end{aligned} \quad (6.20)$$

where  $T_1^+(s)$  and  $T_1^-(s)$  are the interfacial transmission coefficients for forward and backward transmission through the first interface, and  $T_2^+(s)$  and  $T_2^-(s)$  are for the second interface. These transmission coefficients are found for forward and backward transmission as  $T_i^+(s) = 1 + R_i(s)$  and  $T_i^-(s) = 1 - R_i(s)$ , respectively. The reduced



reflection coefficient is thus composed of the transfer functions for the direct path to and from the third interface, divided by the product of the denominators of the reflection coefficients for the single layer structure and the two layer geometry.

Now consider adding a fourth interface to the layered structure, as shown in Figure 6.7. Then, the frequency domain reflection coefficient is given using the wave matrix method as

$$\begin{aligned}\Gamma_{3lay}(s) &= N_3(s)/D_3(s) \\ N_3(s) &= R_1 + R_2 P_1^2 + R_3 P_1^2 P_2^2 + R_1 R_2 R_3 P_2^2 + R_1 R_3 R_4 P_3^2 \\ &\quad + R_2 R_3 R_4 P_1^2 P_3^2 + R_1 R_2 R_4 P_2^2 P_3^2 + R_4 P_1^2 P_2^2 P_3^2 \\ &= N_2(s) + R_4 \left[ N_1(s) R_3 P_3^2 + N_0(s) R_2 P_2^2 P_3^2 + P_1^2 P_2^2 P_3^2 \right] \quad (6.21a)\end{aligned}$$

$$\begin{aligned}D_3(s) &= 1 + R_1 R_2 P_1^2 + R_1 R_3 P_1^2 P_2^2 + R_2 R_3 P_2^2 + R_3 R_4 P_3^2 \\ &\quad + R_1 R_2 R_3 R_4 P_1^2 P_3^2 + R_2 R_4 P_2^2 P_3^2 + R_1 R_4 P_1^2 P_2^2 P_3^2 \\ &= D_2(s) + R_4 \left[ D_1(s) R_3 P_3^2 + D_0 R_2 P_2^2 P_3^2 + R_1 P_1^2 P_2^2 P_3^2 \right] \quad (6.21b)\end{aligned}$$

where the numerator and denominator are given in terms of the numerator and denominator of the reflection coefficients for all of the substructures as described by (6.11), (6.13), and (6.15). The various exponential terms,  $P_1^2(s)$ ,  $P_2^2(s)$ , and  $P_3^2(s)$ , describe the propagation through the three material layers.

To examine the response from the three layer structure, the assumption is made that the early time response, which occurs prior to the two way transit time of the three material layers, will be identical to the reflection from a two layered structure, backed by a material half space. Because of this, the frequency domain reflection coefficient is factored into two components. The first of these is the reflection coefficient for the two layered structure, given by (6.15), and the second is the reduced reflection coefficient. The reduced reflection coefficient is defined for the three layer structure as

the difference between the reflection coefficient for the four interface structure, and the one for the three interface geometry. The reduced reflection coefficient is thus given by

$$\begin{aligned}\Gamma'_{3lay}(s) &= \Gamma_{3lay}(s) - \Gamma_{2lay}(s) \\ &= \frac{N_3(s)D_2(s) - N_2(s)D_3(s)}{D_3(s)D_2(s)}\end{aligned}\quad (6.22)$$

where the various terms in the numerator are found as

$$\begin{aligned}N_3(s)D_2(s) &= (R_1 + R_2P_1^2 + R_3P_1^2P_2^2 + R_1R_2R_3P_2^2 + R_1R_3R_4P_3^2 \\ &\quad + R_2R_3R_4P_1^2P_3^2 + R_1R_2R_4P_2^2P_3^2 + R_4P_1^2P_2^2P_3^2) \times \\ &\quad \times (1 + R_1R_2P_1^2 + R_1R_3P_1^2P_2^2 + R_2R_3P_2^2)\end{aligned}\quad (6.23)$$

and

$$\begin{aligned}N_2(s)D_3(s) &= (R_1 + R_2P_1^2 + R_3P_1^2P_2^2 + R_1R_2R_3P_2^2) \times \\ &\quad \times (1 + R_1R_2P_1^2 + R_1R_3P_1^2P_2^2 + R_2R_3P_2^2 + R_3R_4P_3^2 \\ &\quad + R_1R_2R_3R_4P_1^2P_3^2 + R_2R_4P_2^2P_3^2 + R_1R_4P_1^2P_2^2P_3^2)\end{aligned}\quad (6.24)$$

The difference between these terms can be simplified as

$$\begin{aligned}
N_3(s)D_2(s) - N_2(s)D_3(s) &= R_4P_1^2P_2^2P_3^2 + R_1^2R_2^2R_4P_1^2P_2^2P_3^2 + R_1^2R_3^2R_4P_1^2P_2^2P_3^2 \\
&\quad + R_2^2R_3^2R_4P_1^2P_2^2P_3^2 - R_1^2R_2^2R_3^2R_4P_1^2P_2^2P_3^2 \\
&\quad - R_3^2R_4P_1^2P_2^2P_3^2 - R_2^2R_4P_1^2P_2^2P_3^2 - R_1^2R_4P_1^2P_2^2P_3^2 \\
&= R_4P_1^2P_2^2P_3^2(1 + R_1^2R_2^2 + R_1^2R_3^2 + R_2^2R_3^2 \\
&\quad - R_1^2R_2^2R_3^2 - R_3^2 - R_2^2 - R_1^2) \\
&= R_4P_1^2P_2^2P_3^2(1 - R_1^2)(1 - R_2^2)(1 - R_3^2) \tag{6.25}
\end{aligned}$$

The reduced reflection coefficient for the three layer case is thus given by

$$\begin{aligned}
\Gamma'_{3lay}(s) &= (1 - R_1^2(s))(1 - R_2^2(s))(1 - R_3^2(s)) \frac{R_4(s)P_1^2(s)P_2^2(s)P_3^2(s)}{D_3(s)D_2(s)} \\
&= T_1^+(s)T_1^-(s)T_2^+(s)T_2^-(s)T_3^+(s)T_3^-(s) \frac{R_4(s)P_1^2(s)P_2^2(s)P_3^2(s)}{D_3(s)D_2(s)} \\
&= [T_1^+ P_1 T_2^+ P_2 T_3^+ P_3] \left[ \frac{R_4(s)}{D_3(s)D_2(s)} \right] [T_1^- P_1 T_2^- P_2 T_3^- P_3], \tag{6.26}
\end{aligned}$$

where  $T_1^+(s)$  and  $T_1^-(s)$  are the interfacial transmission coefficients for forward and backward transmission through the first interface,  $T_2^+(s)$  and  $T_2^-(s)$  are for the second interface, and  $T_3^+(s)$  and  $T_3^-(s)$  are for the third interface. These transmission coefficients are found for forward and backward transmission as  $T_3^+(s) = 1 + R_3(s)$  and  $T_3^-(s) = 1 - R_3(s)$ , respectively. The reduced reflection coefficient for the three layer structure is thus composed of the transfer functions for the direct path to and from the fourth interface, divided by the product of the denominators of the reflection coefficients for the two layer structure and the three layer geometry.

Continuing to add interfaces to the geometry, the general case of an N-layer geometry can be addressed. Beginning by examining the processes used to determine the forms of the numerator and denominator of each reflection coefficient for the cases

of one through four interfaces, given by (6.11), (6.13), (6.15), and (6.21), a recursive formula for determining the numerator and denominator of the frequency domain reflection coefficient can be found for any number of interfaces as

$$N_i(s) = N_{i-1}(s) + R_{i+1} \left[ \prod_{j=1}^i P_j^2(s) + \sum_{j=0}^{i-2} N_j(s) R_{j+2}(s) \prod_{k=j+2}^i P_k^2(s) \right] \quad (6.27a)$$

$$D_i(s) = D_{i-1}(s) + R_{i+1} \left[ R_1(s) \prod_{j=1}^i P_j^2(s) + \sum_{j=0}^{i-2} D_j(s) R_{j+2}(s) \prod_{k=j+2}^i P_k^2(s) \right] \quad (6.27b)$$

This form of the numerator and denominator of the frequency domain reflection coefficient can also be obtained through a direct examination of the wave matrix method. This is due to the fashion in which the transmission chain matrices for each material layer are cascaded to give the desired frequency domain reflection coefficient.

Using the form of the numerator and denominator of the frequency domain reflection coefficient given in (6.27), the reflection coefficient of a  $N$ -layered geometry can be written as

$$\Gamma_{Nlay}(s) = N_N(s)/D_N(s)$$

$$N_N(s) = N_{N-1}(s) + R_{N+1} \left[ \prod_{j=1}^N P_j^2(s) + \sum_{i=0}^{N-2} N_i(s) R_{i+2}(s) \prod_{j=i+2}^N P_j^2(s) \right] \quad (6.28a)$$

$$D_N(s) = D_{N-1}(s) + R_{N+1} \left[ R_1(s) \prod_{j=1}^N P_j^2(s) + \sum_{i=0}^{N-2} D_i(s) R_{i+2}(s) \prod_{j=i+2}^N P_j^2(s) \right] \quad (6.28b)$$

where the numerator and denominator are given in terms of the numerator and denominator of the reflection coefficients for all of the substructures comprising the

$N$ -layered geometry. The various exponential terms,  $P_j^2(s)$ , describe the propagation through the different material layers.

To examine the response from this structure, the assumption is made that the early time response, which occurs prior to the two way transit time of the  $N$  material layers, will be identical to the reflection from a  $(N - 1)$ -layered structure, backed by a material half space. Because of this, the frequency domain reflection coefficient is factored into two components. The first of these is the reflection coefficient for the  $(N - 1)$ -layered structure, and the second is the reduced reflection coefficient. The reduced reflection coefficient for the  $N$ -layered geometry is defined as the difference between the reflection coefficient for the  $(N + 1)$  interface structure, and the one for the  $N$  interface geometry. The reduced reflection coefficient is thus given by

$$\begin{aligned}
\Gamma'_{Nlay}(s) &= \Gamma_{Nlay}(s) - \Gamma_{(N-1)lay}(s) \\
&= \frac{N_N(s)D_{N-1}(s) - N_{N-1}(s)D_N(s)}{D_N(s)D_{N-1}(s)} \\
&= \frac{R_{N+1}}{D_N D_{N-1}} \left[ D_{N-1} \left( \prod_{j=1}^N P_j^2(s) + \sum_{i=0}^{N-2} N_i R_{i+2} \prod_{j=i+2}^N P_j^2(s) \right) \right. \\
&\quad \left. - N_{N-1} \left( R_1 \prod_{j=1}^N P_j^2(s) + \sum_{i=0}^{N-2} D_i R_{i+2} \prod_{j=i+2}^N P_j^2(s) \right) \right] \quad (6.29)
\end{aligned}$$

Defining  $A_N = \prod_{j=1}^N P_j^2(s)$  and  $B_{i,N} = \prod_{j=i+2}^N P_j^2(s)$  to simplify notation, and

plugging in  $D_{N-1}$  and  $N_{N-1}$  using (6.27) gives

$$\begin{aligned}
\Gamma'_{Nlay}(s) &= \frac{R_{N+1}}{D_N D_{N-1}} \left[ \left( D_{N-2} + R_N \left[ R_1 A_{N-1} + \sum_{k=0}^{N-3} D_k R_{k+2} B_{k,N-1} \right] \right) \times \right. \\
&\quad \times \left( A_N + \sum_{i=0}^{N-2} N_i R_{i+2} B_{i,N} \right) - \left( N_{N-2} + \right. \\
&\quad \left. \left. + R_N \left[ A_{N-1} + \sum_{k=0}^{N-3} N_k R_{k+2} B_{k,N-1} \right] \right) \left( R_1 A_N + \sum_{i=0}^{N-2} D_i R_{i+2} B_{i,N} \right) \right]
\end{aligned} \tag{6.30}$$

The terms in brackets are multiplied out using

$$\begin{aligned}
&\left( R_1 A_{N-1} + \sum_{k=0}^{N-3} D_k R_{k+2} B_{k,N-1} \right) \left( A_N + \sum_{i=0}^{N-2} N_i R_{i+2} B_{i,N} \right) \\
&- \left( A_{N-1} + \sum_{k=0}^{N-3} N_k R_{k+2} B_{k,N-1} \right) \left( R_1 A_N + \sum_{i=0}^{N-2} D_i R_{i+2} B_{i,N} \right) \\
&= R_1 \left( \sum_{k=0}^{N-3} N_k R_{k+2} (A_{N-1} B_{k,N} - A_N B_{k,N-1}) + A_N N_{N-2} R_N \right) \\
&\quad + \left( \sum_{k=0}^{N-3} D_k R_{k+2} (A_N B_{k,N-1} - A_{N-1} B_{k,N}) - A_N D_{N-2} R_N \right) \\
&\quad + \sum_{k=0}^{N-3} \sum_{i=0}^{N-2} (D_k N_i - D_i N_k) R_{k+2} R_{i+2} B_{k,N-1} B_{i,N}
\end{aligned} \tag{6.31}$$

where summation terms have been combined by pulling the  $N-2$  term out in each of the first two expressions. Plugging in the expressions for  $A_N B_{k,N-1}$  and  $A_{N-1} B_{k,N}$ ,

the single summation terms in (6.31) are exactly zero, giving

$$\begin{aligned}
& \left( R_1 A_{N-1} + \sum_{k=0}^{N-3} D_k R_{k+2} B_{k,N-1} \right) \left( A_N + \sum_{i=0}^{N-2} N_i R_{i+2} B_{i,N} \right) \\
& - \left( A_{N-1} + \sum_{k=0}^{N-3} N_k R_{k+2} B_{k,N-1} \right) \left( R_1 A_N + \sum_{i=0}^{N-2} D_i R_{i+2} B_{i,N} \right) \\
& = R_1 A_N N_{N-2} R_N - A_N D_{N-2} R_N \\
& \quad + \sum_{k=0}^{N-3} \sum_{i=0}^{N-2} (D_k N_i - D_i N_k) R_{k+2} R_{i+2} B_{k,N-1} B_{i,N} \quad (6.32)
\end{aligned}$$

The expression for the reduced reflection coefficient is thus given by

$$\begin{aligned}
\Gamma'_{Nlay}(s) &= \frac{R_{N+1}}{D_N D_{N-1}} \left[ D_{N-2} \left( A_N + \sum_{i=0}^{N-2} N_i R_{i+2} B_{i,N} \right) \right. \\
& \quad - N_{N-2} \left( R_1 A_N + \sum_{i=0}^{N-2} D_i R_{i+2} B_{i,N} \right) + R_1 A_N N_{N-2} R_N^2 \\
& \quad \left. - A_N D_{N-2} R_N^2 + R_N \sum_{k=0}^{N-3} \sum_{i=0}^{N-2} (D_k N_i - D_i N_k) R_{k+2} R_{i+2} B_{k,N-1} B_{i,N} \right] \quad (6.33)
\end{aligned}$$

Next, examining the double summation in (6.33), for indices which occur in both summations, that is for  $i = 0 : N - 3$  and  $k = 0 : N - 3$ , expansion of the summations shows that the double summation is equal to zero. This will leave only the  $i = N - 2$  term, which is a single summation. To see this, take the example of  $N = 5$ . For this

example, the double summation in (6.33) is given as

$$\begin{aligned}
& \sum_{k=0}^2 \sum_{i=0}^3 (D_k N_i - D_i N_k) R_{k+2} R_{i+2} B_{k,4} B_{i,5} \\
&= \sum_{k=0}^2 \sum_{i=0}^2 (D_k N_i - D_i N_k) R_{k+2} R_{i+2} B_{k,4} B_{i,5} \\
&+ \sum_{k=0}^2 (D_k N_3 - D_3 N_k) R_{k+2} R_5 B_{k,4} B_{3,5} \quad (6.34)
\end{aligned}$$

Looking at the double summation term with identical indices for both sums and expanding out the sums gives

$$\begin{aligned}
& \sum_{k=0}^2 \sum_{i=0}^2 (D_k N_i - D_i N_k) R_{k+2} R_{i+2} B_{k,4} B_{i,5} \\
&= (D_0 N_0 - D_0 N_0) R_2^2 B_{0,4} B_{0,5} + (D_1 N_0 - D_0 N_1) R_3 R_2 (B_{1,4} B_{0,5} - B_{0,4} B_{1,5}) \\
&+ (D_1 N_1 - D_1 N_1) R_3^2 B_{1,4} B_{1,5} + (D_2 N_0 - D_0 N_2) R_4 R_2 (B_{2,4} B_{0,5} - B_{0,4} B_{2,5}) \\
&+ (D_2 N_2 - D_2 N_2) R_4^2 B_{2,4} B_{2,5} + (D_1 N_2 - D_2 N_1) R_3 R_4 (B_{1,4} B_{2,5} - B_{2,4} B_{1,5}) \\
&= 0 \quad (6.35)
\end{aligned}$$

where the difference between the products of terms involving  $B_{i,N}$  can be shown to equal zero by plugging the quantities  $B_{i,N} = \prod_{j=i+2}^N P_j^2(s)$  back into (6.35). With this, the reduced reflection coefficient is given as

$$\begin{aligned}
\Gamma'_{Nlay}(s) &= \frac{R_{N+1}}{D_N D_{N-1}} \times \\
&\times \left[ D_{N-2} \left( A_N + \sum_{i=0}^{N-2} N_i R_{i+2} B_{i,N} \right) - N_{N-2} \left( R_1 A_N + \sum_{i=0}^{N-2} D_i R_{i+2} B_{i,N} \right) \right. \\
&\left. + R_N^2 \left( R_1 A_N N_{N-2} - A_N D_{N-2} + \sum_{k=0}^{N-3} (D_k N_{N-2} - D_{N-2} N_k) R_{k+2} B_{k,N} \right) \right] \quad (6.36)
\end{aligned}$$



Rearranging terms to combine the first two summations into one gives

$$\begin{aligned} \Gamma'_{Nlay}(s) = \frac{R_{N+1}}{D_N D_{N-1}} & \left[ (1 - R_N^2)(D_{N-2}A_N - N_{N-2}R_1A_N) \right. \\ & + \sum_{k=0}^{N-2} (D_{N-2}N_k - D_k N_{N-2})R_{k+2}B_{k,N} \\ & \left. + R_N^2 \sum_{k=0}^{N-3} (D_k N_{N-2} - D_{N-2}N_k)R_{k+2}B_{k,N} \right] \quad (6.37) \end{aligned}$$

Now noting that the  $N - 2$  term in the first summation is exactly zero, a  $(1 - R_N^2)$  can be pulled out of the equation, leading to

$$\begin{aligned} \Gamma'_{Nlay}(s) = \frac{R_{N+1}}{D_N D_{N-1}} (1 - R_N^2) & \times \\ & \times \left[ D_{N-2} \left( A_N + \sum_{i=0}^{N-3} N_i R_{i+2} B_{i,N} \right) - N_{N-2} \left( R_1 A_N + \sum_{i=0}^{N-3} D_i R_{i+2} B_{i,N} \right) \right]. \quad (6.38) \end{aligned}$$

At this point, the derivation of the form of the reduced reflection coefficient becomes recursive, because the portion of the equation in brackets can be written generally as

$$\begin{aligned} & D_i \left( A_N + \sum_{j=0}^{i-1} N_j R_{j+2} B_{j,N} \right) - N_i \left( R_1 A_N + \sum_{j=0}^{i-1} D_j R_{j+2} B_{j,N} \right) \\ & = \left( D_{i-1} + R_{i+1} \left[ R_1 A_i + \sum_{k=0}^{i-2} D_k R_{k+2} B_{k,i} \right] \right) \left( A_N + \sum_{j=0}^{i-1} N_j R_{j+2} B_{j,N} \right) \\ & \quad - \left( N_{i-1} + R_{i+1} \left[ A_i + \sum_{k=0}^{i-2} N_k R_{k+2} B_{k,i} \right] \right) \left( R_1 A_N + \sum_{j=0}^{i-1} D_j R_{j+2} B_{j,N} \right) \quad (6.39) \end{aligned}$$

where  $D_i$  and  $N_i$  have been substituted from (6.27). Note that many terms on the right hand side of (6.39) will cancel out, as they did in (6.30). Using analogous steps

to (6.31)-(6.35) gives

$$\begin{aligned}
& D_i \left( A_N + \sum_{j=0}^{i-1} N_j R_{j+2} B_{j,N} \right) - N_i \left( R_1 A_N + \sum_{j=0}^{i-1} D_j R_{j+2} B_{j,N} \right) \\
&= (1 - R_{i+1}^2) \times \\
&\quad \times \left[ D_{i-1} \left( A_N + \sum_{j=0}^{i-2} N_j R_{j+2} B_{j,N} \right) - N_{i-1} \left( R_1 A_N + \sum_{j=0}^{i-2} D_j R_{j+2} B_{j,N} \right) \right]
\end{aligned} \tag{6.40}$$

Continually reapplying (6.40) for decreasing values of  $i$ , until  $i = 3$ , at which point simple expressions for the terms  $N_0$ ,  $D_0$ ,  $N_1$ , and  $D_1$  are available, gives the reduced reflection coefficient as

$$\begin{aligned}
\Gamma'_{Nlay}(s) &= \frac{R_{N+1}}{D_N D_{N-1}} \prod_{i=3}^N (1 - R_i^2) \times \\
&\quad \times \left[ D_1 \left( A_N + N_0 R_2 B_{0,N} \right) - N_1 \left( R_1 A_N + D_0 R_2 B_{0,N} \right) \right].
\end{aligned} \tag{6.41}$$

Plugging in the expressions for  $N_0$ ,  $D_0$ ,  $N_1$ , and  $D_1$ , using (6.11) and (6.13), and writing out the products  $A_N$  and  $B_{0,N}$  gives

$$\begin{aligned}
\Gamma'_{Nlay}(s) &= \frac{R_{N+1}}{D_N D_{N-1}} \prod_{i=3}^N (1 - R_i^2) \times \\
&\quad \times \left[ \left( 1 + R_1 R_2 P_1^2(s) \right) \left( \prod_{j=1}^N P_j^2(s) + R_1 R_2 \prod_{j=2}^N P_j^2(s) \right) \right. \\
&\quad \left. - \left( R_1 + R_2 P_1^2(s) \right) \left( R_1 \prod_{j=1}^N P_j^2(s) + R_2 \prod_{j=2}^N P_j^2(s) \right) \right].
\end{aligned} \tag{6.42}$$

Multiplying out the bracketed terms and rearranging the equation gives

$$\begin{aligned}
\Gamma'_{Nlay}(s) &= \frac{R_{N+1}}{D_N D_{N-1}} \prod_{i=3}^N (1 - R_i^2) \times \\
&\quad \times \left[ \prod_{j=1}^N P_j^2(s) \left[ \left( 1 + R_1 R_2 P_1^2(s) + R_1^2 R_2^2 + R_1 R_2 P_1^{-2} \right) \right. \right. \\
&\quad \left. \left. - \left( R_1^2 + R_1 R_2 P_1^2(s) + R_2^2 + R_1 R_2 P_1^{-2} \right) \right] \right] \\
&= \frac{R_{N+1}}{D_N D_{N-1}} \prod_{i=3}^N (1 - R_i^2) \left[ \prod_{j=1}^N P_j^2(s) \left[ (1 - R_2^2)(1 - R_1^2) \right] \right] \quad (6.43)
\end{aligned}$$

Finally, combining the product terms allows the reduced reflection coefficient for the N-layered material structure backed by a material half space to be written as

$$\begin{aligned}
\Gamma'_{Nlay}(s) &= \Gamma_{Nlay}(s) - \Gamma_{(N-1)lay}(s) \\
&= \frac{R_{N+1}(s)}{D_N(s) D_{N-1}(s)} \prod_{i=1}^N (1 - R_i^2(s)) P_i^2(s) \\
&= \left[ \prod_{i=1}^N T_i^+(s) P_i(s) \right] \left[ \frac{R_{N+1}(s)}{D_N(s) D_{N-1}(s)} \right] \left[ \prod_{i=1}^N T_i^-(s) P_i(s) \right], \quad (6.44)
\end{aligned}$$

where  $T_i^+(s)$  and  $T_i^-(s)$  are the interfacial transmission coefficients for forward and backward transmission though the  $i^{th}$  interface. These transmission coefficients are found for forward and backward transmission as  $T_i^+(s) = 1 + R_i(s)$  and  $T_i^-(s) = 1 - R_i(s)$ , respectively. The reduced reflection coefficient is thus composed of the transfer functions for the direct path to and from the  $N + 1$  interface, divided by the product of the denominators of the reflection coefficients for the  $N$  layer structure and the  $(N - 1)$  layer geometry.

### 6.3 Decomposition of the temporal response using substructure responses

The reflection from a multilayered structure is considered in terms of substructure responses in this section. These substructures are layered material structures backed by material half spaces, which can be identified as components of the larger multilayered geometry.

Begin by considering the temporal response due to reflection from a single interface between two materials as shown in Figure 6.4. The interfacial reflection coefficient is given in the frequency domain by (6.12) in terms of the wave impedance in each region of space. The time domain response is obtained through an inverse Laplace transform of the interfacial reflection coefficient. This reflection coefficient may be multiplied by a unit step function without changing the response, since the system is causal. The time-domain reflection coefficient is thus given for a single interface by

$$\Gamma_{int}(t) = [R_1(t)]u(t) \quad (6.45)$$

This response consists of an impulsive component resulting from the discontinuity between the two regions of space, and, in the case of a lossy half space, an infinite tail which slowly decays. The second of these terms results from conduction currents in the lossy material, and will prohibit a pure natural mode series representation from fully describing the transient response, as long as it is present. A rigorous exploration into the components of this interfacial reflection coefficient can be found in [14].

By adding a second interface to the material structure, a single layer geometry with a material backing as shown in Figure 6.5 is created. The frequency domain reflection coefficient for this structure can be decomposed into two parts. The first of these is the interfacial reflection coefficient given by (6.11), since the response should be identical to that of the single interface during the early time. The second part of

the frequency domain reflection coefficient is the reduced reflection coefficient, which is given by (6.14). Taking the inverse Laplace transform of the frequency domain reflection coefficient yields the temporal response of the layered structure. Because the inverse Laplace transform is a linear operation, the temporal response of the single layered geometry can be found as the sum of the inverse transforms of the components of the frequency domain reflection coefficient. Examining (6.14), the term  $P_1^2(s) = e^{-s\tau_1(s)}$  appears in the numerator. Looking at the behavior of  $\tau_1(s)$  on an infinite contour,

$$\lim_{|s| \rightarrow \infty} \frac{2\Delta_1}{c} \sqrt{\epsilon_1} \sqrt{1 + \frac{\sigma_1}{s\epsilon_0\epsilon_1}} = \frac{2\Delta_1}{c} \sqrt{\epsilon_1} = \tau_1$$

with this, which is the two-way transit time of the material layer as discussed in Section 2.4.1, the inverse transform of the reduced reflection coefficient is found by closing the Laplace inversion integral in the right half plane for  $t < \tau_1$ , and in the left half plane for  $t > \tau_1$ , since  $\tau_1$  is a positive real number. The inverse transform of the reduced reflection coefficient will thus be zero for  $t < \tau_1$ , and nonzero after this time. Thus, the inverse Laplace transform of the frequency domain reflection coefficient for this structure can be multiplied by a unit step function without changing the response. The temporal response for  $t > \tau_1$  is explored in detail in Section 6.4. The response of the two interface geometry is thus given as

$$\Gamma_{2int}(t) = \Gamma_{1int}(t)u(t) + \Gamma'_{2int}(t)u(t - \tau_1) \quad (6.46)$$

Plugging in the definition of the reduced reflection coefficient, which is the difference between the reflection coefficient for the two interface geometry, and that of the single interface structure, the temporal response of the two interface structure can be written

as

$$\begin{aligned}
\Gamma_{2int}(t) &= R_1(t)u(t) + (\Gamma_{2int}(t) - R_1(t))u(t - \tau_1) \\
&= R_1(t)(u(t) - u(t - \tau_1)) + \Gamma_{2int}(t)u(t - \tau_1) \\
&= [R_1(t)u(t)]u(\tau_1 - t) + \Gamma_{2int}(t)u(t - \tau_1) \tag{6.47}
\end{aligned}$$

The temporal response from a single layered structure is thus given by the response of the single interface geometry for a time  $t < \tau_1$ , where  $\tau_1$  is the two way transit time of the material layer. After this time, the response of the single interface substructure turns off, and a late time response from the entire structure turns on. The form of this late time response is considered in Section 6.4. This behavior of one response turning off, and another turning on is an important result. It gives that the branch cut contribution of the interfacial reflection coefficient,  $R_1(t)$ , is exactly cancelled when the response from the next interface arrives at the observation plane. This provides motivation to continue adding interfaces to find out if the turn on and turn off behavior of the responses will continue, yielding an algorithmic approach to finding the time domain reflection coefficient for a structure with an arbitrary number of layers.

Adding a third interface to the material structure creates a two layer, material backed geometry shown in Figure 6.6. The frequency domain reflection coefficient for this structure can be decomposed into two parts. The first of these is the total reflection coefficient for a single layer structure, as given by (6.13). This is used because the response of the multilayered structure should be identical to that of a material backed material layer during the early time. The second part of the frequency domain reflection coefficient is the reduced reflection coefficient, which is given by (6.16). Taking the inverse Laplace transform of the frequency domain reflection coefficient yields the temporal response of the layered structure. Because the inverse Laplace transform is a linear operation, the temporal response of the two layered geometry can be found as

the sum of the inverse transforms of the components of the frequency domain reflection coefficient. Examining (6.16), the term  $P_1^2(s)P_2^2(s) = e^{-s(\tau_1(s)+\tau_2(s))}$  appears in the numerator. Looking at the behavior of  $\tau_1(s) + \tau_2(s)$  on an infinite contour,

$$\lim_{|s| \rightarrow \infty} \left[ \frac{2\Delta_1}{c} \sqrt{\bar{\epsilon}_1} \sqrt{1 + \frac{\sigma_1}{s\epsilon_0\bar{\epsilon}_1}} + \frac{2\Delta_2}{c} \sqrt{\bar{\epsilon}_2} \sqrt{1 + \frac{\sigma_2}{s\epsilon_0\bar{\epsilon}_2}} \right] = \frac{2\Delta_1}{c} \sqrt{\bar{\epsilon}_1} + \frac{2\Delta_2}{c} \sqrt{\bar{\epsilon}_2} = \tau_2$$

with this, which is the two-way transit time of the first two material layers, as discussed in Section 2.4.1, the inverse transform of the reduced reflection coefficient is found by closing the Laplace inversion integral in the right half plane for  $t < \tau_2$ , and in the left half plane for  $t > \tau_2$ , since  $\tau_2$  is a positive real number. The inverse transform of the reduced reflection coefficient will thus be zero for  $t < \tau_2$ , and nonzero after this time, thus, a unit step function can multiply the inverse Laplace transform of the reflection coefficient without changing the response. The temporal response for  $t > \tau_2$  is explored in detail in Section 6.4. The response of the three interface geometry is thus given as

$$\Gamma_{3int}(t) = \Gamma_{2int}(t)u(t) + \Gamma'_{3int}(t)u(t - \tau_2)$$

Plugging in the definition of the reduced reflection coefficient, which is the difference between the reflection coefficient for the three interface geometry, and that of the two interface structure, the temporal response of the three interface structure can be

written as

$$\begin{aligned}
\Gamma_{3int}(t) &= \Gamma_{2int}(t)u(t) + (\Gamma_{3int}(t) - \Gamma_{2int}(t))u(t - \tau_2) \\
&= \Gamma_{2int}(t)(u(t) - u(t - \tau_2)) + \Gamma_{3int}(t)u(t - \tau_2) \\
&= [\Gamma_{2int}(t)u(t)]u(\tau_2 - t) + \Gamma_{3int}(t)u(t - \tau_2) \\
&= [R_1(t)u(t)]u(\tau_1 - t) + [\Gamma_{2int}(t)u(t - \tau_1)]u(\tau_2 - t) + \Gamma_{3int}(t)u(t - \tau_2)
\end{aligned} \tag{6.48}$$

The temporal response from a two layered structure is thus given by the response of the single interface geometry for a time  $t < \tau_1$ , where  $\tau_1$  is the two way transit time of the first material layer. After this time, the response of the single interface substructure turns off, and a late time response from the single layer structure turns on. This response continues until a time  $\tau_2$ , which is the two way transit time of the two material layers. At the time  $\tau_2$ , the response of the single layer geometry turns off, and a late time response for the entire structure turns on. The form of this late time response is considered in Section 6.4.

Continuing to add interfaces to the material structure eventually creates an N layer geometry backed by a material half space, as shown in Figure 6.8. The frequency domain reflection coefficient for this structure can be decomposed into two parts. The first of these is the frequency domain reflection coefficient for the  $(N - 1)$  layer geometry, and the second part is the reduced reflection coefficient, which is given by (6.44). Taking the inverse Laplace transform of the frequency domain reflection coefficient yields the temporal response of the layered structure. Because the inverse Laplace transform is a linear operation, the temporal response of the N-layered geometry can be found as the sum of the inverse transforms of the components of the frequency domain reflection coefficient. Examining (6.44), the term  $\prod_{i=1}^N P_i^2(s) = \prod_{i=1}^N e^{-s\tau_i(s)}$  appears in the numerator.



Looking at the behavior of  $\sum_{i=1}^N \tau_i(s)$  on an infinite contour,

$$\sum_{i=1}^N \tau_i(s) = \lim_{|s| \rightarrow \infty} \sum_{i=1}^N \frac{2\Delta_i}{c} \sqrt{\bar{\epsilon}_i} \sqrt{1 + \frac{\sigma_i}{s\epsilon_0\bar{\epsilon}_i}} = \sum_{i=1}^N \frac{2\Delta_i}{c} \sqrt{\bar{\epsilon}_i} = \tau_N$$

with this, which is the two-way transit time of the  $N$  material layers, the inverse transform of the reduced reflection coefficient is found by closing the Laplace inversion integral in the right half plane for  $t < \tau_N$ , and in the left half plane for  $t > \tau_N$ , since  $\tau_N$  is a positive real number. The inverse transform of the reduced reflection coefficient will thus be zero for  $t < \tau_N$ , and nonzero after this time, thus, a unit step function can multiply the inverse Laplace transform of the reflection coefficient without changing the response. The temporal response for  $t > \tau_N$  is explored in detail in Section 6.4. The response of the  $(N + 1)$  interface geometry is thus given as

$$\begin{aligned} \Gamma_{(N+1)int}(t) &= \Gamma_{Nint}(t)u(t) + \Gamma'_{(N+1)int}(t)u(t - \tau_N) \\ &= \Gamma_{Nint}(t)u(t) + (\Gamma_{(N+1)int}(t) - \Gamma_{Nint}(t))u(t - \tau_N) \\ &= \Gamma_{Nint}(t)(u(t) - u(t - \tau_N)) + \Gamma_{(N+1)int}(t)u(t - \tau_N) \\ &= [R_1(t)u(t)]u(\tau_1 - t) + [\Gamma_{2int}(t)u(t - \tau_1)]u(\tau_2 - t) \\ &\quad + \dots + [\Gamma_{Nint}(t)u(t - \tau_{N-1})]u(\tau_N - t) + \Gamma_{(N+1)int}(t)u(t - \tau_N) \end{aligned} \tag{6.49}$$

The temporal response from a  $N$ -layered structure is thus given by the response of the single interface geometry for a time  $t < \tau_1$ , where  $\tau_1$  is the two way transit time of the first material layer. After this time, the response of the single interface substructure turns off, and a late time response from the single layer structure turns on. This response continues until a time  $\tau_2$ , which is the two way transit time of the first two material layers. At the time  $\tau_2$ , the response of the single layer geometry turns off, and the late time response for the two layer geometry turns on. This turn on and

turn off behavior of the various substructure responses continues until the two way transit time of all  $N$  layers has elapsed, when the late time response for the entire structure turns on. The form of the late time responses are considered in Section 6.4.

#### 6.4 Determination of the branch cut contribution

The recursive forms of the numerator and denominator of the reflection coefficient, given by (6.27), can be expanded out to find explicit forms, which give information on the form of the temporal response. This can be done relatively easily for a small number of layers. However, for many layers, expansion in this way is prohibitively time consuming. For this reason, the recursive nature of the numerator and denominator is exploited in order to show the origin, or existence, of a branch cut contribution to the late time response of a  $N$  layer geometry, without placing the expressions in explicit form. Several products will be employed throughout this derivation in order to simplify equations as much as possible. For notational purposes, these products will be written as

$$\mathbb{A}_{a,b} = \prod_{i=a}^b (Z_{i+1} + Z_i) \quad (6.50a)$$

$$\mathbb{B}_{a,b} = \prod_{i=a}^b P_i^2. \quad (6.50b)$$

Exploration into the origin of the branch cut contributions is carried out by looking at the forms of the denominator and numerator of the reflection coefficient, in Sections 6.4.1 and 6.4.2, respectively. The implications of these forms will be discussed in the context of the frequency domain reflection coefficient in Section 6.4.3.

To begin, the possibility of branch cut contributions due to a product of square roots is examined, since these appear in the wave impedance and propagation terms found in both the numerator and denominator of the reflection coefficient. For a

material region  $i$ , the term which describes propagation through the  $i^{\text{th}}$  region and appears in the frequency domain reflection coefficient is given by

$$P_i^2(s) = e^{-s\tau_i(s)} \quad (6.51)$$

with

$$\begin{aligned} s\tau_i(s) &= \frac{2\Delta_i}{c} \sqrt{\bar{\epsilon}_i} \sqrt{s} \sqrt{s + \frac{\sigma_i}{\bar{\epsilon}_i \epsilon_0}} \\ &= \frac{2\Delta_i}{c} \sqrt{\bar{\epsilon}_i} \sqrt{s} \sqrt{s - s_i}. \end{aligned} \quad (6.52)$$

where  $\Delta_i$  is the physical thickness of the material layer,  $c$  is the speed of light in free space, and  $\bar{\epsilon}_i = \epsilon_{ir} - \sin^2 \theta_{in}$ . Here  $\epsilon_{ir}$  is the relative permittivity of region  $i$ , and  $\theta_{in}$  is the incidence angle of a wave in region 0 impinging on the first interface to the layered material. The wave impedance of region  $i$  is given by

$$Z_i(s) = \begin{cases} \frac{\eta_0 s}{\sqrt{\bar{\epsilon}_i} \sqrt{s} \sqrt{s - s_i}} & \text{perpendicular polarization} \\ \frac{\eta_0 \sqrt{\bar{\epsilon}_i} \sqrt{s} \sqrt{s - s_i}}{s\epsilon_{ir} + \sigma_i/\epsilon_0} & \text{parallel polarization} \end{cases} \quad (6.53)$$

In both the wave impedance and propagation terms, the product of complex square roots  $\sqrt{s} \sqrt{s - s_i}$  appears. These square roots will lead to branch points and corresponding branch cuts in the complex  $s$ -plane. The branch points are given by  $s = 0$  and  $s = s_i$ . The quantity  $s_i = -\sigma_i/\bar{\epsilon}_i \epsilon_0$  is a nonpositive real number, so the branch point is located on the real axis. Branch cuts are taken along the negative real axis for each complex square root, defining the principal branches of the square roots for  $-\pi < \phi_0 \leq \pi$  and  $-\pi < \phi_i \leq \pi$ , each of which is measured from the positive real axis, as shown in Figure 6.9. Looking at this figure, begin by examining the integration paths designated as  $A_+$  and  $A_-$ . For the contour  $A_+$ ,  $\phi_0 = \phi_i = \pi$ . Letting  $s = -x$ ,

where  $x$  is a nonnegative real number, denote a point on the negative real axis, the product of the square root functions found in the wave impedance and propagation terms takes the form

$$\sqrt{s}\sqrt{s-s_i} = \sqrt{r_0}\sqrt{r_i}e^{j(\phi_0+\phi_i)/2} = \sqrt{x}\sqrt{x+s_i}e^{j\pi} = -\sqrt{x}\sqrt{x+s_i} \quad (6.54)$$

on  $A_-$ ,  $\phi_0 = \phi_i = -\pi$ , and the product of square roots is given by

$$\sqrt{s}\sqrt{s-s_i} = \sqrt{x}\sqrt{x+s_i}e^{-j\pi} = -\sqrt{x}\sqrt{x+s_i} \quad (6.55)$$

Equations (6.54) and (6.55) show that the product of the square root functions is analytic when crossing the branch cut along the  $A$  contours, thus

$$Z_i(s)\Big|_{A_+} = Z_i(s)\Big|_{A_-} \quad (6.56)$$

$$s\tau_i(s)\Big|_{A_+} = s\tau_i(s)\Big|_{A_-}. \quad (6.57)$$

On the contour  $B_+$ ,  $\phi_0 = \pi$ ,  $\phi_i = 0$ , and the product of square roots is

$$\sqrt{s}\sqrt{s-s_i} = \sqrt{x}\sqrt{-x-s_i}e^{j\pi/2} = j\sqrt{x}\sqrt{-x-s_i}. \quad (6.58)$$

Analogously, on  $B_-$ ,  $\phi_0 = -\pi$ ,  $\phi_i = 0$  yielding

$$\sqrt{s}\sqrt{s-s_i} = \sqrt{x}\sqrt{-x-s_i}e^{-j\pi/2} = -j\sqrt{x}\sqrt{-x-s_i} \quad (6.59)$$

Plugging (6.58) and (6.59) into (6.52) and (6.53) gives

$$Z_i(s)\Big|_{B_+} = \begin{cases} \frac{-\eta_0 x}{j\sqrt{\epsilon_i}\sqrt{x}\sqrt{-x-s_i}} & \text{perpendicular polarization} \\ \frac{j\eta_0\sqrt{\epsilon_i}\sqrt{x}\sqrt{-x-s_i}}{-x\epsilon_{ir} + \sigma_i/\epsilon_0} & \text{parallel polarization} \end{cases} \quad (6.60)$$

$$Z_i(s)\Big|_{B-} = \begin{cases} \frac{\eta_0 x}{j\sqrt{\epsilon_i}\sqrt{x}\sqrt{-x-s_i}} & \text{perpendicular polarization} \\ \frac{-j\eta_0\sqrt{\epsilon_i}\sqrt{x}\sqrt{-x-s_i}}{-x\epsilon_{ir} + \sigma_i/\epsilon_0} & \text{parallel polarization} \end{cases} \quad (6.61)$$

$$s\tau_i(s)\Big|_{B+} = j\frac{2\Delta_i}{c}\sqrt{\epsilon_i}\sqrt{x}\sqrt{-x-s_i}. \quad (6.62)$$

$$s\tau_i(s)\Big|_{B-} = -j\frac{2\Delta_i}{c}\sqrt{\epsilon_i}\sqrt{x}\sqrt{-x-s_i}. \quad (6.63)$$

thus

$$Z_i(s)\Big|_{B+} = -Z_i(s)\Big|_{B-} \quad (6.64)$$

$$s\tau_i(s)\Big|_{B+} = -s\tau_i(s)\Big|_{B-} \quad (6.65)$$

In order to examine symmetry of various quantities about the portion of the branch cuts along which the  $B$  contours lie, the following quantity is defined

$$\Phi_i = \frac{s\tau_i(s)}{2j}. \quad (6.66)$$

Note that, using (6.65),  $\Phi_i\Big|_{B+} = -\Phi_i\Big|_{B-}$ . Plugging (6.66) into (6.51) leads to

$$P_i = e^{-s\tau_i(s)/2} \quad (6.67)$$

$$= e^{-j\Phi_i} \quad (6.68)$$

which allows the following relationships to be written for the  $B$  contours

$$\begin{aligned} P_i^{-1} - P_i &= e^{j\Phi_i} - e^{-j\Phi_i} \\ &= j2 \sin \Phi_i \end{aligned} \quad (6.69)$$

$$\begin{aligned} P_i^{-1} + P_i &= e^{j\Phi_i} + e^{-j\Phi_i} \\ &= 2 \cos \Phi_i. \end{aligned} \quad (6.70)$$

Finally, even symmetry about the branch cut, which is necessary for cancellation of the integrals taken in opposite directions on the  $B$  contours, can be shown for the following quantities using (6.64) through (6.66), and the even and odd properties of the cosine and sine functions, respectively,

$$Z_i(s) \sin \Phi_i \Big|_{B+} = Z_i(s) \sin \Phi_i \Big|_{B-} \quad (6.71a)$$

$$Z_i^2(s) \Big|_{B+} = Z_i^2(s) \Big|_{B-} \quad (6.71b)$$

$$\cos \Phi_i \Big|_{B+} = \cos \Phi_i \Big|_{B-}. \quad (6.71c)$$

These relationships are used extensively in the examination of the forms of the numerator and denominator of the frequency domain reflection coefficient, which is carried out in Sections 6.4.1 through 6.4.2.

#### 6.4.1 Form of the denominator

In this section, the denominator of the frequency domain reflection coefficient for an  $N$ -layered material structure is manipulated into a form which can be used to help validate a natural mode series representation of the time domain reflection coefficient in the late time of the structure. Here, the late time begins after the two way transit time of the  $N$  regions comprising the  $N$ -material structure. The manipulation of the denominator proceeds by continuously utilizing a recursive form of the denominator

and collapsing the equation by defining quantities which are even about the branch cuts. This is done at each step along the way, eventually leading to a recursive expression which allows for  $N$  steps to be performed. Finally, once the expression is placed in terms of the denominator of the frequency domain reflection coefficient for a two layered structure, explicit expressions for the denominator are substituted in, leaving the expression in terms of quantities which are even about the branch cut, and wave impedances. The wave impedances may be even or odd about the branch cut, depending on the material characteristics of the region.

To this end, begin by establishing some relationships for the  $i^{th}$  layer of a multilayered structure. These relationships will prove extremely useful in the exploration into the form of the transient response from the multilayered structure.

#### 6.4.1.1 Equations for the $i$ -th layer

To utilize the symmetry relationships of (6.71), it is helpful to place the denominator in an alternative form. To do this,  $R_i$  is plugged into (6.27b), and the result is multiplied though by  $A_{0,i}$ , noting a cancellation of terms in  $A_{0,i}$  with the denominators of the interfacial reflection coefficients for indices of 0,  $j$ , and  $i$ . The denominator is then found in terms of the wave impedances, rather than the reflection coefficients as

$$\begin{aligned}
D_i A_{0,i} &= D_{i-1} A_{0,i} + (Z_{i+1} - Z_i) \times \\
&\quad \times \left[ (Z_1 - Z_0) A_{1,i-1} B_{1,i} + \sum_{j=0}^{i-2} D_j (Z_{j+2} - Z_{j+1}) A_{0,j} A_{j+2,i-1} B_{j+2,i} \right] \\
&= \mathcal{X}_{D,i-1} (Z_{i+1} + Z_i) + \mathcal{Y}_{D,i-1} (Z_{i+1} - Z_i)
\end{aligned} \tag{6.72}$$

where dependance of parameters on the complex variable,  $s$ , is suppressed for brevity. Several quantities are defined here in order to aid in the understanding of the steps

used in this derivation. These quantities are given by

$$\begin{aligned}
\mathcal{X}_{D,i} &= D_i \mathbb{A}_{0,i} \\
&= D_{i-1} \mathbb{A}_{0,i-1} (Z_{i+1} + Z_i) + (Z_{i+1} - Z_i) \mathcal{Y}_{D,i-1} \\
&= \mathcal{X}_{D,i-1} (Z_{i+1} + Z_i) + \mathcal{Y}_{D,i-1} (Z_{i+1} - Z_i)
\end{aligned} \tag{6.73a}$$

$$\begin{aligned}
\mathcal{Y}_{D,i} &= \left[ (Z_1 - Z_0) \mathbb{A}_{1,i} \mathbb{B}_{1,i+1} + \sum_{j=0}^{i-1} D_j (Z_{j+2} - Z_{j+1}) \mathbb{A}_{0,j} \mathbb{A}_{j+2,i} \mathbb{B}_{j+2,i+1} \right] \\
&= (Z_{i+1} + Z_i) P_{i+1}^2 \left[ (Z_1 - Z_0) \mathbb{A}_{1,i-1} \mathbb{B}_{1,i} + \right. \\
&\quad \left. + \sum_{j=0}^{i-2} D_j (Z_{j+2} - Z_{j+1}) \mathbb{A}_{0,j} \mathbb{A}_{j+2,i-1} \mathbb{B}_{j+2,i} \right] + (Z_{i+1} - Z_i) P_{i+1}^2 D_{i-1} \mathbb{A}_{0,i-1} \\
&= \mathcal{Y}_{D,i-1} (Z_{i+1} + Z_i) P_{i+1}^2 + \mathcal{X}_{D,i-1} (Z_{i+1} - Z_i) P_{i+1}^2
\end{aligned} \tag{6.73b}$$

Here the  $i - 1$  term was removed from the summation in  $\mathcal{Y}_{D,i}$ , and  $(Z_{i+1} + Z_i) P_{i+1}^2$  was factored out of the remaining terms in order to write  $\mathcal{Y}_{D,i}$  in terms of  $\mathcal{Y}_{D,i-1}$  and  $\mathcal{X}_{D,i-1}$ . Various quantities involving the sum or difference of the expressions in (6.73) are utilized in the exploration of the form of the denominator for an N-layered material. These terms will use the relationships

$$\begin{aligned}
\left( \mathcal{X}_{D,i} \pm \mathcal{Y}_{D,i} \right) &= \left( \mathcal{X}_{D,i-1} (Z_{i+1} + Z_i) + \mathcal{Y}_{D,i-1} (Z_{i+1} - Z_i) \right) \\
&\quad \pm \left( \mathcal{Y}_{D,i-1} (Z_{i+1} + Z_i) P_{i+1}^2 + \mathcal{X}_{D,i-1} (Z_{i+1} - Z_i) P_{i+1}^2 \right) \\
&= Z_{i+1} (1 \pm P_{i+1}^2) \left( \mathcal{X}_{D,i-1} + \mathcal{Y}_{D,i-1} \right) \\
&\quad + Z_i (1 \mp P_{i+1}^2) \left( \mathcal{X}_{D,i-1} - \mathcal{Y}_{D,i-1} \right).
\end{aligned} \tag{6.74}$$

Because of various operations carried out on the denominator, the two quantities given by (6.74) appear in various combinations, including the squaring of either of



the quantities, given by

$$\begin{aligned}
(\mathcal{X}_{D,i} \pm \mathcal{Y}_{D,i})^2 &= Z_{i+1}^2(1 \pm P_{i+1}^2)^2(\mathcal{X}_{D,i-1} + \mathcal{Y}_{D,i-1})^2 \\
&\quad + Z_i^2(1 \mp P_{i+1}^2)^2(\mathcal{X}_{D,i-1} - \mathcal{Y}_{D,i-1})^2 \\
&\quad + 2Z_{i+1}Z_i(1 + P_{i+1}^2)(1 - P_{i+1}^2)(\mathcal{X}_{D,i-1} + \mathcal{Y}_{D,i-1})(\mathcal{X}_{D,i-1} - \mathcal{Y}_{D,i-1}),
\end{aligned} \tag{6.75}$$

and the product of the two quantities, which takes the form

$$\begin{aligned}
&(\mathcal{X}_{D,i} + \mathcal{Y}_{D,i})(\mathcal{X}_{D,i} - \mathcal{Y}_{D,i}) \\
&= (1 + P_{i+1}^2)(1 - P_{i+1}^2) \left[ Z_{i+1}^2(\mathcal{X}_{D,i-1} + \mathcal{Y}_{D,i-1})^2 + Z_i^2(\mathcal{X}_{D,i-1} - \mathcal{Y}_{D,i-1})^2 \right] \\
&\quad + Z_{i+1}Z_i \left[ (1 + P_{i+1}^2)^2 + (1 - P_{i+1}^2)^2 \right] (\mathcal{X}_{D,i-1} + \mathcal{Y}_{D,i-1})(\mathcal{X}_{D,i-1} - \mathcal{Y}_{D,i-1}).
\end{aligned} \tag{6.76}$$

The products of (6.75) and (6.76) appear often in the denominator of the frequency domain reflection coefficient. The following recursive formula, which appears in the course of this derivation and is utilized heavily, contains all combinations of (6.75) and (6.76).

$$\begin{aligned}
&4^{-1}P_{(N-i)}^{-2} \left[ (\mathcal{G}_{1,i-1} + jZ_{N+1}\mathcal{G}_{2,i-1})(\mathcal{X}_{D,N-(i+1)} + \mathcal{Y}_{D,N-(i+1)})^2 \right. \\
&\quad + (\tilde{\mathcal{G}}_{1,i} + jZ_{N+1}\tilde{\mathcal{G}}_{2,i})(\mathcal{X}_{D,N-(i+1)} - \mathcal{Y}_{D,N-(i+1)})^2 + (\mathcal{G}_{3,i-1}Z_{i-1} + j\mathcal{G}_{4,i-1}) \times \\
&\quad \left. \times Z_{N-i}(\mathcal{X}_{D,N-(i+1)} + \mathcal{Y}_{D,N-(i+1)})(\mathcal{X}_{D,N-(i+1)} - \mathcal{Y}_{D,N-(i+1)}) \right] \\
&= (\mathcal{G}_{1,i} + jZ_{N+1}\mathcal{G}_{2,i})(\mathcal{X}_{D,N-(i+2)} + \mathcal{Y}_{D,N-(i+2)})^2 \\
&\quad + (\tilde{\mathcal{G}}_{1,i+1} + jZ_{N+1}\tilde{\mathcal{G}}_{2,i+1})(\mathcal{X}_{D,N-(i+2)} - \mathcal{Y}_{D,N-(i+2)})^2 + (\mathcal{G}_{3,i}Z_{N+1} + j\mathcal{G}_{4,i}) \times \\
&\quad \times Z_{N-(i+1)}(\mathcal{X}_{D,N-(i+2)} + \mathcal{Y}_{D,N-(i+2)})(\mathcal{X}_{D,N-(i+2)} - \mathcal{Y}_{D,N-(i+2)})
\end{aligned} \tag{6.77}$$

where the following quantities arise from application of (6.73) through (6.76)

$$\begin{aligned}
\mathcal{G}_{1,i} &= Z_{N-i}^2 \left[ \mathcal{G}_{1,i-1} \cos^2 \Phi_{N-i} - \tilde{\mathcal{G}}_{1,i} \sin^2 \Phi_{N-i} \right. \\
&\quad \left. - \mathcal{G}_{4,i-1} (Z_{N-i} \sin \Phi_{N-i}) \cos \Phi_{N-i} \right] \\
\mathcal{G}_{2,i} &= Z_{N-i}^2 \left[ \mathcal{G}_{2,i-1} \cos^2 \Phi_{N-i} - \tilde{\mathcal{G}}_{2,i} \sin^2 \Phi_{N-i} \right. \\
&\quad \left. + \mathcal{G}_{3,i-1} (Z_{N-i} \sin \Phi_{N-i}) \cos \Phi_{N-i} \right] \\
\tilde{\mathcal{G}}_{1,i+1} &= Z_{N-(i+1)}^2 \left[ \tilde{\mathcal{G}}_{1,i} \cos^2 \Phi_{N-i} - \mathcal{G}_{1,i-1} \sin^2 \Phi_{N-i} \right. \\
&\quad \left. - \mathcal{G}_{4,i-1} (Z_{N-i} \sin \Phi_{N-i}) \cos \Phi_{N-i} \right] \\
\tilde{\mathcal{G}}_{2,i+1} &= Z_{N-(i+1)}^2 \left[ \tilde{\mathcal{G}}_{2,i} \cos^2 \Phi_{N-i} - \mathcal{G}_{2,i-1} \sin^2 \Phi_{N-i} \right. \\
&\quad \left. + \mathcal{G}_{3,i-1} (Z_{N-i} \sin \Phi_{N-i}) \cos \Phi_{N-i} \right] \\
\mathcal{G}_{3,i} &= Z_{N-i}^2 \left[ \cos^2 \Phi_{N-i} - \sin^2 \Phi_{N-i} \right] \mathcal{G}_{3,i-1} \\
&\quad - 2 \left[ \mathcal{G}_{2,i-1} + \tilde{\mathcal{G}}_{2,i} \right] (Z_{N-i} \sin \Phi_{N-i}) \cos \Phi_{N-i} \\
\mathcal{G}_{4,i} &= Z_{N-i}^2 \left[ \cos^2 \Phi_{N-i} - \sin^2 \Phi_{N-i} \right] \mathcal{G}_{4,i-1} \\
&\quad + 2 \left[ \mathcal{G}_{1,i-1} + \tilde{\mathcal{G}}_{1,i} \right] (Z_{N-i} \sin \Phi_{N-i}) \cos \Phi_{N-i}.
\end{aligned}$$

#### 6.4.1.2 N-Layer geometry

Consider the  $N$ -material, planar layered geometry shown in Figure 6.8, where region 0 is free space, and region  $N + 1$  is a material which may or may not be lossy. The denominator of the frequency domain reflection coefficient, multiplied by  $\mathbf{A}_{0,N}$ , is given by (6.72) for  $i = N$  as

$$D_N \mathbf{A}_{0,N} = \mathcal{X}_{D,N-1} (Z_{N+1} + Z_N) + \mathcal{Y}_{D,N-1} (Z_{N+1} - Z_N) \quad (6.78)$$

To explore the properties of the denominator of the reflection coefficient, begin by plugging in expressions for  $\mathcal{X}_{D,N-1}$  and  $\mathcal{Y}_{D,N-1}$  using (6.73). Doing this gives

$$\begin{aligned} D_N \mathbf{A}_{0,N} &= \left[ \mathcal{X}_{D,N-2}(Z_N + Z_{N-1}) + \mathcal{Y}_{D,N-2}(Z_N - Z_{N-1}) \right] (Z_{N+1} + Z_N) \\ &\quad + \left[ \mathcal{Y}_{D,N-2}(Z_N + Z_{N-1})P_{i+1}^2 + \mathcal{X}_{D,N-2}(Z_N - Z_{N-1})P_N^2 \right] (Z_{N+1} - Z_N). \end{aligned} \quad (6.79)$$

Rearranging terms to separate the  $\mathcal{X}_{D,N-2}$  and  $\mathcal{Y}_{D,N-2}$  terms gives

$$\begin{aligned} D_N \mathbf{A}_{0,N} &= \mathcal{X}_{D,N-2} \left[ (Z_{N+1} + Z_N)(Z_N + Z_{N-1}) + (Z_{N+1} - Z_N)(Z_N - Z_{N-1})P_N^2 \right] \\ &\quad + \mathcal{Y}_{D,N-2} \left[ (Z_{N+1} + Z_N)(Z_N - Z_{N-1}) + (Z_{N+1} - Z_N)(Z_N + Z_{N-1})P_N^2 \right]. \end{aligned} \quad (6.80)$$

Multiplying out the wave impedance terms in brackets and regrouping gives

$$\begin{aligned} D_N \mathbf{A}_{0,N} &= \mathcal{X}_{D,N-2} \left[ Z_N(Z_{N+1} + Z_{N-1})(1 + P_N^2) + (Z_N^2 + Z_{N+1}Z_{N-1})(1 - P_N^2) \right] \\ &\quad + \mathcal{Y}_{D,N-2} \left[ Z_N(Z_{N+1} - Z_{N-1})(1 + P_N^2) + (Z_N^2 - Z_{N+1}Z_{N-1})(1 - P_N^2) \right] \\ &= \mathcal{A}(1 + P_N^2) + j\mathcal{B}\left(\frac{1 - P_N^2}{j}\right) \end{aligned} \quad (6.81)$$

where the quantities  $\mathcal{A}$  and  $\mathcal{B}$  are defined as

$$\mathcal{A} = \mathcal{X}_{D,N-2}(Z_{N+1}Z_N + Z_NZ_{N-1}) + \mathcal{Y}_{D,N-2}(Z_{N+1}Z_N - Z_NZ_{N-1}) \quad (6.82a)$$

$$\mathcal{B} = \mathcal{X}_{D,N-2}(Z_N^2 + Z_{N+1}Z_{N-1}) + \mathcal{Y}_{D,N-2}(Z_N^2 - Z_{N+1}Z_{N-1}) \quad (6.82b)$$

Multiplying the denominator by  $\left(\mathcal{A}(1 + P_N^2) - j\mathcal{B}\left(\frac{1 - P_N^2}{j}\right)\right)4^{-1}P_N^{-2}$  in order to take advantage of (6.69) through (6.71) gives

$$\begin{aligned}\bar{D}_N &= D_N \mathbb{A}_{0,N} \left( \mathcal{A}(1 + P_N^2) - j\mathcal{B}\left(\frac{1 - P_N^2}{j}\right) \right) 4^{-1} P_N^{-2} \\ &= \mathcal{A}^2 \left( \frac{P_N^{-1} + P_N}{2} \right)^2 + \mathcal{B}^2 \left( \frac{P_N^{-1} - P_N}{j2} \right)^2 \\ &= \mathcal{A}^2 \cos^2 \Phi_N + \mathcal{B}^2 \sin^2 \Phi_N\end{aligned}\quad (6.83)$$

where  $\Phi_N$  is defined by (6.66) as  $s\tau_N(s)/2j$ , and (6.69) through (6.70) are utilized.

Plugging  $\mathcal{A}^2$  and  $\mathcal{B}^2$  into (6.83) using (6.82) gives

$$\begin{aligned}\bar{D}_N &= \left[ Z_{N+1}^2 Z_N^2 (\mathcal{X}_{D,N-2} + \mathcal{Y}_{D,N-2})^2 + Z_N^2 Z_{N-1}^2 (\mathcal{X}_{D,N-2} - \mathcal{Y}_{D,N-2})^2 \right] \cos^2 \Phi_N \\ &\quad + \left[ Z_N^4 (\mathcal{X}_{D,N-2} + \mathcal{Y}_{D,N-2})^2 + Z_{N+1}^2 Z_{N-1}^2 (\mathcal{X}_{D,N-2} - \mathcal{Y}_{D,N-2})^2 \right] \sin^2 \Phi_N \\ &\quad + 2Z_{N+1} Z_N^2 Z_{N-1} (\mathcal{X}_{D,N-2} + \mathcal{Y}_{D,N-2}) (\mathcal{X}_{D,N-2} - \mathcal{Y}_{D,N-2})\end{aligned}\quad (6.84)$$

Rearranging (6.84) to organize the equation in terms of various products of  $(\mathcal{X}_{D,N-2} \pm \mathcal{Y}_{D,N-2})$  gives

$$\begin{aligned}\bar{D}_N &= \left[ Z_{N+1}^2 Z_N^2 \cos^2 \Phi_N + Z_N^4 \sin^2 \Phi_N \right] (\mathcal{X}_{D,N-2} + \mathcal{Y}_{D,N-2})^2 \\ &\quad + \left[ Z_N^2 Z_{N-1}^2 \cos^2 \Phi_N + Z_{N+1}^2 Z_{N-1}^2 \sin^2 \Phi_N \right] (\mathcal{X}_{D,N-2} - \mathcal{Y}_{D,N-2})^2 \\ &\quad + \left[ 2Z_N^2 \right] Z_{N+1} Z_{N-1} (\mathcal{X}_{D,N-2} + \mathcal{Y}_{D,N-2}) (\mathcal{X}_{D,N-2} - \mathcal{Y}_{D,N-2}) \\ &= F_1 (\mathcal{X}_{D,N-2} + \mathcal{Y}_{D,N-2})^2 + F_2 (\mathcal{X}_{D,N-2} - \mathcal{Y}_{D,N-2})^2 \\ &\quad + F_3 Z_{N+1} Z_{N-1} (\mathcal{X}_{D,N-2} + \mathcal{Y}_{D,N-2}) (\mathcal{X}_{D,N-2} - \mathcal{Y}_{D,N-2}).\end{aligned}\quad (6.85)$$

Here the functions  $F_1$  through  $F_3$  are even about the branch cut, since they are defined in terms of wave impedances and trigonometric functions which are raised to

even powers. Plugging in expressions for the various products of  $(\mathcal{X}_{D,N-2} \pm \mathcal{Y}_{D,N-2})$  using (6.75) and (6.76) with  $i = N - 2$  gives

$$\begin{aligned}
\bar{D}_N = & F_1 \left[ Z_{N-1}^2 (1 + P_{N-1}^2)^2 (\mathcal{X}_{D,N-3} + \mathcal{Y}_{D,N-3})^2 + Z_{N-2}^2 (1 - P_{N-1}^2)^2 \times \right. \\
& \times (\mathcal{X}_{D,N-3} - \mathcal{Y}_{D,N-3})^2 + 2Z_{N-1}Z_{N-2}(1 + P_{N-1}^2)(1 - P_{N-1}^2) \times \\
& \left. \times (\mathcal{X}_{D,N-3} + \mathcal{Y}_{D,N-3})(\mathcal{X}_{D,N-3} - \mathcal{Y}_{D,N-3}) \right] \\
& + F_2 \left[ Z_{N-1}^2 (1 - P_{N-1}^2)^2 (\mathcal{X}_{D,N-3} + \mathcal{Y}_{D,N-3})^2 + Z_{N-2}^2 (1 + P_{N-1}^2)^2 \times \right. \\
& \times (\mathcal{X}_{D,N-3} - \mathcal{Y}_{D,N-3})^2 + 2Z_{N-1}Z_{N-2}(1 + P_{N-1}^2)(1 - P_{N-1}^2) \times \\
& \left. \times (\mathcal{X}_{D,N-3} + \mathcal{Y}_{D,N-3})(\mathcal{X}_{D,N-3} - \mathcal{Y}_{D,N-3}) \right] \\
& + F_3 Z_{N+1} Z_{N-1} \left[ (1 + P_{N-1}^2)(1 - P_{N-1}^2) \left[ Z_{N-1}^2 (\mathcal{X}_{D,N-3} + \mathcal{Y}_{D,N-3})^2 \right. \right. \\
& \left. \left. + Z_{N-2}^2 (\mathcal{X}_{D,N-3} - \mathcal{Y}_{D,N-3})^2 \right] + Z_{N-1} Z_{N-2} \left[ (1 + P_{N-1}^2)^2 \right. \right. \\
& \left. \left. + (1 - P_{N-1}^2)^2 \right] (\mathcal{X}_{D,N-3} + \mathcal{Y}_{D,N-3})(\mathcal{X}_{D,N-3} - \mathcal{Y}_{D,N-3}) \right]. \quad (6.86)
\end{aligned}$$

Rearranging (6.86) to organize in terms of the various products of  $(\mathcal{X}_{D,N-3} \pm \mathcal{Y}_{D,N-3})$  gives

$$\begin{aligned}
\bar{D}_N = & Z_{N-1}^2 \left[ F_1 (1 + P_{N-1}^2)^2 + F_2 (1 - P_{N-1}^2)^2 \right. \\
& \left. + F_3 Z_{N+1} Z_{N-1} (1 + P_{N-1}^2)(1 - P_{N-1}^2) \right] (\mathcal{X}_{D,N-3} + \mathcal{Y}_{D,N-3})^2 \\
& + Z_{N-2}^2 \left[ F_1 (1 - P_{N-1}^2)^2 + F_2 (1 + P_{N-1}^2)^2 \right. \\
& \left. + F_3 Z_{N+1} Z_{N-1} (1 + P_{N-1}^2)(1 - P_{N-1}^2) \right] (\mathcal{X}_{D,N-3} - \mathcal{Y}_{D,N-3})^2 \\
& + Z_{N-1} Z_{N-2} \left[ 2[F_1 + F_2](1 + P_{N-1}^2)(1 - P_{N-1}^2) \right. \\
& \left. + F_3 Z_{N+1} Z_{N-1} [(1 + P_{N-1}^2)^2 + (1 - P_{N-1}^2)^2] \right] \times \\
& \times (\mathcal{X}_{D,N-3} + \mathcal{Y}_{D,N-3})(\mathcal{X}_{D,N-3} - \mathcal{Y}_{D,N-3}). \quad (6.87)
\end{aligned}$$

Multiplying through by  $4^{-1} P_{N-1}^{-2}$  in order to take advantage of (6.69) through (6.71)

gives

$$\begin{aligned}
4^{-1}P_{N-1}^{-2}\bar{D}_N &= Z_{N-1}^2 \left[ F_1 \cos^2 \Phi_{N-1} - F_2 \sin^2 \Phi_{N-1} \right. \\
&\quad \left. + jF_3 Z_{N+1} (Z_{N-1} \sin \Phi_{N-1}) \cos \Phi_{N-1} \right] \left( \mathcal{X}_{D,N-3} + \mathcal{Y}_{D,N-3} \right)^2 \\
&\quad + Z_{N-2}^2 \left[ -F_1 \sin^2 \Phi_{N-1} + F_2 \cos^2 \Phi_{N-1} \right. \\
&\quad \left. + jF_3 Z_{N+1} (Z_{N-1} \sin \Phi_{N-1}) \cos \Phi_{N-1} \right] \left( \mathcal{X}_{D,N-3} - \mathcal{Y}_{D,N-3} \right)^2 \\
&\quad + Z_{N-2} \left[ 2j[F_1 + F_2] (Z_{N-1} \sin \Phi_{N-1}) \cos \Phi_{N-1} \right. \\
&\quad \left. + F_3 Z_{N+1} Z_{N-1}^2 [\cos^2 \Phi_{N-1} - \sin^2 \Phi_{N-1}] \right] \times \\
&\quad \times \left( \mathcal{X}_{D,N-3} + \mathcal{Y}_{D,N-3} \right) \left( \mathcal{X}_{D,N-3} - \mathcal{Y}_{D,N-3} \right) \\
&= (\mathcal{G}_{1,1} + jZ_{N+1}\mathcal{G}_{2,1}) \left( \mathcal{X}_{D,N-3} + \mathcal{Y}_{D,N-3} \right)^2 \\
&\quad + (\tilde{\mathcal{G}}_{1,2} + jZ_{N+1}\tilde{\mathcal{G}}_{2,2}) \left( \mathcal{X}_{D,N-3} - \mathcal{Y}_{D,N-3} \right)^2 + (\mathcal{G}_{3,1}Z_{N+1} + j\mathcal{G}_{4,1}) \times \\
&\quad \times Z_{N-2} \left( \mathcal{X}_{D,N-3} + \mathcal{Y}_{D,N-3} \right) \left( \mathcal{X}_{D,N-3} - \mathcal{Y}_{D,N-3} \right) \quad (6.88)
\end{aligned}$$

where  $\Phi_{N-1}$  is defined by (6.66) as  $s\tau_{N-1}(s)/2j$ , and

$$\begin{aligned}
\mathcal{G}_{1,1} &= Z_{N-1}^2 \left[ F_1 \cos^2 \Phi_{N-1} - F_2 \sin^2 \Phi_{N-1} \right] \\
\mathcal{G}_{2,1} &= F_3 (Z_{N-1} \sin \Phi_{N-1}) Z_{N-1}^2 \cos \Phi_{N-1} \\
\tilde{\mathcal{G}}_{1,2} &= Z_{N-2}^2 \left[ F_2 \cos^2 \Phi_{N-1} - F_1 \sin^2 \Phi_{N-1} \right] \\
\tilde{\mathcal{G}}_{2,2} &= F_3 (Z_{N-1} \sin \Phi_{N-1}) Z_{N-2}^2 \cos \Phi_{N-1} \\
\mathcal{G}_{3,1} &= F_3 Z_{N-1}^2 \left[ \cos^2 \Phi_{N-1} - \sin^2 \Phi_{N-1} \right] \\
\mathcal{G}_{4,1} &= 2 \left[ F_1 + F_2 \right] (Z_{N-1} \sin \Phi_{N-1}) \cos \Phi_{N-1}.
\end{aligned}$$

Note that the quantities  $\mathcal{G}_{1,1}$  through  $\mathcal{G}_{4,1}$  are defined in terms of  $F_1$  through  $F_3$ , wave impedances, and trigonometric functions, thus  $\mathcal{G}_{1,1}$  through  $\mathcal{G}_{4,1}$  are even about the branch cut as shown by using (6.71) and evenness of  $F_1$  through  $F_3$ .

Multiplying by  $4^{-1}P_{N-2}^{-2}$ , the right hand side of (6.86) has the form of the left hand side of (6.77) for  $i = 2$ , thus,

$$\begin{aligned}
4^{-2}P_{N-1}^{-2}P_{N-2}^{-2}\bar{D}_N &= (\mathcal{G}_{1,2} + jZ_{N+1}\mathcal{G}_{2,2})\left(\mathcal{X}_{D,N-4} + \mathcal{Y}_{D,N-4}\right)^2 \\
&+ (\tilde{\mathcal{G}}_{1,3} + jZ_{N+1}\tilde{\mathcal{G}}_{2,3})\left(\mathcal{X}_{D,N-4} - \mathcal{Y}_{D,N-4}\right)^2 + (\mathcal{G}_{3,2}Z_{N+1} + j\mathcal{G}_{4,2}) \times \\
&\times Z_{N-3}\left(\mathcal{X}_{D,N-4} + \mathcal{Y}_{D,N-4}\right)\left(\mathcal{X}_{D,N-4} - \mathcal{Y}_{D,N-4}\right) \quad (6.89)
\end{aligned}$$

with

$$\begin{aligned}
\mathcal{G}_{1,2} &= Z_{N-2}^2 \left[ \mathcal{G}_{1,1} \cos^2 \Phi_{N-2} - \tilde{\mathcal{G}}_{1,2} \sin^2 \Phi_{N-2} - \mathcal{G}_{4,1} (Z_{N-2} \sin \Phi_{N-2}) \cos \Phi_{N-2} \right] \\
\mathcal{G}_{2,2} &= Z_{N-2}^2 \left[ \mathcal{G}_{2,1} \cos^2 \Phi_{N-2} - \tilde{\mathcal{G}}_{2,2} \sin^2 \Phi_{N-2} + \mathcal{G}_{3,1} (Z_{N-2} \sin \Phi_{N-2}) \cos \Phi_{N-2} \right] \\
\tilde{\mathcal{G}}_{1,3} &= Z_{N-3}^2 \left[ \tilde{\mathcal{G}}_{1,2} \cos^2 \Phi_{N-2} - \mathcal{G}_{1,1} \sin^2 \Phi_{N-2} - \mathcal{G}_{4,1} (Z_{N-2} \sin \Phi_{N-2}) \cos \Phi_{N-2} \right] \\
\tilde{\mathcal{G}}_{2,3} &= Z_{N-3}^2 \left[ \tilde{\mathcal{G}}_{2,2} \cos^2 \Phi_{N-2} - \mathcal{G}_{2,1} \sin^2 \Phi_{N-2} + \mathcal{G}_{3,1} (Z_{N-2} \sin \Phi_{N-2}) \cos \Phi_{N-2} \right] \\
\mathcal{G}_{3,2} &= Z_{N-2}^2 \left[ \cos^2 \Phi_{N-2} - \sin^2 \Phi_{N-2} \right] \mathcal{G}_{3,1} \\
&\quad - 2 \left[ \mathcal{G}_{2,1} + \tilde{\mathcal{G}}_{2,2} \right] (Z_{N-2} \sin \Phi_{N-2}) \cos \Phi_{N-2} \\
\mathcal{G}_{4,2} &= Z_{N-2}^2 \left[ \cos^2 \Phi_{N-2} - \sin^2 \Phi_{N-2} \right] \mathcal{G}_{4,1} \\
&\quad + 2 \left[ \mathcal{G}_{1,1} + \tilde{\mathcal{G}}_{1,2} \right] (Z_{N-2} \sin \Phi_{N-2}) \cos \Phi_{N-2}
\end{aligned}$$

Note that the quantities  $\mathcal{G}_{1,2}$  through  $\mathcal{G}_{4,2}$  are defined in terms of  $\mathcal{G}_{1,1}$  through  $\mathcal{G}_{4,1}$ , wave impedances, and trigonometric functions. Thus,  $\mathcal{G}_{1,2}$  through  $\mathcal{G}_{4,2}$  are even about the branch cut using (6.71) and evenness of  $\mathcal{G}_{1,1}$  through  $\mathcal{G}_{4,1}$ .

Multiplying by  $4^{-1}P_{N-3}^{-2}$ , the right hand side of (6.89) again has the form of the left hand side of (6.77), this time with  $i = 3$ . This leads to terms  $\mathcal{G}_{1,3}$  through  $\mathcal{G}_{4,3}$ , which are defined by (6.77) in terms of  $\mathcal{G}_{1,2}$  through  $\mathcal{G}_{4,2}$ , wave impedances, and trigonometric functions, thus  $\mathcal{G}_{1,3}$  through  $\mathcal{G}_{4,3}$  are even about the branch cut using (6.71) and evenness of  $\mathcal{G}_{1,2}$  through  $\mathcal{G}_{4,2}$ . Continuing to multiply through by

$4^{-1}P_{N-i}^{-2}$  and applying (6.77) for increasing values of  $i$ , until  $i = N - 3$ , and then multiplying by  $4^{-2}P_1^{-2}P_2^{-2}$  leads to

$$\begin{aligned}
4^{-(N-1)} \prod_{i=1}^{N-1} P_i^{-2} \bar{D}_N &= (\mathcal{G}_{1,N-3} + jZ_{N+1}\mathcal{G}_{2,N-3}) \left[ 4^{-2}P_1^{-2}P_2^{-2} (\mathcal{X}_{D,1} + \mathcal{Y}_{D,1})^2 \right] \\
&+ (\tilde{\mathcal{G}}_{1,N-2} + jZ_{N+1}\tilde{\mathcal{G}}_{2,N-2}) \left[ 4^{-2}P_1^{-2}P_2^{-2} (\mathcal{X}_{D,1} - \mathcal{Y}_{D,1})^2 \right] \\
&+ (\mathcal{G}_{3,N-3}Z_{N+1} + j\mathcal{G}_{4,N-3}) \times \\
&\times Z_2 \left[ 4^{-2}P_1^{-2}P_2^{-2} (\mathcal{X}_{D,1} + \mathcal{Y}_{D,1}) (\mathcal{X}_{D,1} - \mathcal{Y}_{D,1}) \right] \tag{6.90}
\end{aligned}$$

with

$$\begin{aligned}
\mathcal{G}_{1,N-3} &= Z_3^2 \left[ \mathcal{G}_{1,N-4} \cos^2 \Phi_2 - \tilde{\mathcal{G}}_{1,N-3} \sin^2 \Phi_2 - \mathcal{G}_{4,N-4} (Z_2 \sin \Phi_2) \cos \Phi_2 \right] \\
\mathcal{G}_{2,N-3} &= Z_3^2 \left[ \mathcal{G}_{2,N-4} \cos^2 \Phi_2 - \tilde{\mathcal{G}}_{2,N-3} \sin^2 \Phi_2 + \mathcal{G}_{3,N-4} (Z_2 \sin \Phi_2) \cos \Phi_2 \right] \\
\tilde{\mathcal{G}}_{1,N-2} &= Z_2^2 \left[ \tilde{\mathcal{G}}_{1,N-3} \cos^2 \Phi_2 - \mathcal{G}_{1,N-4} \sin^2 \Phi_2 - \mathcal{G}_{4,N-4} (Z_2 \sin \Phi_2) \cos \Phi_2 \right] \\
\tilde{\mathcal{G}}_{2,N-2} &= Z_2^2 \left[ \tilde{\mathcal{G}}_{2,N-3} \cos^2 \Phi_2 - \mathcal{G}_{2,N-4} \sin^2 \Phi_2 + \mathcal{G}_{3,N-4} (Z_2 \sin \Phi_2) \cos \Phi_2 \right] \\
\mathcal{G}_{3,N-3} &= Z_3^2 \left[ \cos^2 \Phi_2 - \sin^2 \Phi_2 \right] \mathcal{G}_{3,N-4} - 2 \left[ \mathcal{G}_{2,N-4} + \tilde{\mathcal{G}}_{2,N-3} \right] (Z_2 \sin \Phi_2) \cos \Phi_2 \\
\mathcal{G}_{4,N-3} &= Z_3^2 \left[ \cos^2 \Phi_2 - \sin^2 \Phi_2 \right] \mathcal{G}_{4,N-4} + 2 \left[ \mathcal{G}_{1,N-4} + \tilde{\mathcal{G}}_{1,N-3} \right] (Z_2 \sin \Phi_2) \cos \Phi_2
\end{aligned}$$

Here  $\mathcal{G}_{1,N-3}$  through  $\mathcal{G}_{4,N-3}$ , which are defined by (6.77) in terms of  $\mathcal{G}_{1,N-4}$  through  $\mathcal{G}_{4,N-4}$ , wave impedances, and trigonometric functions, are even about the branch cut using (6.71) and evenness of  $\mathcal{G}_{1,N-4}$  through  $\mathcal{G}_{4,N-4}$ . This symmetry about the branch cut is established through the continual reapplication of (6.77) leading to the form of (6.90).

At this point, the expressions for  $(\mathcal{X}_{D,1} \pm \mathcal{Y}_{D,1})$  are simple enough to be written



out explicitly. These expressions are found as

$$\begin{aligned}
(\mathcal{X}_{D,1} \pm \mathcal{Y}_{D,1}) &= D_1 \mathbf{A}_{0,1} \pm [(Z_1 - Z_0) \mathbf{A}_{1,1} \mathbf{B}_{1,2} + D_0 (Z_2 - Z_1) \mathbf{A}_{0,0} \mathbf{B}_{2,2}] \\
&= \left(1 + \frac{(Z_2 - Z_1)(Z_1 - Z_0)}{(Z_2 + Z_1)(Z_1 + Z_0)} P_1^2\right) (Z_2 + Z_1)(Z_1 + Z_0) \\
&\quad \pm [(Z_1 - Z_0)(Z_2 + Z_1) P_1^2 P_2^2 + (Z_2 - Z_1)(Z_1 + Z_0) P_2^2] \\
&= Z_2(1 \pm P_2^2)(Z_1(1 + P_1^2) + Z_0(1 - P_1^2)) \\
&\quad + Z_1(1 \mp P_2^2)(Z_1(1 - P_1^2) + Z_0(1 + P_1^2)) \tag{6.91}
\end{aligned}$$

The expressions for  $(\mathcal{X}_{D,1} \pm \mathcal{Y}_{D,1})^2$  and  $(\mathcal{X}_{D,1} + \mathcal{Y}_{D,1})(\mathcal{X}_{D,1} - \mathcal{Y}_{D,1})$  can thus be written out explicitly as

$$\begin{aligned}
(\mathcal{X}_{D,1} \pm \mathcal{Y}_{D,1})^2 &= Z_2^2(1 \pm P_2^2)^2 [Z_1^2(1 + P_1^2)^2 + Z_0^2(1 - P_1^2)^2 \\
&\quad + 2Z_0Z_1(1 + P_1^2)(1 - P_1^2)] + Z_1^2(1 \mp P_2^2)^2 \times \\
&\quad \times [Z_1^2(1 - P_1^2)^2 + Z_0^2(1 + P_1^2)^2 + 2Z_0Z_1(1 + P_1^2)(1 - P_1^2)] \\
&\quad + 2Z_1Z_2(1 + P_2^2)(1 - P_2^2) \times \\
&\quad \times [(Z_1^2 + Z_0^2)(1 + P_1^2)(1 - P_1^2) + Z_0Z_1[(1 + P_1^2)^2 + (1 - P_1^2)^2]] \tag{6.92}
\end{aligned}$$

and

$$\begin{aligned}
(\mathcal{X}_{D,1} + \mathcal{Y}_{D,1})(\mathcal{X}_{D,1} - \mathcal{Y}_{D,1}) &= (1 + P_2^2)(1 - P_2^2) [Z_2^2 [Z_1^2(1 + P_1^2)^2 + Z_0^2(1 - P_1^2)^2 \\
&\quad + 2Z_0Z_1(1 + P_1^2)(1 - P_1^2)] + Z_1^2 [Z_1^2(1 - P_1^2)^2 + Z_0^2(1 + P_1^2)^2 \\
&\quad + 2Z_0Z_1(1 + P_1^2)(1 - P_1^2)] + Z_1Z_2 [(1 + P_2^2)^2 + (1 - P_2^2)^2] \times \\
&\quad \times [(Z_1^2 + Z_0^2)(1 + P_1^2)(1 - P_1^2) + Z_0Z_1[(1 + P_1^2)^2 + (1 - P_1^2)^2]] \tag{6.93}
\end{aligned}$$

Thus, the expressions in square brackets in (6.90) can be written explicitly. The first

of these is given as

$$\begin{aligned}
& 4^{-2} P_1^{-2} P_2^{-2} (\mathcal{X}_{D,1} + \mathcal{Y}_{D,1})^2 \\
&= Z_2^2 \cos^2 \Phi_2 \left[ Z_1^2 \cos^2 \Phi_1 - Z_0^2 \sin^2 \Phi_1 + 2j Z_0 (Z_1 \sin \Phi_1) \cos \Phi_1 \right] \\
&\quad - Z_1^2 \sin^2 \Phi_2 \left[ Z_0^2 \cos^2 \Phi_1 - Z_1^2 \sin^2 \Phi_1 + 2j Z_0 (Z_1 \sin \Phi_1) \cos \Phi_1 \right] \\
&\quad + 2j (Z_2 \sin \Phi_2) \cos \Phi_2 \left[ j (Z_1 \sin \Phi_1) \cos \Phi_1 (Z_1^2 + Z_0^2) + Z_0 Z_1^2 [\cos^2 \Phi_1 - \sin^2 \Phi_1] \right] \\
&= \left[ Z_2^2 \cos^2 \Phi_2 [Z_1^2 \cos^2 \Phi_1 - Z_0^2 \sin^2 \Phi_1] - Z_1^2 \sin^2 \Phi_2 [Z_0^2 \cos^2 \Phi_1 - Z_1^2 \sin^2 \Phi_1] \right. \\
&\quad \left. - 2 (Z_2 \sin \Phi_2) \cos \Phi_2 (Z_1 \sin \Phi_1) \cos \Phi_1 (Z_1^2 + Z_0^2) \right] + j Z_0 \left[ 2 (Z_1 \sin \Phi_1) \cos \Phi_1 \times \right. \\
&\quad \left. \times [Z_2^2 \cos^2 \Phi_2 - Z_1^2 \sin^2 \Phi_2] + 2 Z_1^2 [\cos^2 \Phi_1 - \sin^2 \Phi_1] (Z_2 \sin \Phi_2) \cos \Phi_2 \right] \\
&\triangleq H_1 + j Z_0 H_2 \tag{6.94}
\end{aligned}$$

where  $\Phi_2$  and  $\Phi_1$  are defined by (6.66). The quantities defined here as  $H_1$  and  $H_2$  are only functions of wave impedances and trigonometric functions, and are even about the branch cut using (6.71). The second expression found in square brackets in (6.90) is given by

$$\begin{aligned}
& 4^{-2} P_1^{-2} P_2^{-2} (\mathcal{X}_{D,1} - \mathcal{Y}_{D,1})^2 \\
&= - Z_2^2 \sin^2 \Phi_2 \left[ Z_1^2 \cos^2 \Phi_1 - Z_0^2 \sin^2 \Phi_1 + 2j Z_0 (Z_1 \sin \Phi_1) \cos \Phi_1 \right] \\
&\quad + Z_1^2 \cos^2 \Phi_2 \left[ Z_0^2 \cos^2 \Phi_1 - Z_1^2 \sin^2 \Phi_1 + 2j Z_0 (Z_1 \sin \Phi_1) \cos \Phi_1 \right] \\
&\quad + 2j (Z_2 \sin \Phi_2) \cos \Phi_2 \left[ j (Z_1 \sin \Phi_1) \cos \Phi_1 (Z_1^2 + Z_0^2) + Z_0 Z_1^2 [\cos^2 \Phi_1 - \sin^2 \Phi_1] \right] \\
&= \left[ - Z_2^2 \sin^2 \Phi_2 [Z_1^2 \cos^2 \Phi_1 - Z_0^2 \sin^2 \Phi_1] + Z_1^2 \cos^2 \Phi_2 [Z_0^2 \cos^2 \Phi_1 - Z_1^2 \sin^2 \Phi_1] \right. \\
&\quad \left. - 2 (Z_2 \sin \Phi_2) \cos \Phi_2 (Z_1 \sin \Phi_1) \cos \Phi_1 (Z_1^2 + Z_0^2) \right] + j Z_0 \left[ 2 (Z_1 \sin \Phi_1) \cos \Phi_1 \times \right. \\
&\quad \left. \times [Z_1^2 \cos^2 \Phi_2 - Z_2^2 \sin^2 \Phi_2] + 2 Z_1^2 [\cos^2 \Phi_1 - \sin^2 \Phi_1] (Z_2 \sin \Phi_2) \cos \Phi_2 \right] \\
&\triangleq \tilde{H}_1 + j Z_0 \tilde{H}_2 \tag{6.95}
\end{aligned}$$

The quantities defined here as  $\tilde{H}_1$  and  $\tilde{H}_2$  are only functions of wave impedances and trigonometric functions, and are even about the branch cut using (6.71). Finally, the third expression found in square brackets in (6.90) is given by

$$\begin{aligned}
& Z_2 \left[ 4^{-2} P_1^{-2} P_2^{-2} \left( \mathcal{X}_{D,1} + \mathcal{Y}_{D,1} \right) \left( \mathcal{X}_{D,1} - \mathcal{Y}_{D,1} \right) \right] \\
&= j(Z_2 \sin \Phi_2) \cos \Phi_2 \left[ Z_2^2 [Z_1^2 \cos^2 \Phi_1 - Z_0^2 \sin^2 \Phi_1 + 2jZ_0(Z_1 \sin \Phi_1) \cos \Phi_1] \right. \\
&\quad \left. + Z_1^2 [Z_0^2 \cos^2 \Phi_1 - Z_1^2 \sin^2 \Phi_1 + 2jZ_0(Z_1 \sin \Phi_1) \cos \Phi_1] \right] \\
&\quad + Z_2^2 \left[ j[\cos^2 \Phi_2 - \sin^2 \Phi_2] [(Z_1^2 + Z_0^2)(Z_1 \sin \Phi_1) \cos \Phi_1] \right. \\
&\quad \left. + Z_0 Z_1^2 (\cos^2 \Phi_1 - \sin^2 \Phi_1) \right] \\
&= Z_0 \left[ Z_2^2 Z_1^2 (\cos^2 \Phi_1 - \sin^2 \Phi_1) - 2[Z_2^2 + Z_1^2] Z_2 \sin \Phi_2 \cos \Phi_2 (Z_1 \sin \Phi_1) \cos \Phi_1 \right] \\
&\quad + j \left[ Z_2 \sin \Phi_2 \cos \Phi_2 \left[ Z_2^2 [Z_1^2 \cos^2 \Phi_1 - Z_0^2 \sin^2 \Phi_1] + Z_1^2 [Z_0^2 \cos^2 \Phi_1 - Z_1^2 \sin^2 \Phi_1] \right] \right. \\
&\quad \left. + Z_2^2 [\cos^2 \Phi_2 - \sin^2 \Phi_2] (Z_1^2 + Z_0^2) (Z_1 \sin \Phi_1) \cos \Phi_1 \right] \\
&\triangleq H_3 Z_0 + jH_4 \tag{6.96}
\end{aligned}$$

The quantities defined here as  $H_3$  and  $H_4$  are only functions of wave impedances and trigonometric functions, and are even about the branch cut using (6.71).

Plugging (6.94) through (6.96) into (6.90) gives

$$\begin{aligned}
4^{-(N-1)} \prod_{i=1}^{N-1} P_i^{-2} \overline{D}_N &= (\mathcal{G}_{1,N-3} + jZ_{N+1} \mathcal{G}_{2,N-3}) (H_1 + jZ_0 H_2) \\
&\quad + (\tilde{\mathcal{G}}_{1,N-2} + jZ_{N+1} \tilde{\mathcal{G}}_{2,N-2}) (\tilde{H}_1 + jZ_0 \tilde{H}_2) \\
&\quad + (\mathcal{G}_{3,N-3} Z_{N+1} + j\mathcal{G}_{4,N-3}) (H_3 Z_0 + jH_4) \tag{6.97}
\end{aligned}$$

Examining this equation, it can be seen that all quantities in the equation are even about the branch cut, with the possible exceptions of  $Z_0$  and  $Z_{N+1}$ . These wave impedances will exhibit an evenness about the branch cut if the regions they corre-

respond to are lossless. This occurs because the wave impedance of a lossless region of space is independent of the complex variable,  $s$ . However, if these regions are lossy, the wave impedances will display an odd symmetry about the branch cut by (6.64). Implications of the wave impedances displaying either even or odd symmetry about the branch cut on the form of the transient field are discussed in Section 6.4.3.

## 6.4.2 Form of the numerator

In this section, the numerator of the frequency domain reflection coefficient for an  $N$ -layered material structure is manipulated into a form which can be used to examine the form of the time domain reflection coefficient in the late time of the structure. Here, the late time begins after the two way transit time of the  $N$  regions comprising the  $N$ -material structure. The manipulation of the numerator proceeds by continuously utilizing a recursive form of the numerator and collapsing the equation by defining quantities which are even about the branch cuts. This is done at each step along the way, eventually leading to a recursive expression that allows  $N$  steps to be performed. Finally, once the expression is placed in terms of the numerator and denominator of the frequency domain reflection coefficient for a two layered structure, explicit expressions for the numerator and denominator are substituted in, leaving the expression in terms of quantities which are even about the branch cut, and wave impedances. The wave impedances may be even or odd about the branch cut, depending on the material characteristics of the region.

To this end, begin by establishing some relationships for the  $i^{th}$  layer of a multilayered structure. These relationships will prove extremely useful in the exploration into the form of the transient response from the multilayered structure.

### 6.4.2.1 Equations for the $i$ -th layer

To utilize the symmetry relationships of (6.71), it is helpful to place the numerator in an alternative form. To do this,  $R_i$  is plugged into (6.27a), and the result is multiplied

though by  $\mathbb{A}_{0,i}$ , noting a cancellation of terms in  $\mathbb{A}_{0,i}$  with the denominators of the interfacial reflection coefficients for indices of  $j$ , and  $i$ . The numerator is then found in terms of the wave impedances, rather than the reflection coefficients, as

$$\begin{aligned}
N_i \mathbb{A}_{0,i} &= N_{i-1} \mathbb{A}_{0,i} + (Z_{i+1} - Z_i) \times \\
&\times \left[ \mathbb{A}_{0,i-1} \mathbb{B}_{1,i} + \sum_{j=0}^{i-2} N_j (Z_{j+2} - Z_{j+1}) \mathbb{A}_{0,j} \mathbb{A}_{j+2,i-1} \mathbb{B}_{j+2,i} \right] \\
&= \mathcal{X}_{N,i-1} (Z_{i+1} + Z_i) + \mathcal{Y}_{N,i-1} (Z_{i+1} - Z_i)
\end{aligned} \tag{6.98}$$

where dependence of parameters on the complex variable,  $s$ , is suppressed for brevity. Several quantities are defined here in order to aid in understanding of the steps used in this derivation. These quantities are given by

$$\begin{aligned}
\mathcal{X}_{N,i} &= N_i \mathbb{A}_{0,i} \\
&= \mathcal{X}_{N,i-1} (Z_{i+1} + Z_i) + \mathcal{Y}_{N,i-1} (Z_{i+1} - Z_i)
\end{aligned} \tag{6.99a}$$

$$\begin{aligned}
\mathcal{Y}_{N,i} &= \left[ \mathbb{A}_{0,i} \mathbb{B}_{1,i+1} + \sum_{j=0}^{i-1} N_j (Z_{j+2} - Z_{j+1}) \mathbb{A}_{0,j} \mathbb{A}_{j+2,i} \mathbb{B}_{j+2,i+1} \right] \\
&= (Z_{i+1} + Z_i) P_{i+1}^2 \left[ \mathbb{A}_{0,i-1} \mathbb{B}_{1,i} + \sum_{j=0}^{i-2} N_j (Z_{j+2} - Z_{j+1}) \mathbb{A}_{0,j} \mathbb{A}_{j+2,i-1} \mathbb{B}_{j+2,i} \right] \\
&\quad + (Z_{i+1} - Z_i) P_{i+1}^2 N_{i-1} \mathbb{A}_{0,i-1} \\
&= \mathcal{Y}_{N,i-1} (Z_{i+1} + Z_i) P_{i+1}^2 + \mathcal{X}_{N,i-1} (Z_{i+1} - Z_i) P_{i+1}^2
\end{aligned} \tag{6.99b}$$

Here the  $i - 1$  term was removed from the summation in  $\mathcal{Y}_{N,i}$ , and  $(Z_{i+1} + Z_i) P_{i+1}^2$  was factored out of the remaining terms in order to write  $\mathcal{Y}_{N,i}$  in terms of  $\mathcal{Y}_{N,i-1}$  and  $\mathcal{X}_{N,i-1}$ . Various quantities involving the sum or difference of the expressions in (6.99) are utilized in the exploration of the form of the numerator for an N-layered

material. These terms will use the relationships

$$\begin{aligned}
(\mathcal{X}_{N,i} \pm \mathcal{Y}_{N,i}) &= (\mathcal{X}_{N,i-1}(Z_{i+1} + Z_i) + \mathcal{Y}_{N,i-1}(Z_{i+1} - Z_i)) \\
&\quad \pm (\mathcal{Y}_{N,i-1}(Z_{i+1} + Z_i)P_{i+1}^2 + \mathcal{X}_{N,i-1}(Z_{i+1} - Z_i)P_{i+1}^2) \\
&= Z_{i+1}(1 \pm P_{i+1}^2)(\mathcal{X}_{N,i-1} + \mathcal{Y}_{N,i-1}) \\
&\quad + Z_i(1 \mp P_{i+1}^2)(\mathcal{X}_{N,i-1} - \mathcal{Y}_{N,i-1}) \tag{6.100}
\end{aligned}$$

Because of various operations carried out on the denominator in 6.4.1, the two quantities given by (6.100) appear in various combinations with the quantities  $(\mathcal{X}_{D,i} \pm \mathcal{Y}_{D,i})$ , given by (6.74) when these same operations are performed on the numerator. Terms which appear include the combinations of

$$\begin{aligned}
&(\mathcal{X}_{D,i} \pm \mathcal{Y}_{D,i})(\mathcal{X}_{N,i} \pm \mathcal{Y}_{N,i}) \\
&= Z_{i+1}^2(1 \pm P_{i+1}^2)^2(\mathcal{X}_{D,i-1} + \mathcal{Y}_{D,i-1})(\mathcal{X}_{N,i-1} + \mathcal{Y}_{N,i-1}) \\
&\quad + Z_i^2(1 \mp P_{i+1}^2)^2(\mathcal{X}_{D,i-1} - \mathcal{Y}_{D,i-1})(\mathcal{X}_{N,i-1} - \mathcal{Y}_{N,i-1}) \\
&\quad + Z_{i+1}Z_i(1 \pm P_{i+1}^2)(1 \mp P_{i+1}^2) \left[ (\mathcal{X}_{D,i-1} + \mathcal{Y}_{D,i-1})(\mathcal{X}_{N,i-1} - \mathcal{Y}_{N,i-1}) \right. \\
&\quad \left. + (\mathcal{X}_{D,i-1} - \mathcal{Y}_{D,i-1})(\mathcal{X}_{N,i-1} + \mathcal{Y}_{N,i-1}) \right] \tag{6.101}
\end{aligned}$$

and

$$\begin{aligned}
&(\mathcal{X}_{D,i} \pm \mathcal{Y}_{D,i})(\mathcal{X}_{N,i} \mp \mathcal{Y}_{N,i}) \\
&= Z_{i+1}^2(1 \pm P_{i+1}^2)(1 \mp P_{i+1}^2)(\mathcal{X}_{D,i-1} + \mathcal{Y}_{D,i-1})(\mathcal{X}_{N,i-1} + \mathcal{Y}_{N,i-1}) \\
&\quad + Z_i^2(1 \pm P_{i+1}^2)(1 \mp P_{i+1}^2)(\mathcal{X}_{D,i-1} - \mathcal{Y}_{D,i-1})(\mathcal{X}_{N,i-1} - \mathcal{Y}_{N,i-1}) \\
&\quad + Z_{i+1}Z_i \left[ (1 \pm P_{i+1}^2)^2(\mathcal{X}_{D,i-1} + \mathcal{Y}_{D,i-1})(\mathcal{X}_{N,i-1} - \mathcal{Y}_{N,i-1}) \right. \\
&\quad \left. + (1 \mp P_{i+1}^2)^2(\mathcal{X}_{D,i-1} - \mathcal{Y}_{D,i-1})(\mathcal{X}_{N,i-1} + \mathcal{Y}_{N,i-1}) \right]. \tag{6.102}
\end{aligned}$$

The products of (6.101) and (6.102) appear often throughout the manipulation of the numerator of the frequency domain reflection coefficient. The following recursive formula, which appears in the course of this derivation and is utilized heavily, contains all combinations of (6.101) and (6.102).

$$\begin{aligned}
& 4P_{N-i}^{-2} \left[ (\mathcal{H}_{1,i-1} + jZ_{N+1}\mathcal{H}_{2,i-1}) \times \right. \\
& \quad \times \left( \mathcal{X}_{D,N-(i+1)} + \mathcal{Y}_{D,N-(i+1)} \right) \left( \mathcal{X}_{N,N-(i+1)} + \mathcal{Y}_{N,N-(i+1)} \right) \\
& + (\tilde{\mathcal{H}}_{1,i} + jZ_{N+1}\tilde{\mathcal{H}}_{2,i}) \times \\
& \quad \times \left( \mathcal{X}_{D,N-(i+1)} - \mathcal{Y}_{D,N-(i+1)} \right) \left( \mathcal{X}_{N,N-(i+1)} - \mathcal{Y}_{N,N-(i+1)} \right) \\
& + (\mathcal{H}_{3,i-1}Z_{i-1} + j\mathcal{H}_{4,i-1}) \times \\
& \quad \times Z_{N-i} \left( \mathcal{X}_{D,N-(i+1)} + \mathcal{Y}_{D,N-(i+1)} \right) \left( \mathcal{X}_{N,N-(i+1)} - \mathcal{Y}_{N,N-(i+1)} \right) \\
& + (\mathcal{H}_{3,i-1}Z_{i-1} + j\tilde{\mathcal{H}}_{4,i-1}) \times \\
& \quad \times Z_{N-i} \left( \mathcal{X}_{D,N-(i+1)} - \mathcal{Y}_{D,N-(i+1)} \right) \left( \mathcal{X}_{N,N-(i+1)} + \mathcal{Y}_{N,N-(i+1)} \right) \left. \right] \\
& = (\mathcal{H}_{1,i} + jZ_{N+1}\mathcal{H}_{2,i}) \times \\
& \quad \times \left( \mathcal{X}_{D,N-(i+2)} + \mathcal{Y}_{D,N-(i+2)} \right) \left( \mathcal{X}_{N,N-(i+2)} + \mathcal{Y}_{N,N-(i+2)} \right) \\
& + (\tilde{\mathcal{H}}_{1,i+1} + jZ_{N+1}\tilde{\mathcal{H}}_{2,i+1}) \times \\
& \quad \times \left( \mathcal{X}_{D,N-(i+2)} - \mathcal{Y}_{D,N-(i+2)} \right) \left( \mathcal{X}_{N,N-(i+2)} - \mathcal{Y}_{N,N-(i+2)} \right) \\
& + (\mathcal{H}_{3,i}Z_{N+1} + j\mathcal{H}_{4,i})Z_{N-(i+1)} \times \\
& \quad \times \left( \mathcal{X}_{D,N-(i+2)} + \mathcal{Y}_{D,N-(i+2)} \right) \left( \mathcal{X}_{N,N-(i+2)} - \mathcal{Y}_{N,N-(i+2)} \right) \\
& + (\mathcal{H}_{3,i}Z_{N+1} + j\tilde{\mathcal{H}}_{4,i})Z_{N-(i+1)} \times \\
& \quad \times \left( \mathcal{X}_{D,N-(i+2)} - \mathcal{Y}_{D,N-(i+2)} \right) \left( \mathcal{X}_{N,N-(i+2)} + \mathcal{Y}_{N,N-(i+2)} \right) \quad (6.103)
\end{aligned}$$

where the following quantities arise from application of (6.99) through (6.102)

$$\begin{aligned}
\mathcal{H}_{1,i} &= Z_{N-i}^2 \left[ \mathcal{H}_{1,i-1} \cos^2 \Phi_{N-i} - \tilde{\mathcal{H}}_{1,i} \sin^2 \Phi_{N-i} \right. \\
&\quad \left. - [\mathcal{H}_{4,i-1} + \tilde{\mathcal{H}}_{4,i-1}] (Z_{N-i} \sin \Phi_{N-i}) \cos \Phi_{N-i} \right] \\
\mathcal{H}_{2,i} &= Z_{N-i}^2 \left[ \mathcal{H}_{2,i-1} \cos^2 \Phi_{N-i} - \tilde{\mathcal{H}}_{2,i} \sin^2 \Phi_{N-i} \right. \\
&\quad \left. + 2\mathcal{H}_{3,i-1} (Z_{N-i} \sin \Phi_{N-i}) \cos \Phi_{N-i} \right] \\
\tilde{\mathcal{H}}_{1,i+1} &= Z_{N-(i+1)}^2 \left[ \tilde{\mathcal{H}}_{1,i} \cos^2 \Phi_{N-i} - \mathcal{H}_{1,i-1} \sin^2 \Phi_{N-i} \right. \\
&\quad \left. - [\mathcal{H}_{4,i-1} + \tilde{\mathcal{H}}_{4,i-1}] (Z_{N-i} \sin \Phi_{N-i}) \cos \Phi_{N-i} \right] \\
\tilde{\mathcal{H}}_{2,i+1} &= Z_{N-(i+1)}^2 \left[ \tilde{\mathcal{H}}_{2,i} \cos^2 \Phi_{N-i} - \mathcal{H}_{2,i-1} \sin^2 \Phi_{N-i} \right. \\
&\quad \left. + 2\mathcal{H}_{3,i-1} (Z_{N-i} \sin \Phi_{N-i}) \cos \Phi_{N-i} \right] \\
\mathcal{H}_{3,i} &= Z_{N-i}^2 \left[ \cos^2 \Phi_{N-i} - \sin^2 \Phi_{N-i} \right] \mathcal{H}_{3,i-1} \\
&\quad - [\mathcal{H}_{2,i-1} + \tilde{\mathcal{H}}_{2,i}] (Z_{N-i} \sin \Phi_{N-i}) \cos \Phi_{N-i} \\
\mathcal{H}_{4,i} &= Z_{N-i}^2 \left[ \mathcal{H}_{4,i-1} \cos^2 \Phi_{N-i} - \tilde{\mathcal{H}}_{4,i-1} \sin^2 \Phi_{N-i} \right] \\
&\quad + [\mathcal{H}_{1,i-1} + \tilde{\mathcal{H}}_{1,i}] (Z_{N-i} \sin \Phi_{N-i}) \cos \Phi_{N-i} \\
\tilde{\mathcal{H}}_{4,i} &= Z_{N-i}^2 \left[ \tilde{\mathcal{H}}_{4,i-1} \cos^2 \Phi_{N-i} - \mathcal{H}_{4,i-1} \sin^2 \Phi_{N-i} \right] \\
&\quad + [\mathcal{H}_{1,i-1} + \tilde{\mathcal{H}}_{1,i}] (Z_{N-i} \sin \Phi_{N-i}) \cos \Phi_{N-i}
\end{aligned}$$

#### 6.4.2.2 N-Layer geometry

Consider the  $N$ -material, planar layered geometry shown in Figure 6.8, where region 0 is free space, and region  $N + 1$  is a material which may or may not be lossy. The numerator of the frequency domain reflection coefficient, multiplied by  $\mathbb{A}_{0,N}$ , is given by (6.98) for  $i = N$  as

$$N_N \mathbb{A}_{0,N} = \mathcal{X}_{N,N-1} (Z_{N+1} + Z_N) + \mathcal{Y}_{N,N-1} (Z_{N+1} - Z_N) \quad (6.104)$$



To explore the properties of the numerator of the reflection coefficient, begin by plugging in expressions for  $\mathcal{X}_{N,N-1}$  and  $\mathcal{Y}_{N,N-1}$  using (6.99). Doing this gives

$$\begin{aligned} N_N \mathbf{A}_{0,N} &= (\mathcal{X}_{N,N-2}(Z_N + Z_{N-1}) + \mathcal{Y}_{N,N-2}(Z_N - Z_{N-1}))(Z_{N+1} + Z_N) \\ &\quad + (\mathcal{Y}_{N,N-2}(Z_N + Z_{N-1})P_N^2 + \mathcal{X}_{N,N-2}(Z_N - Z_{N-1})P_N^2)(Z_{N+1} - Z_N) \end{aligned} \quad (6.105)$$

Rearranging terms to separate the  $\mathcal{X}_{N,N-2}$  and  $\mathcal{Y}_{N,N-2}$  terms gives

$$\begin{aligned} N_N \mathbf{A}_{0,N} &= \mathcal{X}_{N,N-2} \left[ (Z_{N+1} + Z_N)(Z_N + Z_{N-1}) + (Z_{N+1} - Z_N)(Z_N - Z_{N-1})P_N^2 \right] \\ &\quad + \mathcal{Y}_{N,N-2} \left[ (Z_{N+1} + Z_N)(Z_N - Z_{N-1}) + (Z_{N+1} - Z_N)(Z_N + Z_{N-1})P_N^2 \right] \end{aligned} \quad (6.106)$$

Multiplying out the wave impedance terms in brackets and regrouping gives

$$\begin{aligned} N_N \mathbf{A}_{0,N} &= \mathcal{X}_{N,N-2} \left[ Z_N(Z_{N+1} + Z_{N-1})(1 + P_N^2) + (Z_N^2 + Z_{N+1}Z_{N-1})(1 - P_N^2) \right] \\ &\quad + \mathcal{Y}_{N,N-2} \left[ Z_N(Z_{N+1} - Z_{N-1})(1 + P_N^2) + (Z_N^2 - Z_{N+1}Z_{N-1})(1 - P_N^2) \right] \\ &= \mathcal{C}(1 + P_N^2) + j\mathcal{D} \left( \frac{1 - P_N^2}{j} \right) \end{aligned} \quad (6.107)$$

where the quantities  $\mathcal{C}$  and  $\mathcal{D}$  are defined as

$$\mathcal{C} = \mathcal{X}_{N,N-2}(Z_{N+1}Z_N + Z_NZ_{N-1}) + \mathcal{Y}_{N,N-2}(Z_{N+1}Z_N - Z_NZ_{N-1}) \quad (6.108a)$$

$$\mathcal{D} = \mathcal{X}_{N,N-2}(Z_N^2 + Z_{N+1}Z_{N-1}) + \mathcal{Y}_{N,N-2}(Z_N^2 - Z_{N+1}Z_{N-1}) \quad (6.108b)$$

Utilizing  $\Phi_i = \left( \frac{s\tau_i(s)}{2j} \right)$ , and multiplying through by  $\left( \mathcal{A}(1 + P_N^2) - j\mathcal{B} \left( \frac{1 - P_N^2}{j} \right) \right) 4^{-1} P_N^{-2}$ , which is the same term the denominator is multiplied by in

Section 6.4.1, leads to

$$\begin{aligned}
\bar{N}_N &= N_N \mathbb{A}_{0,N} \left( \mathcal{A}(1 + P_N^2) - j\mathcal{B} \left( \frac{1 - P_N^2}{j} \right) \right) 4^{-1} P_N^{-2} \\
&= \left( \mathcal{C}(1 + P_N^2) + j\mathcal{D} \left( \frac{1 - P_N^2}{j} \right) \right) \left( \mathcal{A}(1 + P_N^2) - j\mathcal{B} \left( \frac{1 - P_N^2}{j} \right) \right) 4^{-1} P_N^{-2} \\
&= \mathcal{AC} \cos^2 \Phi_N + \mathcal{BD} \sin^2 \Phi_N + j(\mathcal{AD} - \mathcal{BC}) \sin \Phi_N \cos \Phi_N \quad (6.109)
\end{aligned}$$

Here, the terms  $\mathcal{AC}$ ,  $\mathcal{BD}$ ,  $\mathcal{AD}$ , and  $\mathcal{BC}$  are calculated using (6.82) and (6.108). The first term is given by

$$\begin{aligned}
\mathcal{AC} &= \mathcal{X}_{N,N-2} \mathcal{X}_{D,N-2} (Z_{N+1} Z_N + Z_N Z_{N-1})^2 \\
&\quad + \mathcal{Y}_{N,N-2} \mathcal{Y}_{D,N-2} (Z_{N+1} Z_N - Z_N Z_{N-1})^2 \\
&\quad + (\mathcal{X}_{D,N-2} \mathcal{Y}_{N,N-2} + \mathcal{X}_{N,N-2} \mathcal{Y}_{D,N-2}) (Z_{N+1}^2 Z_N^2 - Z_N^2 Z_{N-1}^2) \\
&= Z_{N+1}^2 Z_N^2 (\mathcal{X}_{D,N-2} + \mathcal{Y}_{D,N-2}) (\mathcal{X}_{N,N-2} + \mathcal{Y}_{N,N-2}) \\
&\quad + Z_N^2 Z_{N-1}^2 (\mathcal{X}_{D,N-2} - \mathcal{Y}_{D,N-2}) (\mathcal{X}_{N,N-2} - \mathcal{Y}_{N,N-2}) \\
&\quad + 2Z_{N+1} Z_N^2 Z_{N-1} \left[ (\mathcal{X}_{D,N-2} - \mathcal{Y}_{D,N-2}) (\mathcal{X}_{N,N-2} + \mathcal{Y}_{N,N-2}) \right. \\
&\quad \left. + (\mathcal{X}_{D,N-2} + \mathcal{Y}_{D,N-2}) (\mathcal{X}_{N,N-2} - \mathcal{Y}_{N,N-2}) \right]. \quad (6.110)
\end{aligned}$$

Next,  $\mathcal{BD}$  is found as

$$\begin{aligned}
\mathcal{BD} &= \mathcal{X}_{N,N-2} \mathcal{X}_{D,N-2} (Z_N^2 + Z_{N+1} Z_{N-1})^2 + \mathcal{Y}_{N,N-2} \mathcal{Y}_{D,N-2} (Z_N^2 - Z_{N+1} Z_{N-1})^2 \\
&\quad + (\mathcal{X}_{D,N-2} \mathcal{Y}_{N,N-2} + \mathcal{X}_{N,N-2} \mathcal{Y}_{D,N-2}) (Z_N^4 - Z_{N+1}^2 Z_{N-1}^2) \\
&= Z_N^4 (\mathcal{X}_{D,N-2} + \mathcal{Y}_{D,N-2}) (\mathcal{X}_{N,N-2} + \mathcal{Y}_{N,N-2}) \\
&\quad + Z_{N+1}^2 Z_{N-1}^2 (\mathcal{X}_{D,N-2} - \mathcal{Y}_{D,N-2}) (\mathcal{X}_{N,N-2} - \mathcal{Y}_{N,N-2}) \\
&\quad + 2Z_{N+1} Z_N^2 Z_{N-1} \left[ (\mathcal{X}_{D,N-2} - \mathcal{Y}_{D,N-2}) (\mathcal{X}_{N,N-2} + \mathcal{Y}_{N,N-2}) \right. \\
&\quad \left. + (\mathcal{X}_{D,N-2} + \mathcal{Y}_{D,N-2}) (\mathcal{X}_{N,N-2} - \mathcal{Y}_{N,N-2}) \right]. \quad (6.111)
\end{aligned}$$

$\mathcal{AD}$  and  $\mathcal{BC}$  are given by

$$\begin{aligned}
\mathcal{AD} &= \mathcal{X}_{N,N-2}\mathcal{X}_{D,N-2}(Z_{N+1}Z_N + Z_N Z_{N-1})(Z_N^2 + Z_{N+1}Z_{N-1}) \\
&\quad + \mathcal{Y}_{N,N-2}\mathcal{Y}_{D,N-2}(Z_{N+1}Z_N - Z_N Z_{N-1})(Z_N^2 - Z_{N+1}Z_{N-1}) \\
&\quad + \mathcal{X}_{D,N-2}\mathcal{Y}_{N,N-2}(Z_{N+1}Z_N + Z_N Z_{N-1})(Z_N^2 - Z_{N+1}Z_{N-1}) \\
&\quad + \mathcal{X}_{N,N-2}\mathcal{Y}_{D,N-2}(Z_{N+1}Z_N - Z_N Z_{N-1})(Z_N^2 + Z_{N+1}Z_{N-1}) \\
&= Z_{N+1}Z_N^3(\mathcal{X}_{D,N-2} + \mathcal{Y}_{D,N-2})(\mathcal{X}_{N,N-2} + \mathcal{Y}_{N,N-2}) \\
&\quad + Z_N^3 Z_{N-1}(\mathcal{X}_{D,N-2} - \mathcal{Y}_{D,N-2})(\mathcal{X}_{N,N-2} + \mathcal{Y}_{N,N-2}) \\
&\quad + Z_{N+1}^2 Z_N Z_{N-1}(\mathcal{X}_{D,N-2} + \mathcal{Y}_{D,N-2})(\mathcal{X}_{N,N-2} - \mathcal{Y}_{N,N-2}) \\
&\quad + Z_{N+1} Z_N Z_{N-1}^2(\mathcal{X}_{D,N-2} - \mathcal{Y}_{D,N-2})(\mathcal{X}_{N,N-2} - \mathcal{Y}_{N,N-2}) \tag{6.112}
\end{aligned}$$

$$\begin{aligned}
\mathcal{BC} &= \mathcal{X}_{N,N-2}\mathcal{X}_{D,N-2}(Z_{N+1}Z_N + Z_N Z_{N-1})(Z_N^2 + Z_{N+1}Z_{N-1}) \\
&\quad + \mathcal{Y}_{N,N-2}\mathcal{Y}_{D,N-2}(Z_{N+1}Z_N - Z_N Z_{N-1})(Z_N^2 - Z_{N+1}Z_{N-1}) \\
&\quad + \mathcal{X}_{D,N-2}\mathcal{Y}_{N,N-2}(Z_{N+1}Z_N - Z_N Z_{N-1})(Z_N^2 + Z_{N+1}Z_{N-1}) \\
&\quad + \mathcal{X}_{N,N-2}\mathcal{Y}_{D,N-2}(Z_{N+1}Z_N + Z_N Z_{N-1})(Z_N^2 - Z_{N+1}Z_{N-1}) \\
&= Z_{N+1}Z_N^3(\mathcal{X}_{D,N-2} + \mathcal{Y}_{D,N-2})(\mathcal{X}_{N,N-2} + \mathcal{Y}_{N,N-2}) \\
&\quad + Z_N^3 Z_{N-1}(\mathcal{X}_{D,N-2} + \mathcal{Y}_{D,N-2})(\mathcal{X}_{N,N-2} - \mathcal{Y}_{N,N-2}) \\
&\quad + Z_{N+1}^2 Z_N Z_{N-1}(\mathcal{X}_{D,N-2} - \mathcal{Y}_{D,N-2})(\mathcal{X}_{N,N-2} + \mathcal{Y}_{N,N-2}) \\
&\quad + Z_{N+1} Z_N Z_{N-1}^2(\mathcal{X}_{D,N-2} - \mathcal{Y}_{D,N-2})(\mathcal{X}_{N,N-2} - \mathcal{Y}_{N,N-2}). \tag{6.113}
\end{aligned}$$

The difference between (6.112) and (6.113) is then given as

$$\begin{aligned}
\mathcal{AD} - \mathcal{BC} &= (Z_N^2 - Z_{N+1}^2)Z_N Z_{N-1} \left[ (\mathcal{X}_{D,N-2} - \mathcal{Y}_{D,N-2})(\mathcal{X}_{N,N-2} + \mathcal{Y}_{N,N-2}) \right. \\
&\quad \left. - (\mathcal{X}_{D,N-2} + \mathcal{Y}_{D,N-2})(\mathcal{X}_{N,N-2} - \mathcal{Y}_{N,N-2}) \right] \tag{6.114}
\end{aligned}$$

Plugging (6.110) through (6.114) back into (6.109) gives

$$\begin{aligned}
\bar{N}_N = & \left[ Z_{N+1}^2 Z_N^2 (\mathcal{X}_{D,N-2} + \mathcal{Y}_{D,N-2}) (\mathcal{X}_{N,N-2} + \mathcal{Y}_{N,N-2}) \right. \\
& + \left. Z_N^2 Z_{N-1}^2 (\mathcal{X}_{D,N-2} - \mathcal{Y}_{D,N-2}) (\mathcal{X}_{N,N-2} - \mathcal{Y}_{N,N-2}) \right] \cos^2 \Phi_N \\
& + \left[ Z_N^4 (\mathcal{X}_{D,N-2} + \mathcal{Y}_{D,N-2}) (\mathcal{X}_{N,N-2} + \mathcal{Y}_{N,N-2}) \right. \\
& + \left. Z_{N+1}^2 Z_{N-1}^2 (\mathcal{X}_{D,N-2} - \mathcal{Y}_{D,N-2}) (\mathcal{X}_{N,N-2} - \mathcal{Y}_{N,N-2}) \right] \sin^2 \Phi_N \\
& + 2Z_{N+1} Z_N^2 Z_{N-1} \left[ (\mathcal{X}_{D,N-2} - \mathcal{Y}_{D,N-2}) (\mathcal{X}_{N,N-2} + \mathcal{Y}_{N,N-2}) \right. \\
& + \left. (\mathcal{X}_{D,N-2} + \mathcal{Y}_{D,N-2}) (\mathcal{X}_{N,N-2} - \mathcal{Y}_{N,N-2}) \right] + j(Z_N^2 - Z_{N+1}^2) \times \\
& \times Z_N Z_{N-1} \sin \Phi_N \cos \Phi_N \left[ (\mathcal{X}_{D,N-2} - \mathcal{Y}_{D,N-2}) (\mathcal{X}_{N,N-2} + \mathcal{Y}_{N,N-2}) \right. \\
& - \left. (\mathcal{X}_{D,N-2} + \mathcal{Y}_{D,N-2}) (\mathcal{X}_{N,N-2} - \mathcal{Y}_{N,N-2}) \right] \quad (6.115)
\end{aligned}$$

Rearranging (6.115) to organize the equation in terms of various products of  $(\mathcal{X}_{D,N-2} \pm \mathcal{Y}_{D,N-2})$  and  $(\mathcal{X}_{N,N-2} \pm \mathcal{Y}_{N,N-2})$  gives

$$\begin{aligned}
\bar{N}_N = & \left[ Z_{N+1}^2 Z_N^2 \cos^2 \Phi_N + Z_N^4 \sin^2 \Phi_N \right] (\mathcal{X}_{D,N-2} + \mathcal{Y}_{D,N-2}) \times \\
& \times (\mathcal{X}_{N,N-2} + \mathcal{Y}_{N,N-2}) + \left[ Z_N^2 Z_{N-1}^2 \cos^2 \Phi_N + Z_{N+1}^2 Z_{N-1}^2 \sin^2 \Phi_N \right] \times \\
& \times (\mathcal{X}_{D,N-2} - \mathcal{Y}_{D,N-2}) (\mathcal{X}_{N,N-2} - \mathcal{Y}_{N,N-2}) + \left[ 2Z_{N+1} Z_N^2 + j(Z_N^2 - \right. \\
& - \left. Z_{N+1}^2) Z_N \sin \Phi_N \cos \Phi_N \right] Z_{N-1} (\mathcal{X}_{D,N-2} - \mathcal{Y}_{D,N-2}) (\mathcal{X}_{N,N-2} + \mathcal{Y}_{N,N-2}) \\
& + \left[ 2Z_{N+1} Z_N^2 - j(Z_N^2 - Z_{N+1}^2) Z_N \sin \Phi_N \cos \Phi_N \right] \times \\
& \times Z_{N-1} (\mathcal{X}_{D,N-2} + \mathcal{Y}_{D,N-2}) (\mathcal{X}_{N,N-2} - \mathcal{Y}_{N,N-2}) \\
= & \tilde{F}_1 (\mathcal{X}_{D,N-2} + \mathcal{Y}_{D,N-2}) (\mathcal{X}_{N,N-2} + \mathcal{Y}_{N,N-2}) \\
& + \tilde{F}_2 (\mathcal{X}_{D,N-2} - \mathcal{Y}_{D,N-2}) (\mathcal{X}_{N,N-2} - \mathcal{Y}_{N,N-2}) \\
& + (Z_{N+1} \tilde{F}_3 + j\tilde{F}_4) Z_{N-1} (\mathcal{X}_{D,N-2} - \mathcal{Y}_{D,N-2}) (\mathcal{X}_{N,N-2} + \mathcal{Y}_{N,N-2}) \\
& + (Z_{N+1} \tilde{F}_3 - j\tilde{F}_4) Z_{N-1} (\mathcal{X}_{D,N-2} + \mathcal{Y}_{D,N-2}) (\mathcal{X}_{N,N-2} - \mathcal{Y}_{N,N-2}) \quad (6.116)
\end{aligned}$$

Here the functions  $\tilde{F}_1$  through  $\tilde{F}_3$  are even about the branch cut, since they are defined in terms of wave impedances and trigonometric functions which are raised to even powers. Multiplying through by  $4^{-1}P_{N-1}^{-2}$ , plugging in the expressions for  $(\mathcal{X}_{D,N-2} \pm \mathcal{Y}_{D,N-2})$  and  $(\mathcal{X}_{N,N-2} \pm \mathcal{Y}_{N,N-2})$ , and rearranging terms gives

$$\begin{aligned}
4^{-1}P_{N-1}^{-2}\bar{N}_N &= Z_{N-1}^2 \left[ \tilde{F}_1 \cos^2 \Phi_{N-1} - \tilde{F}_2 \sin^2 \Phi_{N-1} + j(Z_{N+1}\tilde{F}_3 + \right. \\
&+ j\tilde{F}_4)Z_{N-1} \sin \Phi_{N-1} \cos \Phi_{N-1} + j(Z_{N+1}\tilde{F}_3 - j\tilde{F}_4)Z_{N-1} \sin \Phi_{N-1} \cos \Phi_{N-1} \left. \right] \times \\
&\times \left( \mathcal{X}_{D,N-3} + \mathcal{Y}_{D,N-3} \right) \left( \mathcal{X}_{N,N-3} + \mathcal{Y}_{N,N-3} \right) + Z_{N-2}^2 \left[ \tilde{F}_2 \cos^2 \Phi_{N-1} - \right. \\
&- \tilde{F}_1 \sin^2 \Phi_{N-1} + j(Z_{N+1}\tilde{F}_3 + j\tilde{F}_4)Z_{N-1} \sin \Phi_{N-1} \cos \Phi_{N-1} \\
&+ j(Z_{N+1}\tilde{F}_3 - j\tilde{F}_4)Z_{N-1} \sin \Phi_{N-1} \cos \Phi_{N-1} \left. \right] \times \\
&\times \left( \mathcal{X}_{D,N-3} - \mathcal{Y}_{D,N-3} \right) \left( \mathcal{X}_{N,N-3} - \mathcal{Y}_{N,N-3} \right) \\
&+ Z_{N-2} \left[ j[\tilde{F}_1 + \tilde{F}_2](Z_{N-1} \sin \Phi_{N-1}) \cos \Phi_{N-1} + (Z_{N+1}\tilde{F}_3 + j\tilde{F}_4) \cos^2 \Phi_{N-1} \right. \\
&- \left. (Z_{N+1}\tilde{F}_3 - j\tilde{F}_4) \sin^2 \Phi_{N-1} \right] \left( \mathcal{X}_{D,N-3} + \mathcal{Y}_{D,N-3} \right) \left( \mathcal{X}_{N,N-3} - \mathcal{Y}_{N,N-3} \right) \\
&+ Z_{N-2} \left[ j[\tilde{F}_1 + \tilde{F}_2](Z_{N-1} \sin \Phi_{N-1}) \cos \Phi_{N-1} - (Z_{N+1}\tilde{F}_3 + j\tilde{F}_4) \cos^2 \Phi_{N-1} \right. \\
&+ \left. (Z_{N+1}\tilde{F}_3 - j\tilde{F}_4) \sin^2 \Phi_{N-1} \right] \left( \mathcal{X}_{D,N-3} - \mathcal{Y}_{D,N-3} \right) \left( \mathcal{X}_{N,N-3} + \mathcal{Y}_{N,N-3} \right) \\
&= (\mathcal{H}_{1,1} + jZ_{N+1}\mathcal{H}_{2,1}) \left( \mathcal{X}_{D,N-3} + \mathcal{Y}_{D,N-3} \right) \left( \mathcal{X}_{N,N-3} + \mathcal{Y}_{N,N-3} \right) \\
&+ (\tilde{\mathcal{H}}_{1,2} + jZ_{N+1}\tilde{\mathcal{H}}_{2,2}) \left( \mathcal{X}_{D,N-3} - \mathcal{Y}_{D,N-3} \right) \left( \mathcal{X}_{N,N-3} - \mathcal{Y}_{N,N-3} \right) \\
&+ (\mathcal{H}_{3,1}Z_{N+1} + j\mathcal{H}_{4,1})Z_{N-2} \left( \mathcal{X}_{D,N-3} + \mathcal{Y}_{D,N-3} \right) \left( \mathcal{X}_{N,N-3} - \mathcal{Y}_{N,N-3} \right) \\
&+ (\mathcal{H}_{3,1}Z_{N+1} + j\tilde{\mathcal{H}}_{4,1})Z_{N-2} \left( \mathcal{X}_{D,N-3} - \mathcal{Y}_{D,N-3} \right) \left( \mathcal{X}_{N,N-3} + \mathcal{Y}_{N,N-3} \right) \quad (6.117)
\end{aligned}$$

with  $\Phi_{N-1}$  defined by (6.66) as  $s\tau_{N-1}(s)/2j$ , and

$$\begin{aligned}
\mathcal{H}_{1,1} &= Z_{N-1}^2 \left[ \tilde{F}_1 \cos^2 \Phi_{N-1} - \tilde{F}_2 \sin^2 \Phi_{N-1} \right] \\
\mathcal{H}_{2,1} &= 2\tilde{F}_3 Z_{N-1}^2 (Z_{N-1} \sin \Phi_{N-1}) \cos \Phi_{N-1} \\
\tilde{\mathcal{H}}_{1,2} &= Z_{N-2}^2 \left[ \tilde{F}_2 \cos^2 \Phi_{N-1} - \tilde{F}_1 \sin^2 \Phi_{N-1} \right] \\
\tilde{\mathcal{H}}_{2,2} &= 2\tilde{F}_3 Z_{N-2}^2 (Z_{N-1} \sin \Phi_{N-1}) \cos \Phi_{N-1} \\
\mathcal{H}_{3,1} &= \tilde{F}_3 Z_{N-1}^2 \left[ \cos^2 \Phi_{N-1} - \sin^2 \Phi_{N-1} \right] \\
\mathcal{H}_{4,1} &= \left[ \tilde{F}_1 + \tilde{F}_2 \right] (Z_{N-1} \sin \Phi_{N-1}) \cos \Phi_{N-1} + \tilde{F}_4 Z_{N-1}^2 \\
\tilde{\mathcal{H}}_{4,1} &= \left[ \tilde{F}_1 + \tilde{F}_2 \right] (Z_{N-1} \sin \Phi_{N-1}) \cos \Phi_{N-1} - \tilde{F}_4 Z_{N-1}^2
\end{aligned}$$

Note that the quantities  $\mathcal{H}_{1,1}$  through  $\mathcal{H}_{4,1}$  are defined in terms of  $\tilde{F}_1$  through  $\tilde{F}_3$ , wave impedances, and trigonometric functions. Thus,  $\mathcal{H}_{1,1}$  through  $\mathcal{H}_{4,1}$  are even about the branch cut using (6.71) and evenness of  $\tilde{F}_1$  through  $\tilde{F}_3$ .

Multiplying by  $4^{-1}P_{N-2}^{-2}$ , the right hand side of (6.117) has the form of the left hand side of (6.103) for  $i = 2$ , thus,

$$\begin{aligned}
&4^{-2}P_{N-1}^{-2}P_{N-2}^{-2}\bar{N}_N \\
&= (\mathcal{H}_{1,2} + jZ_{N+1}\mathcal{H}_{2,2})\left(\mathcal{X}_{D,N-4} + \mathcal{Y}_{D,N-4}\right)\left(\mathcal{X}_{N,N-4} + \mathcal{Y}_{N,N-4}\right) \\
&\quad + (\tilde{\mathcal{H}}_{1,3} + jZ_{N+1}\tilde{\mathcal{H}}_{2,3})\left(\mathcal{X}_{D,N-4} - \mathcal{Y}_{D,N-4}\right)\left(\mathcal{X}_{N,N-4} - \mathcal{Y}_{N,N-4}\right) \\
&\quad + (\mathcal{H}_{3,2}Z_{N+1} + j\mathcal{H}_{4,2})Z_{N-3}\left(\mathcal{X}_{D,N-4} + \mathcal{Y}_{D,N-4}\right)\left(\mathcal{X}_{N,N-4} - \mathcal{Y}_{N,N-4}\right) \\
&\quad + (\mathcal{H}_{3,2}Z_{N+1} + j\tilde{\mathcal{H}}_{4,2})Z_{N-3}\left(\mathcal{X}_{D,N-4} - \mathcal{Y}_{D,N-4}\right)\left(\mathcal{X}_{N,N-4} + \mathcal{Y}_{N,N-4}\right)
\end{aligned} \tag{6.118}$$

with

$$\begin{aligned}
\mathcal{H}_{1,2} &= Z_{N-2}^2 \left[ \mathcal{H}_{1,1} \cos^2 \Phi_{N-2} - \tilde{\mathcal{H}}_{1,2} \sin^2 \Phi_{N-2} \right. \\
&\quad \left. - \left[ \mathcal{H}_{4,1} + \tilde{\mathcal{H}}_{4,1} \right] (Z_{N-2} \sin \Phi_{N-2}) \cos \Phi_{N-2} \right] \\
\mathcal{H}_{2,2} &= Z_{N-2}^2 \left[ \mathcal{H}_{2,1} \cos^2 \Phi_{N-2} - \tilde{\mathcal{H}}_{2,2} \sin^2 \Phi_{N-2} \right. \\
&\quad \left. + 2\mathcal{H}_{3,1} (Z_{N-2} \sin \Phi_{N-2}) \cos \Phi_{N-2} \right] \\
\tilde{\mathcal{H}}_{1,3} &= Z_{N-3}^2 \left[ \tilde{\mathcal{H}}_{1,2} \cos^2 \Phi_{N-2} - \mathcal{H}_{1,1} \sin^2 \Phi_{N-2} \right. \\
&\quad \left. - \left[ \mathcal{H}_{4,1} + \tilde{\mathcal{H}}_{4,1} \right] (Z_{N-2} \sin \Phi_{N-2}) \cos \Phi_{N-2} \right] \\
\tilde{\mathcal{H}}_{2,3} &= Z_{N-3}^2 \left[ \tilde{\mathcal{H}}_{2,2} \cos^2 \Phi_{N-2} - \mathcal{H}_{2,1} \sin^2 \Phi_{N-2} \right. \\
&\quad \left. + 2\mathcal{H}_{3,1} (Z_{N-2} \sin \Phi_{N-2}) \cos \Phi_{N-2} \right] \\
\mathcal{H}_{3,2} &= Z_{N-2}^2 \left[ \cos^2 \Phi_{N-2} - \sin^2 \Phi_{N-2} \right] \mathcal{H}_{3,1} \\
&\quad - \left[ \mathcal{H}_{2,1} + \tilde{\mathcal{H}}_{2,2} \right] (Z_{N-2} \sin \Phi_{N-2}) \cos \Phi_{N-2} \\
\mathcal{H}_{4,2} &= Z_{N-2}^2 \left[ \mathcal{H}_{4,1} \cos^2 \Phi_{N-2} - \tilde{\mathcal{H}}_{4,1} \sin^2 \Phi_{N-2} \right] \\
&\quad + \left[ \mathcal{H}_{1,1} + \tilde{\mathcal{H}}_{1,2} \right] (Z_{N-2} \sin \Phi_{N-2}) \cos \Phi_{N-2} \\
\tilde{\mathcal{H}}_{4,2} &= Z_{N-2}^2 \left[ \tilde{\mathcal{H}}_{4,1} \cos^2 \Phi_{N-2} - \mathcal{H}_{4,1} \sin^2 \Phi_{N-2} \right] \\
&\quad + \left[ \mathcal{H}_{1,1} + \tilde{\mathcal{H}}_{1,2} \right] (Z_{N-2} \sin \Phi_{N-2}) \cos \Phi_{N-2}
\end{aligned}$$

Note that the quantities  $\mathcal{H}_{1,2}$  through  $\mathcal{H}_{4,2}$  are defined in terms of  $\mathcal{H}_{1,1}$  through  $\mathcal{H}_{4,1}$ , wave impedances, and trigonometric functions. Thus  $\mathcal{H}_{1,2}$  through  $\mathcal{H}_{4,2}$  are even about the branch cut using (6.71) and evenness of  $\mathcal{H}_{1,1}$  through  $\mathcal{H}_{4,1}$ .

Multiplying by  $4^{-1}P_{N-3}^{-2}$ , the right hand side of (6.118) has the form of the left hand side of (6.103), with  $i = 3$ . This leads to terms  $\mathcal{H}_{1,3}$  through  $\mathcal{H}_{4,3}$ , which are defined by (6.103) in terms of  $\mathcal{H}_{1,2}$  through  $\mathcal{H}_{4,2}$ , wave impedances, and trigonometric functions. Thus  $\mathcal{H}_{1,3}$  through  $\mathcal{H}_{4,3}$  are even about the branch cut using (6.71) and evenness of  $\mathcal{H}_{1,2}$  through  $\mathcal{H}_{4,2}$ . Continuing to multiply through by  $4^{-1}P_{N-i}^{-2}$  and

applying (6.103) for increasing values of  $i$ , until  $i = N - 3$ , and then multiplying by  $4^{-2}P_1^{-2}P_2^{-2}$ , leads to

$$\begin{aligned}
& 4^{-(N-1)} \prod_{i=1}^{N-1} P_i^{-2} \bar{N}_N \\
&= (\mathcal{H}_{1,N-3} + jZ_{N+1}\mathcal{H}_{2,N-3}) \left[ 4^{-2}P_1^{-2}P_2^{-2} (\mathcal{X}_{D,1} + \mathcal{Y}_{D,1}) (\mathcal{X}_{N,1} + \mathcal{Y}_{N,1}) \right] \\
&+ (\tilde{\mathcal{H}}_{1,N-2} + jZ_{N+1}\tilde{\mathcal{H}}_{2,N-2}) \left[ 4^{-2}P_1^{-2}P_2^{-2} (\mathcal{X}_{D,1} - \mathcal{Y}_{D,1}) (\mathcal{X}_{N,1} - \mathcal{Y}_{N,1}) \right] \\
&+ (\mathcal{H}_{3,N-3}Z_{N+1} + j\mathcal{H}_{4,N-3})Z_2 \left[ 4^{-2}P_1^{-2}P_2^{-2} (\mathcal{X}_{D,1} + \mathcal{Y}_{D,1}) (\mathcal{X}_{N,1} - \mathcal{Y}_{N,1}) \right] \\
&+ (\mathcal{H}_{3,N-3}Z_{N+1} + j\tilde{\mathcal{H}}_{4,N-3})Z_2 \left[ 4^{-2}P_1^{-2}P_2^{-2} (\mathcal{X}_{D,1} - \mathcal{Y}_{D,1}) (\mathcal{X}_{N,1} + \mathcal{Y}_{N,1}) \right]
\end{aligned} \tag{6.119}$$

with

$$\begin{aligned}
\mathcal{H}_{1,N-3} &= Z_3^2 \left[ \mathcal{H}_{1,N-4} \cos^2 \Phi_2 - \tilde{\mathcal{H}}_{1,N-3} \sin^2 \Phi_2 \right. \\
&\quad \left. - \left[ \mathcal{H}_{4,N-4} + \tilde{\mathcal{H}}_{4,N-4} \right] (Z_2 \sin \Phi_2) \cos \Phi_2 \right] \\
\mathcal{H}_{2,N-3} &= Z_3^2 \left[ \mathcal{H}_{2,N-4} \cos^2 \Phi_2 - \tilde{\mathcal{H}}_{2,N-3} \sin^2 \Phi_2 + 2\mathcal{H}_{3,N-4} (Z_2 \sin \Phi_2) \cos \Phi_2 \right] \\
\tilde{\mathcal{H}}_{1,N-2} &= Z_2^2 \left[ \tilde{\mathcal{H}}_{1,N-3} \cos^2 \Phi_2 - \mathcal{H}_{1,N-4} \sin^2 \Phi_2 \right. \\
&\quad \left. - \left[ \mathcal{H}_{4,N-4} + \tilde{\mathcal{H}}_{4,N-4} \right] (Z_2 \sin \Phi_2) \cos \Phi_2 \right] \\
\tilde{\mathcal{H}}_{2,N-2} &= Z_2^2 \left[ \tilde{\mathcal{H}}_{2,N-3} \cos^2 \Phi_2 - \mathcal{H}_{2,N-4} \sin^2 \Phi_2 + 2\mathcal{H}_{3,N-4} (Z_2 \sin \Phi_2) \cos \Phi_2 \right] \\
\mathcal{H}_{3,N-3} &= Z_3^2 \left[ \cos^2 \Phi_2 - \sin^2 \Phi_2 \right] \mathcal{H}_{3,N-4} - \left[ \mathcal{H}_{2,N-4} + \tilde{\mathcal{H}}_{2,N-3} \right] (Z_2 \sin \Phi_2) \cos \Phi_2 \\
\mathcal{H}_{4,N-3} &= Z_3^2 \left[ \mathcal{H}_{4,N-4} \cos^2 \Phi_2 - \tilde{\mathcal{H}}_{4,N-4} \sin^2 \Phi_2 \right] \\
&\quad + \left[ \mathcal{H}_{1,N-4} + \tilde{\mathcal{H}}_{1,N-3} \right] (Z_2 \sin \Phi_2) \cos \Phi_2 \\
\tilde{\mathcal{H}}_{4,N-3} &= Z_3^2 \left[ \tilde{\mathcal{H}}_{4,N-4} \cos^2 \Phi_2 - \mathcal{H}_{4,N-4} \sin^2 \Phi_2 \right] \\
&\quad + \left[ \mathcal{H}_{1,N-4} + \tilde{\mathcal{H}}_{1,N-3} \right] (Z_2 \sin \Phi_2) \cos \Phi_2
\end{aligned}$$

Here  $\mathcal{H}_{1,N-3}$  through  $\mathcal{H}_{4,N-3}$ , which are defined by (6.103) in terms of  $\mathcal{H}_{1,N-4}$



through  $\mathcal{H}_{4,N-4}$ , wave impedances, and trigonometric functions, are even about the branch cut using (6.71) and evenness of  $\mathcal{H}_{1,N-4}$  through  $\mathcal{H}_{4,N-4}$ . This symmetry about the branch cut is established through the continual reapplication of (6.103) leading to the form of (6.119).

At this point, the expressions for  $(\mathcal{X}_{D,1} \pm \mathcal{Y}_{D,1})$  and  $(\mathcal{X}_{N,1} \pm \mathcal{Y}_{N,1})$  are simple enough to be written out explicitly. These expressions are found as

$$\begin{aligned}
(\mathcal{X}_{N,1} \pm \mathcal{Y}_{N,1}) &= N_1 \mathbb{A}_{0,1} \pm \left[ \mathbb{A}_{0,1} \mathbb{B}_{1,2} + N_0 (Z_2 - Z_1) \mathbb{A}_{0,0} \mathbb{B}_{2,2} \right] \\
&= (Z_2 + Z_1)(Z_1 - Z_0) + (Z_2 - Z_1)(Z_1 + Z_0) P_1^2 \\
&\quad \pm \left[ (Z_2 + Z_1)(Z_1 + Z_0) P_1^2 P_2^2 + (Z_2 - Z_1)(Z_1 - Z_0) P_2^2 \right] \\
&= Z_2 (1 \pm P_2^2) (Z_1 (1 + P_1^2) - Z_0 (1 - P_1^2)) \\
&\quad + Z_1 (1 \mp P_2^2) (Z_1 (1 - P_1^2) - Z_0 (1 + P_1^2)) \tag{6.120}
\end{aligned}$$

Repeating (6.91),  $(\mathcal{X}_{D,1} \pm \mathcal{Y}_{D,1})$  is given by

$$\begin{aligned}
(\mathcal{X}_{D,1} \pm \mathcal{Y}_{D,1}) &= Z_2 (1 \pm P_2^2) (Z_1 (1 + P_1^2) + Z_0 (1 - P_1^2)) \\
&\quad + Z_1 (1 \mp P_2^2) (Z_1 (1 - P_1^2) + Z_0 (1 + P_1^2)) \tag{6.121}
\end{aligned}$$

The expressions in brackets in (6.119) can be written using (6.120) through (6.121).

The first of these terms is given by

$$\begin{aligned}
&4^{-2} P_1^{-2} P_2^{-2} (\mathcal{X}_{D,1} + \mathcal{Y}_{D,1}) (\mathcal{X}_{N,1} + \mathcal{Y}_{N,1}) \\
&= \left[ Z_2 \cos \Phi_2 (Z_1 \cos \Phi_1 + j Z_0 \sin \Phi_1) + j Z_1 \sin \Phi_2 (j Z_1 \sin \Phi_1 + Z_0 \cos \Phi_1) \right] \times \\
&\quad \times \left[ Z_2 \cos \Phi_2 (Z_1 \cos \Phi_1 - j Z_0 \sin \Phi_1) + j Z_1 \sin \Phi_2 (j Z_1 \sin \Phi_1 - Z_0 \cos \Phi_1) \right] \\
&= Z_2^2 \cos^2 \Phi_2 (Z_1^2 \cos^2 \Phi_1 + Z_0^2 \sin^2 \Phi_1) + Z_1^2 \sin^2 \Phi_2 (Z_1^2 \sin^2 \Phi_1 + Z_0^2 \cos^2 \Phi_1) \\
&\quad + 2 (Z_2 \sin \Phi_2) \cos \Phi_2 (Z_1 \sin \Phi_1) \cos \Phi_1 (Z_0^2 - Z_1^2) \triangleq G_1 \tag{6.122}
\end{aligned}$$

The quantity defined here as  $G_1$  is only a function of wave impedances and trigonometric functions, and is even about the branch cut using (6.71). The second expression found in brackets in (6.119) is given by

$$\begin{aligned}
& 4^{-2}P_1^{-2}P_2^{-2}\left(\mathcal{X}_{D,1} - \mathcal{Y}_{D,1}\right)\left(\mathcal{X}_{N,1} - \mathcal{Y}_{N,1}\right) \\
&= \left[ jZ_2 \sin \Phi_2 (Z_1 \cos \Phi_1 + jZ_0 \sin \Phi_1) + Z_1 \cos \Phi_2 (jZ_1 \sin \Phi_1 + Z_0 \cos \Phi_1) \right] \times \\
&\quad \times \left[ jZ_2 \sin \Phi_2 (Z_1 \cos \Phi_1 - jZ_0 \sin \Phi_1) + Z_1 \cos \Phi_2 (jZ_1 \sin \Phi_1 - Z_0 \cos \Phi_1) \right] \\
&= -Z_2^2 \sin^2 \Phi_2 \left( Z_1^2 \cos^2 \Phi_1 + Z_0^2 \sin^2 \Phi_1 \right) - Z_1^2 \cos^2 \Phi_2 \left( Z_1^2 \sin^2 \Phi_1 + Z_0^2 \cos^2 \Phi_1 \right) \\
&\quad + 2(Z_2 \sin \Phi_2) \cos \Phi_2 (Z_1 \sin \Phi_1) \cos \Phi_1 \left( Z_0^2 - Z_1^2 \right) \triangleq \tilde{G}_1 \tag{6.123}
\end{aligned}$$

The quantity defined here as  $\tilde{G}_1$  is only a function of wave impedances and trigonometric functions, and is even about the branch cut using (6.71). The third expression found in brackets in (6.119) is given by

$$\begin{aligned}
& Z_2 \left[ 4^{-2}P_1^{-2}P_2^{-2}\left(\mathcal{X}_{D,1} + \mathcal{Y}_{D,1}\right)\left(\mathcal{X}_{N,1} - \mathcal{Y}_{N,1}\right) \right] \\
&= Z_2 \left[ \left[ Z_2 \cos \Phi_2 (Z_1 \cos \Phi_1 + jZ_0 \sin \Phi_1) + jZ_1 \sin \Phi_2 (jZ_1 \sin \Phi_1 + Z_0 \cos \Phi_1) \right] \times \right. \\
&\quad \left. \times \left[ jZ_2 \sin \Phi_2 (Z_1 \cos \Phi_1 - jZ_0 \sin \Phi_1) + Z_1 \cos \Phi_2 (jZ_1 \sin \Phi_1 - Z_0 \cos \Phi_1) \right] \right] \\
&= Z_2^2 Z_1^2 Z_0 + j \left[ (Z_2 \sin \Phi_2) \cos \Phi_2 \left( Z_2^2 (Z_1^2 \cos^2 \Phi_1 + Z_0^2 \sin^2 \Phi_1) - Z_1^2 (Z_1^2 \sin^2 \Phi_1 \right. \right. \\
&\quad \left. \left. + Z_0^2 \cos^2 \Phi_1) \right) + Z_2^2 (Z_1 \sin \Phi_1) \cos \Phi_1 \left( Z_1^2 - Z_0^2 \right) \left( \cos^2 \Phi_2 - \sin^2 \Phi_2 \right) \right] \\
&\triangleq G_3 Z_0 + jG_4 \tag{6.124}
\end{aligned}$$

The quantities defined here as  $G_3$  and  $G_4$  are only functions of wave impedances and trigonometric functions, and are even about the branch cut using (6.71). Finally, the

fourth expression found in brackets in (6.119) is given by

$$\begin{aligned}
& Z_2 \left[ 4^{-2} P_1^{-2} P_2^{-2} (\mathcal{X}_{D,1} - \mathcal{Y}_{D,1}) (\mathcal{X}_{N,1} + \mathcal{Y}_{N,1}) \right] \\
&= Z_2 \left[ \left[ j Z_2 \sin \Phi_2 (Z_1 \cos \Phi_1 + j Z_0 \sin \Phi_1) + Z_1 \cos \Phi_2 (j Z_1 \sin \Phi_1 + Z_0 \cos \Phi_1) \right] \times \right. \\
&\quad \left. \times \left[ Z_2 \cos \Phi_2 (Z_1 \cos \Phi_1 - j Z_0 \sin \Phi_1) + j Z_1 \sin \Phi_2 (j Z_1 \sin \Phi_1 - Z_0 \cos \Phi_1) \right] \right] \\
&= Z_2^2 Z_1^2 Z_0 + j \left[ (Z_2 \sin \Phi_2) \cos \Phi_2 \left( Z_2^2 (Z_1^2 \cos^2 \Phi_1 + Z_0^2 \sin^2 \Phi_1) - Z_1^2 (Z_1^2 \sin^2 \Phi_1 \right. \right. \\
&\quad \left. \left. + Z_0^2 \cos^2 \Phi_1) \right) + Z_2^2 (Z_1 \sin \Phi_1) \cos \Phi_1 \left( Z_1^2 - Z_0^2 \right) \left( \cos^2 \Phi_2 - \sin^2 \Phi_2 \right) \right] \\
&= Z_2 \left[ 4^{-2} P_1^{-2} P_2^{-2} (\mathcal{X}_{D,1} + \mathcal{Y}_{D,1}) (\mathcal{X}_{N,1} - \mathcal{Y}_{N,1}) \right] \tag{6.125}
\end{aligned}$$

Plugging into (6.119) gives

$$\begin{aligned}
4^{-(N-1)} \prod_{i=1}^{N-1} P_i^{-2} \bar{N}_N &= (\mathcal{H}_{1,N-3} + j Z_{N+1} \mathcal{H}_{2,N-3}) G_1 \\
&\quad + (\tilde{\mathcal{H}}_{1,N-2} + j Z_{N+1} \tilde{\mathcal{H}}_{2,N-2}) \tilde{G}_1 \\
&\quad + (2\mathcal{H}_{3,N-3} Z_{N+1} + j(\mathcal{H}_{4,N-3} + \tilde{\mathcal{H}}_{4,N-3}))(G_3 Z_0 + j G_4) \tag{6.126}
\end{aligned}$$

Examining this equation, it can be seen that all quantities in the equation are even about the branch cut, with the possible exceptions of  $Z_0$  and  $Z_{N+1}$ . These wave impedances will exhibit an evenness about the branch cut if the regions they correspond to are lossless. This occurs because the wave impedance of a lossless region of space is independent of the complex variable,  $s$ . However, if these regions are lossy, the wave impedances will display an odd symmetry about the branch cut by (6.64). Implications of the wave impedances displaying either even or odd symmetry about the branch cut on the form of the transient field are discussed in Section 6.4.3.

### 6.4.3 Form of the reflection coefficient

The frequency domain reflection coefficient is given by

$$\Gamma_{Nlay}(s) = \frac{N_N(s)}{D_N(s)} = \frac{\bar{N}_N(s)}{\bar{D}_N(s)} \quad (6.127)$$

where  $\bar{N}_N(s)$  and  $\bar{D}_N(s)$  are defined by (6.109) and (6.83), respectively. Multiplying and dividing by  $4^{-(N-1)} \prod_{i=1}^{N-1} P_i^{-2}$  gives

$$\Gamma_{Nlay}(s) = \frac{4^{-(N-1)} \prod_{i=1}^{N-1} P_i^{-2} \bar{N}_N}{4^{-(N-1)} \prod_{i=1}^{N-1} P_i^{-2} \bar{D}_N}. \quad (6.128)$$

Here, the numerator is given by

$$\begin{aligned} 4^{-(N-1)} \prod_{i=1}^{N-1} P_i^{-2} \bar{N}_N &= (\mathcal{H}_{1,N-3} + jZ_{N+1}\mathcal{H}_{2,N-3})G_1 \\ &+ (\tilde{\mathcal{H}}_{1,N-2} + jZ_{N+1}\tilde{\mathcal{H}}_{2,N-2})\tilde{G}_1 \\ &+ (2\mathcal{H}_{3,N-3}Z_{N+1} + j(\mathcal{H}_{4,N-3} + \tilde{\mathcal{H}}_{4,N-3}))(G_3Z_0 + jG_4) \end{aligned} \quad (6.129)$$

and the denominator by

$$\begin{aligned} 4^{-(N-1)} \prod_{i=1}^{N-1} P_i^{-2} \bar{D}_N &= (\mathcal{G}_{1,N-3} + jZ_{N+1}\mathcal{G}_{2,N-3})(H_1 + jZ_0H_2) \\ &+ (\tilde{\mathcal{G}}_{1,N-2} + jZ_{N+1}\tilde{\mathcal{G}}_{2,N-2})(\tilde{H}_1 + jZ_0\tilde{H}_2) \\ &+ (\mathcal{G}_{3,N-3}Z_{N+1} + j\mathcal{G}_{4,N-3})(H_3Z_0 + jH_4) \end{aligned} \quad (6.130)$$

Both the numerator and denominator are given in terms of wave impedances for regions 0 and  $(N+1)$ , and quantities which are even about the branch cuts. Quantities displaying evenness about the branch cut lead to identical expressions on each side of the branch cut. Thus, since all other quantities are even about the branch cut, there is

only a possibility of a branch cut contribution due to the material properties of regions 0 and  $(N + 1)$  in the late time of the  $N$ -layered system. Since region 0 is assumed to be free space, only the properties of the backing material region will determine the form of the late time response. If this region is lossless, the wave impedance will be even about the branch cut. This will lead to evenness about the branch cut for the frequency domain reflection coefficient and the cancellation of integral contributions due to integration paths located on opposite sides of the branch cut. Thus, if region  $(N + 1)$  is lossless,

$$\sum_i \int_{l_i} f(s)e^{st} ds = 0. \quad (6.131)$$

The integration along the Bromwich path is then given by

$$\int_{Br} f(s)e^{st} ds = \sum [Res(f(s)e^{st}), poles] \quad (6.132)$$

Thus, for an  $N$ -layered material structure backed by a lossless material half space, the late time response is a natural mode series, assuming that region 0 is free space. This development also validates a natural mode series representation for substructures of the multilayered structure, during the late times of these substructures, provided that the backing material of the substructure is lossless. If the  $N$  layer material structure is backed by a lossy half space, it is likely that there will be a branch cut contribution which pollutes the natural resonance response. Examining 6.129 and 6.130, it appears that a pure natural resonance representation of the time domain reflection coefficient is not possible with a lossy backing layer, however this has not been shown explicitly, and proving this is left as future work.

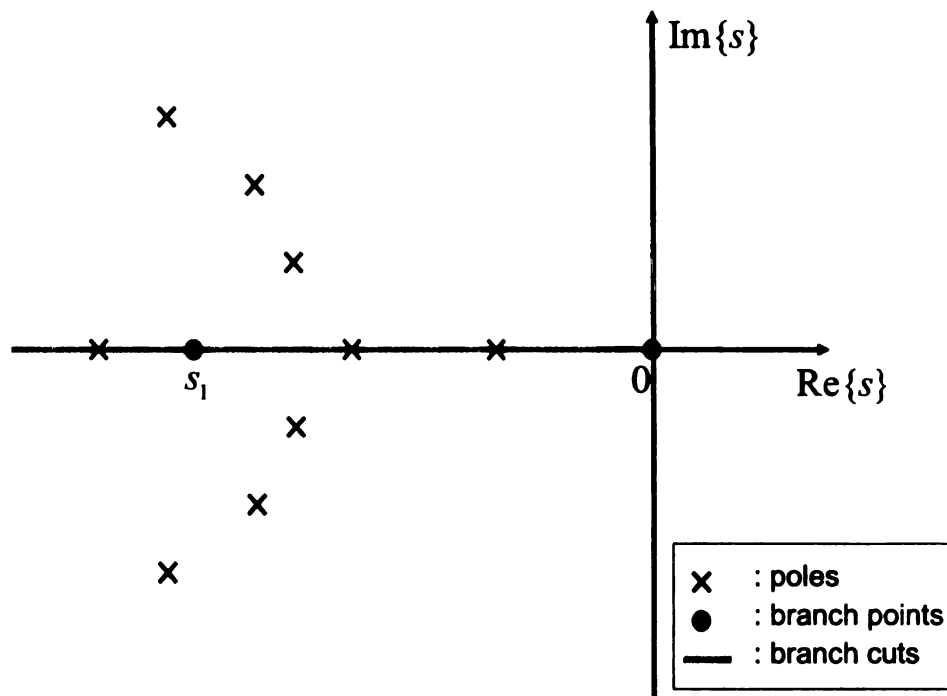


Figure 6.1. Singularities of the frequency domain reflection coefficient

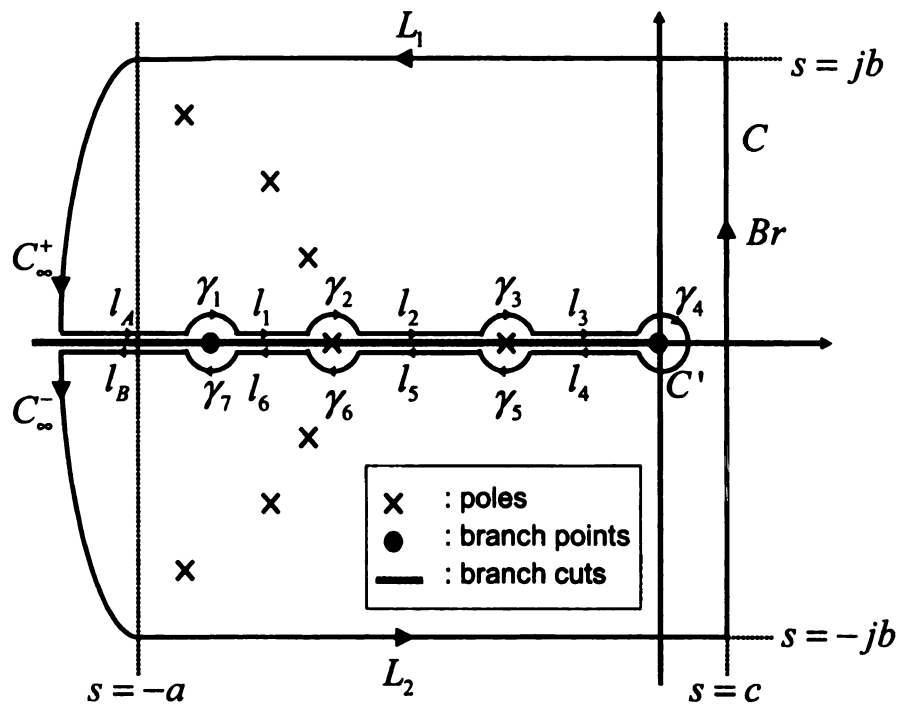


Figure 6.2. Left half plane closure of the integration path.  $|a|, |b| \rightarrow \infty, 0 < c < \infty$

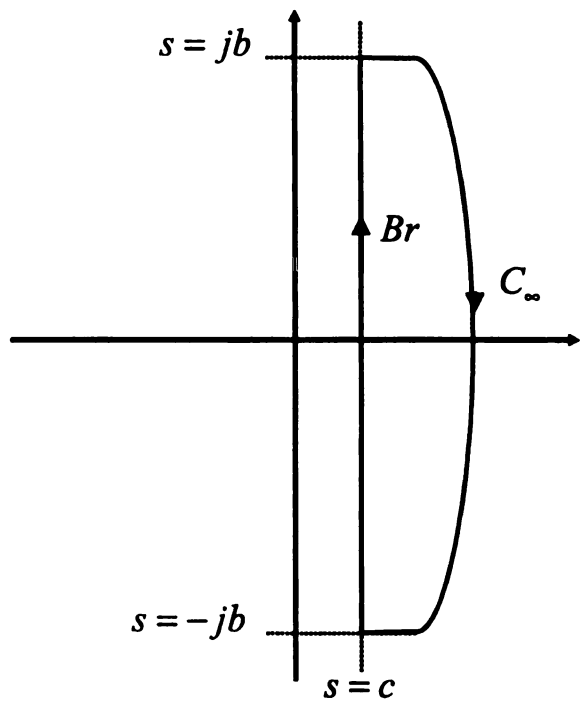


Figure 6.3. Right half plane closure of the integration path.  $|b| \rightarrow \infty, 0 < c < \infty$



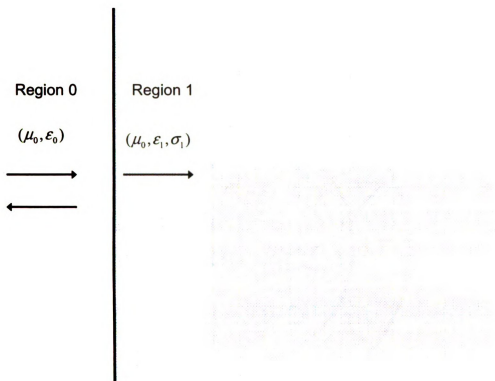


Figure 6.4. Single interface between two material half spaces

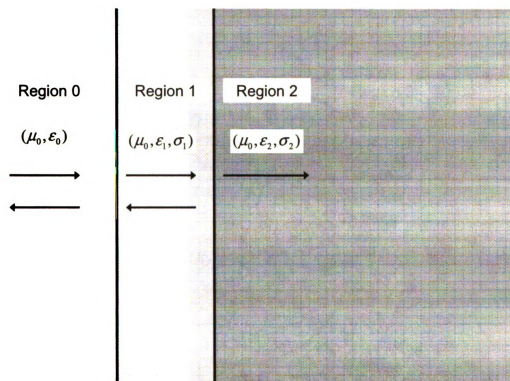


Figure 6.5. Single layer geometry backed by a material half space

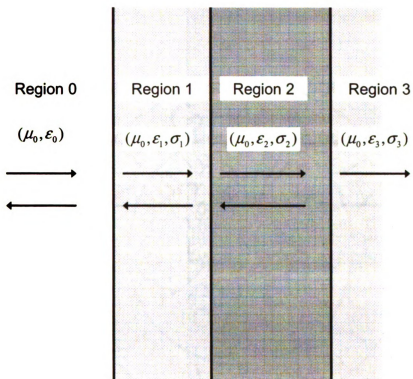


Figure 6.6. Two layer geometry backed by a material half space

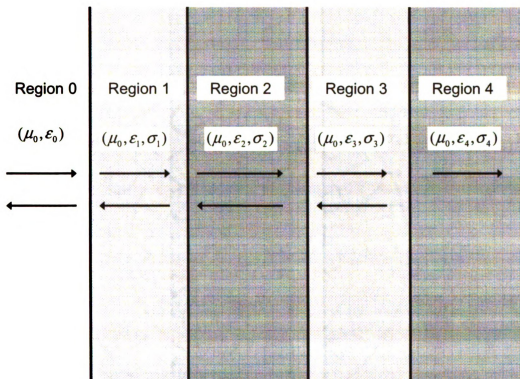


Figure 6.7. Three layer geometry backed by a material half space

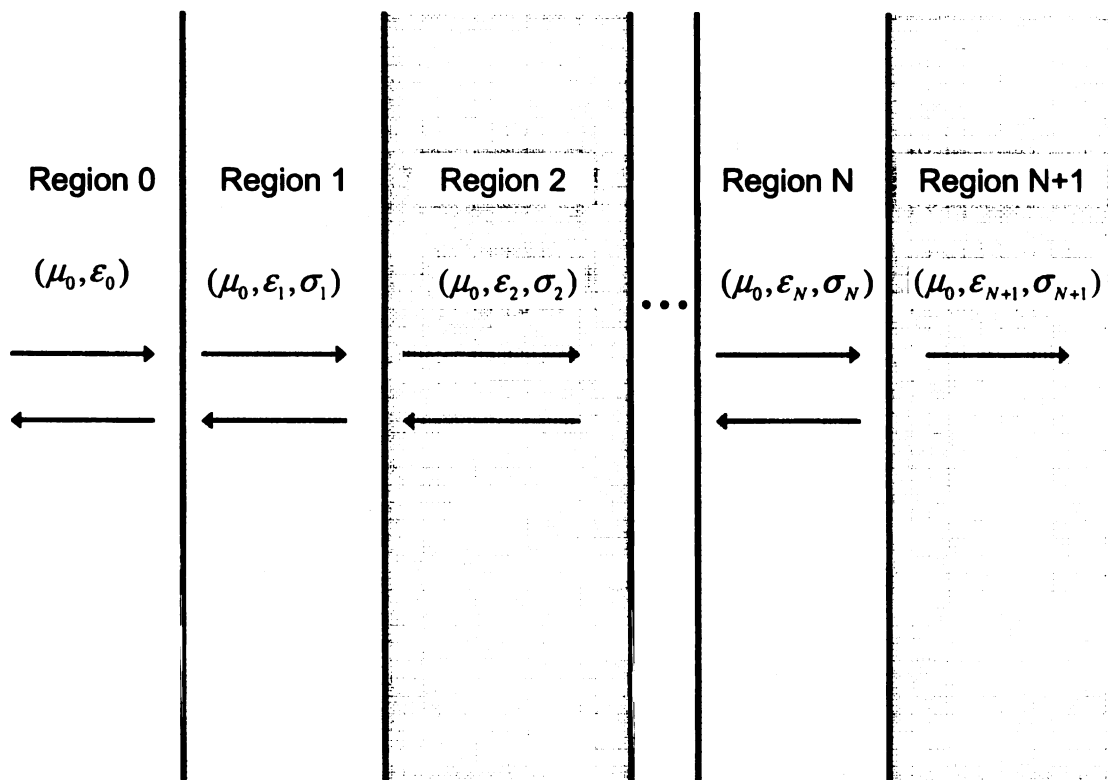


Figure 6.8. N-layered structure backed by a material half space

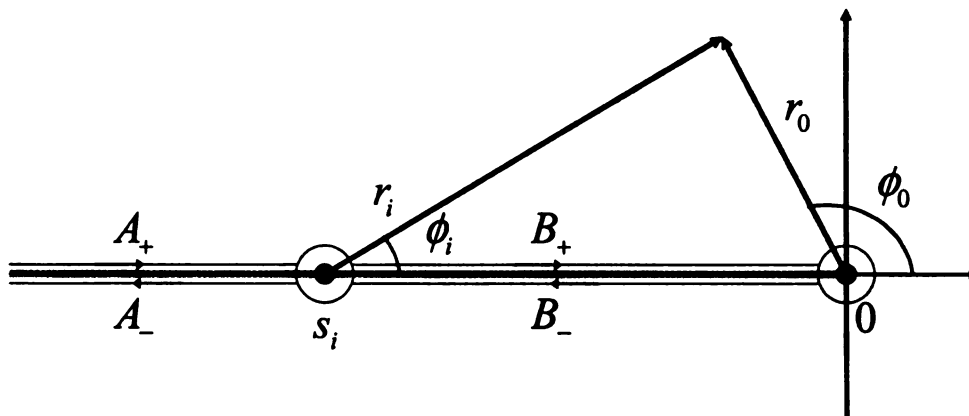


Figure 6.9. Inner contour integration paths for left half plane closure

## CHAPTER 7

### TIME AND FREQUENCY DOMAIN MEASUREMENTS

In this chapter, the experimental setup and procedure for obtaining a measured response from layered material is examined. An overview of time-domain and frequency-domain measurement systems is given in Section 7.1, including benefits and drawbacks of each measurement system. Determination of experimental parameters and calibration procedures for each of these measurement systems are discussed in Section 7.2, and results of measurements for various material sheets are given in Section 7.3. Comparisons of the two measurement systems are provided throughout the chapter.

#### 7.1 Measurement Systems

Time-domain and frequency-domain measurement techniques for scattering from planar layered dielectric materials are examined here. Included are descriptions of measurement systems and calibration techniques for both time and frequency-domain setups. For both systems, reflection measurements are made using the MSU reflectivity arch range. The arch range is a circular structure measuring 6.096 meters in diameter with transmitting and receiving horn antennas and dielectric lenses placed at a height of 1.219 meters. The horn antennas have a 2 GHz to 18 GHz bandwidth and are manufactured by American Electronics Laboratories, Inc. (AEL), model H-1498. These horn antennas can be placed at arbitrary locations on the perimeter of the arch, as shown in Figure 7.1. To measure the backscattered fields the two horn antennas are placed adjacent to each other in order to approximate a mono-static configuration.

Comparisons of the data measured using the frequency-domain and time-domain systems are given in Section 7.3.3. It is shown there that nearly equivalent temporal results may be obtained using the two systems, and that these results compare favor-

ably with theory. Importantly, the performance of each system is “tuned” through the adjustment of the various measurement parameters. Thus, the comparison between systems reflects trade-offs regarding measurement time and measurement accuracy chosen using the best judgment of the operator. With the signal levels allowed by the various sources, the noise reduction allowed by using a reasonable number of averages, the attenuation in the cables, the dynamic ranges of the systems, the bandwidth of the antennas, and the geometrical positioning of the samples, equally good time-domain results may be obtained using the two systems.

### **7.1.1 Time Domain Measurement System**

True time-domain measurements are made using a digital sampling oscilloscope (DSO), a pulse generator, and the MSU reflectivity arch range. Scattering targets are placed at the center of the arch range and are supported by a metallic pedestal that centers two foot by two foot material sheets at a height of 1.219 meters, which is the height of the horn antennas. This setup provides the most uniform incident field for the reflection measurements [18]. The time domain response is measured using a Hewlett Packard HP84750A digitizing oscilloscope with HP54753A TDR module. The TDR module is a plug-in which allows for time-domain reflectometry / time-domain transmission measurements through 18 GHz and 20 GHz input channels. The TDR unit uses an integrated step generator to send a 200 mV step with a 45 ps rise time from channel 3 of the DSO to the trigger input of a Picosecond Pulse Labs (PSPL) 4015B step generator. This trigger signal is shown in Figure 7.2. The PSPL 4015B step generator creates another step using a PSPL 4015RHP remote pulse head. This -9 volt step output with 15 ps fall time is sent into the PSPL 5208 pulse-generating network, creating 20 ps, approximately gaussian pulses, whose amplitudes are -3 volts, as shown in Figure 7.3. The spectrum of this pulse is obtained through a fast Fourier transform (FFT) and is shown in Figure 7.4. Significant spectral content is visible in the range 2-18 GHz.



The output pulse from the pulse-generating network is transmitted by an AEL H-1498 horn antenna mounted 35 cm behind a dielectric lens. This horn antenna is mounted for horizontal polarization. The receiving antenna is an identical horn antenna placed adjacent to the transmitting horn, also mounted for horizontal polarization and placed behind a dielectric lens, as shown in Figure 7.5. This setup is meant to approximate a mono-static arrangement; however, the antennas are separated by 70 cm at their apertures, corresponding to a bistatic angle of 11.5 degrees. The receiving antenna is connected to channel 4 of the DSO, where the voltage is sampled using 1024 sample points (which is the maximum number of samples allowed) in a typical 5-20 ns time window.

#### **7.1.1.1 Benefits of the time-domain system**

While both systems have many benefits, several important ones are discussed here for the time-domain measurement system.

*Data is collected directly in the time domain.* Since the temporal response of the material is desired, the time-domain system gives this directly. However, calibration must still be done in the frequency domain (see drawbacks in Section 7.1.1.2).

*Time gating of multipath signals is easily done to raw measurements.* Since the time domain data is directly available, no processing is required to remove undesired clutter not present in the background response (such as multipath reflections).

*Broadband data is obtained with a single measurement, which can be quite rapid.* By using a short-duration pulse, data over the entire equivalent band is produced from a single measurement. This measurement can be done quite quickly. However, to improve the SNR, many averages are usually taken, which increases the measurement time (see drawbacks in Section 7.1.1.2). Typical measurement time for the data presented here is 15-20 seconds.

*Receiver (oscilloscope) can be replaced with a high-quality digitizer (can be miniaturized).* Although a relatively expensive digitizing oscilloscope was used as the re-

ceiver in the laboratory experiments, this can be replaced with widely available high speed A/D converters and signal amplifiers. This would be useful in a portable version of the system. However, producing the required pulse might be difficult (see drawbacks in Section 7.1.1.2).

*Can measure the response of nonlinear materials.* The reflected-field response of nonlinear material samples is directly available in the time domain data.

#### **7.1.1.2 Drawbacks of the time-domain system**

As with every measurement system, the time-domain measurement system has its drawbacks. Several of these, which are important to the measurements of interest, are discussed here.

*Many averages or high pulse amplitude required for good SNR.* Unlike with the frequency domain system, the time domain system cannot make use of narrow filters to eliminate noise. Thus, the SNR is increased through the use of averaging. This increases the measurement time. The SNR can also be increased by reducing the distance between the antennas and the sample, and by using a pulse with a higher amplitude. The distance to the sample is set to provide approximately uniform illumination of the samples, and increased pulse amplitude requires the use of a high-power, linear, wideband amplifier.

*Calibration is done in the frequency domain.* Even though the data is collected in the time domain, calibration is performed in the frequency domain. Thus, the data must be transformed into the frequency domain, and the calibrated data must be windowed before transforming back into the time domain. Direct time-domain calibrations are possible, but these often prove difficult to implement.

*Narrow pulse width required to get equivalent wideband data.* A pulse of very short duration (about 10 ps) is required to get data in a band equivalent to that available from the network analyzer used in the frequency domain system (2-18 GHz). Producing a narrow pulse of sufficient amplitude is difficult, especially in a portable

system.

*Drifting of time reference can cause lowering of SNR.* An important tradeoff exists between the number of averages and the resulting drift in the time reference of the receiver. As the number of averages is increased, the SNR increases. However, as the measurement time increases, inaccuracies in the time reference due to thermal drifting increase. Thus, there is an optimal number of averages to use.

*Receiver is "wide open" and thus prone to interference from external sources.* The bandwidth of the input stage of the receiver is only limited by the response time of the electronics. Thus, any strong external CW signals will be passed through and measured by the receiver, appearing as "noise."

*The receiver has a low dynamic range.* The dynamic range (ratio of largest to smallest measurable signal) of the sampling oscilloscope is relatively low – roughly 40 dB. However, by setting the time window of the measurement appropriately, only the reflected signal must be measured. Thus the large direct coupling signal between the transmit and receive antennas can be omitted. This is not possible with the frequency- domain system, since the direct coupling is present at all frequencies, and thus a larger dynamic range is required with the frequency-domain system.

### **7.1.2 Frequency Domain Measurement System**

The frequency domain measurement system consists of a Hewlett Packard 8510C vector network analyzer (VNA) and the MSU reflectivity arch range. For reflection measurements, scattering targets are placed at the center of the arch range and supported by a metallic pedestal at a height of 1.219 meters; this places the center of the two foot by two foot target at the height of the horn antennas. This arrangement provides the most uniform incident field for measurement of the reflected field. [18] The frequency response is measured using the HP 8510C vector network analyzer with HP 8517B S-parameter test set, which has a bandwidth of 45 MHz to 50 GHz. Port 1 of the S-parameter test set is attached directly to the transmit antenna and

port 2 is connected to the receive antenna as shown in Figure 7.6; both transmit and receive antennas are AEL H-1498 horn antennas with 2 to 18 GHz bandwidths. The horn antennas are both mounted 35 cm behind dielectric lenses and configured for horizontal polarization. The arrangement of the transmit and receive horns is shown in Figure 7.5. This setup is meant to approximate a mono-static arrangement; however, the antennas are separated by 70 cm at their apertures, corresponding to a bistatic angle of 11.5 degrees.

#### **7.1.2.1 Benefits of the frequency-domain system**

While both systems have many benefits, several important ones are discussed here for the frequency-domain measurement system.

*VNA has a very stable signal source.* The synthesized signal source in the HP 8510C VNA is highly accurate (with 1 Hz resolution) and not prone to drifting. With a properly chosen dwell time, the frequency can be considered as stable.

*VNA has a large dynamic range.* The dynamic range (ratio of the largest to the smallest measurable signal) of the VNA is over 120 dB. This allows the small reflected signals to be separated from the large signals due to the direct-path coupling between the transmitting and receiving antennas.

*Calibration is done in the frequency domain.* The data is measured in the frequency domain, where the calibration takes place. However, the data must first be transformed into the time domain to gate out multipath reflections, which cannot be subtracted as background clutter (see drawbacks in Section 7.1.2.2).

*Receiver is phase locked and therefore not prone to external interference.* Since the received signal is phase-locked to the transmitted signal, interference from external signals at the same frequency is reduced.

### 7.1.2.2 Drawbacks of the frequency-domain system

As with every measurement system, the frequency-domain measurement system has its drawbacks. Several of these, which are important to the measurements of interest, are discussed here.

*Time-domain aliasing requires fine sample interval and large number of frequency points.* This is a very serious problem with the frequency-domain system. The frequency sample interval determines the span of the time-domain signal (through the FFT time/frequency relationship). This span must include all of the significant events in the time response. Problems occur when reflections from distant objects (walls, ceilings) or multipath signals are present in the data. If the frequency step size is not fine enough to provide a time span that will encompass these events, the events will wrap around and overlap with the desired sample response. Often these events cannot be subtracted as background clutter, because they originate as reflections from the target, and thus are not present in the background measurement. Experience shows that the sampling rate of the 8510C cannot be set high enough to accommodate the distant reflections within the laboratory unless absorbing material is used to eliminate the reflections altogether. Thus, a field unit might be prone to this difficulty.

*Long measurement times, especially with long dwell time.* VNA measurements can take a considerable amount of time to complete. As mentioned earlier, a tradeoff is used between measurement time and accuracy. For the measurements presented here, a typical time to acquire one measured waveform is 60-90 seconds.

*Averaging required to gain full benefit of dynamic range.* While the dynamic range of the 8510C is quite impressive, only signals above the noise level can be measured. Thus averaging is used to improve the SNR. This increases the measurement time.

*Must convert data into the time domain to do time gating.* Time gating is used to eliminate reflections not present in the background measurement and direct interactions between the antennas. The measured data must be converted into the time

domain via the FFT in order to do the time gating. This requires the application of a windowing function which is thus present in the final data.

*Equipment is very complicated and costly – difficult to miniaturize.* A good VNA is a very expensive item requiring significant maintenance. A portable system with the capabilities of a VNA would be hard to produce. The VNA can be replaced by a source and a receiver, but with reduced capabilities producing inferior measured results.

*Cannot measure the time response of nonlinear materials.* Data obtained from a frequency-stepped system cannot be used to determine the time response of a nonlinear material. That is, for a given radiated frequency, the nonlinear reflected-field response of the material is manifested through higher harmonics, which are not measured by the VNA.

### 7.1.3 Arch Range Calibration

In order to obtain the desired reflected-field response, the system response and the effects of the surrounding environment need to be removed through an appropriate calibration. The techniques described in [19]-[21] are employed. The system response is a function of the cables, antennas, antenna coupling, dielectric lenses, mutual interactions, and arch-range clutter. A block diagram of the measurement system is given in Figure 7.7. Examining this figure, the measured waveform of an unknown target is formulated as

$$R_T(f) = E(f)H_T(f)H_R(f)\{H_A(f) + H_{TL}(f)H_{RL}(f)[H_S^T(f) + H_{SC}^T(f) + H_C(f)]\} + N(f). \quad (7.1)$$

Here  $H_S^T(f)$  is the unknown response of the target and  $N(f)$  is the background noise present in the environment. Examining Equation (7.1) and Figure 7.7, the measured waveform is formulated beginning with the source pulse,  $E(f)$ . This pulse

arrives at the transmitting horn antenna, which has a transfer function of  $H_T(f)$ . Next, the field is radiated by the horn antenna and is either passed through a collimating lens, with a transfer function of  $H_{TL}(f)$ , or it directly couples to the receiving antenna, with this path represented by the transfer function  $H_A(f)$ . The portion of the field passing through the collimating lens is then either reflected by the target directly, which is the scattered response  $H_S^T(f)$ , or it is involved in interactions with objects in the laboratory environment. Interactions with the environment are either direct, which are referred to as arch-range clutter with transfer function  $H_C(f)$ , or they are mutual interactions between the target and the environment, represented by the transfer function  $H_{SC}^T(f)$ . With all three of these paths, the signal returns through another collimating lens, which has a transfer function of  $H_{RL}(f)$ . Finally, the signal passes through the receiving horn, with transfer function  $H_R(f)$ , and arrives at the receiver. The receiver will also pick up background noise, which is included through the term  $N(f)$ .

To obtain the desired target response, several measurements are required to eliminate undesired components of the response. The first of these measurements is used to eliminate the effects of the laboratory environment, and is carried out by taking a measurement with the material holder left empty. This background measurement includes the same responses as the measurement target, with the exception of the scattering and mutual interaction terms. Thus the background measurement is given as

$$R_b(f) = E(f)H_T(f)H_R(f)\{H_A(f) + H_{TL}(f)H_{RL}(f)H_C(f)\} + N(f). \quad (7.2)$$

By taking this background measurement immediately following other measurements, the error introduced by the background noise,  $N(f)$ , is minimized. By subtracting

the background response from the target response, the following result is obtained:

$$\begin{aligned} R_{T-b}(f) &= E(f)H_T(f)H_R(f)H_{TL}(f)H_{RL}(f)[H_S^T(f) + H_{SC}(f)] \\ &= S(f)[H_S^T(f) + H_{SC}^T(f)]. \end{aligned} \quad (7.3)$$

This result is in terms of a transfer function of the measurement system,  $S(f)$ , the desired target response  $H_S^T(f)$ , and a mutual interaction term,  $H_{SC}^T(f)$ , which represents interactions between the target and objects in the environment, such as the metal stand used to hold the material sheets. Thus the desired target response can be obtained if the system transfer function is known and the mutual interaction terms are assumed negligible. (In fact, these terms are often quite important and must be removed using time gating). To acquire the system transfer function, the response of a calibration target must be measured. The response of the calibration measurement with the background measurement removed is found to be

$$R_{C-b}(f) = S(f)[H_S^C(f) + H_{SC}^C(f)]. \quad (7.4)$$

Here  $H_S^C(f)$  is the theoretically known response of the calibration target. By assuming the mutual interaction between the calibration target and the surrounding environment,  $H_{SC}^C(f)$ , can be neglected or removed, the system response is obtained as

$$S(f) = \frac{R_{C-b}(f)}{H_S^C(f)}. \quad (7.5)$$

This system transfer function is used to obtain the unknown target response as

$$H_S^T(f) = \frac{R_{T-b}(f)}{S(f)}. \quad (7.6)$$

Calibration procedures using the developments of (7.1) through (7.6) are covered



in Sections 7.2.2 and 7.2.3 for the time-domain and frequency-domain measurement systems, respectively.

## **7.2 Experimental Procedures**

In this section, procedures involved with selection of experimental parameters are discussed, along with calibration procedures and examples for both the time domain and frequency domain measurement systems. Included in the calibration procedures are necessary measurements and weighting techniques needed to obtain the desired response from raw measured data, and to reproduce the results contained in Sections 7.3.1 through 7.3.3.

### **7.2.1 Determination of Experiment Parameters**

Before carrying out measurements of the material sheets, various experiment parameters needed to be determined. Many of these parameters were selected to either maximize the signal-to-noise ratio (SNR) or minimize the effect of mutual interactions on the measurements. Increasing SNR provides for more accurate results in arch range measurements, while minimizing the mutual interactions in the measurements allows the system response and the desired target response to be obtained using the calibration procedures outlined in Section 7.1.3 and detailed for the time-domain system in Section 7.2.2 and for the frequency-domain system in Section 7.2.3.

Other things that need to be considered in order to obtain meaningful, accurate results are the affect of the metal stand on measurements, in comparison to the Styro-foam stands used in many arch range studies, and the tradeoffs between measurement time and accuracy. Experimental parameters for both the time-domain system and the frequency-domain system are explored here.

### 7.2.1.1 Time Domain Measurement System

By maximizing signal-to-noise ratio, more accurate results can be obtained from the arch range measurements. In general, increasing the number of averages will increase the SNR [20]; however, when the background noise is high, the subtraction of the background noise measurement can worsen the results due to small time drifts in longer sampling processes. It has been found that 1024 averages provide a good SNR without an excessively long sampling process. [18]

In order to minimize the affect of mutual interactions on the measurement, absorbing foam and time-gating are used. Typical time-windows are 5-20 ns as mentioned earlier. Based on the duration of the target response, 10 ns windows were chosen for measurements taken with the time-domain measurement system. This allows the response of the material to the incident field to be measured, while the effect of mutual interactions between the material and surrounding objects is removed if they are sufficiently separated in time. It also allows the strong direct interaction between the horns, which is difficult to completely remove through subtraction, to be windowed out, since it occurs much earlier in time than the target response. Due to the proximity of the metallic pedestal used to support the scattering targets, further determination of its effect on the measured results is required. To accommodate this, measurements are taken using a 2 foot by 2 foot conducting plate atop both the metallic support structure and a Styrofoam pedestal. A comparison of these measurements is shown in Figure 7.8. For comparison purposes, measurements of several spherical targets were also taken on both metal and Styrofoam pedestals. The results for a 14 inch spherical calibration target are shown in Figure 7.9. It can be seen by comparing these figures that interactions between the spherical structures and the metallic pedestal are significant, while the interactions between the planar structures and the metallic pedestal are negligible. Since the materials used here are planar layers, and an aluminum plate is used for calibration purposes, the effect of the metallic support

pedestal is found to be negligible.

### **7.2.1.2 Frequency Domain Measurement System**

In order to maximize signal-to-noise ratio in the frequency domain system, several measures were taken. First, the source amplitude was set at 15dBm, which is what was determined to be a safe level, just short of the maximum rating of the S-parameter test set, which is 17dBm. In addition to increasing the signal strength, averaging was used. In general, increasing the number of averages will increase the SNR [20]; however, when the background noise is high, the subtraction of the background noise measurement can worsen the results due to small time drifts in longer sampling processes. [18] To determine the number of averages to use, measurements were taken using 2, 4, 8, 16, 32, 64, 128, 256, and 512 averages, all for 201 sample points. Results are summarized in Table 7.1 and Table 7.2. Table 7.1 uses the measurements taken using 256 averages as the baseline measurements for comparison to the other cases. This table shows that increasing the number of averages decreases the difference between the cases, as expected. Table 7.2 uses the measurements taken using 512 averages as the baseline measurements for comparison to other cases. Examining this table, it is seen that increasing the number of averages does not decrease the difference between the cases. This is because the small time drifts encountered in the longer measurement process cause the background subtraction to worsen. For this reason, a maximum of 256 averages are chosen for measurements using 201 sample points.

Another parameter which determines the amount of time that a given measurement takes is the dwell time. This quantity is the amount of time that the network analyzer waits before taking measurements, after the source has settled at a point in the frequency list. To determine a minimum dwell time for the arch range measurements, dwell times ranging from 1 to 25 milliseconds were tested. All measurements were taken using 201 points over the 2 to 18 GHz band with averaging turned off.

It was found that measurements for dwell times between 10ms and 25ms showed no differences across the band, while measurements for shorter dwell times differed for the lowest frequencies in the band.

As with the time domain system, the affect of the metallic support pedestal was found to be negligible.

### **7.2.2 Calibration of the Time Domain System**

Measurements made using the time domain system were calibrated using an aluminum plate. To illustrate this calibration procedure, the measurement of a 25 millimeter thick garolite sheet backed by a conductor is considered. Examining the calibration procedure outlined in Section 7.1.3, three measurements are required for this calibration: measurement of the material, shown in Figure 7.10, a background measurement, given in Figure 7.11, and a calibrator measurement. The calibrator used for this work was a conducting plate of the same size as the samples, whose measured response is shown in Figure 7.12.

To obtain the system transfer function (7.5) is used. The background measurement is subtracted from the measured response of the conducting plate and is time windowed to exclude multi-path interactions, which are not considered in the theoretical response. This response, which is shown in Figure 7.13, is then fast-Fourier transformed. Upon dividing by the theoretical reflection coefficient of the calibrator plate, which is negative unity, the system transfer function is obtained. This transfer function, also called the system response, is shown in Figure 7.14.

Subtracting the background measurement, applying a time window, and fast-Fourier transforming the material measurement gives the result shown in Figure 7.15. This response is divided by the system response found previously according to (7.6) to give the calibrated response of the material measurement in the frequency domain, as shown in Figure 7.16. The data is then truncated to include only the band from 2 to 18 GHz, since the rest of the data is outside of the bandwidth of the horn antennas,

and is thus not meaningful.

To obtain the time-domain response, a windowing function is applied to smooth the roll off of the data around 2 and 18 GHz; this is used to avoid excessive oscillation in the time domain response due to an abrupt truncation of the bandwidth, analogous to weighting with a rectangular window. A cosine-taper window is chosen because it retains more of the energy in the waveform under transformation than does a Gaussian window centered at 10 GHz, allowing more of the response to be seen.[19] Applying the cosine-taper window gives the response in Figure 7.17, and fast-Fourier transforming gives the calibrated material response in the time domain. Figure 7.18 shows the calibrated material response compared to simulation results obtained using the wave matrix method with  $\epsilon_r = 4.75$ , which are fast Fourier transformed using the same windowing function. It can be seen here that the measured result matches well with the theoretical response.

### 7.2.3 Calibration of the Frequency Domain System

The frequency-domain measurement system is calibrated using a two-level approach. This involves a full two-port calibration of the network analyzer and a calibration using a conducting plate.

The primary calibration for the frequency domain system is a full two-port calibration which uses the HP85056A 2.4 mm calibration kit. This kit is used to calibrate to the end of the 2.4 mm cables which connect directly to the S-parameter test set. The full two-port calibration is carried out through three types of measurements: reflection, transmission, and isolation. Reflection measurements are taken using short circuit, open circuit, and broadband matched-terminated standards on both ports 1 and 2. After reflection measurements are completed, transmission measurements are taken. This involves four measurements with the cables connected directly to one another. Next, isolation measurements are taken if desired. For this work, isolation measurements were omitted from the calibration. From this point on, a correction

is automatically applied to the measured data on the network analyzer, which calibrates out the affects of everything between the sources and the plane of the 2.4mm connectors.

Further calibration of the system is carried out using a conducting plate. This calibration requires that three measurements be taken: a material measurement, a background measurement, and a calibrator measurement. The calibrator measurement is made using a conducting plate, whose theoretical reflection coefficient is negative unity. To obtain the system response, the background measurement is subtracted from the calibrator response using either a math function in the network analyzer or a computer program and a division by the theoretical reflection coefficient. The result is shown in Figure 7.19. Comparing this to the system response found using the time-domain system, Figure 7.20 shows that the results are nearly the similar, except for the strong oscillations on the data from the frequency-domain system. This oscillation occurs because time gating has not been applied to this measurement as this was done to the sample measurements, rather than the system response. Next, the background measurement is subtracted from the material measurement. The result is then divided by the system response found previously to give the calibrated response of the material measurement in the frequency domain, as shown in Figure 7.21. The data is then truncated to include only the band from 2 to 18 GHz, since the rest of the data is outside of the bandwidth of the horn antennas.

To obtain the time domain response, a cosine-taper window is applied to smooth the roll off of the data around 2 and 18 GHz. Applying this windowing function gives the response in Figure 7.22, and fast-Fourier transforming gives the calibrated material response in the time domain. Figure 7.23 shows the calibrated material response compared to simulation results obtained using the wave matrix method, which is fast-Fourier transformed using the same windowing function. It can be seen here that the measured result matches up well with the theoretical response.

### 7.3 Measurement Results

Measurements for cast acrylic, polyvinyl chloride (PVC), and garolite material sheets are considered here. Each of these samples is square, two feet by two feet on a side, and one inch thick. Only the PVC has a dielectric constant specified by the manufacturer:  $\epsilon_r = 3.19$ . The dielectric constant of cast acrylic is estimated from published data to be around  $\epsilon_r = 2.5$ . The dielectric constant of garolite is assumed to be close to bakelite at  $\epsilon_r = 4.75$ .

The results of measurements taken with the time-domain and frequency-domain systems are presented in Sections 7.3.1 and 7.3.2, respectively. Each material was measured with both an air backing and a conductor (PEC) backing (using an aluminum sheet). In addition to single layer measurements, various two layer measurements were also taken with both air and PEC backing. All results are calibrated using a conducting plate, as discussed in 7.2.2 and 7.2.3, and are weighted using cosine-taper windows. Measurements are compared to simulation results found using the inverse fast-Fourier transform of the reflection coefficient obtained via the wave matrix method. In all of these theoretical responses the materials are assumed to be perfect, lossless, nonmagnetic dielectrics, with permittivities that are independent of frequency.

#### 7.3.1 Time Domain System Measurements

Measurements were taken using the time-domain system, with 1024 samples, 1024 averages, and a 10ns time window. All materials measured were two feet by two feet and approximately one inch thick. Both air-backed and conductor-backed measurements were taken with material sheets supported by a metallic pedestal.

The calibrated, time-domain measured response for an acrylic sheet backed by a conductor is shown in Figure 7.24. Figure 7.24(a) is the temporal response, which matches well with the theoretical response found using the wave matrix method.

Figure 7.24(b) is the frequency-domain response, which also matches relatively well with the theoretical response. There are some differences that show up more in the frequency-domain response than in the time-domain response. These differences are due both to variations in the thickness of the acrylic sheet, and to loss in the materials that are not accounted for in the simulations. Figure 7.25 shows the response of the air-backed acrylic sheet. It can again be seen that the time domain response matches very well with theory, while some differences show up in the frequency-domain response. Figure 7.26 and Figure 7.27 are responses for conductor and air backed garolite, respectively. In both of these cases, there is good agreement with theory for the time-domain response, however, the material shows some loss, causing deviations from the theoretical response which was assumed lossless. The frequency-domain response matches reasonably well, but again there is some loss and some variation in the thickness of the garolite sheet. Figure 7.28 and Figure 7.29 are the conductor and air backed responses for measurement of polyvinyl chloride (PVC).

Two layer measurements were also taken using the time-domain measurement system. These include a garolite-acrylic stack, with the response for the conductor-backed material stack shown in Figure 7.30, and the response for the air backed material stack in Figure 7.31. Figure 7.32 is the response for an air-backed acrylic-garolite material stack. All of these measurements agree well with theory for the time domain response, while the frequency domain responses deviate from theory as discussed above for the single layer cases.

### **7.3.2 Frequency Domain System Measurements**

Measurements were taken with the frequency domain system using 201 sample points across the frequency band from 2 to 18 GHz, 32 averages, and a dwell time of 10 ms. All materials measured were two feet by two feet and approximately one inch thick. Both air-backed and conductor-backed measurements were taken with material sheets supported by a metallic pedestal.



The calibrated, frequency domain measured response for the conductor backed and air backed acrylic sheet are shown in Figure 7.33 and Figure 7.34, respectively. Figure 7.35 and Figure 7.36 are the measured responses for the conductor backed and air backed garolite sheet. Measurements of the polyvinyl chloride (PVC) sheet are shown in Figure 7.37 and Figure 7.38 for the conductor-backed and air-backed cases. The time-domain responses shown in these figures match up very well with the theoretical responses found using the wave matrix method. The only difference found in these responses is in Figure 7.35, where there is evidently loss in the material, since the measured signal dies off faster than the theoretical response, in which the material was assumed lossless. The frequency-domain responses shown in these figures also match up well, with deviations from the theoretical response again occurring due to loss in the materials and variations in the thickness of the material sheets.

Two-layer measurements were also taken using the frequency-domain system. The response for a conductor backed garolite-acrylic material stack is shown in Figure 7.39. Figure 7.40 shows the response for a conductor backed PVC-garolite material stack. The time domain responses shown in both of these figures match up well with the theoretical responses found using the wave matrix method. The only deviations from the simulated results occur because of loss in the material, which can be seen in the later portion of the time-domain results. The frequency-domain responses also match well.

### **7.3.3 Comparison of Results from the Time-Domain and Frequency-Domain Systems**

In comparing time-domain measured data to frequency-domain measured data, very good agreement is seen between the measured time-domain response results in all cases. Measurements of an acrylic sheet with conductor and air backing are shown in Figure 7.41 and Figure 7.42, respectively. Figure 7.43 and Figure 7.44 show conductor-backed and air-backed garolite measurements, comparing the time domain measure-

ments to the frequency domain measurements. Measurements of polyvinyl chloride (PVC) are compared in Figure 7.45 and Figure 7.46 for conductor-backed and air-backed cases. The comparison of a two layer material stack is shown in Figure 7.47, for a conductor-backed garolite-acrylic stack. Although the time-domain responses found using both systems are nearly identical, there are some differences in the magnitudes of the frequency domain responses. The “noise” in the magnitude of the frequency-domain responses measured by the frequency-domain system is due both to less averages being used with the frequency-domain system, and the fact that time gating of later multipath signals was not done for the system response; because of this, time-aliasing can occur and creates oscillations in the measured results. The time-domain responses agree quite well because the phases of the frequency-domain responses (which are not shown, to save space) agree well.

Averages	Frequency					
<i>Amplitude</i>	2 MHz	8 MHz	12 MHz	16 MHz	18 MHz	Average
1	0.085	1.296	0.999	1.810	1.499	0.814
2	-0.253	1.206	0.750	1.905	1.941	0.770
4	0.296	1.100	0.586	1.485	2.042	0.627
8	-0.500	1.078	0.681	1.655	1.902	0.600
16	-0.163	0.986	0.665	1.555	2.009	0.567
32	-0.648	0.977	0.622	1.531	2.047	0.516
64	0.133	0.971	0.512	1.386	1.672	0.451
128	-0.224	0.816	0.377	1.275	1.189	0.341
256	0.000	0.000	0.000	0.000	0.000	0.000
512	-0.116	1.550	1.882	2.344	2.804	1.326
<i>Phase</i>	2 MHz	8 MHz	12 MHz	16 MHz	18 MHz	Average
1	0.355	-1.540	-0.656	-0.730	-0.440	0.145
2	0.039	-1.388	-0.623	-0.684	-0.566	0.028
4	0.584	-1.303	-0.491	-0.487	-0.570	0.000
8	0.152	-1.204	-0.417	-0.482	-0.351	0.034
16	0.697	-1.188	-0.411	-0.470	-0.354	-0.005
32	0.147	-1.205	-0.403	-0.435	-0.272	0.000
64	0.131	-1.097	-0.372	-0.413	-0.316	-0.084
128	0.240	-0.993	-0.257	-0.186	-0.239	-0.129
256	0.000	0.000	0.000	0.000	0.000	0.000
512	0.376	-0.843	-0.170	0.369	0.166	0.026

Table 7.1. Percent difference between measurement with given number of averages, and measurement with 256 averages

Averages	Frequency					
<i>Amplitude</i>	2 MHz	8 MHz	12 MHz	16 MHz	18 MHz	Average
1	0.201	-0.251	-0.867	-0.522	-1.269	-0.503
2	-0.137	-0.339	-1.110	-0.429	-0.839	-0.546
4	0.413	-0.443	-1.271	-0.840	-0.741	-0.687
8	-0.384	-0.465	-1.178	-0.674	-0.877	-0.714
16	-0.047	-0.556	-1.194	-0.772	-0.773	-0.746
32	-0.533	-0.564	-1.236	-0.795	-0.736	-0.796
64	0.249	-0.571	-1.344	-0.937	-1.101	-0.860
128	-0.108	-0.723	-1.477	-1.045	-1.570	-0.968
256	0.116	-1.527	-1.847	-2.291	-2.727	-1.300
512	0.000	0.000	0.000	0.000	0.000	0.000
<i>Phase</i>	2 MHz	8 MHz	12 MHz	16 MHz	18 MHz	Average
1	-0.020	-0.703	-0.486	-1.095	-0.605	0.134
2	-0.335	-0.549	-0.453	-1.049	-0.730	0.019
4	0.207	-0.464	-0.321	-0.853	-0.735	-0.012
8	-0.222	-0.364	-0.247	-0.848	-0.516	0.021
16	0.321	-0.348	-0.241	-0.835	-0.519	-0.018
32	-0.227	-0.364	-0.233	-0.801	-0.437	-0.012
64	-0.244	-0.256	-0.202	-0.779	-0.481	-0.096
128	-0.135	-0.151	-0.087	-0.553	-0.404	-0.141
256	-0.374	0.851	0.171	-0.367	-0.166	-0.012
512	0.000	0.000	0.000	0.000	0.000	0.000

Table 7.2. Percent difference between measurement with given number of averages, and measurement with 512 averages

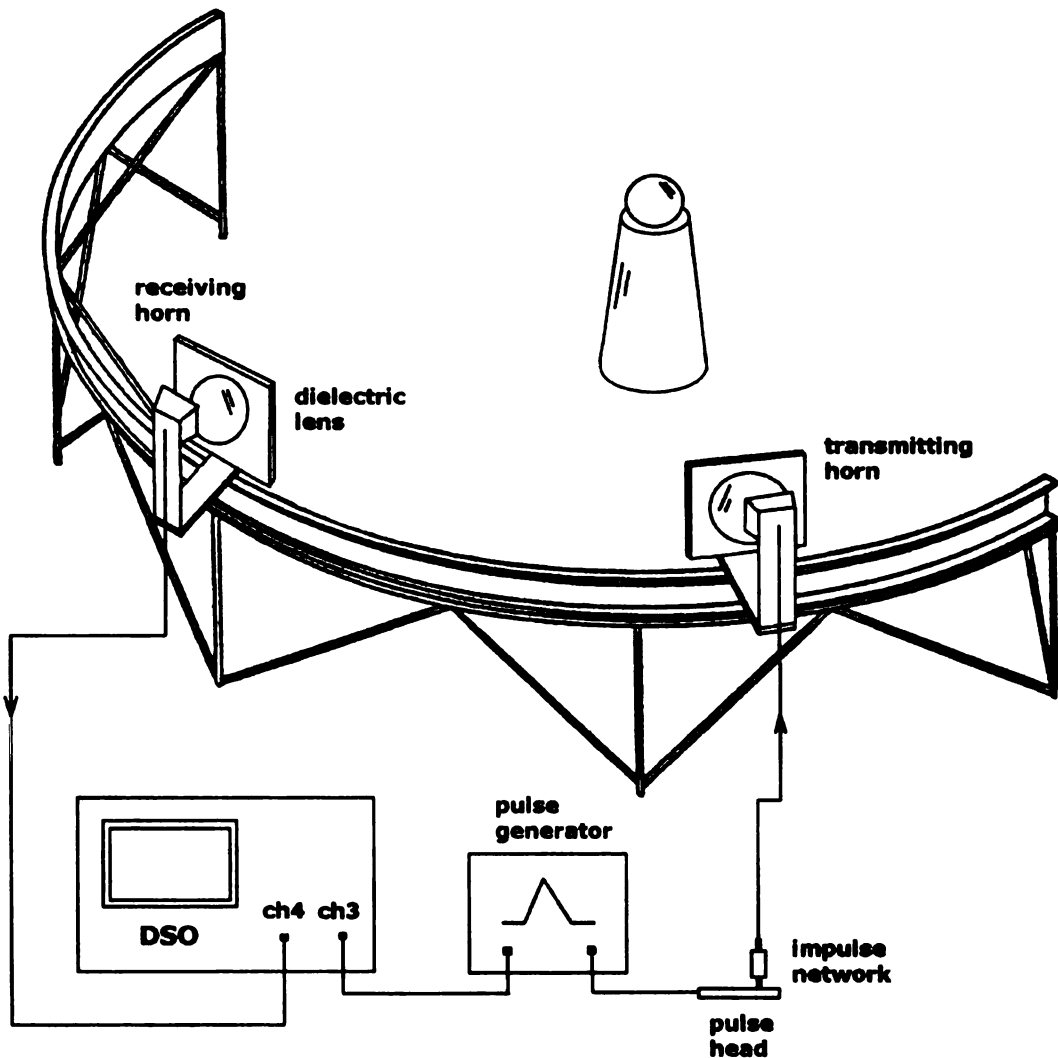


Figure 7.1. Arch range setup for the time-domain measurement system

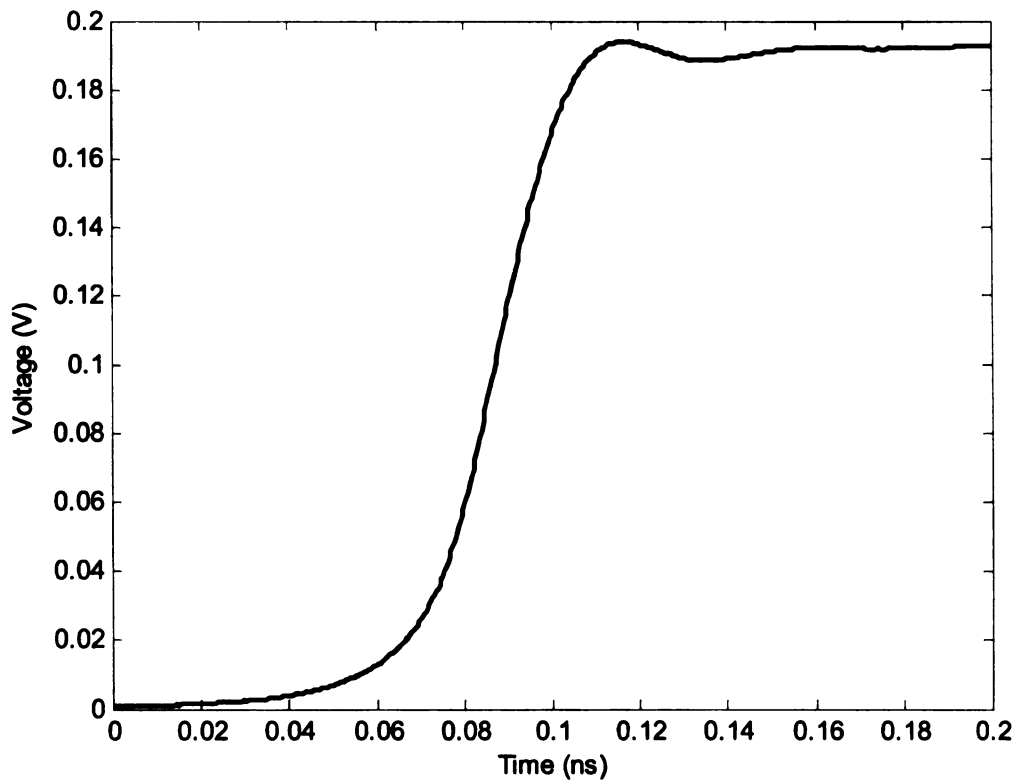


Figure 7.2. Step output from channel 3 of the HP54750A used as trigger for the PSPL 4015B step generator

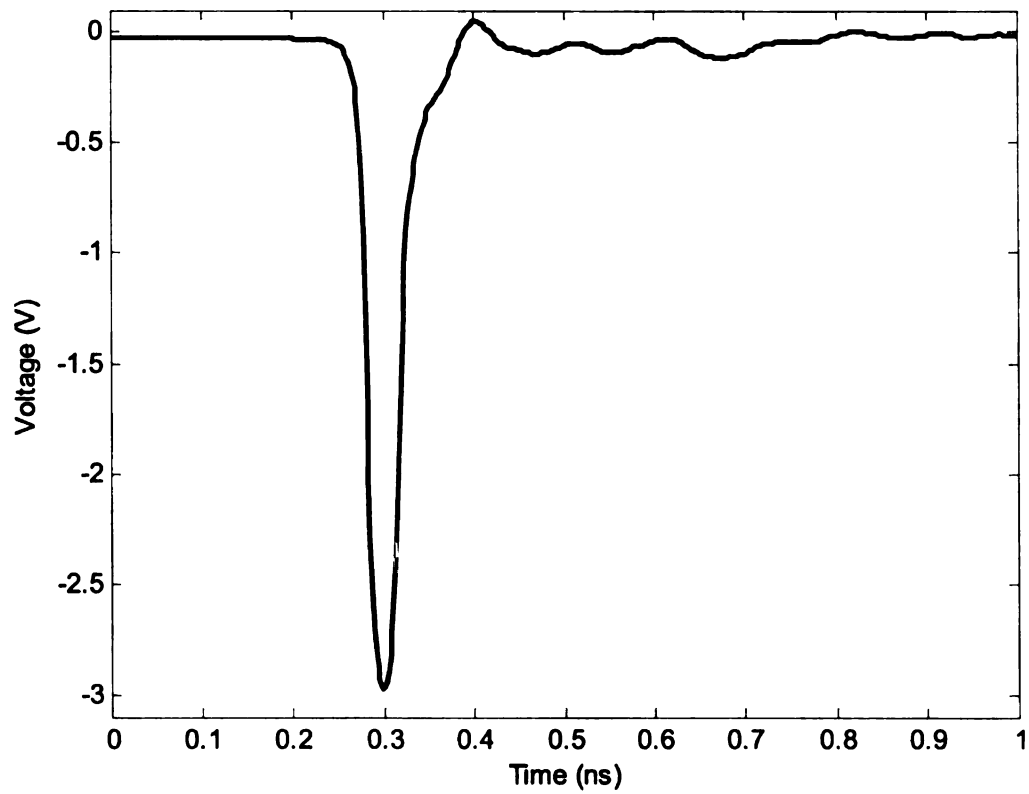


Figure 7.3. Transmitted pulse created by the PSPL 5208 pulse-generating network

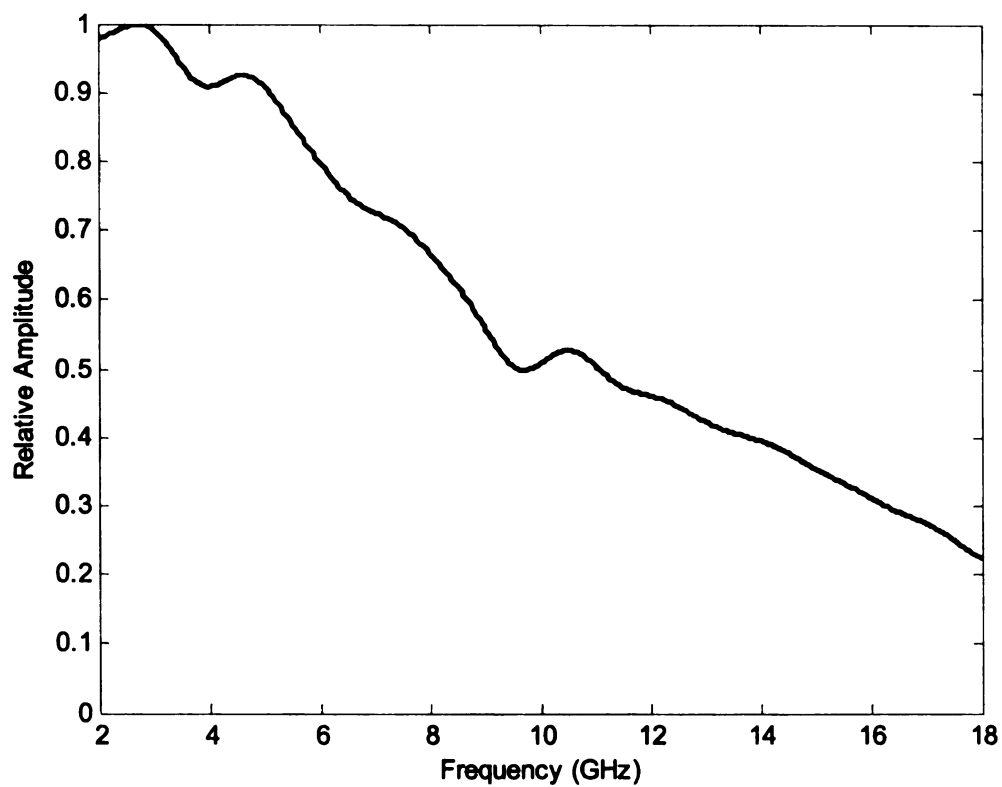


Figure 7.4. Spectrum of transmitted pulse created by the PSPL 5208 pulse-generating network



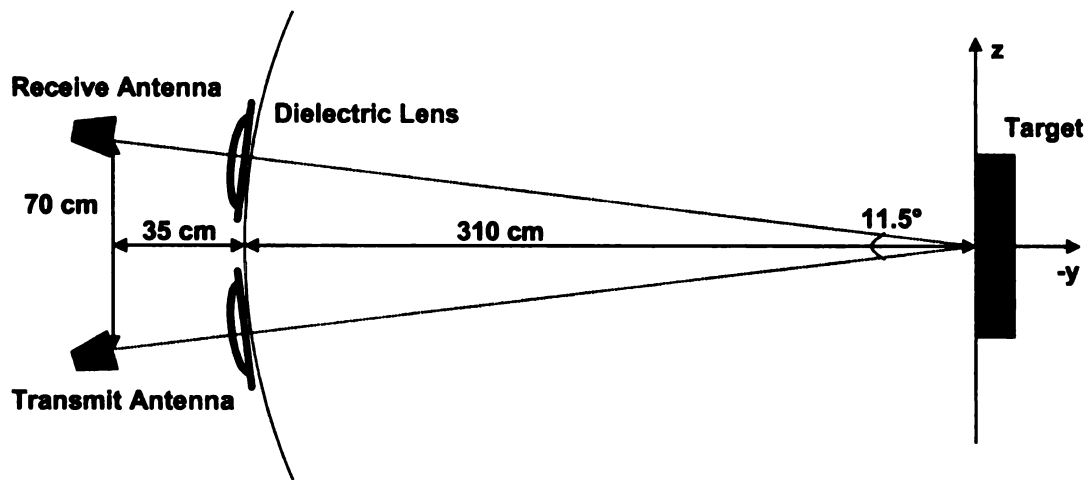


Figure 7.5. Top view of arch range setup

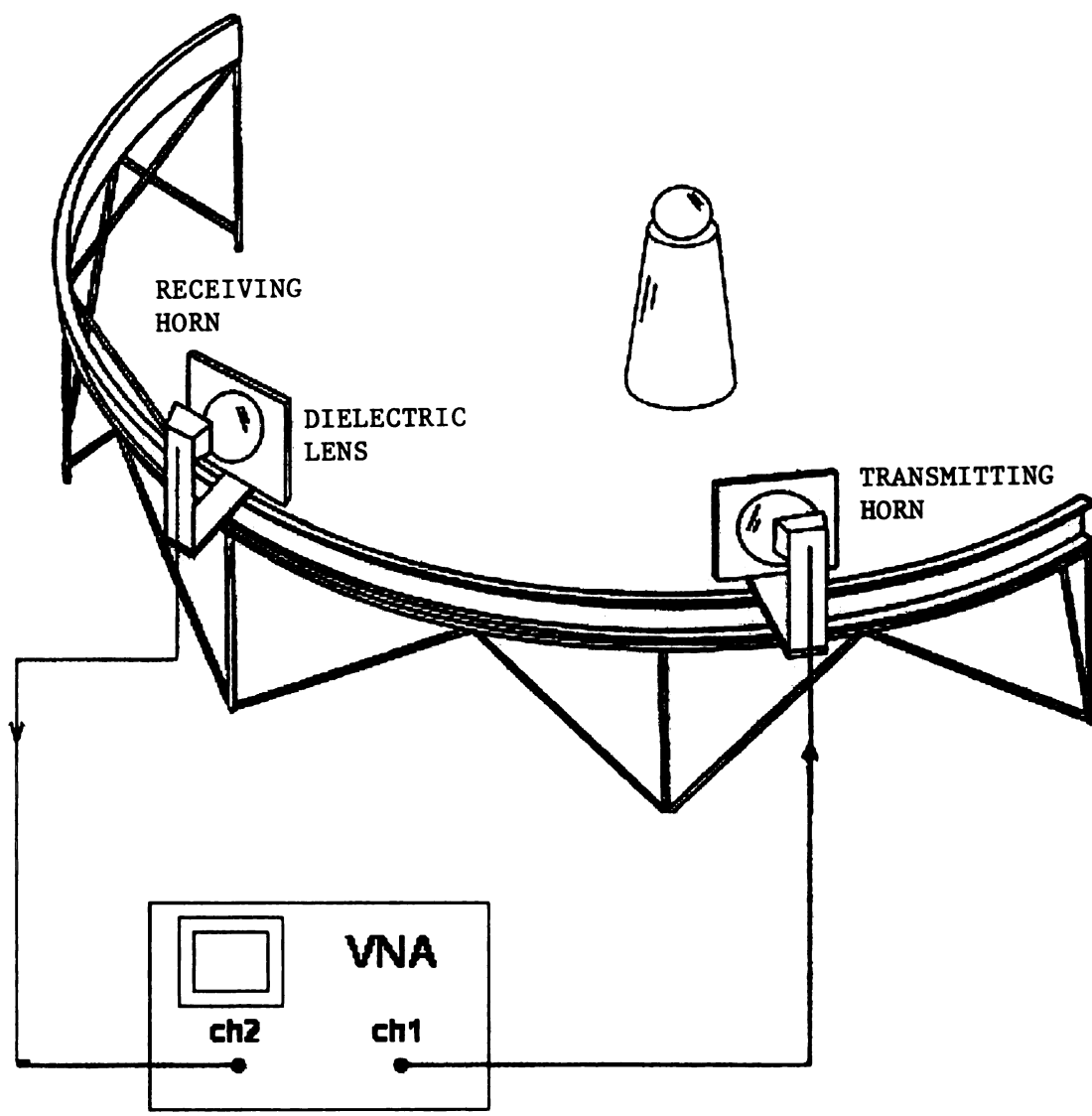


Figure 7.6. Arch range setup for the frequency-domain measurement system

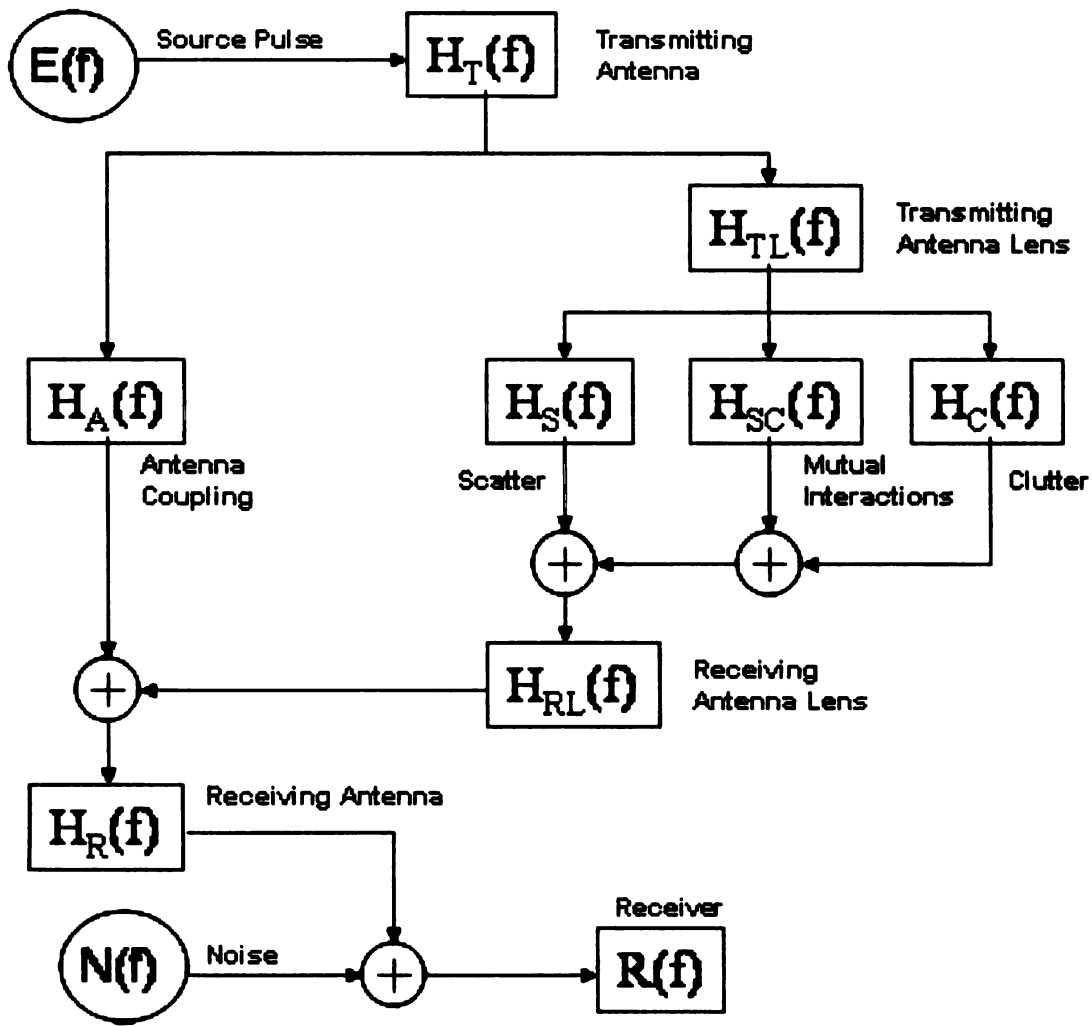


Figure 7.7. Block diagram of the measurement system

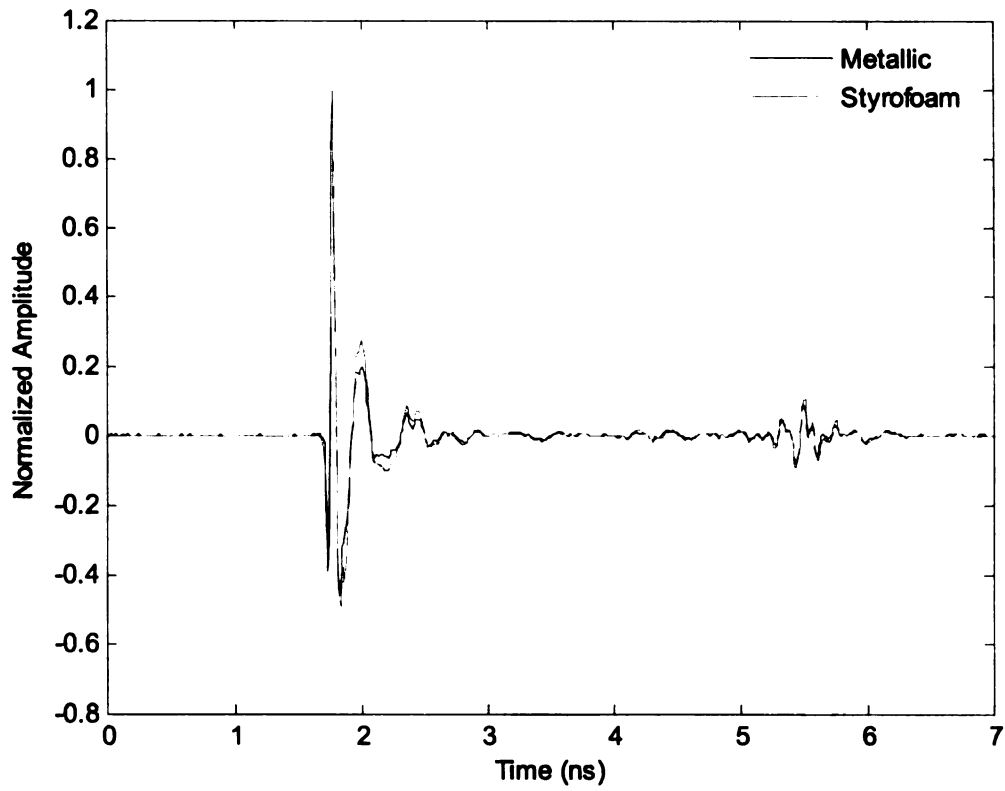


Figure 7.8. Comparison of raw measured data for a conducting plate measured with a metallic pedestal and a styrofoam pedestal

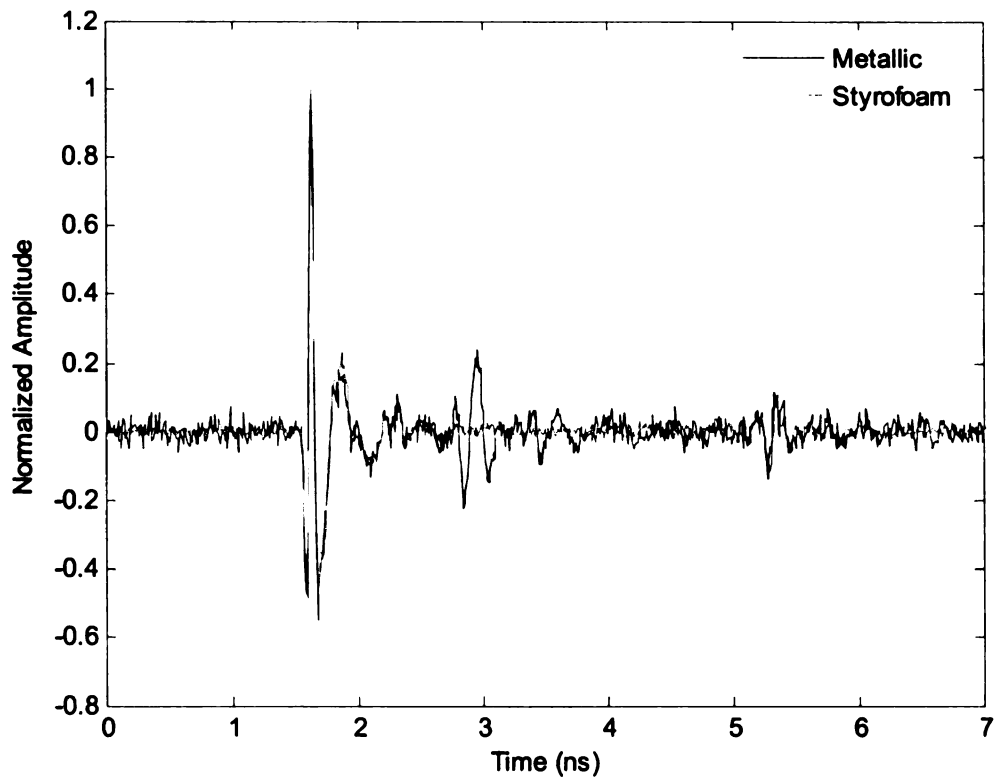


Figure 7.9. Comparison of raw measured data for a 14 inch sphere measured with a metallic pedestal and a styrofoam pedestal

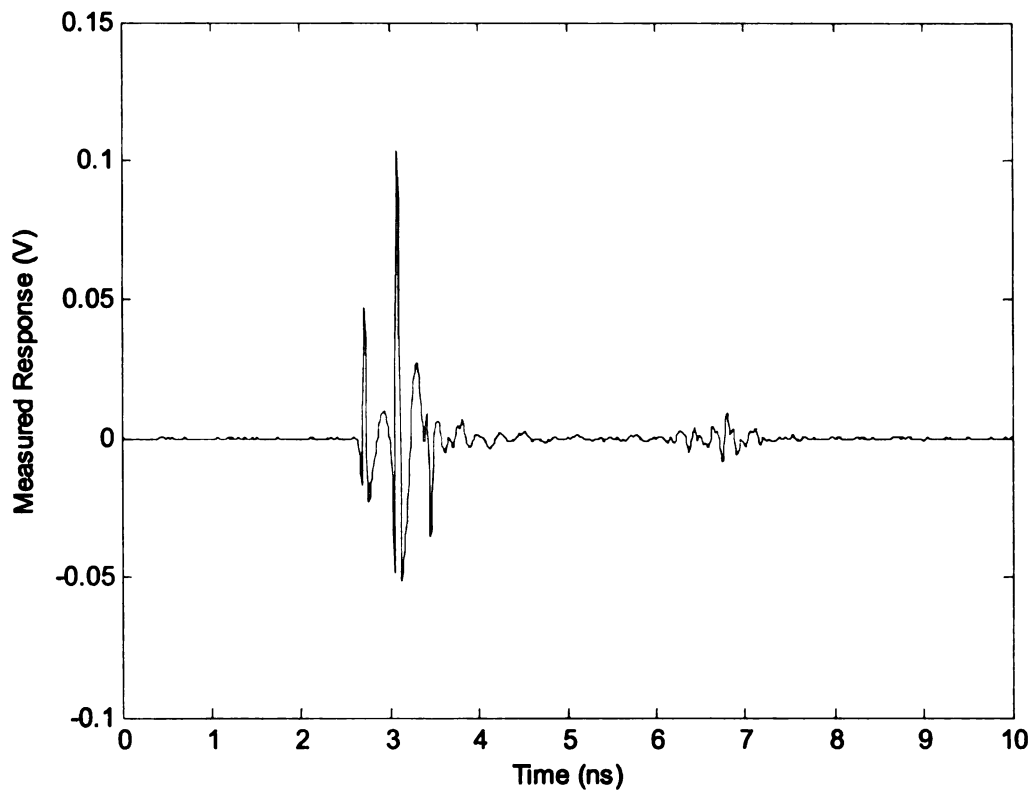


Figure 7.10. Raw measurement for a conductor-backed garolite sheet

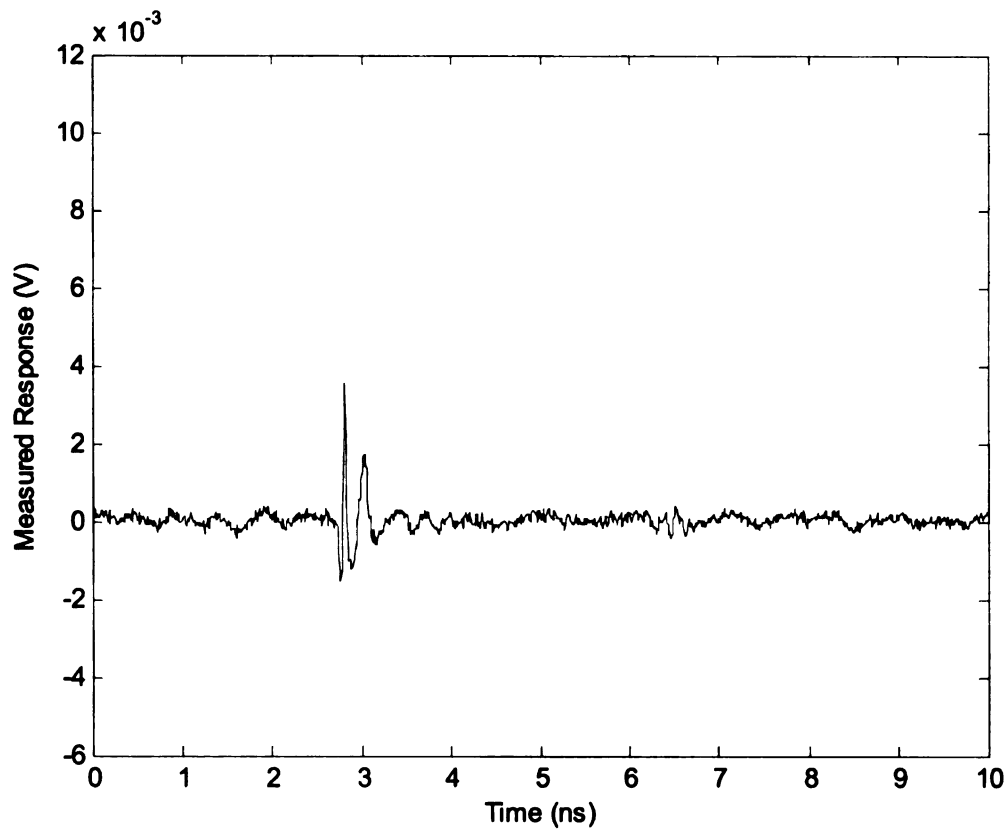


Figure 7.11. A typical background measurement for the time-domain measurement system (Note the change in scale)

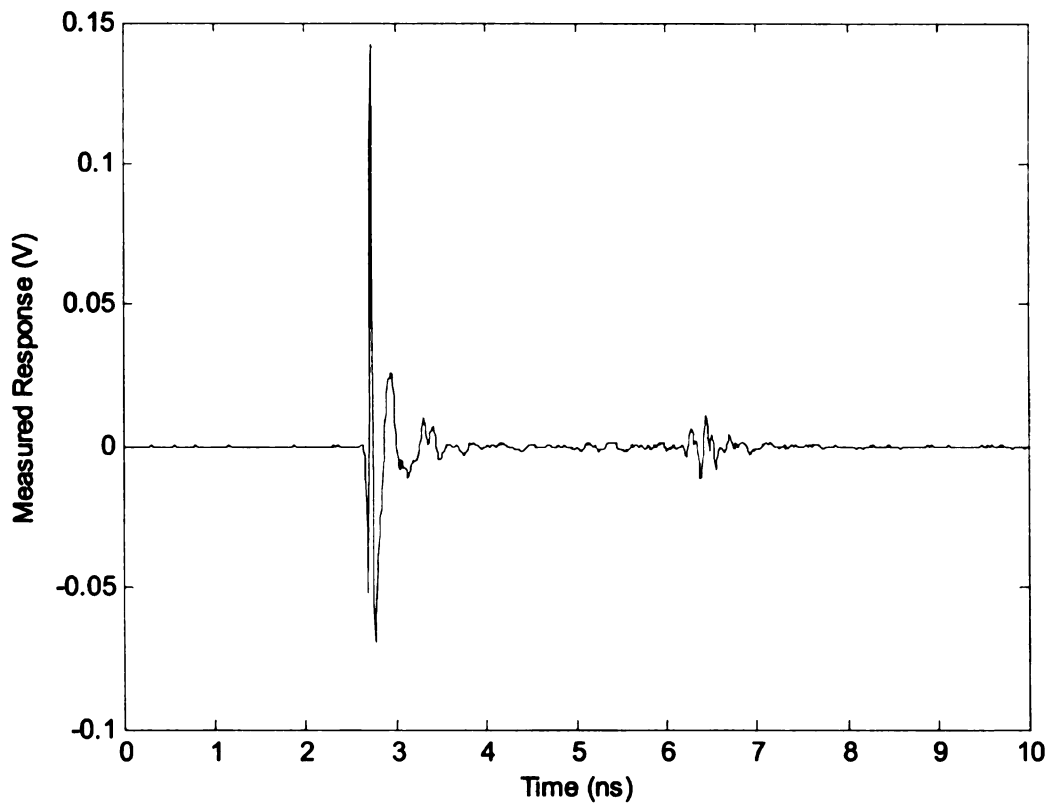


Figure 7.12. Raw conducting-plate calibration measurement



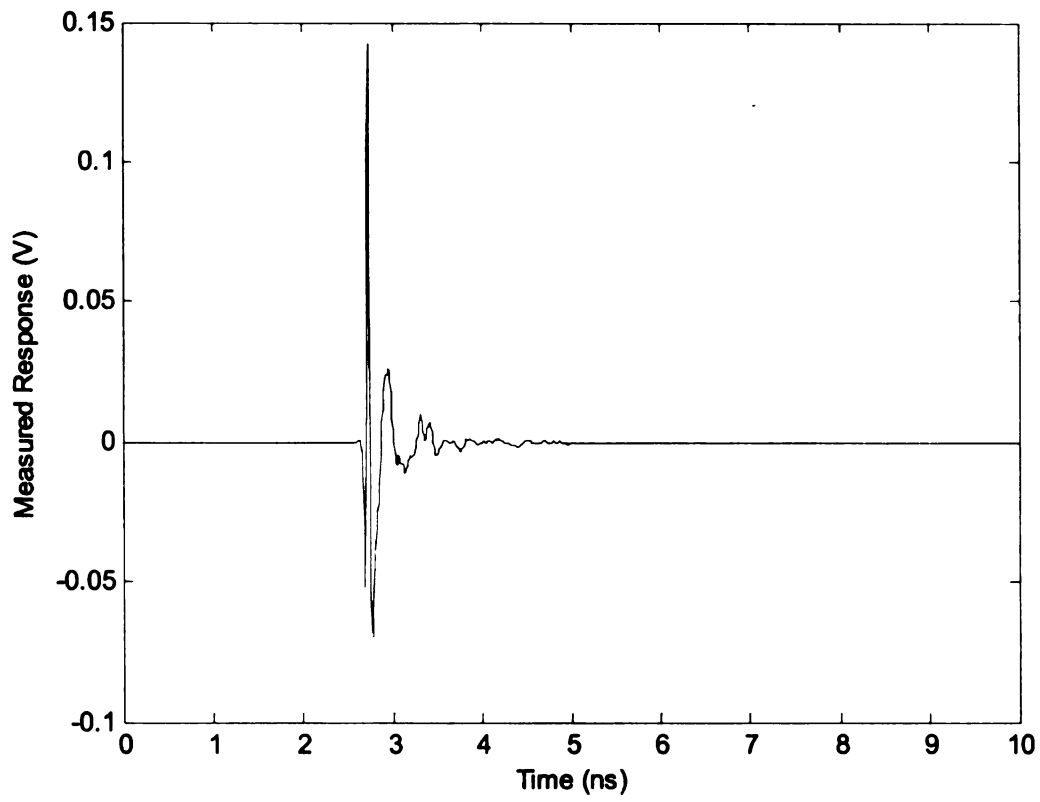


Figure 7.13. Time-gated conducting-plate calibrator measurement

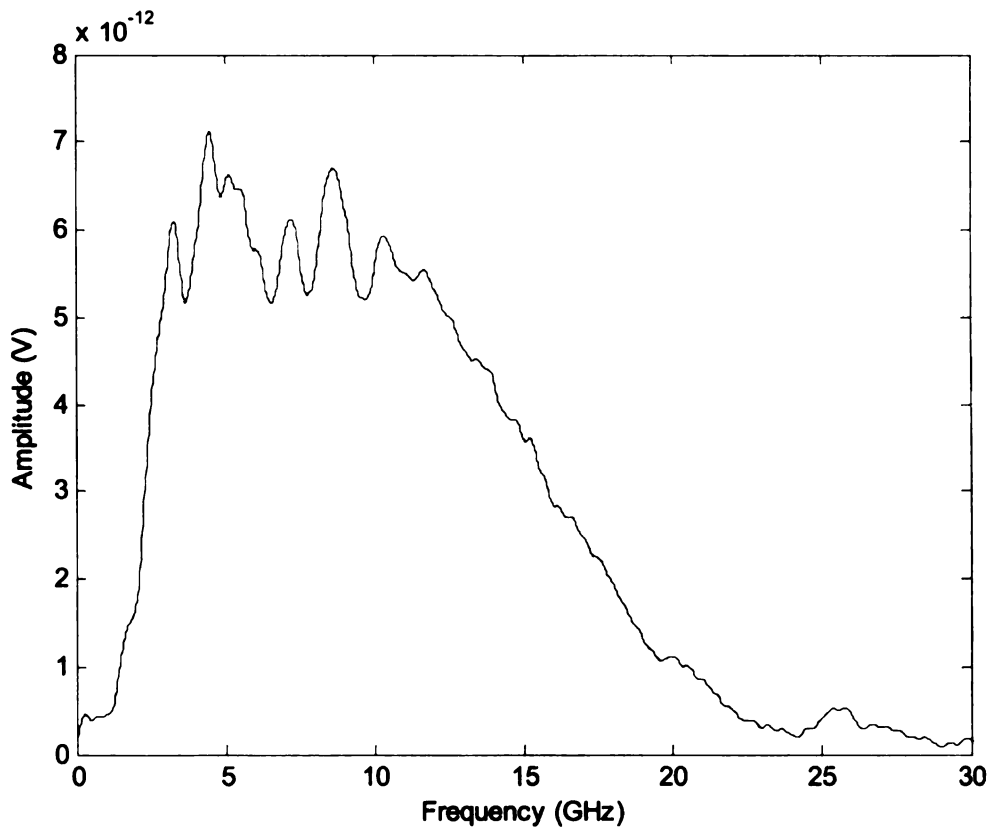


Figure 7.14. System response for the time-domain measurement system

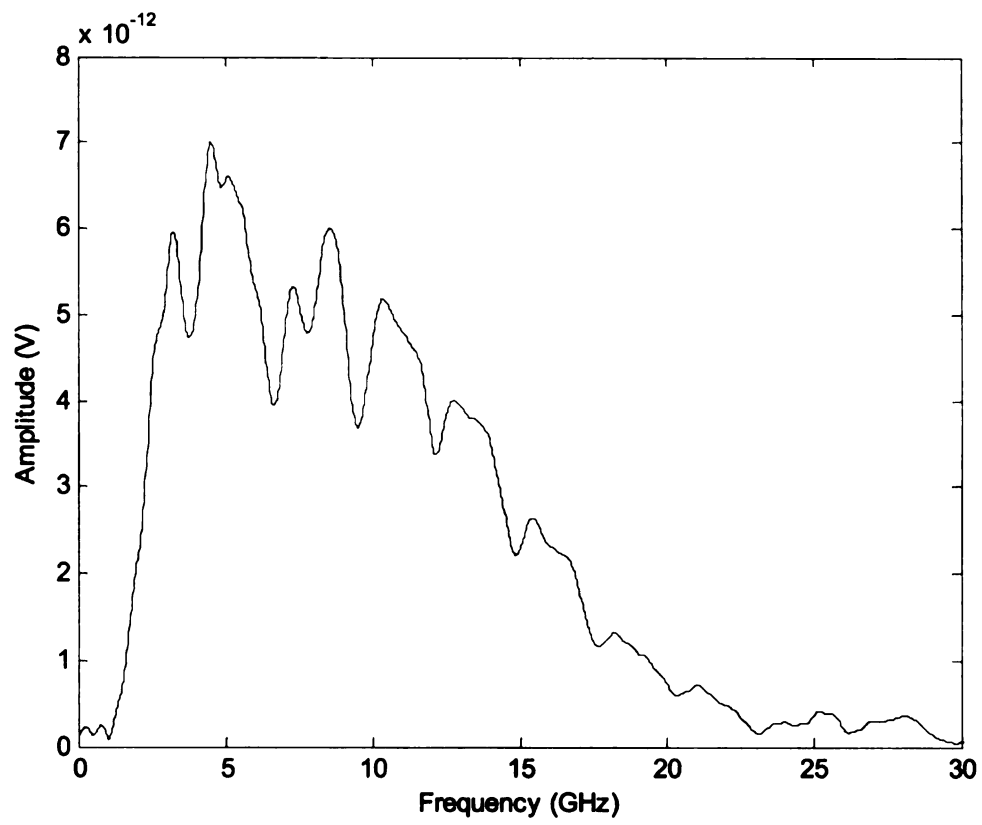


Figure 7.15. Time-gated, Fourier transformed PEC-backed material measurement

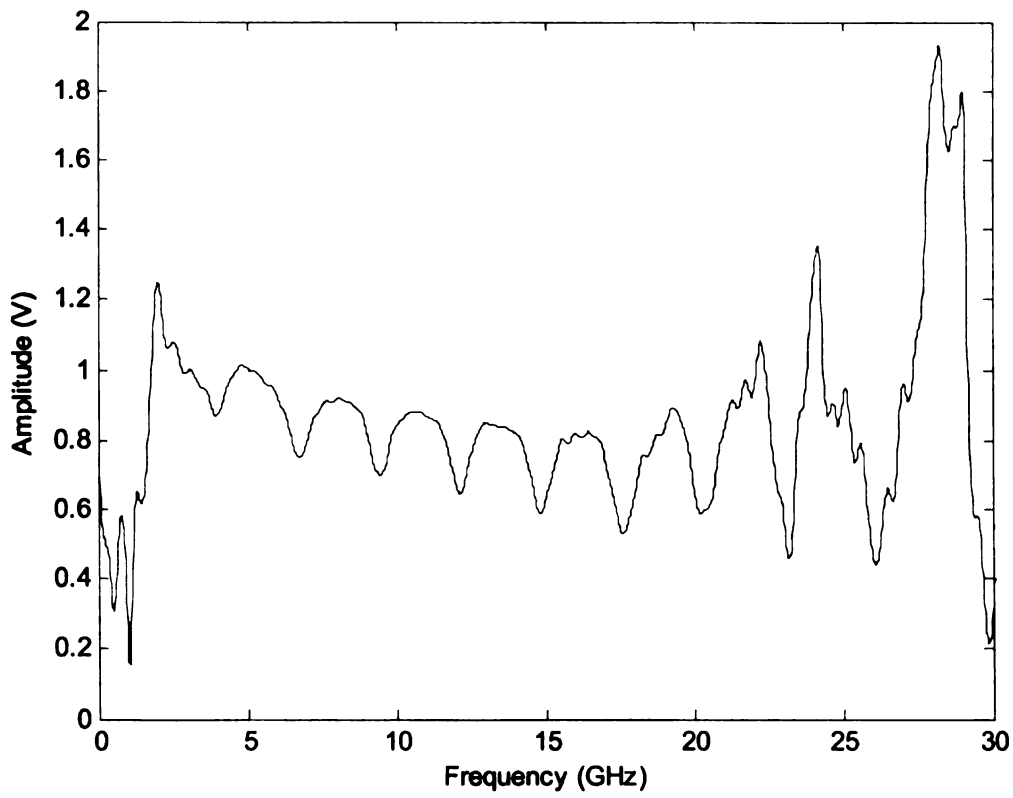


Figure 7.16. Measured PEC-backed garolite data after division by system response

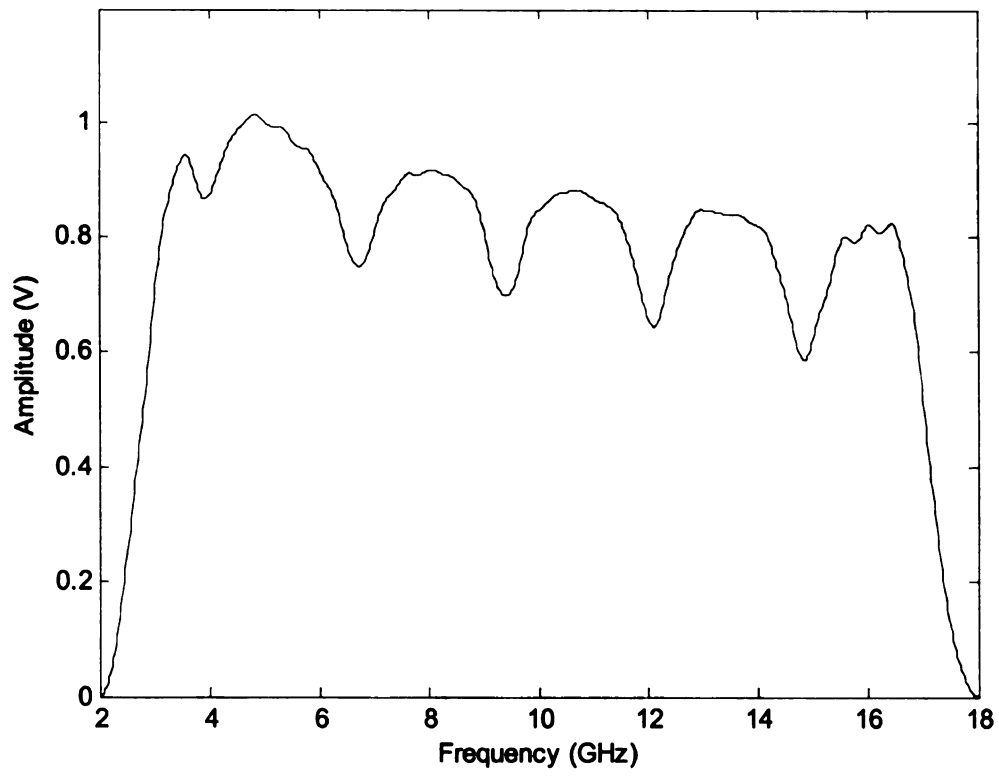


Figure 7.17. Spectrum of PEC-backed garolite sheet weighted by a cosine taper

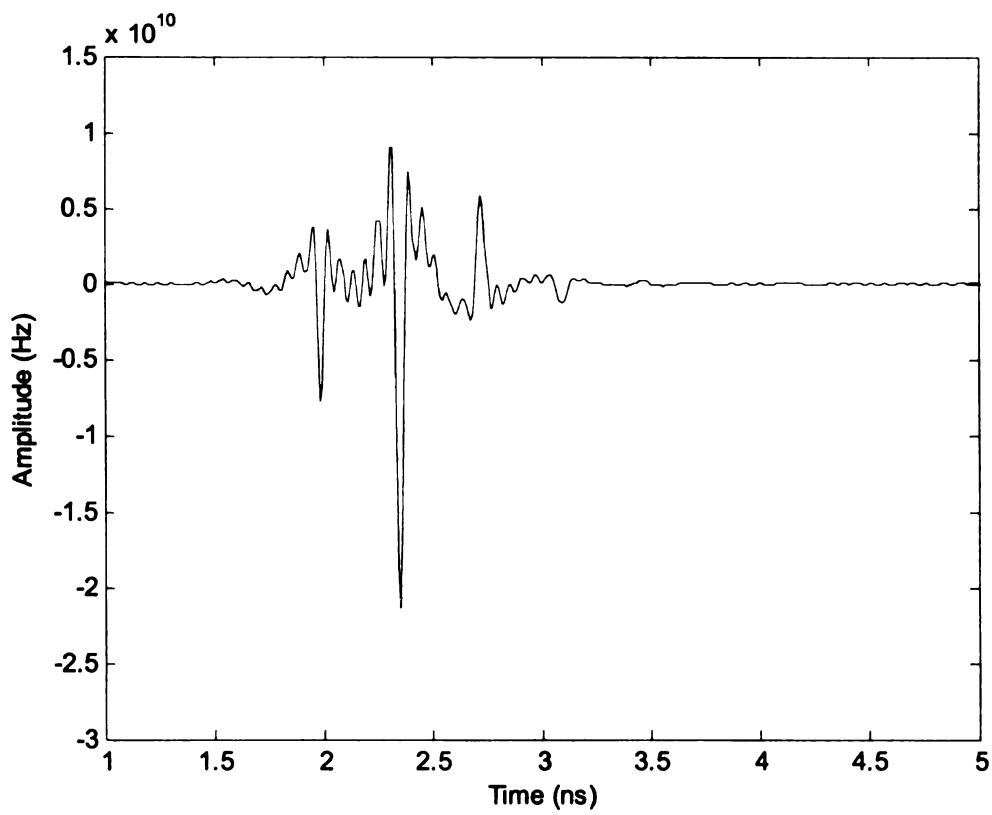


Figure 7.18. Calibrated temporal response of PEC-backed garolite sheet measured with the time-domain system

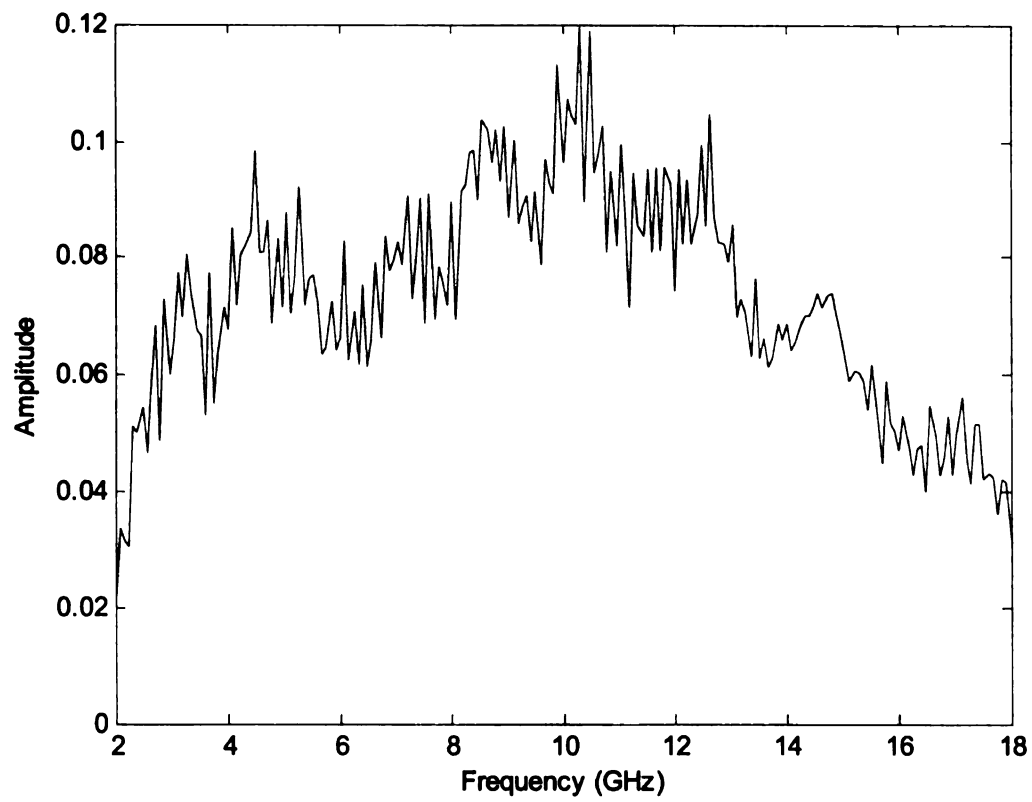


Figure 7.19. System response of the frequency-domain measurement system

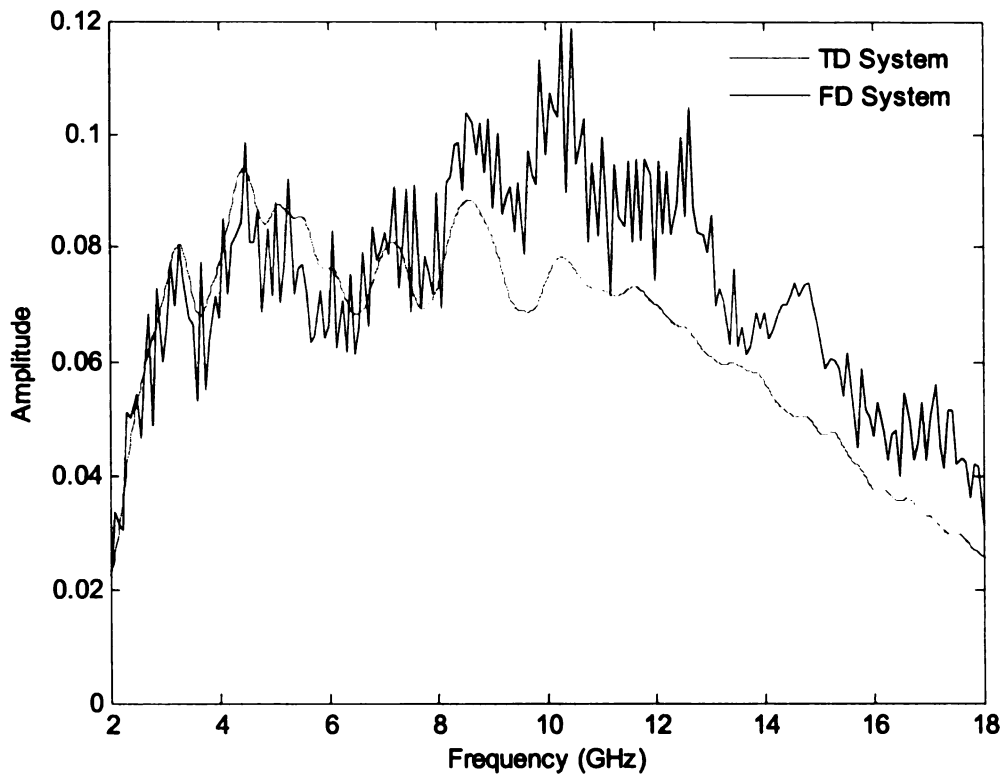


Figure 7.20. Comparison of the system responses for the time-domain and frequency-domain measurement systems



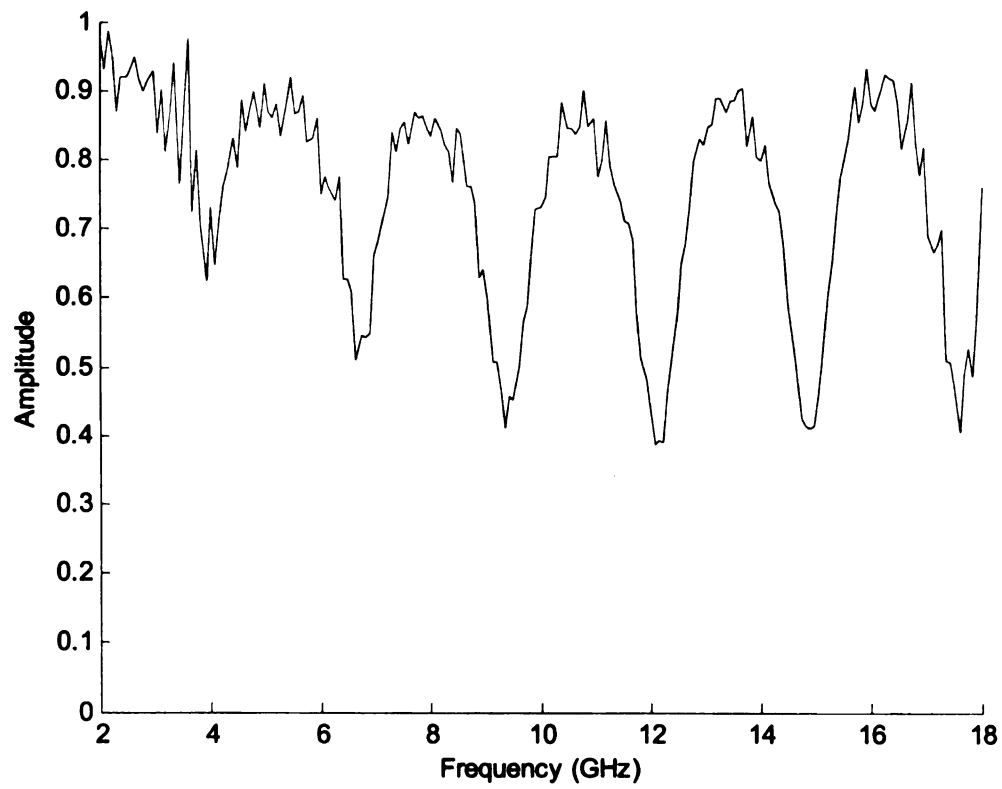


Figure 7.21. Spectrum of a PEC-backed garolite sheet measured using the frequency-domain system

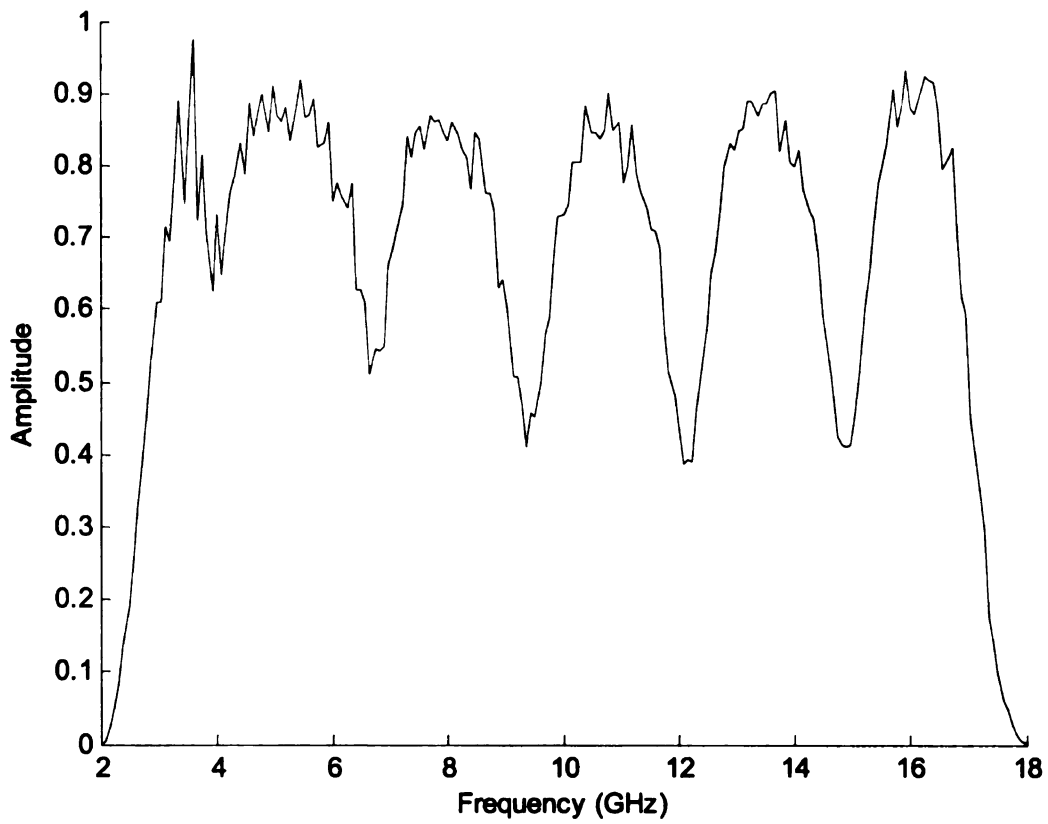


Figure 7.22. Spectrum of a PEC-backed garolite sheet measured using the frequency-domain system and weighted with a cosine taper window

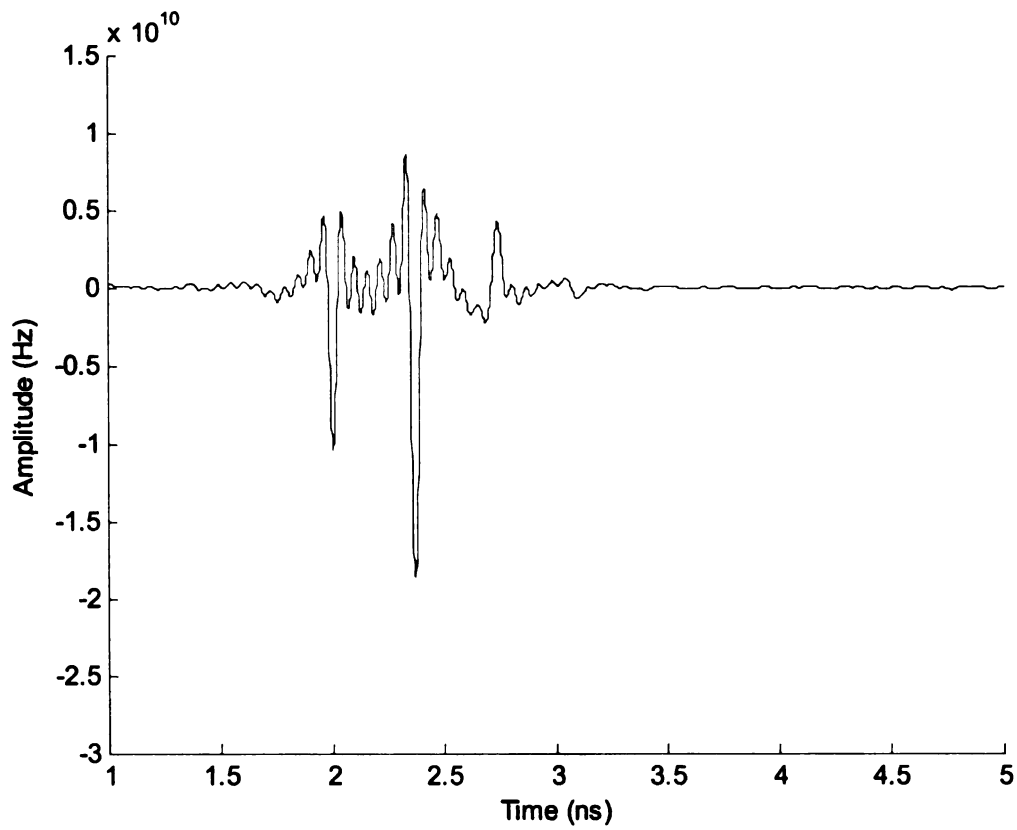


Figure 7.23. Calibrated temporal response of PEC-backed garolite sheet measured with the frequency domain system

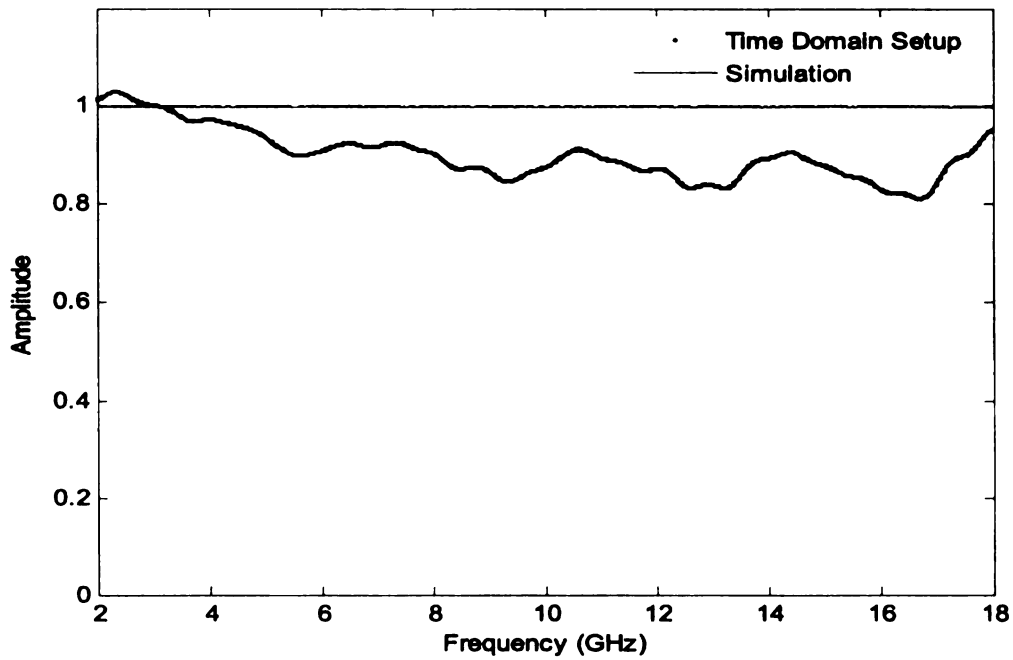
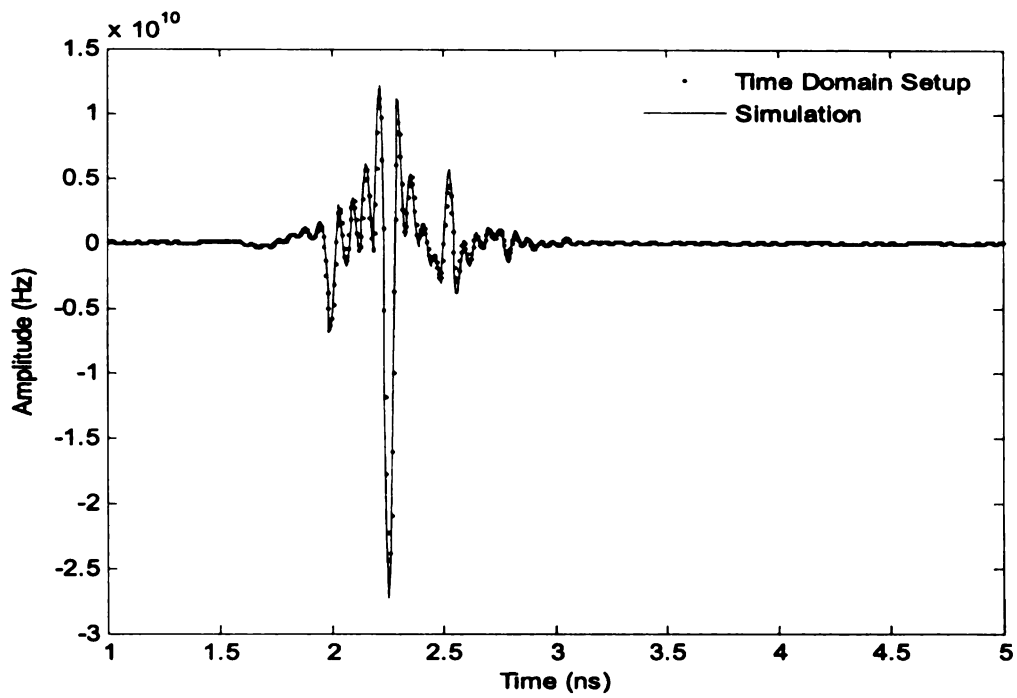


Figure 7.24. PEC-backed acrylic - Measurement using time-domain system (a)temporal response and (b)spectral response

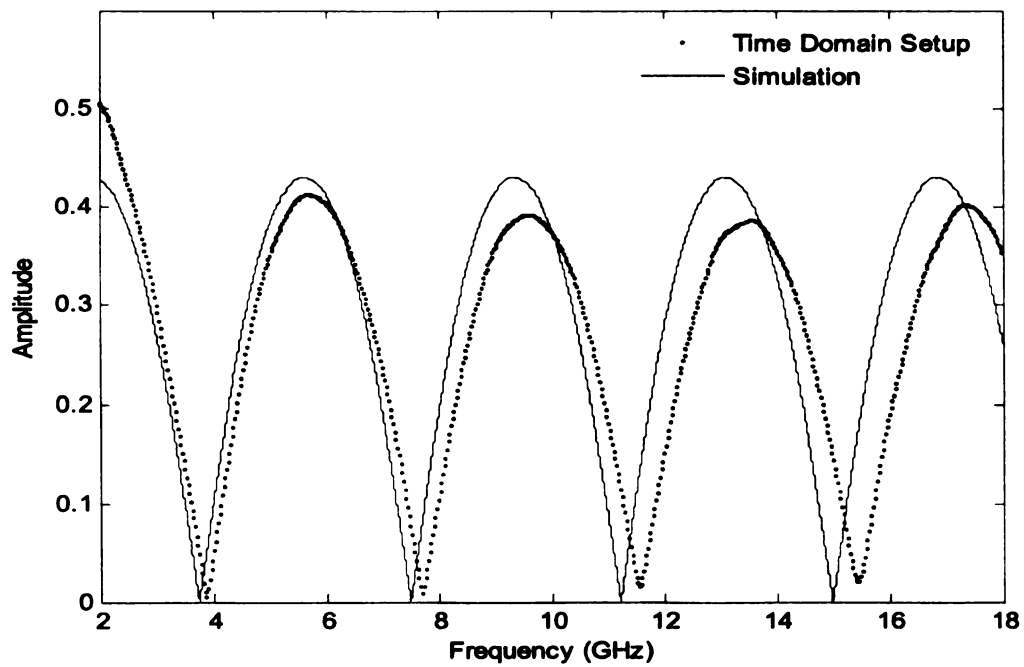
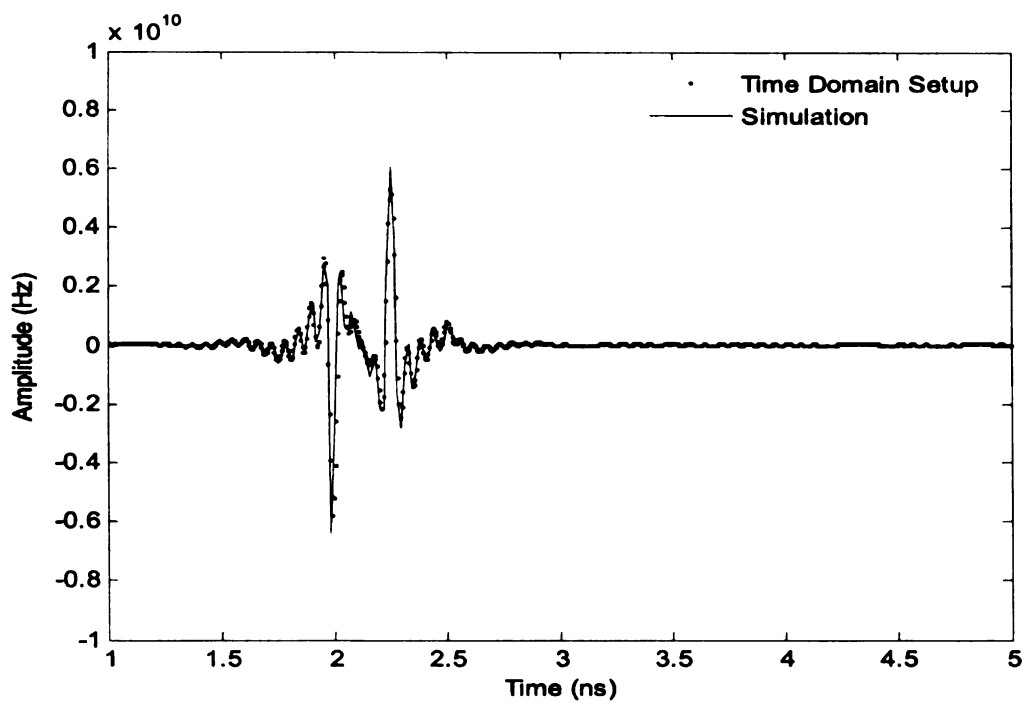


Figure 7.25. Air-backed acrylic - Measurement using time-domain system (a)temporal response and (b)spectral response

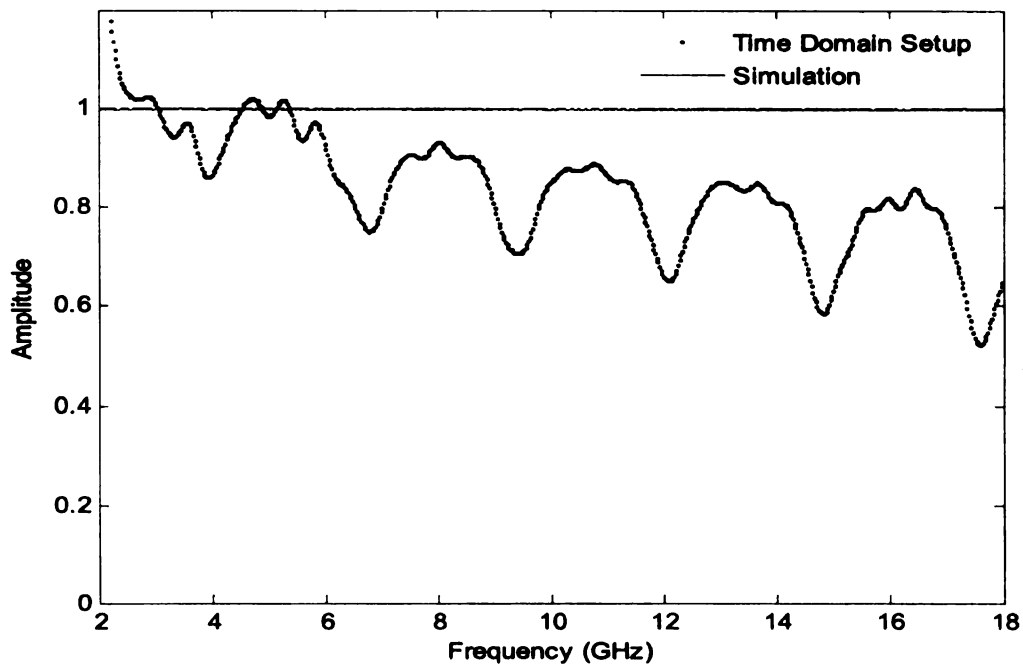
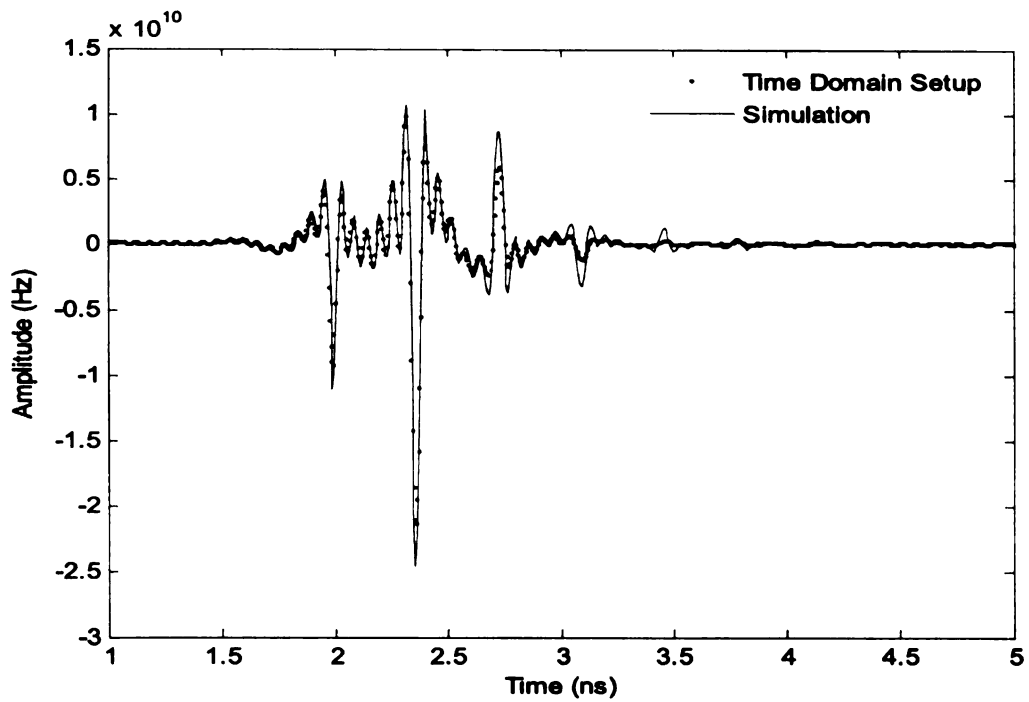


Figure 7.26. PEC-backed garolite - Measurement using time-domain system (a)temporal response and (b)spectral response

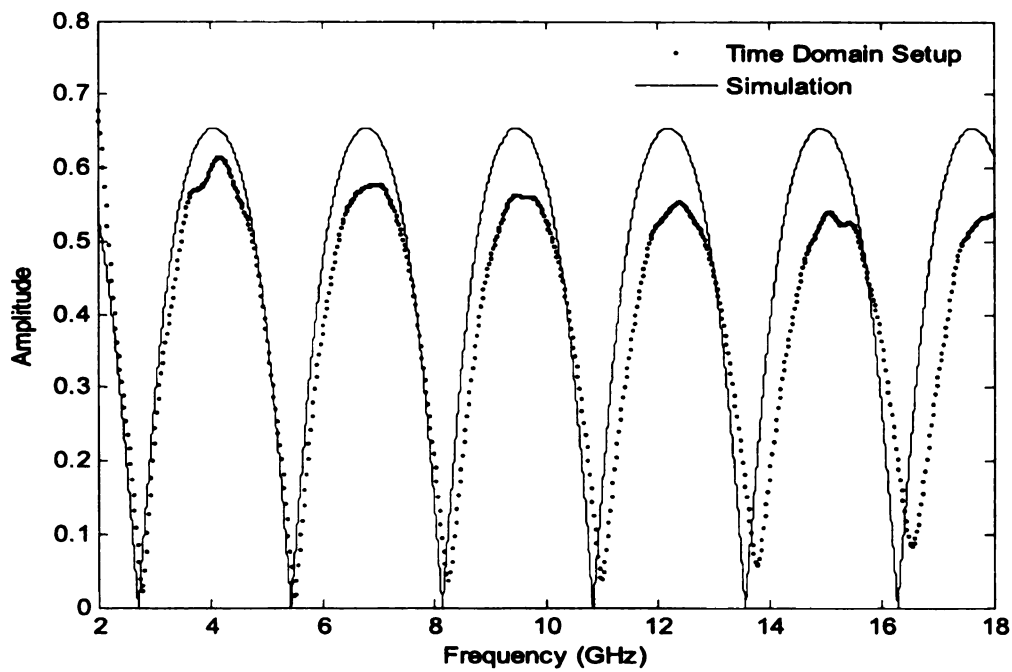
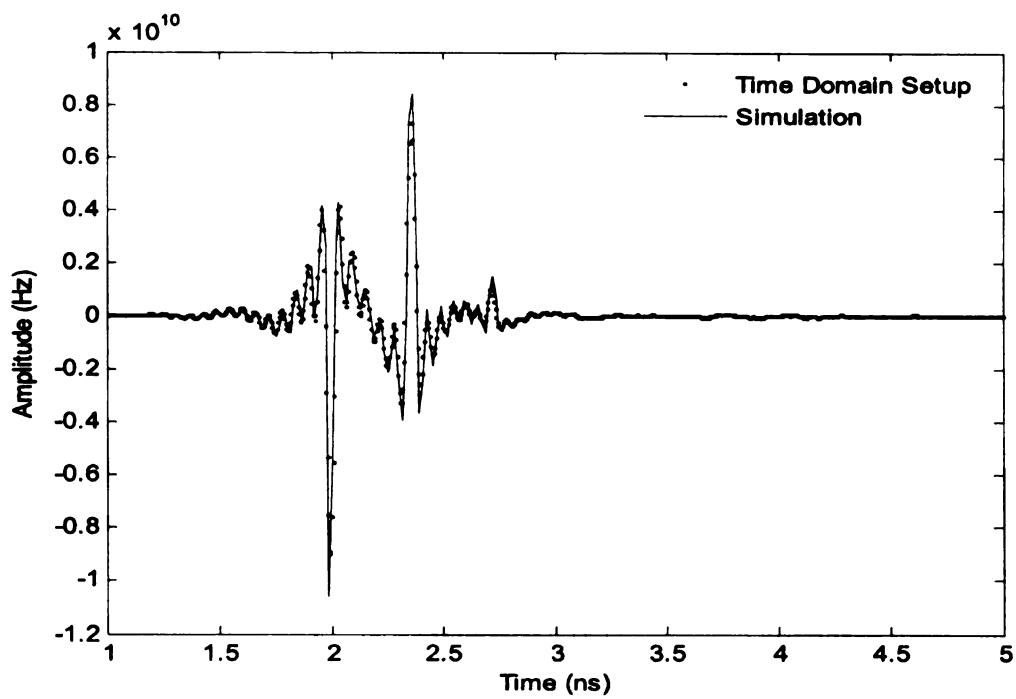


Figure 7.27. Air-backed garolite - Measurement using time-domain system (a)temporal response and (b)spectral response

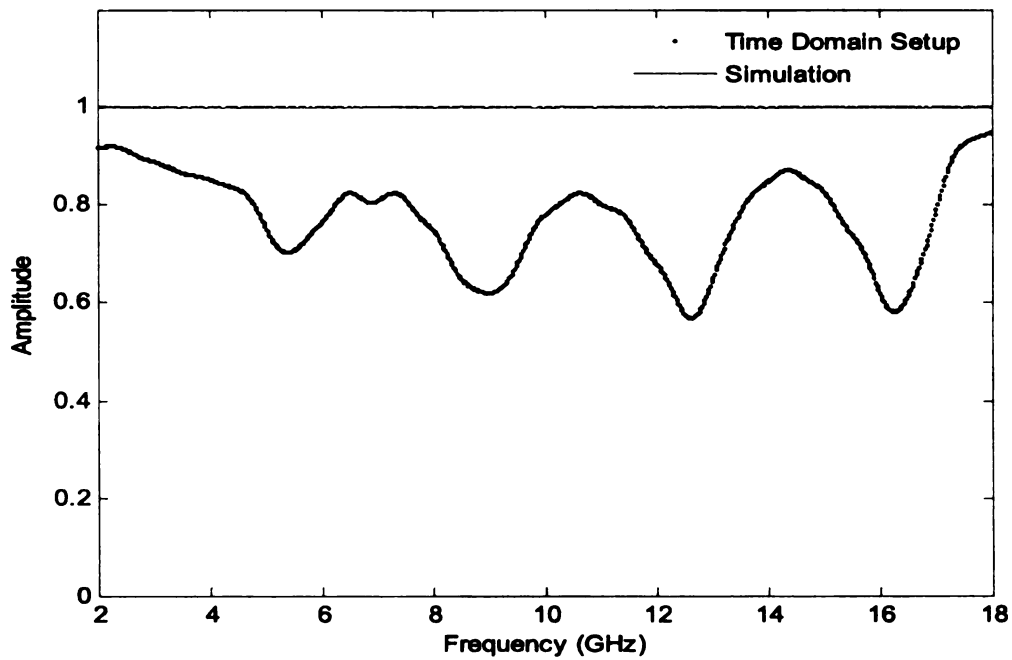
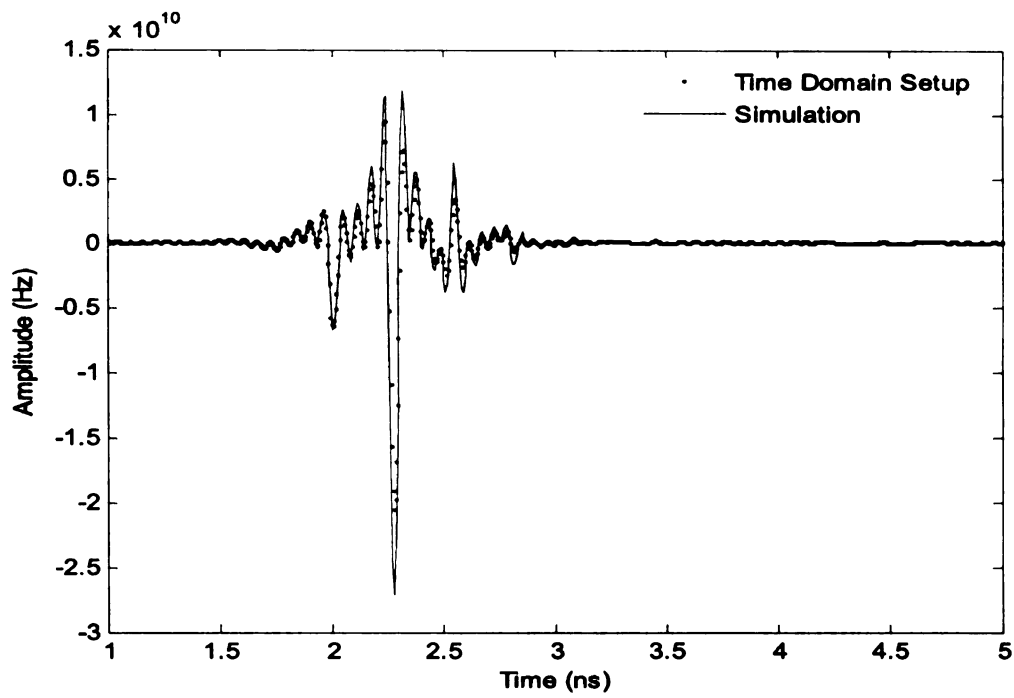


Figure 7.28. PEC-backed PVC - Measurement using time-domain system (a)temporal response and (b)spectral response



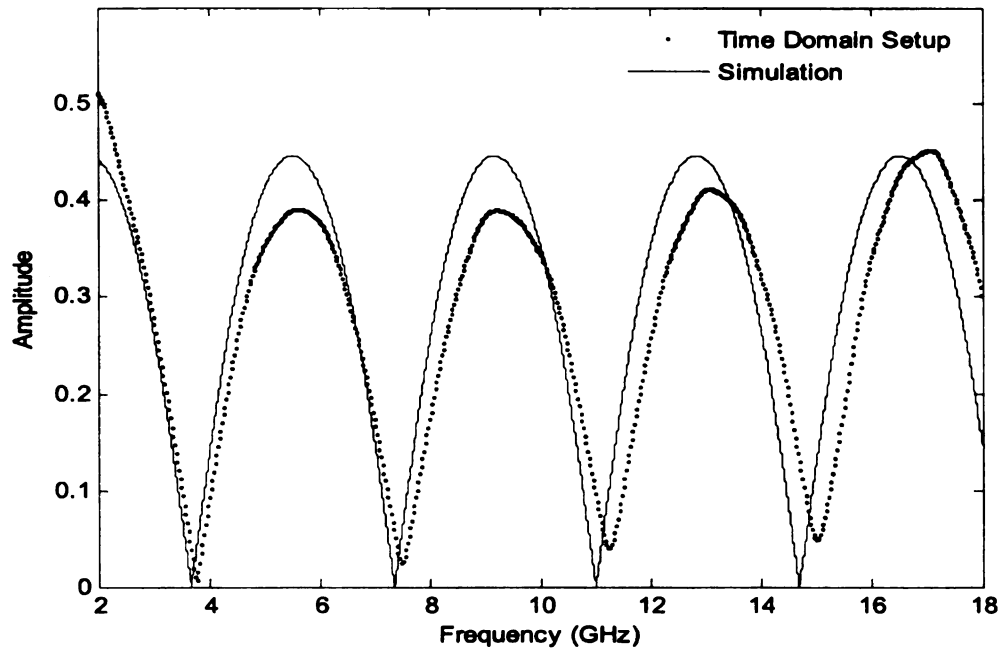
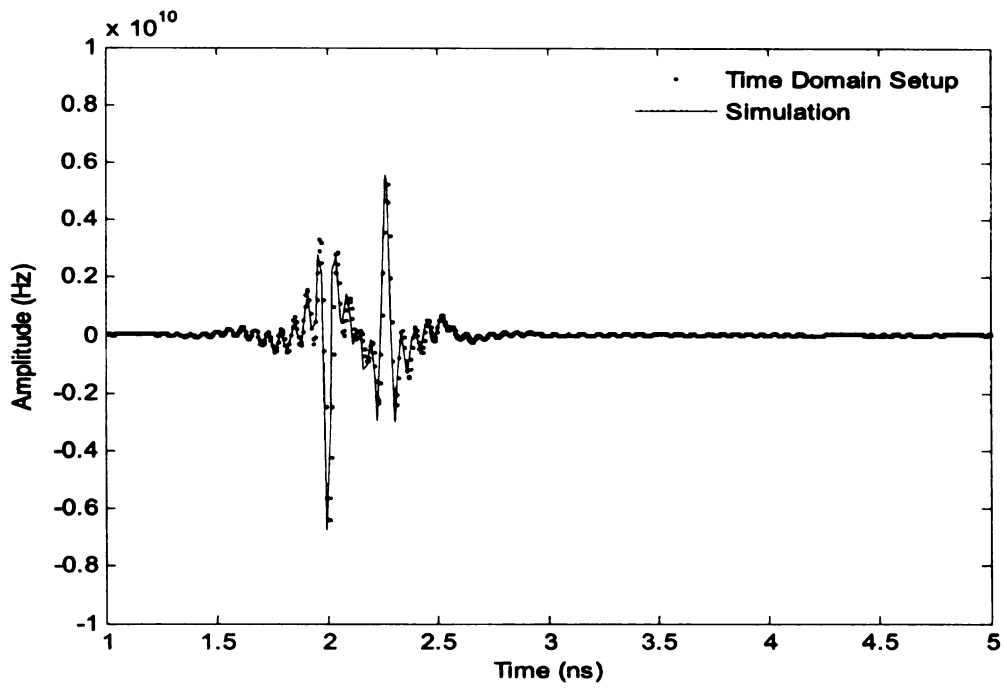


Figure 7.29. Air-backed PVC - Measurement using time-domain system (a)temporal response and (b)spectral response

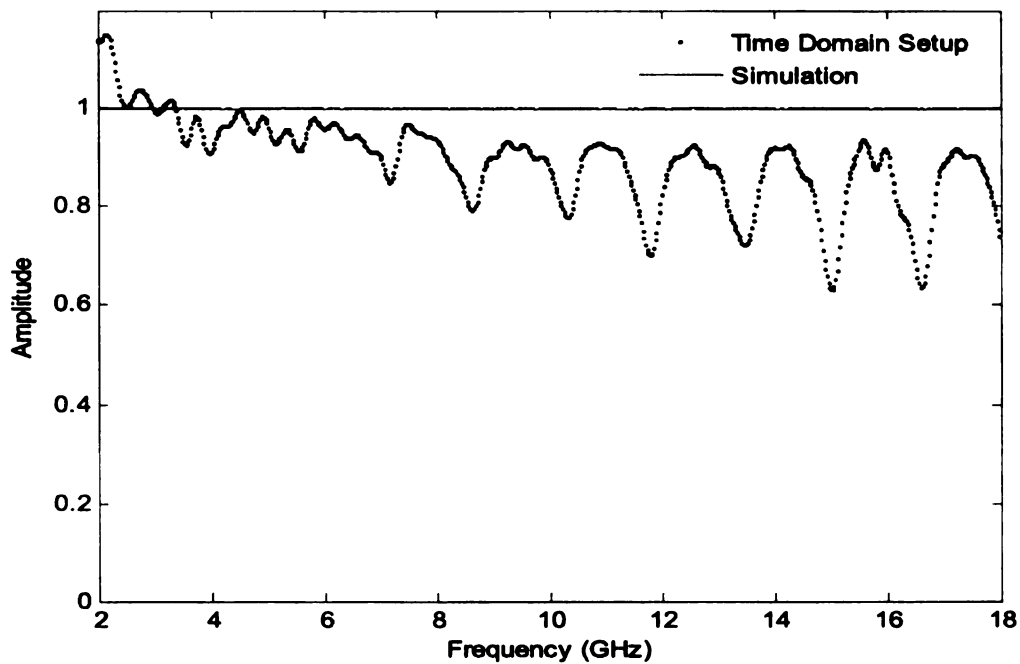
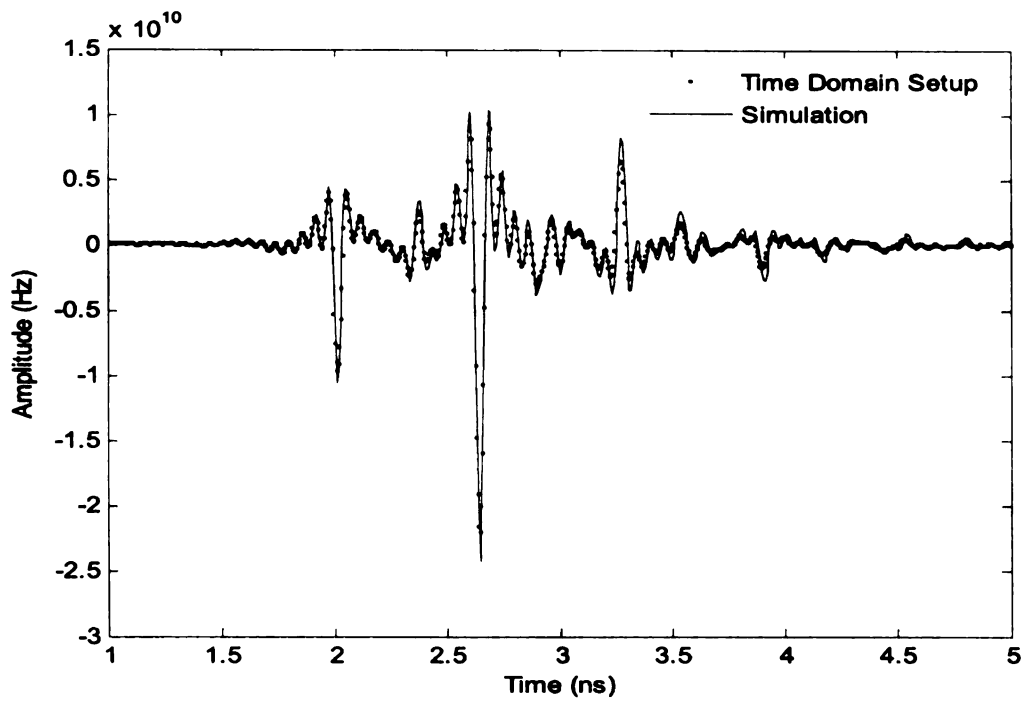


Figure 7.30. PEC-backed garolite-acrylic stack - Measurement using time-domain system (a)temporal response and (b)spectral response

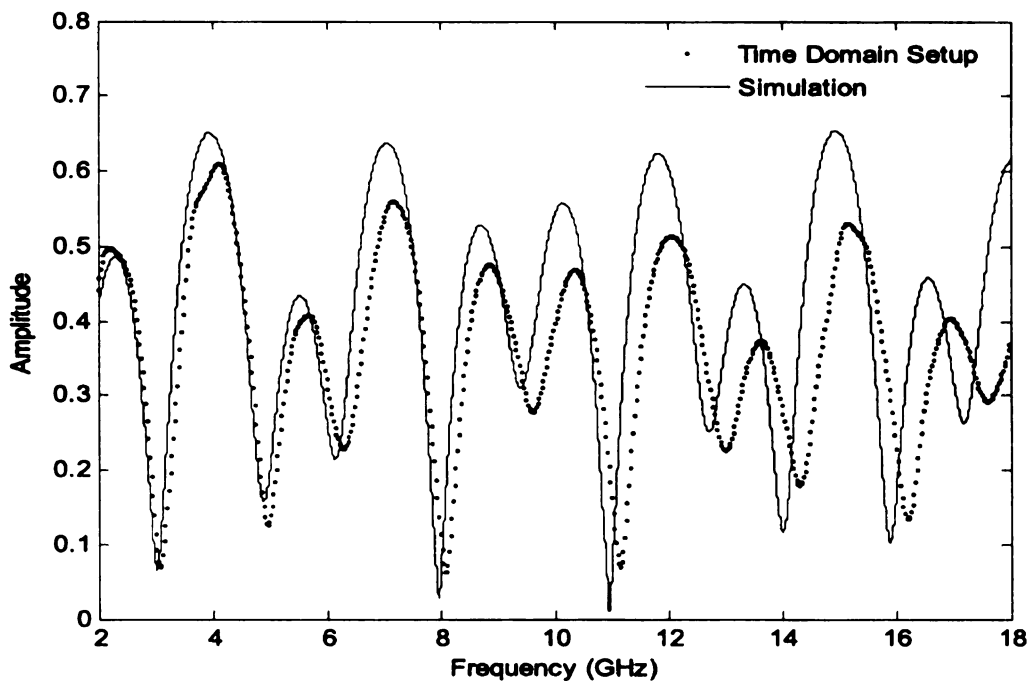
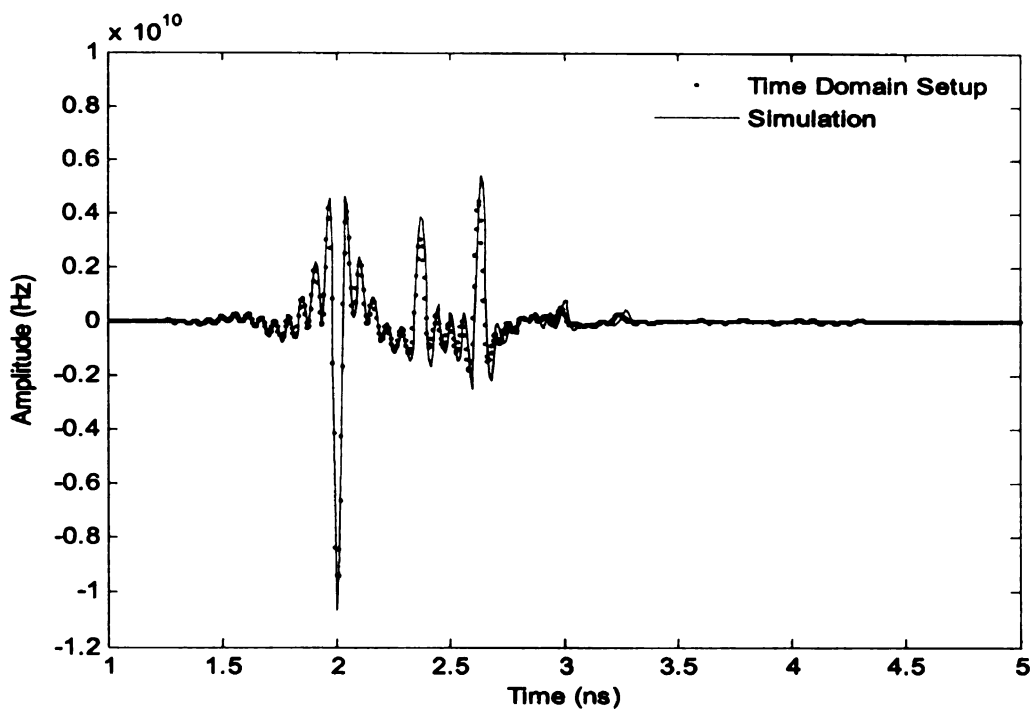


Figure 7.31. Air-backed garolite-acrylic stack - Measurement using time-domain system (a)temporal response and (b)spectral response

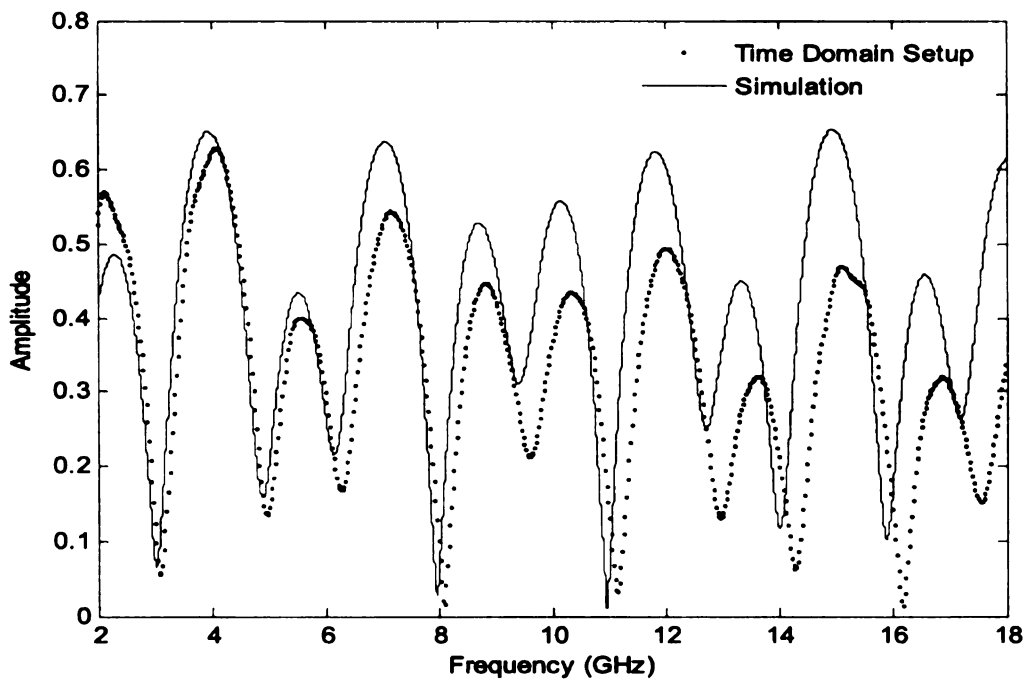
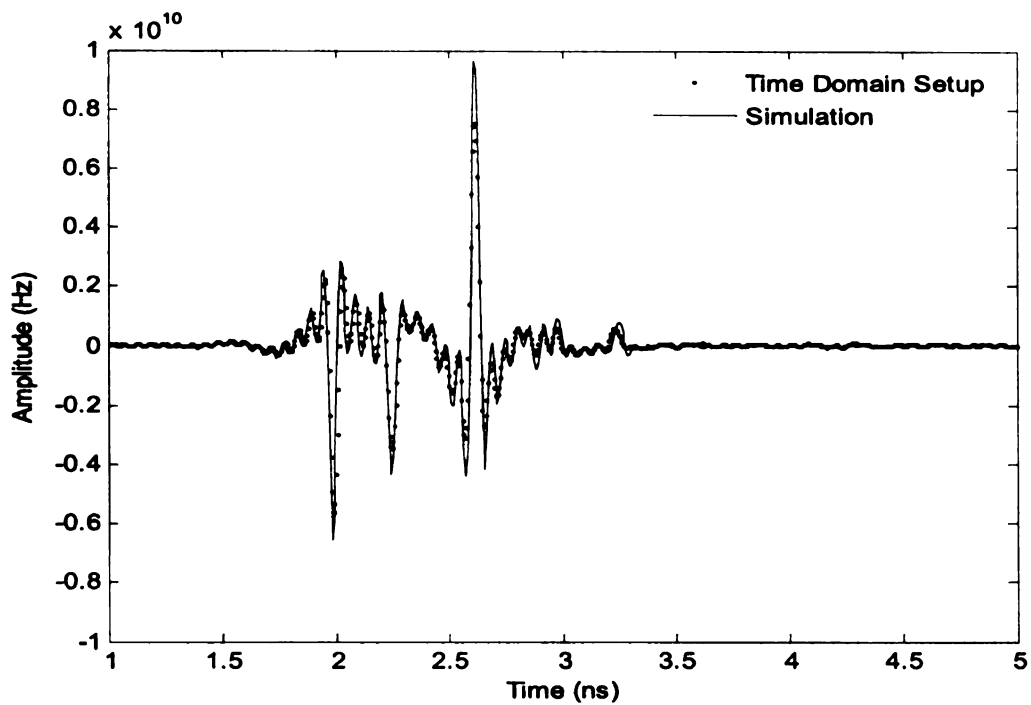


Figure 7.32. Air-backed acrylic-garolite stack - Measurement using time-domain system (a)temporal response and (b)spectral response

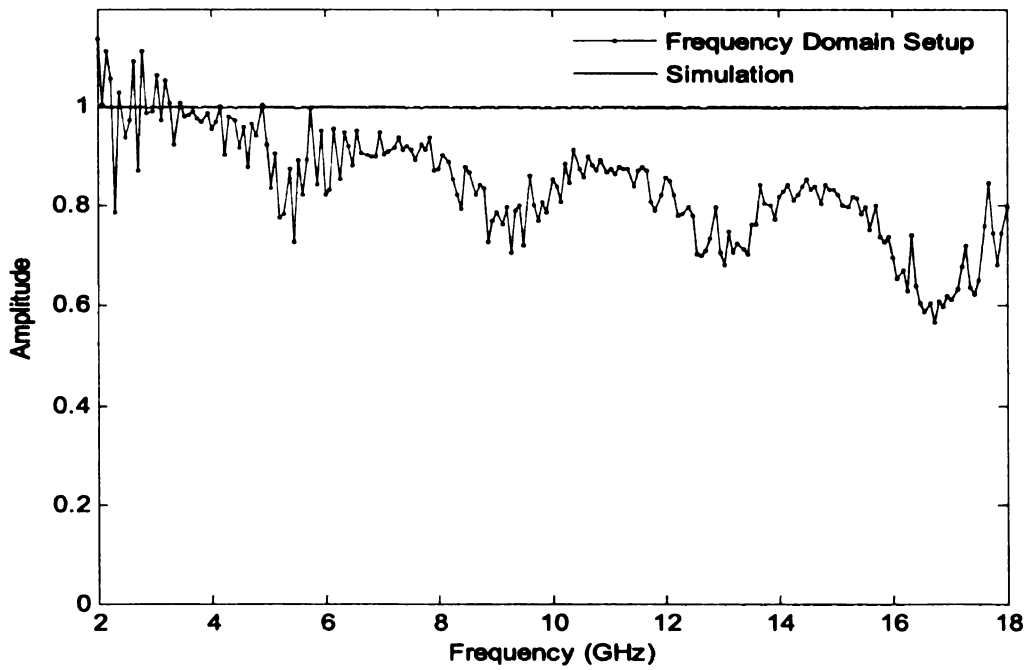
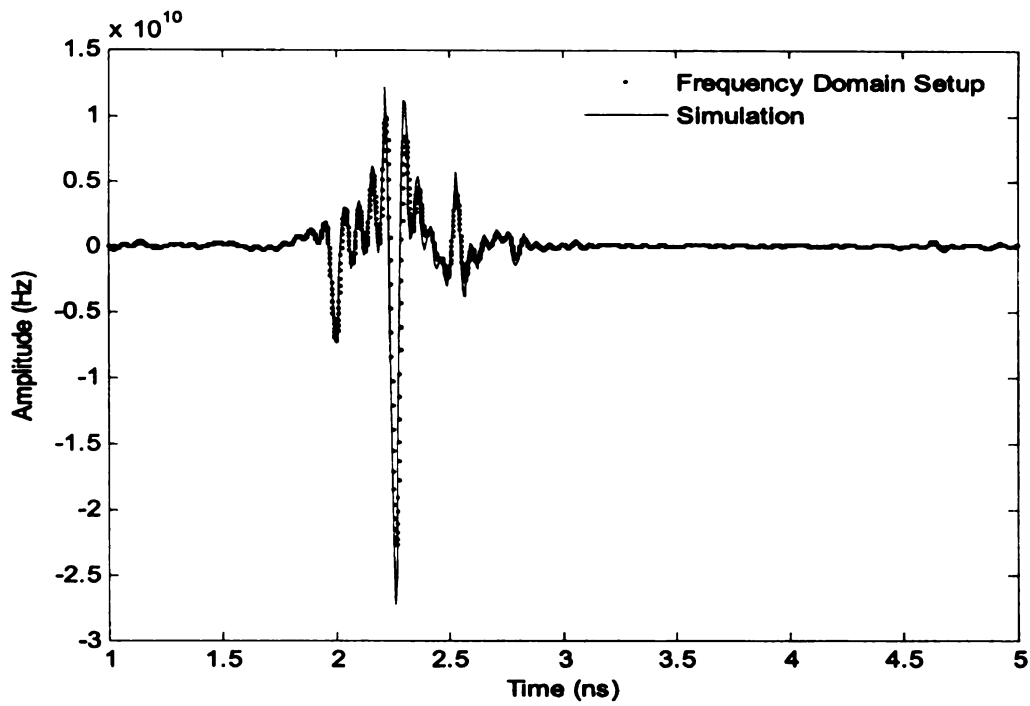


Figure 7.33. PEC-backed acrylic - Measurement using frequency-domain system (a)temporal response and (b)spectral response

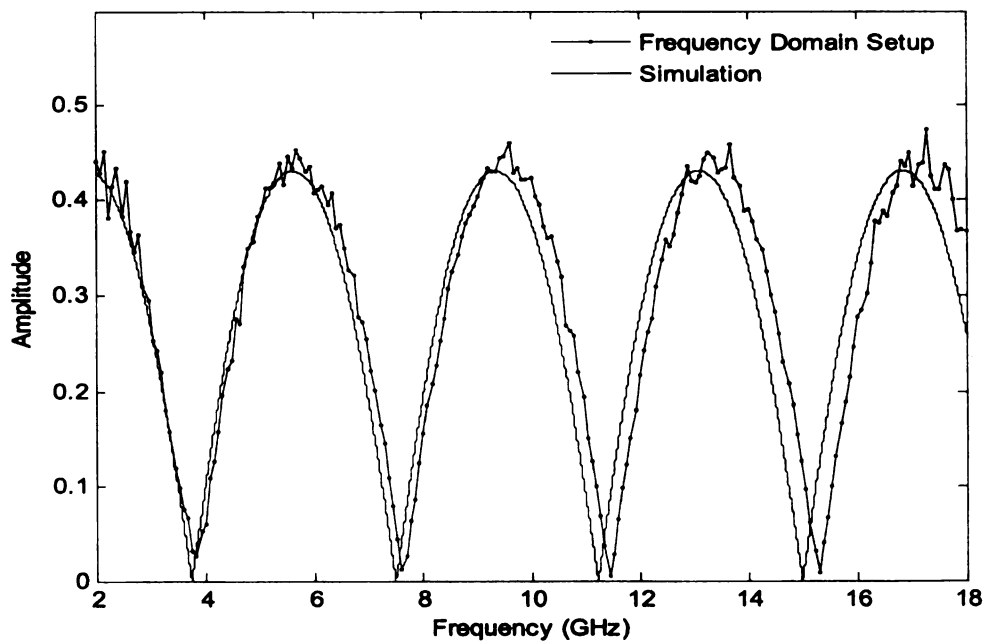
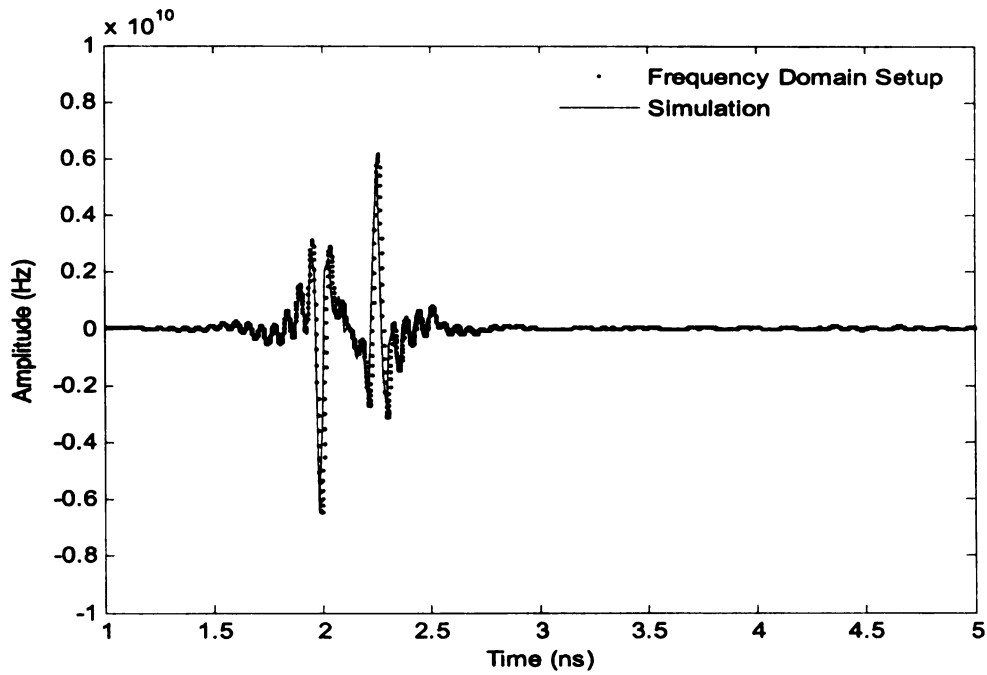


Figure 7.34. Air-backed acrylic - Measurement using frequency-domain system (a)temporal response and (b)spectral response

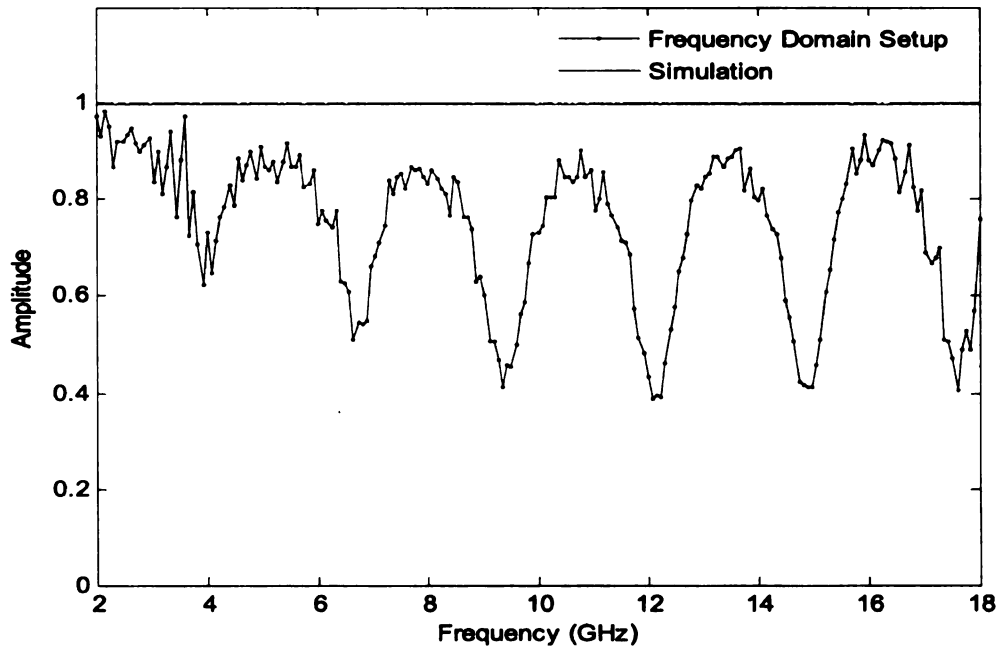
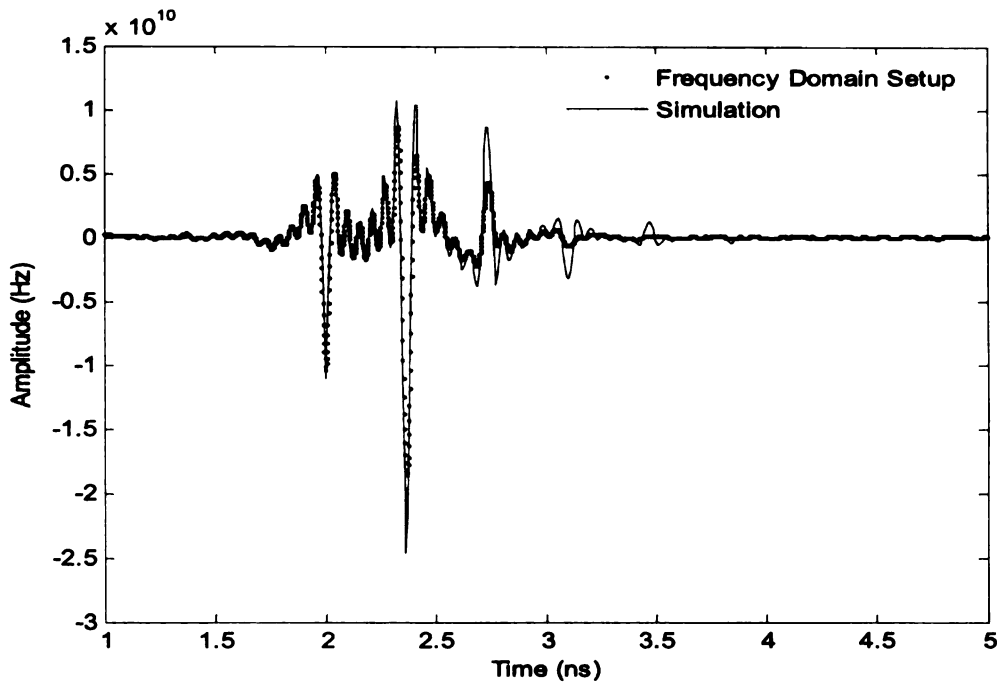


Figure 7.35. PEC-backed garolite - Measurement using frequency-domain system (a)temporal response and (b)spectral response

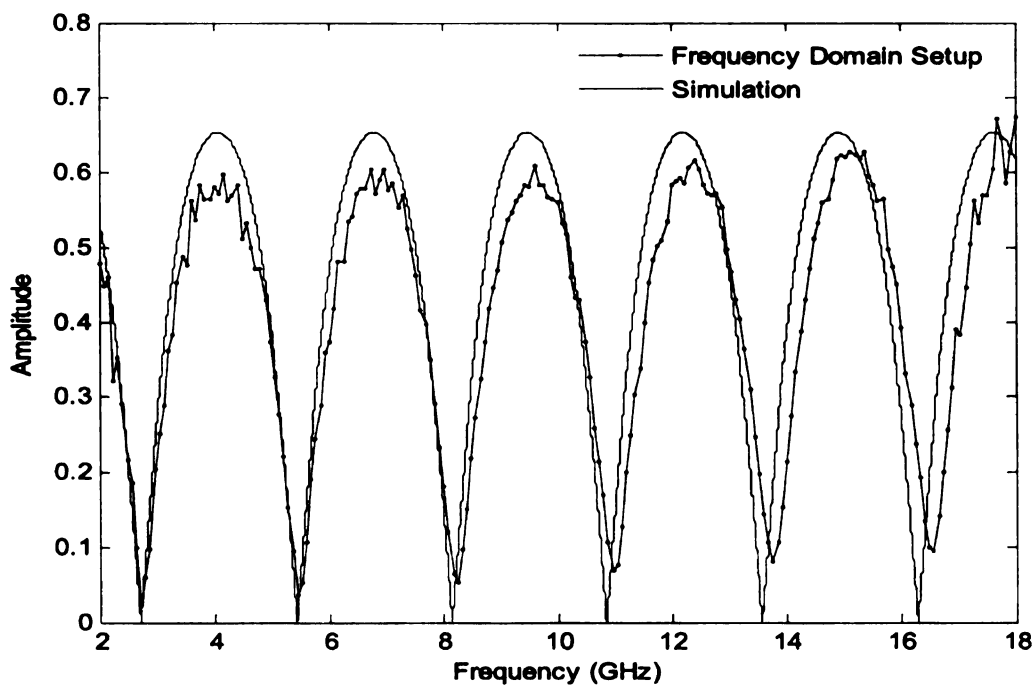
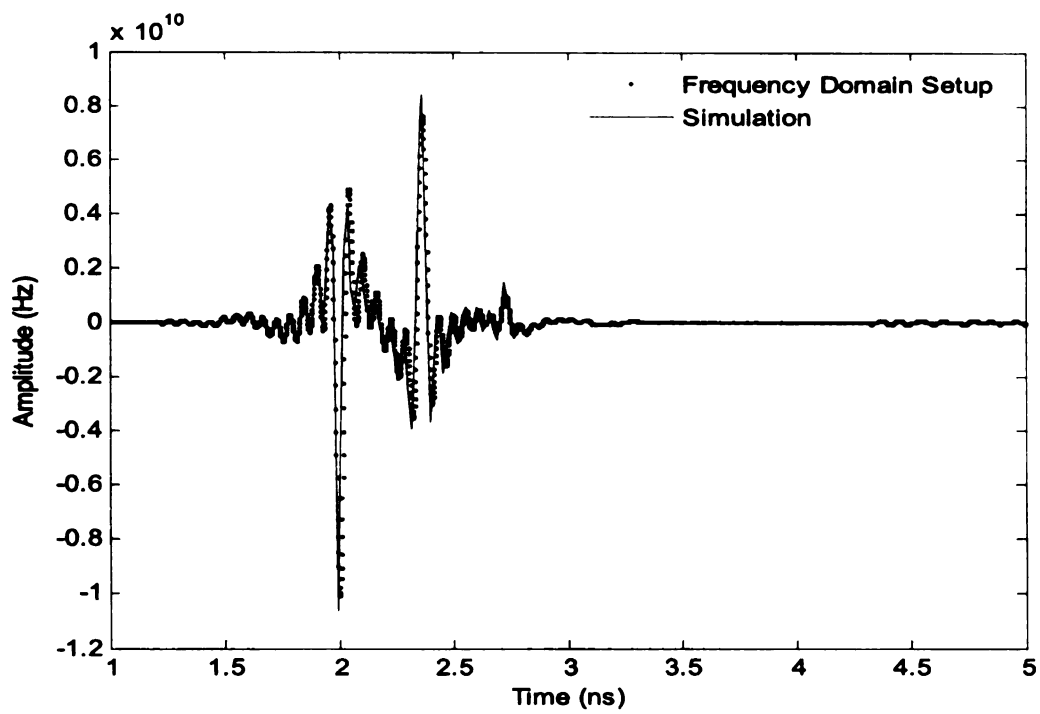


Figure 7.36. Air-backed garolite - Measurement using frequency-domain system  
 (a)temporal response and (b)spectral response



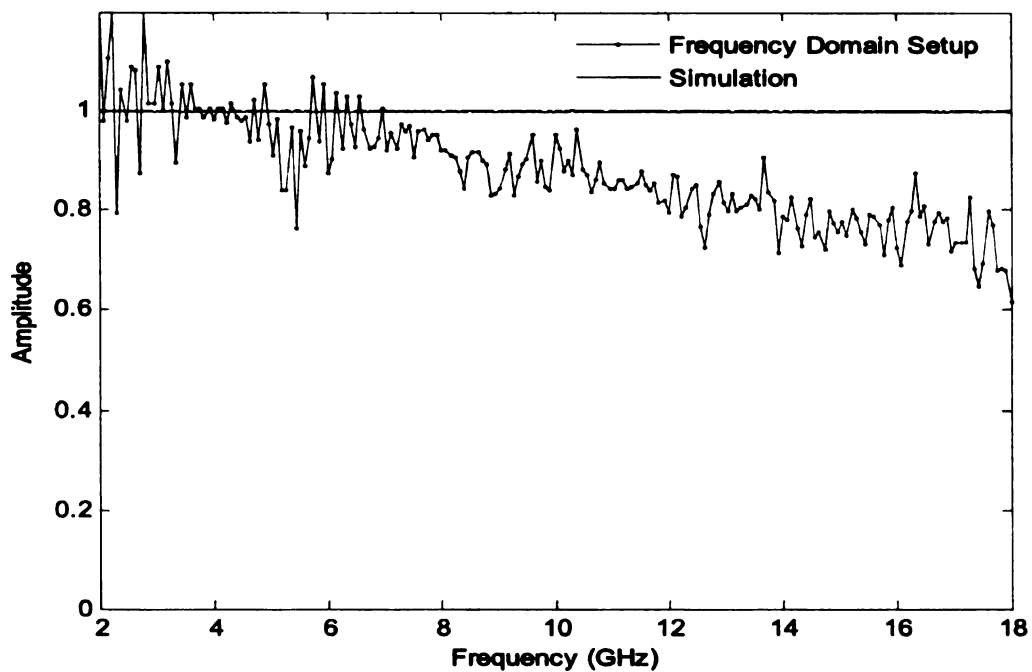
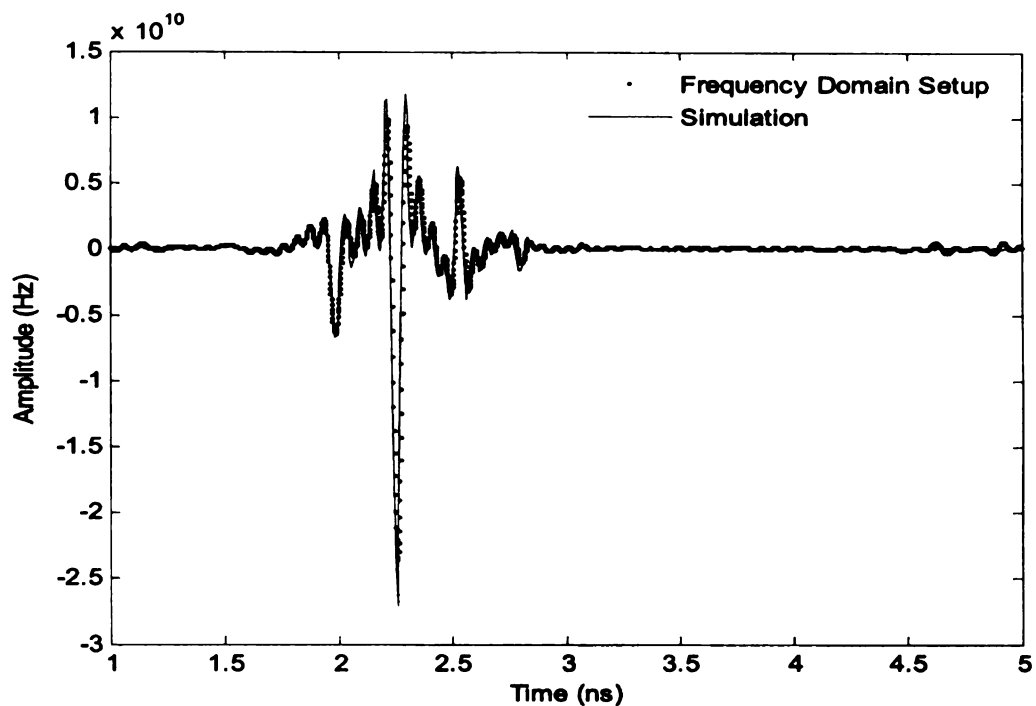


Figure 7.37. PEC-backed PVC - Measurement using frequency-domain system (a)temporal response and (b)spectral response

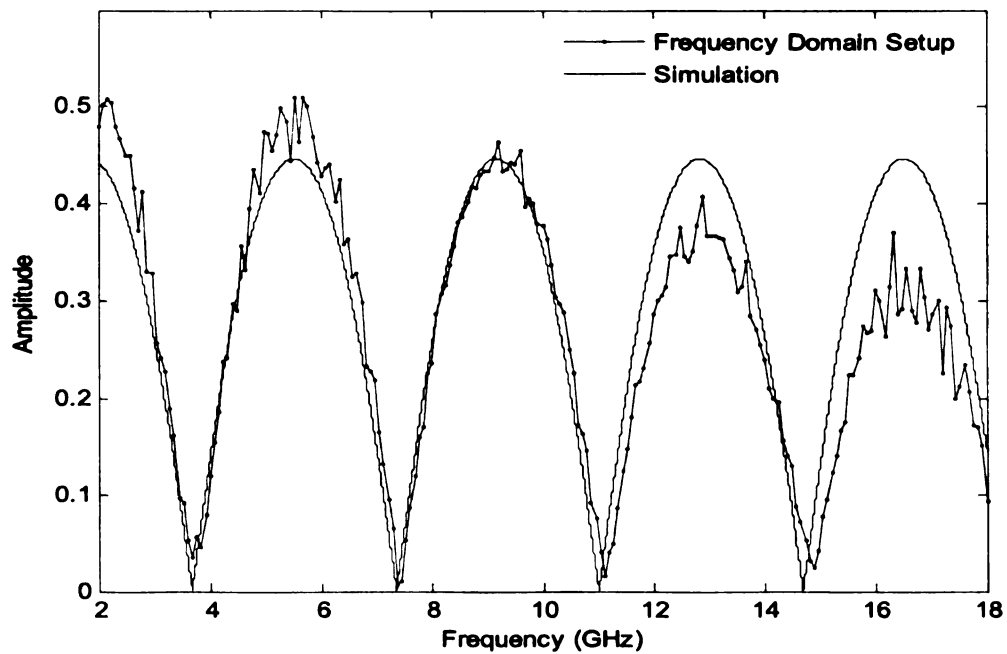
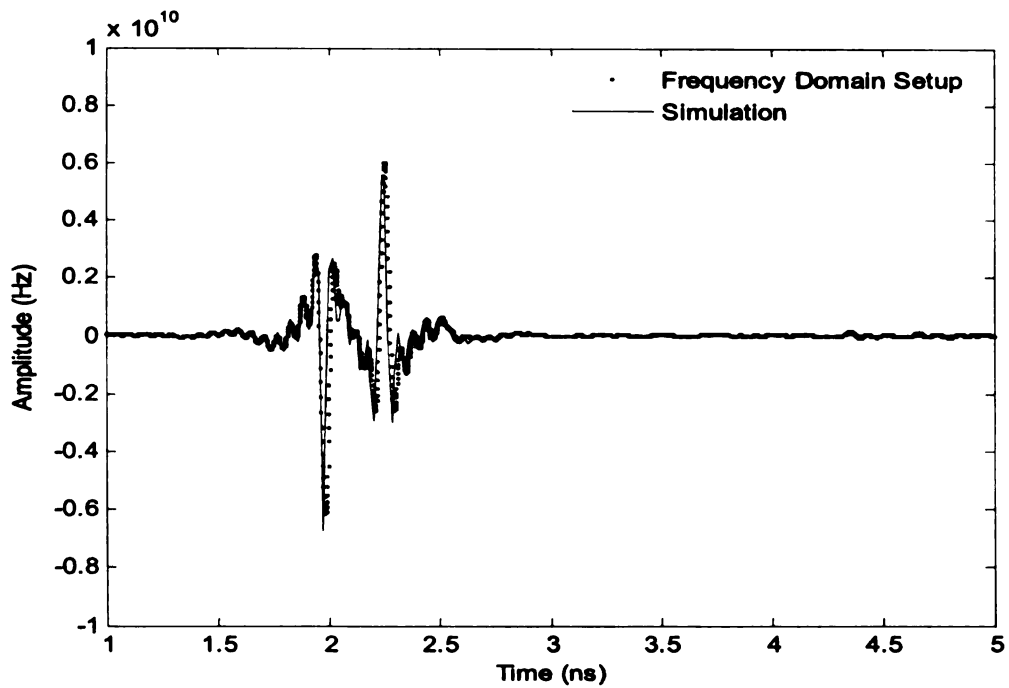


Figure 7.38. Air-backed PVC - Measurement using frequency-domain system (a)temporal response and (b)spectral response

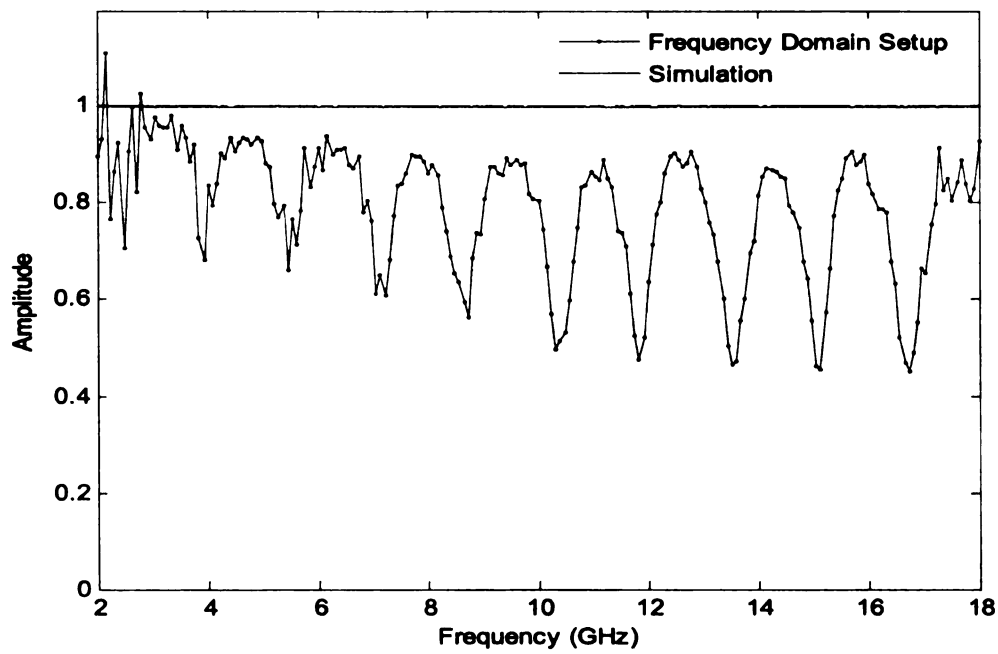
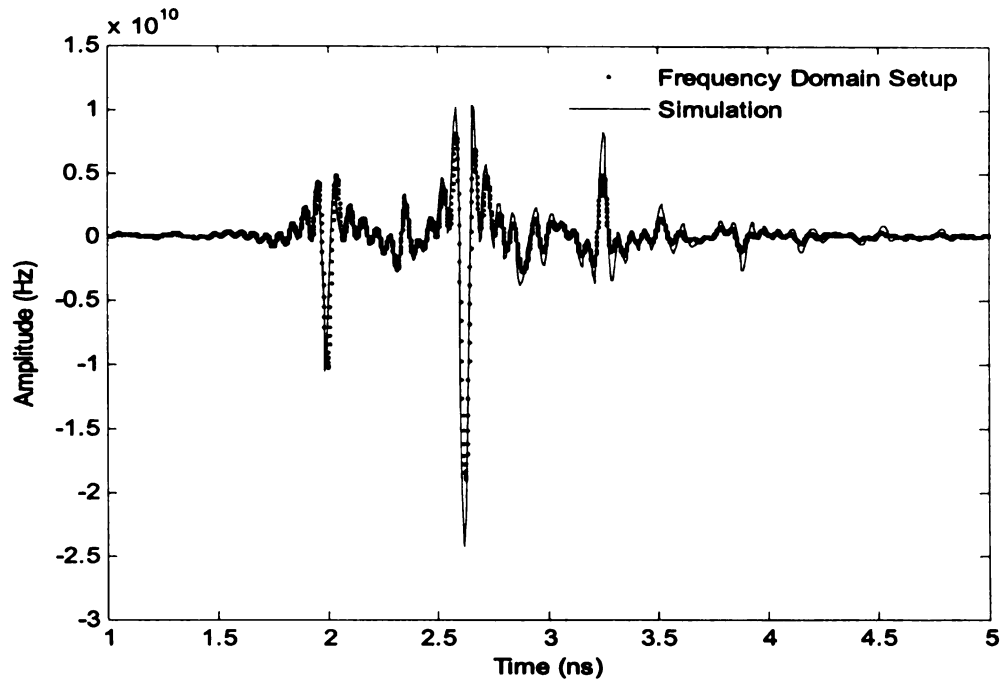


Figure 7.39. PEC-backed garolite-acrylic stack - Measurement using frequency-domain system (a)temporal response and (b)spectral response

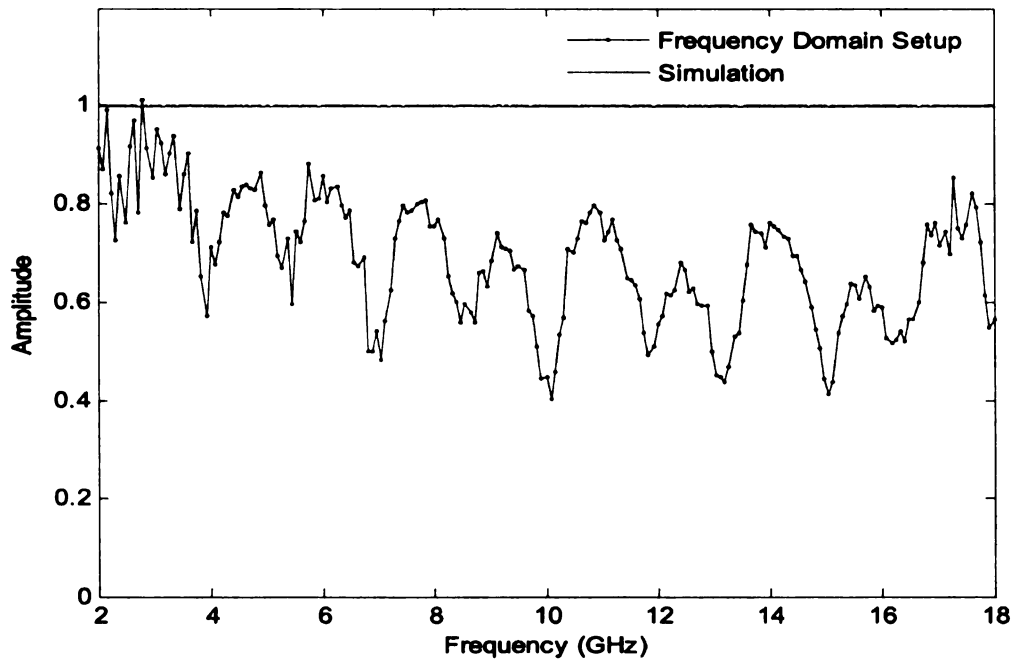
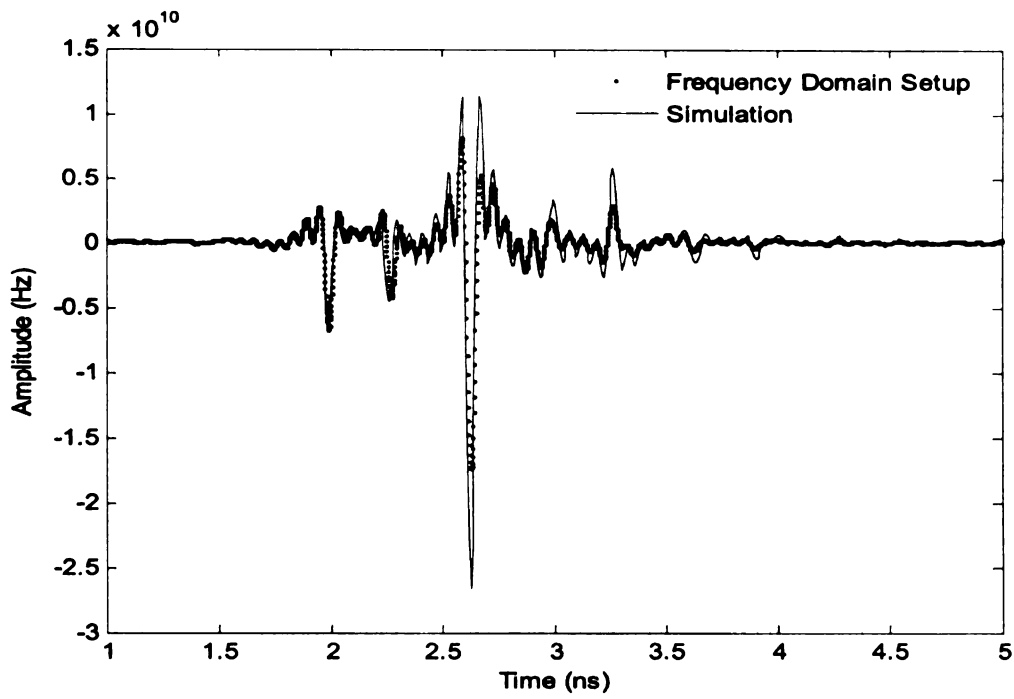


Figure 7.40. PEC-backed PVC-garolite stack - Measurement using frequency-domain system (a)temporal response and (b)spectral response

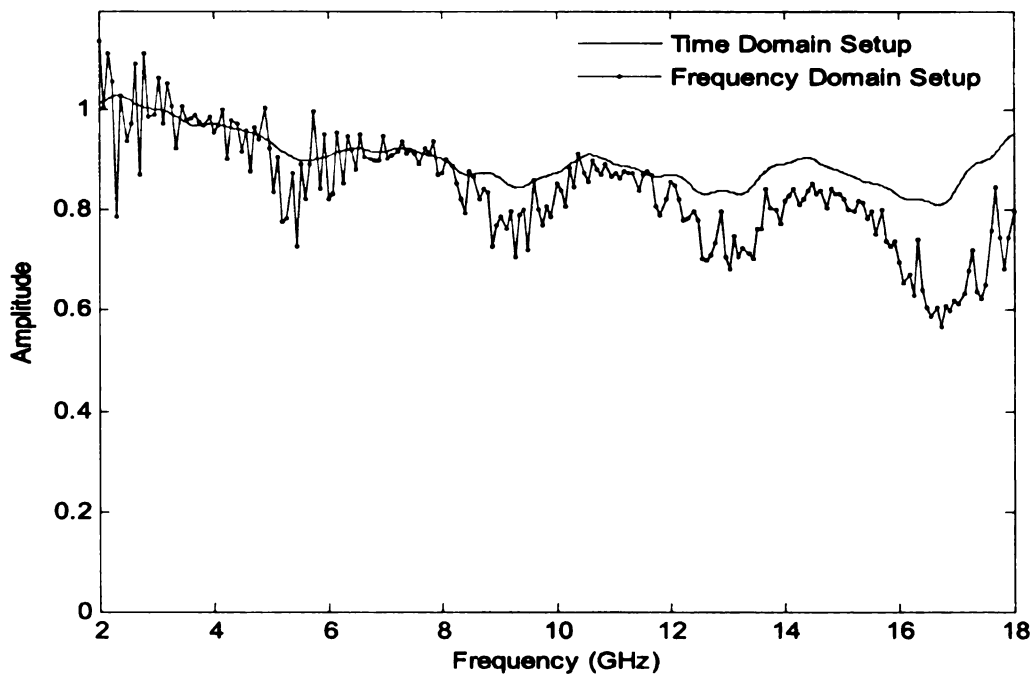
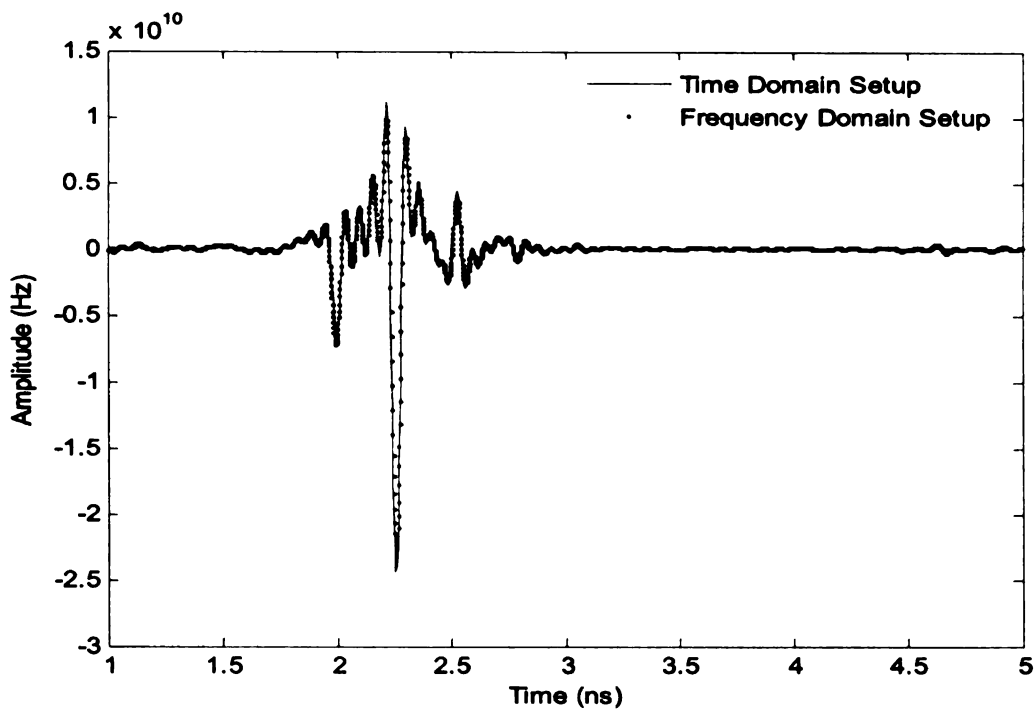


Figure 7.41. PEC-backed acrylic - Comparison of measurement systems (a)temporal response and (b)spectral response

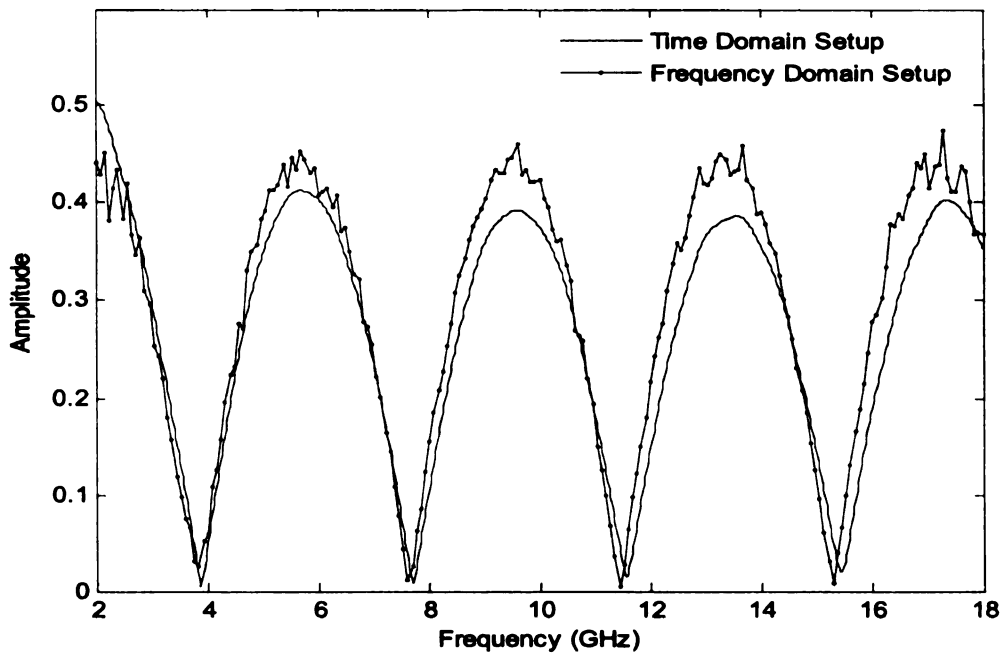
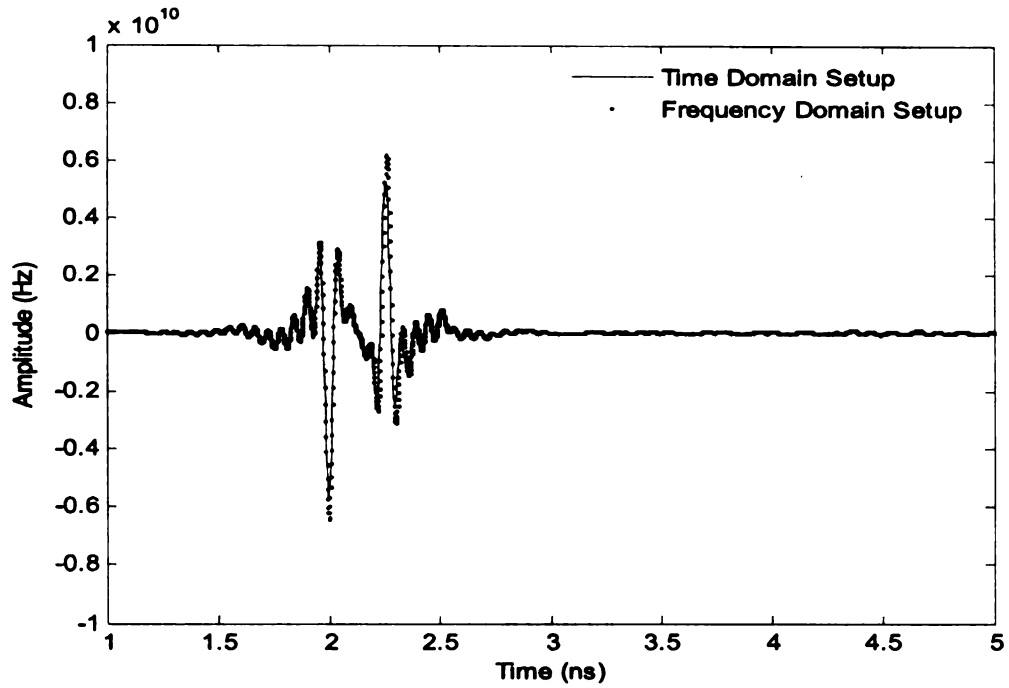


Figure 7.42. Air-backed acrylic - Comparison of measurement systems (a)temporal response and (b)spectral response

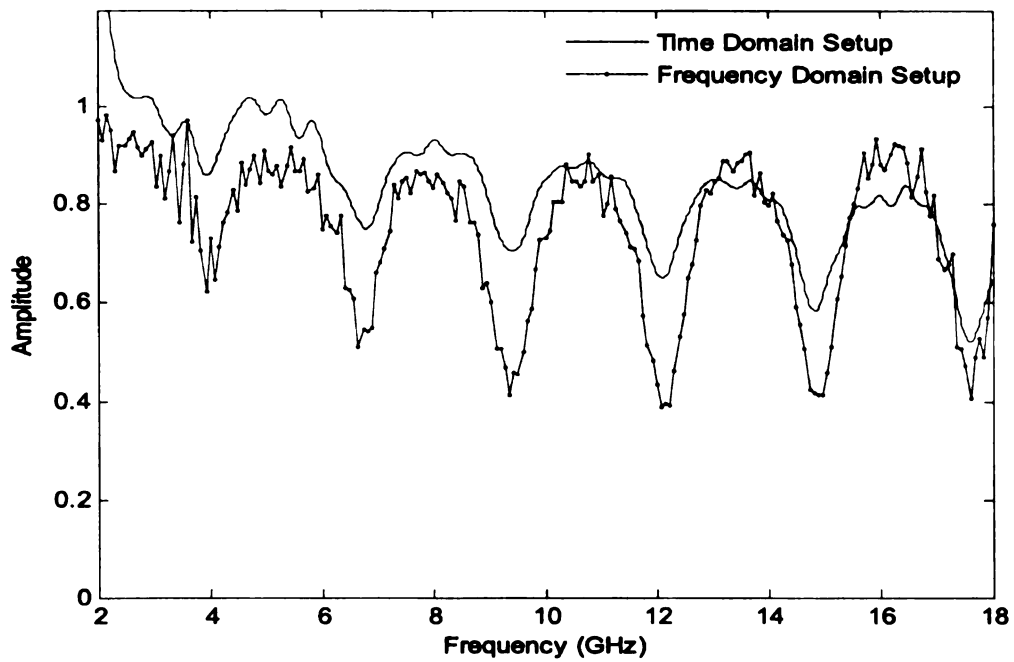
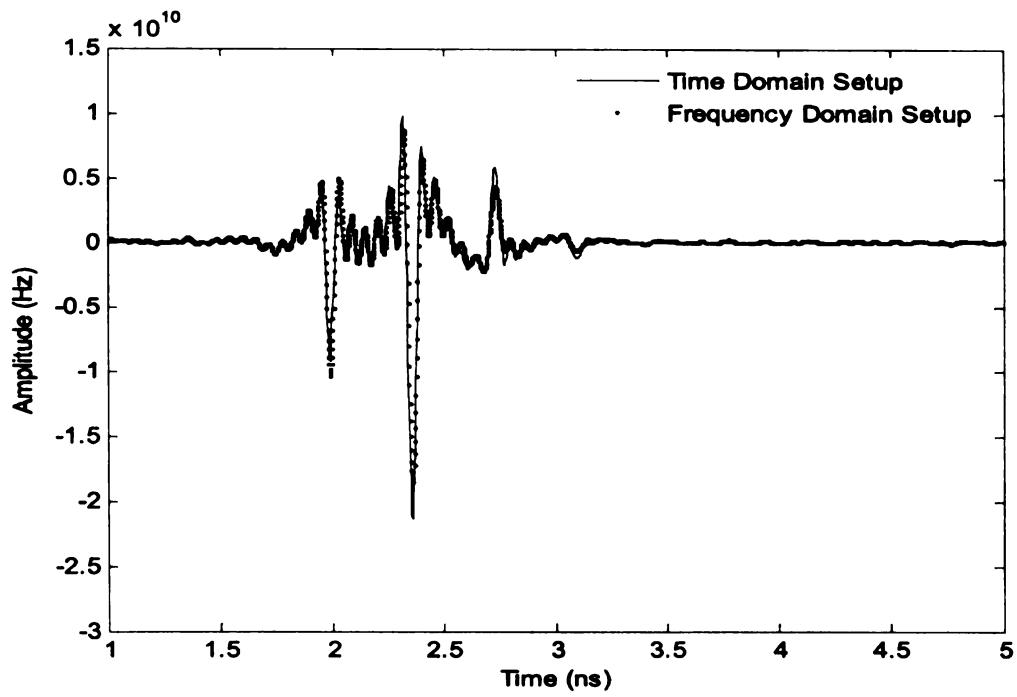


Figure 7.43. PEC-backed garolite - Comparison of measurement systems (a)temporal response and (b)spectral response

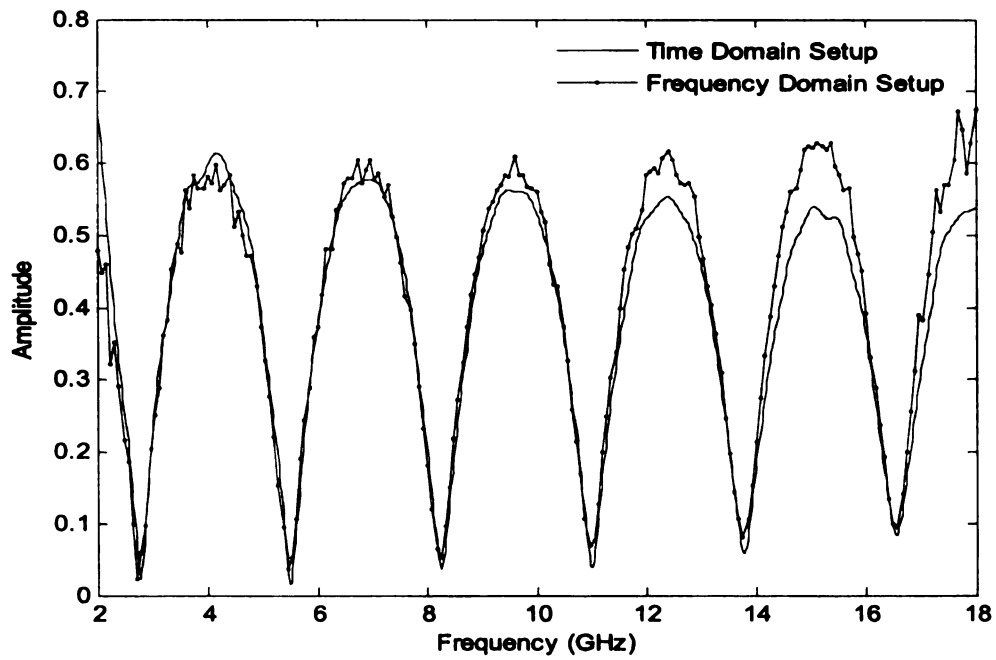
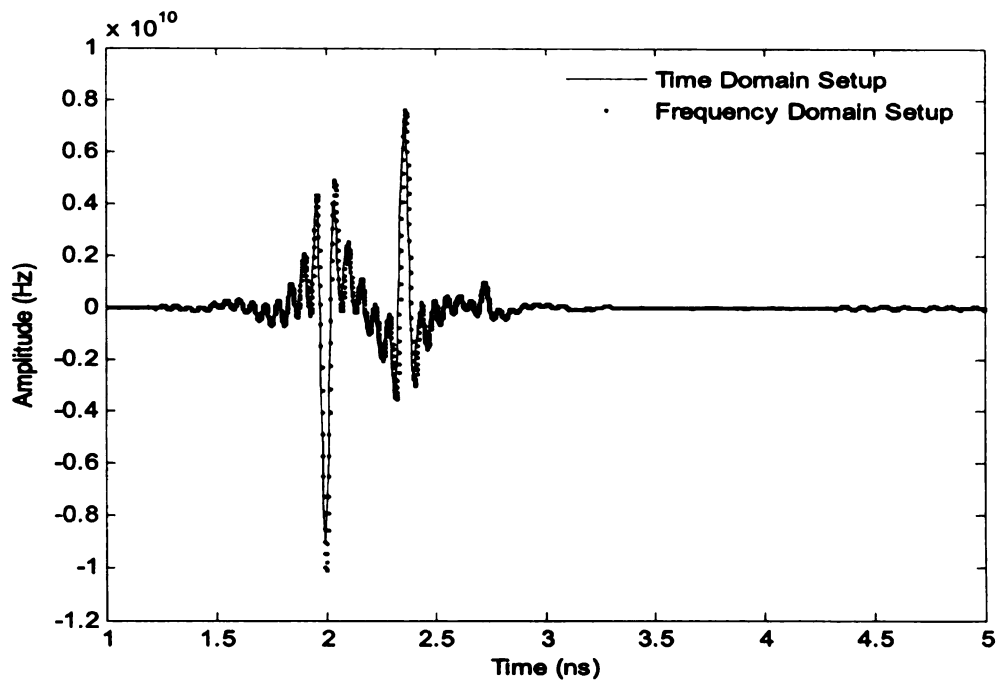


Figure 7.44. Air-backed garolite - Comparison of measurement systems (a)temporal response and (b)spectral response



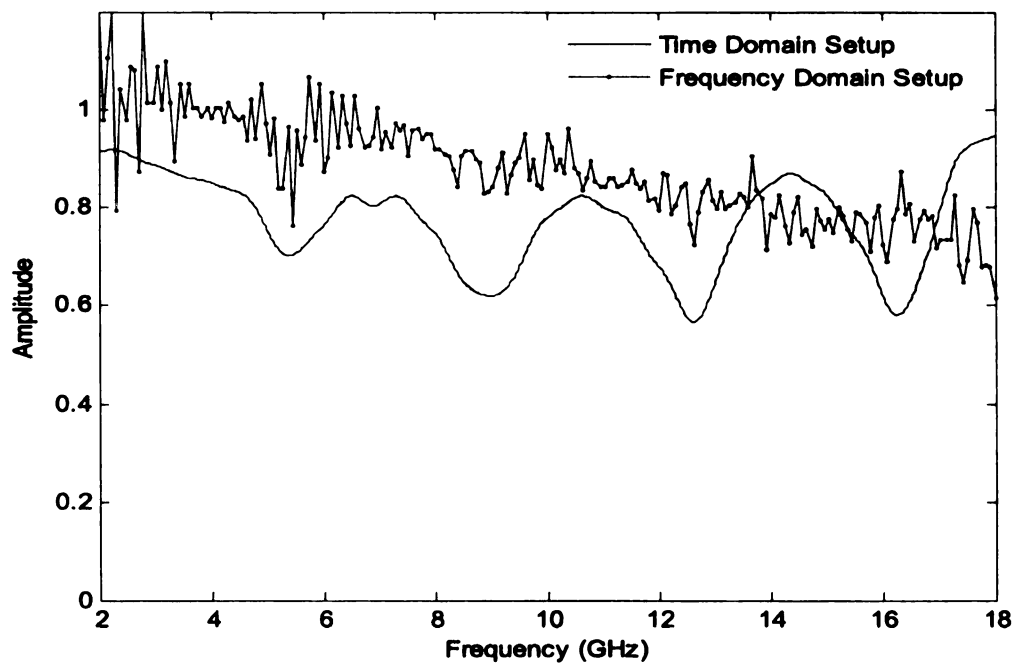
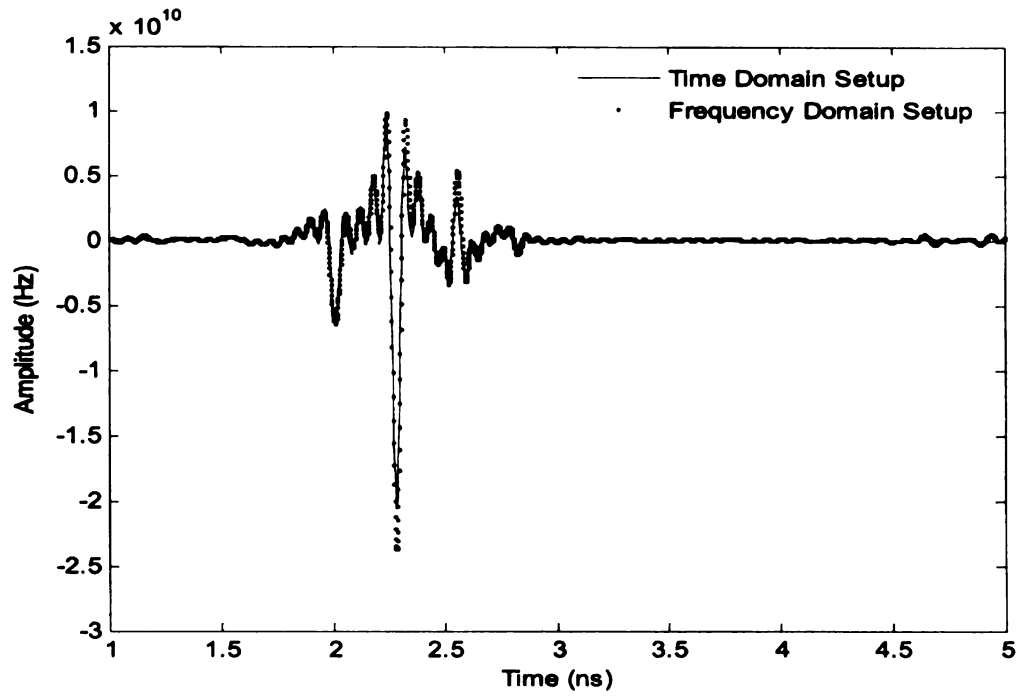


Figure 7.45. PEC-backed PVC - Comparison of measurement systems (a)temporal response and (b)spectral response

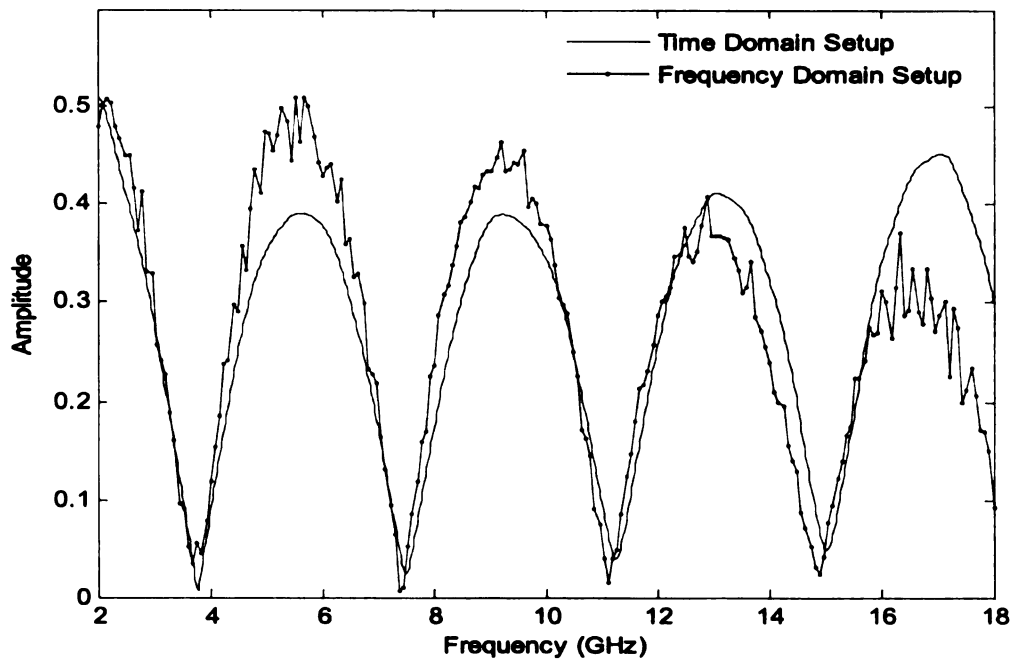
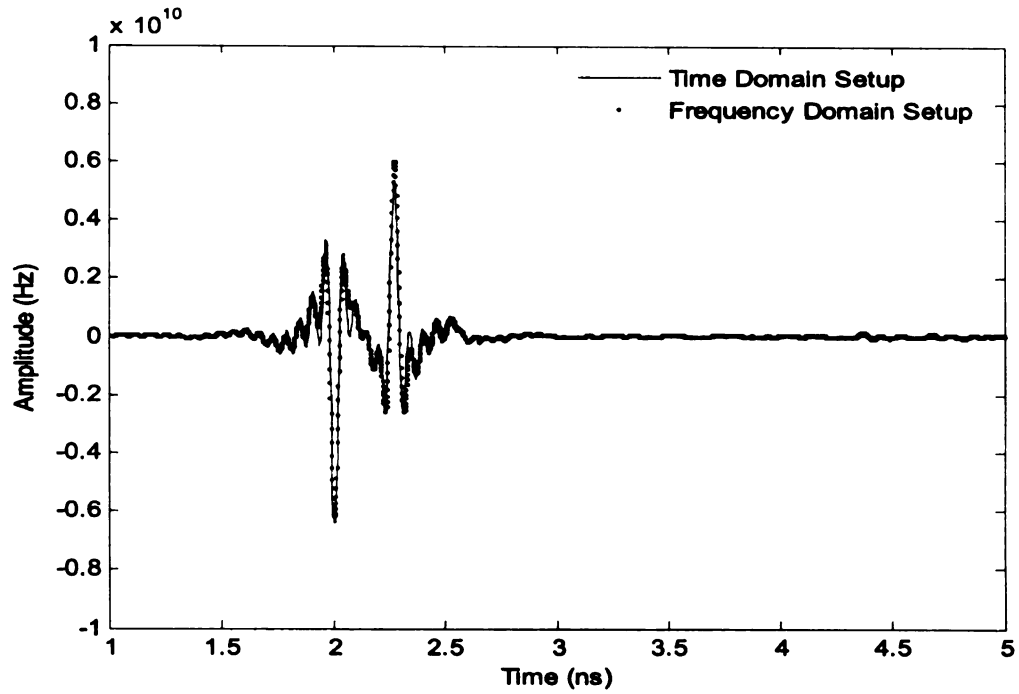


Figure 7.46. Air-backed PVC - Comparison of measurement systems (a)temporal response and (b)spectral response

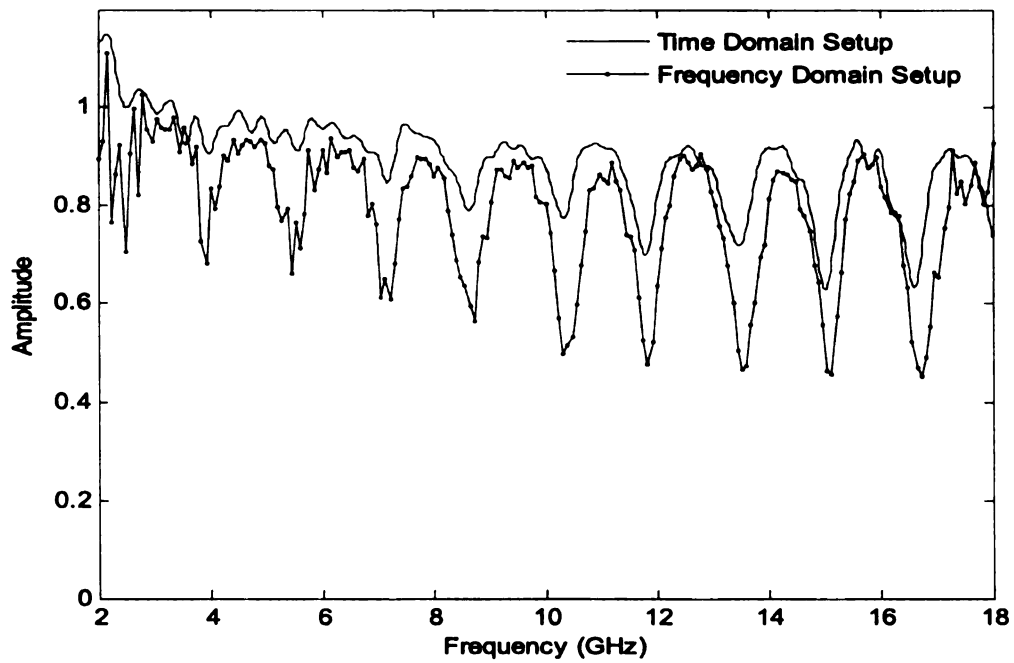
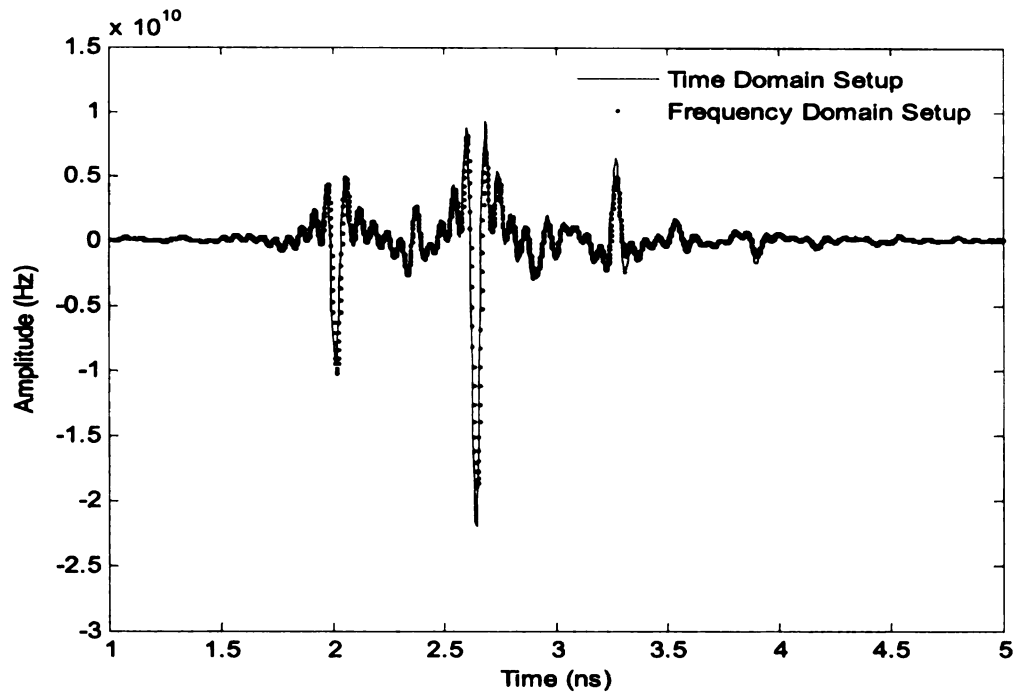


Figure 7.47. PEC-backed garolite-acrylic stack - Comparison of measurement systems (a)temporal response and (b)spectral response

## CHAPTER 8

### CONCLUSIONS

In this thesis, the temporal response for reflection from an  $n$ -layer material structure is explored. This work builds on work done by Oh, which showed that the late time response of a single layer backed by either free space or a conductor is a natural mode series. Oh's work leads one to consider what conditions lead to the late time response of a material stack with more than a single layer having a natural resonance representation. To answer this question, the reflection from an air backed single lossy layer terminated by a perfect electric conductor is first considered. Physical reasoning suggests, and the analysis shows, that there is a middle time during which the response of the structure is a natural mode series identical to that of the single air-backed layer, since the incident wave has not reached the conductor backing and thus no information about the position of this backing is available in the reflected response. The middle time period is found to correspond to the time between the observation of the response due to reflection from the second interface, and the observation of the response from the conductor at an observation plane. After this middle time period there is a late time during which the response is an entirely new natural mode series related to the poles of the frequency domain reflection coefficient for the entire problem. Hence, the response of the air-backed lossy layer present during the middle time period is turned off, and replaced by a different natural mode response.

With this knowledge of the response from a multilayered structure, properties of the backing layer and their relationship to the presence of a pure natural mode series in the late time are considered. To study this, examination of the response of a single lossy layer, backed by a material layer, either lossless or lossy, is undertaken. It is found that whether or not the late time response of this structure is a natural mode

series is dependent only on the properties of the material backing. When a lossless backing half space is considered, the response is found to have a natural resonance representation in the late time. However, when a lossy half space is considered, it is found that a pure natural resonance representation may not be possible, as there may be a branch cut contribution to the temporal response. This is found to be the case regardless of the properties of the first material layer.

Thus, a single lossy layer, backed by a perfect conductor, or a lossless half space, will have a late time response that is a pure natural mode series. However, when that same layer is backed by a lossy region, the late time natural mode response may be augmented by a branch cut contribution which is not time-limited. The portion of the response due to this branch cut contribution is an infinite tail which pollutes the natural mode response.

Next, the properties of the backing layer in an  $n$ -layer material stack are explored in order to determine their affect on the form of the response in the late time of the structure. For this, a stack consisting of two lossy layers backed by a perfect conductor is considered. It is found in this exploration that the response of the two-layered material structure backed by a perfect conductor is a natural mode series during the late time. This implies that the branch cut contribution that is present in the middle time of the response is turned off when the reflection from the conductor backing reaches the observation plane; that is, at the start of the late time. Thus, the presence of the conductor terminates the infinite tail in the response of the single layer backed by a lossy material, and initiates a pure natural mode series.

All of these results lead to the following hypothesis about the response of an  $n$ -layer system. First, it is hypothesized that the late time reflected field response of an  $n$ -layer system is a pure natural mode series if the backing layer is lossless or a perfect electric conductor. Also, if the backing layer is lossy, the late time reflected field response is hypothesized to be is a natural mode series augmented by a non-time

limited branch cut contribution. This hypothesis proves to be true, with the backing layer being the determining factor as to whether the late time response is a pure natural mode series. It is also found that the addition of another interface, which produces a new  $n + 1$  layer structure, has an the early time response that is identical to the total response of the  $n$ -layer structure. This response turns off completely at a time associated with the reflection from the new interface with the backing material, and a late time response turns on consisting of a natural mode series that is only augmented by a branch cut contribution if the new backing is lossy. If the  $n$ -layer structure has a non-time limited component in its late time, this component turns off at the start of the late time of the  $n + 1$  layer structure.

## 8.1 Suggestions for Future Work

In this work, a lot of emphasis was placed on the determination of the branch cut contributions to the temporal response of layered material structures. There is still a great deal of work to be done in exploring layered material problems. Some suggestions for this work include:

*Tracing of pole trajectories for the air-backed lossy layer terminated by a perfect conductor* for oblique incidence, as a function of both the position of the conductor, and the incidence angle. This investigation should be straight forward for incidence angles below the Brewster angle, but may become intriguing as grazing incidence is considered.

*Tracing of pole trajectories and numerical evaluation of the branch cut contribution* for the lossy material-backed material layer as the backing material is varied from a lossless material to a highly lossy one. This becomes interesting because of the nonexistence of branch cut contributions for both the lossless case, and the perfect conductor case, while at points in between, a branch cut contribution may occur.

*Verification of integral contributions from the paths around branch points vanish-*

*ing.* It was assumed in this thesis that these paths yield no contributions to the inverse transform, however, this was not verified for the  $n$ -layered case. This assumption was based on these contributions being zero for all cases examined.

*Determination of whether there will be a branch cut contribution during the late time response* when the backing material is lossy. This thesis shows rigorously that there will not be a branch cut contribution if the backing material is lossless, however the mandatory inclusion of a branch cut contribution when the material is lossy has not been shown rigorously. That is to say, there was not an evaluation done to find out if a branch cut contribution is guaranteed when the material is lossy. Determination of the form of the branch cut contribution as a non-time limited wave has not been shown rigorously for the layered case either, it was assumed based on the developments of [14].

*Consideration of transmission through material stacks* has not been considered here. It would be interesting to explore the properties of the transmitted field through a stack of materials to find out if a natural resonance series exists. If so, does it exist at all times for the transmitted response, or is there a distinction of time periods as in the reflection case?

These are only a few of the many open questions which warrant exploration in this field.

## **BIBLIOGRAPHY**



## BIBLIOGRAPHY

- [1] C.E. Baum, E.J. Rothwell, K.M. Chen and D.P. Nyquist, "The singularity expansion method and its application to target identification," *Proc. IEEE*, vol. 79, no. 10, pp. 1481-1491, 1991.
- [2] E.J. Rothwell, D.P. Nyquist, K.M. Chen and B. Drachman, "Radar target discrimination using the extinction-pulse technique," *IEEE Trans. Antennas Propagat.*, vol. AP-33, pp. 929-937, Sept. 1985.
- [3] E.J. Rothwell, K.M. Chen, D.P. Nyquist and W. Sun, "Frequency domain E-pulse synthesis and target discrimination," *IEEE Trans. Antennas Propagat.*, vol. AP-35, pp. 426-434, Apr. 1987.
- [4] G.J. Stenholm, E.J. Rothwell, D.P. Nyquist, L.C. Kempel and K.M. Chen, "E-pulse diagnostics for layered materials," *URSI Radio Science Meeting*, Boston, Mass., 2001.
- [5] D. Batrakov, S. Shulga and N. Zhuck, "Application of the extinction pulse technique to non-destructive control of dielectric materials," *IEEE AP-S Int. Symp. Dig.*, Ann Arbor, MI, vol.2, pp. 880-883, 1993.
- [6] L.B. Felson, ed., *Transient Electromagnetic Fields*, Springer-Verlag, Berlin, 1976, Chapter 3 (C.E. Baum).
- [7] A.G. Alexander, "Theoretical and practical aspects of singularity and eigenmode expansion methods," *IEEE Trans. Antennas Propagat.*, vol. AP-28, no. 6, pp. 897-901, Nov. 1980.
- [8] M.A. Morgan, "Singularity expansion representations of fields and currents in transient scattering," *IEEE Trans. Antennas Propagat.*, vol. AP-32, no. 5, pp. 466-473, May 1984.
- [9] L.B. Felson, "Comments on early time SEM," *IEEE Trans. Antennas Propagat.*, vol. AP-33, no. 1, pp. 118-119, Jan. 1985.
- [10] D.G. Dudley, "Comments on SEM and the parameter inverse problem," *IEEE Trans. Antennas Propagat.*, vol. AP-33, no.1 pp. 119-120, Jan. 1985.
- [11] A.G. Tihuis and H. Block, "SEM approach to the transient scattering by and inhomogeneous, lossy dielectric slab; Part 1: the homogeneous case," *Wave Motion*, vol. 6, pp. 61-78, 1984.

- [12] A.G. Tihuis and H. Block, "SEM approach to the transient scattering by and inhomogeneous, lossy dielectric slab; Part 2: the inhomogeneous case," *Wave Motion*, vol. 6, pp. 167-182, 1984.
- [13] J.C. Oh, "Natural resonance representation of the transient field reflected by a planar layered lossy dielectric," Ph.D. Dissertation, Michigan State University, East Lansing, MI, 2002.
- [14] J. Suk, "Transient analysis of plane wave scattering in a layered medium," Ph.D. Dissertation, Michigan State University, East Lansing, MI, 2000.
- [15] W.R. LePage, *Complex Variables and the Laplace Transform for Engineers*, McGraw-Hill, New York, 1961, pp. 353-357.
- [16] R.E. Collin, *Field Theory of Guided Waves*, Second Edition, IEEE Press, Piscataway, NJ, 1991.
- [17] E.J. Rothwell and M.J. Cloud, *Electromagnetics*, CRC Press, Boca Raton, Florida, 2001.
- [18] A. Kizilay, "A perturbation method for transient multipath scattering from targets above periodic surfaces," Ph.D. Dissertation, Michigan State University, East Lansing, MI, 2000.
- [19] J. Ross, III. "Application of transient electromagnetic fields to radar target discrimination," Ph.D. Dissertation, Michigan State University, East Lansing, MI, 1992.
- [20] Michael A. Morgan, "Ultra-Wideband Impulse Scattering Measurements," *IEEE Transactions on Antennas and Propagation*, vol. 42, no.6, pp. 840-852, June 1994.
- [21] M.A. Morgan and B.W. McDaniel, "Transient Electromagnetic Scattering: Data Acquisition and Signal Processing," *IEEE Transactions on Instrumentation and Measurement*, vol. 36, no.2, pp. 263-267, June 1994.
- [22] R.F. Harrington, *Time-Harmonic Electromagnetic Fields*, McGraw-Hill, New York, 1961.
- [23] T.M.R. Ellis, I.R. Phillips and T.M. Lahey, *Fortran 90 Programming*, Addison Wesley, England, 1994.

MICHIGAN STATE UNIVERSITY LIBRARIES



3 1293 02736 5265